nagra.

# Arbeitsbericht NAB 22-01

## TBO Stadel-3-1: Data Report

## Dossier VIII
## Rock Properties, Porewater Characterisation and Natural Tracer Profiles

June 2022

L. Aschwanden, L. Camesi, E. Gaucher,
T. Gimmi, A. Jenni, M. Kiczka, U. Mäder,
M. Mazurek, D. Rufer, H.N. Waber,
P. Wersin, C. Zwahlen & D. Traber

National Cooperative
for the Disposal of
Radioactive Waste

Hardstrasse 73
P.O. Box
5430 Wettingen
Switzerland
Tel. +41 56 437 11 11

www.nagra.ch

nagra.

# Arbeitsbericht NAB 22-01

## TBO Stadel-3-1: Data Report

## Dossier VIII
## Rock Properties, Porewater Characterisation and Natural Tracer Profiles

June 2022

L. Aschwanden[1], L. Camesi[1], E. Gaucher[1], T. Gimmi[1], A. Jenni[1], M. Kiczka[1], U. Mäder[1,2], M. Mazurek[1], D. Rufer[1], H.N. Waber[1,3], P. Wersin[1], C. Zwahlen[1] & D. Traber[4]

[1] Rock-Water Interaction, University of Bern
[2] Rock-Water Consulting, Boll
[3] WaterGeoChem Consulting, Bern
[4] Nagra

**Keywords:**
STA3-1, Nördlich Lägern, TBO, deep drilling campaign, petrophysical parameters, water content, porosity, mineralogy, clay content, clay mineral composition, porewater chemistry, natural tracer profiles

**National Cooperative for the Disposal of Radioactive Waste**

Hardstrasse 73
P.O. Box
5430 Wettingen
Switzerland
Tel. +41 56 437 11 11

www.nagra.ch

Nagra Arbeitsberichte ("Working Reports") present the results of work in progress that have not necessarily been subject to a comprehensive review. They are intended to provide rapid dissemination of current information.

This NAB aims at reporting drilling results at an early stage. Additional borehole-specific data will be published elsewhere.

In the event of inconsistencies between dossiers of this NAB, the dossier addressing the specific topic takes priority. In the event of discrepancies between Nagra reports, the chronologically later report is generally considered to be correct. Data sets and interpretations laid out in this NAB may be revised in subsequent reports. The reasoning leading to these revisions will be detailed there.

This report was finalised in March 2023.

This Dossier was prepared by the Rock-Water Interaction Group of the University of Bern (authors are listed in the individual chapters). D. Traber was the responsible Nagra project manager.

The authors warmly acknowledge the laboratory work of:
P. Bähler and C. Pichler efficiently produced a substantial part of the data presented in this report.
U. Eggenberger, J. Krbanjevic, M. Wolffers, W. Zucha and F. Gfeller provided data for mineralogical and BET analyses as well as evaluation tools.
D. Roos, J. Richards and L. de Doliwa Zielinski performed sampling and core processing.
Th. Siegenthaler expertly machined core samples for advective-displacement experiments.
T. Oyama (CRIEPI, Japan) kindly collaborated in the context of porewater squeezing.
N. Schwendener from IRM University of Bern provided X-ray CT scans of a substantial number of core samples.

We are also grateful for the excellent work of the drill-site team who successfully provided sealed core samples according to our specifications.

We thank P. Blaser and M. Unger for editorial work.

Text, clarity and discussions were improved by a thorough review by A. Gautschi.

# Table of Contents

## List of Tables

## List of Figures

# Electronic Appendices

App. A: Comprehensive database with results of laboratory analyses (xls format)

App. B: Detailed documentation of advective-displacement experiments (xls format)

*Note: Appendices are available upon request.*

# 1 Introduction

## 1.1 Context

To provide input for site selection and the safety case for deep geological repositories for radioactive waste, Nagra has drilled a series of deep boreholes ("Tiefbohrungen", TBO) in Northern Switzerland. The aim of the drilling campaign is to characterise the deep underground of the three remaining siting regions located at the edge of the Northern Alpine Molasse Basin (Fig. 1-1).

In this report, we present the results from the Stadel-3-1 borehole.

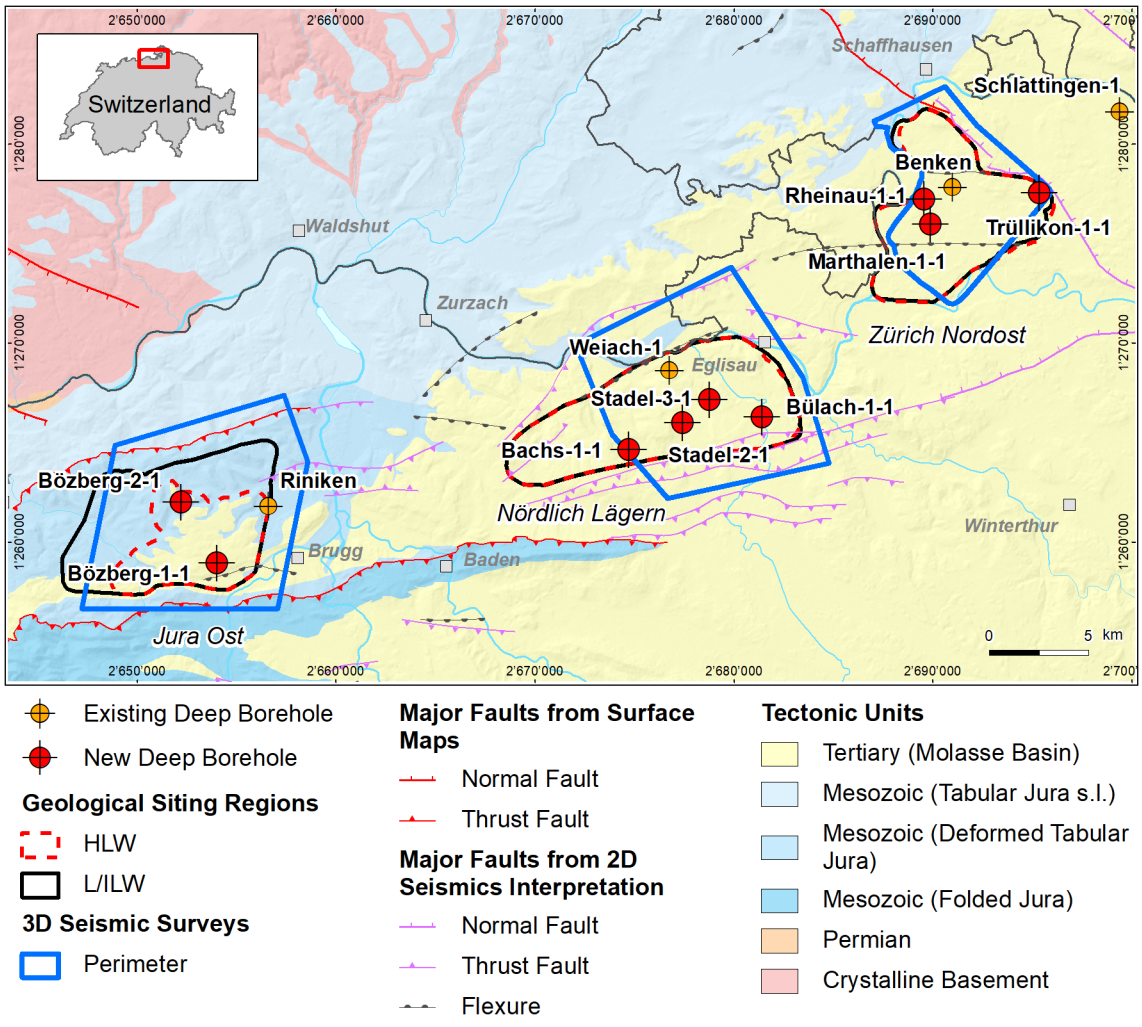


Fig. 1-1: Tectonic overview map with the three siting regions under investigation

## 1.2 Location and specifications of the borehole

The Stadel-3-1 (STA3-1) exploratory borehole is the sixth borehole drilled within the framework of the TBO project. The drill site is located in the central part of the Nördlich Lägern siting region (Fig. 1-2). The vertical borehole reached a final depth of 1'280.88 m (MD)[1]. The borehole specifications are provided in Tab. 1-1.

Tab. 1-1: General information about the STA3-1 borehole

| | |
|---|---|
| **Siting region** | Nördlich Lägern |
| **Municipality** | Stadel (Canton Zürich / ZH), Switzerland |
| **Drill site** | Stadel-3 (STA3) |
| **Borehole** | Stadel-3-1 (STA3-1) |
| **Coordinates** | LV95: 2'678'792.885 / 1'267'161.988 |
| **Elevation** | Ground level = top of rig cellar: 408.74 m above sea level (asl) |
| **Borehole depth** | 1'280.88 m measured depth (MD) below ground level (bgl) |
| **Drilling period** | 17th December 2020 – 25th June 2021 (spud date to end of rig release) |
| **Drilling company** | PR Marriott Drilling Ltd |
| **Drilling rig** | Rig-16 Drillmec HH102 |
| **Drilling fluid** | Water-based mud with various amounts of different components such as[2]:<br>0.0 – 439.0 m: Polymers<br>439.0 – 640.0[3] m: Sodium chloride & polymers<br>640.0 – 1'035.0 m: Potassium silicate & polymers<br>1'035.0 – 1'101.0 m: Polymers<br>1'101.0 – 1'280.9 m: Sodium chloride & polymers |

The lithostratigraphic profile and the casing scheme are shown in Fig. 1-3. The comparison of the core versus log depth[4] of the main lithostratigraphic boundaries in the STA3-1 borehole is shown in Tab. 1-2.

[1] Measured depth (MD) refers to the position along the borehole trajectory, starting at ground level, which for this borehole is the top of the rig cellar. For a perfectly vertical borehole, MD below ground level (bgl) and true vertical depth (TVD) are the same. In all Dossiers depth refers to MD unless stated otherwise.

[2] For detailed information see Dossier I.

[3] Borehole uncased below casing shoe at 437.4 m after drilling fluid exchange.

[4] Core depth refers to the depth marked on the drill cores. Log depth results from the depth observed during geophysical wireline logging. Note that the petrophysical logs have not been shifted to core depth, hence log depth differs from core depth.

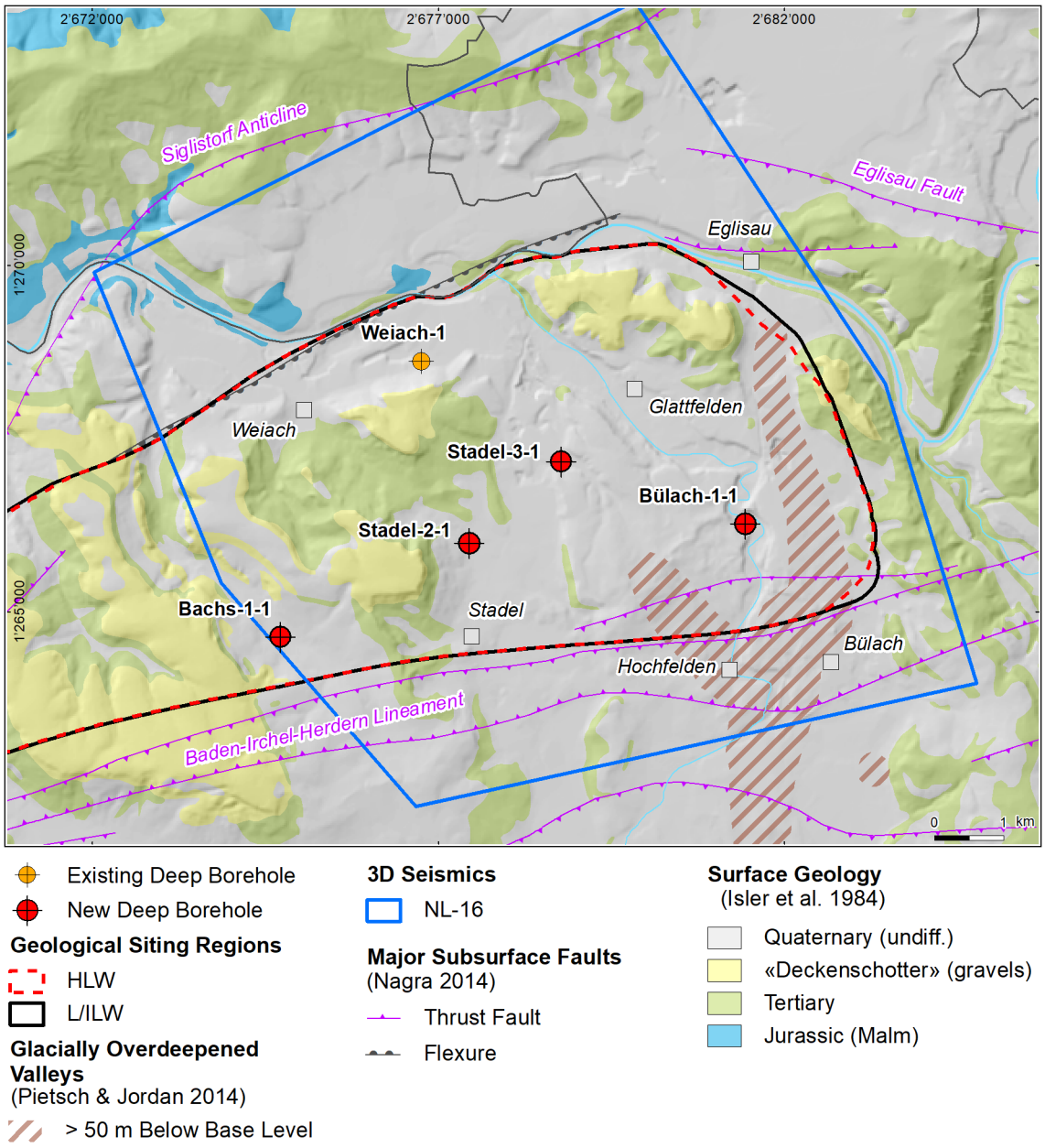


Fig. 1-2: Overview map of the investigation area in the Nördlich Lägern siting region with the location of the STA3-1 borehole in relation to the boreholes Weiach-1, BUL1-1, STA2-1 and BAC1-1

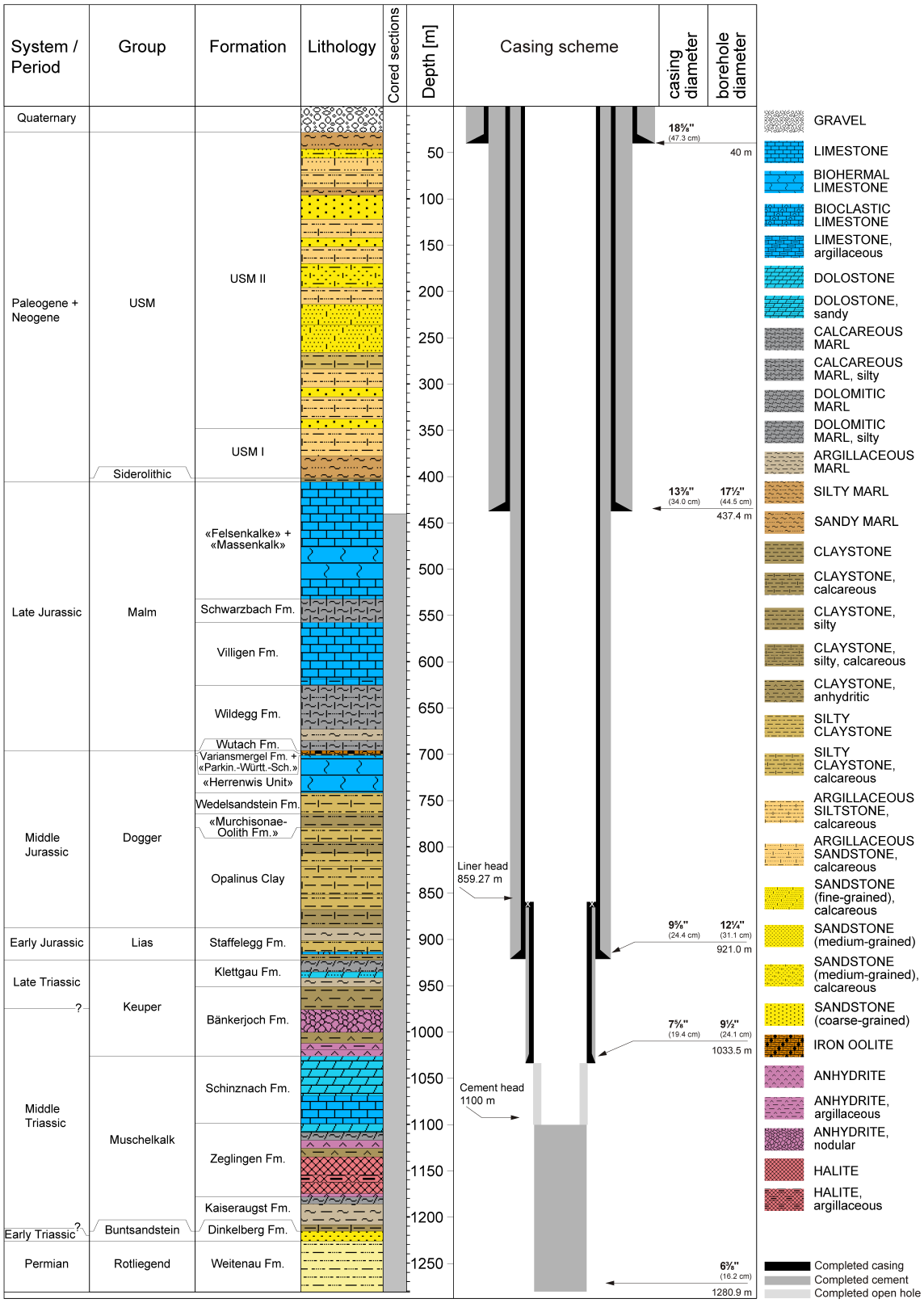


Fig. 1-3: Lithostratigraphic profile and casing scheme for the STA3-1 borehole[5]

[5] For detailed information see Dossier I and III.

Tab. 1-2: Core and log depth for the main lithostratigraphic boundaries in the STA3-1 borehole[6]

| System / Period | Group | Formation | | Core depth in m (MD) | Log depth in m (MD) | |
|---|---|---|---|---|---|---|
| Quaternary | | | | | **28.0** | — |
| Paleogene + Neogene | USM | | | | 402.0 | — |
| | Siderolithic | | | | **406.0** | — |
| Jurassic | Malm | «Felsenkalke» + «Massenkalk» | | 532.55 | 532.65 | — |
| | | Schwarzbach Formation | | 557.93 | 558.11 | — |
| | | Villigen Formation | | 625.58 | 625.64 | — |
| | | Wildegg Formation | | 696.03 | 696.15 | — |
| | Dogger | Wutach Formation | | 699.47 | 699.59 | — |
| | | Variansmergel Formation + «Parkinsoni-Württembergica-Schichten» | | 701.65 | 701.77 | — |
| | | «Herrenwis Unit» | | 742.00 | 742.03 | — |
| | | Wedelsandstein Formation | | 764.97 | 764.94 | — |
| | | «Murchisonae-Oolith Formation» | | 779.26 | 779.16 | — |
| | | Opalinus Clay | | 887.94 | 887.72 | — |
| | Lias | Staffelegg Formation | | **922.71** | **922.44** | — |
| Triassic | Keuper | Klettgau Formation | | 951.13 | 951.57 | — |
| | | Bänkerjoch Formation | | 1026.62 | 1026.96 | — |
| | Muschelkalk | Schinznach Formation | | 1099.03 | 1099.64 | — |
| | | Zeglingen Formation | | 1178.43 | 1178.73 | — |
| | | Kaiseraugst Formation | | 1215.50 | 1215.74 | — |
| | Buntsandstein | Dinkelberg Formation | | **1226.38** | **1226.68** | — |
| Permian | Rotliegend | Weitenau Formation | final depth | 1280.88 | 1281.08 | |

[6] For details regarding lithostratigraphic boundaries see Dossier III and IV; for details about depth shifts (core goniometry) see Dossier V.

## 1.3 Documentation structure for the STA3-1 borehole

NAB 22-01 documents the majority of the investigations carried out in the STA3-1 borehole, including laboratory investigations on core material. The NAB comprises a series of stand-alone dossiers addressing individual topics and a final dossier with a summary composite plot (Tab. 1-3).

This documentation aims at early publication of the data collected in the STA3-1 borehole. It includes most of the data available approximately one year after completion of the borehole. Some analyses are still ongoing (e.g. diffusion experiments, analysis of veins, hydrochemical interpretation of water samples) and results will be published in separate reports.

The current borehole report will provide an important basis for the integration of datasets from different boreholes. The integration and interpretation of the results in the wider geological context will be documented later in separate geoscientific reports.

Tab. 1-3: List of dossiers included in NAB 22-01

Black indicates the dossier at hand.

| Dossier | Title | Authors |
|---|---|---|
| I | TBO Stadel-3-1: Drilling | M. Ammen & P.-J. Palten |
| II | TBO Stadel-3-1: Core Photography | D. Kaehr & M. Gysi |
| III | TBO Stadel-3-1: Lithostratigraphy | P. Schürch, P. Jordan, M. Schwarz, H. Naef, R. Felber, T. Ibele & M. Gysi |
| IV | TBO Stadel-3-1: Microfacies, Bio- and Chemostratigraphic Analyses | S. Wohlwend, H.R. Bläsi, S. Feist-Burkhardt, B. Hostettler, U. Menkveld-Gfeller, V. Dietze & G. Deplazes |
| V | TBO Stadel-3-1: Structural Geology | A. Ebert, S. Cioldi, E. Hägerstedt & M. Gysi |
| VI | TBO Stadel-3-1: Wireline Logging, Micro-hydraulic Fracturing and Pressure-meter Testing | J. Gonus, E. Bailey, J. Desroches & R. Garrard |
| VII | TBO Stadel-3-1: Hydraulic Packer Testing | R. Schwarz, M. Willmann, H. Fisch, M. Voß & A. Pechstein |
| VIII | TBO Stadel-3-1: Rock Properties, Porewater Characterisation and Natural Tracer Profiles | L. Aschwanden, L. Camesi, E. Gaucher, T. Gimmi, A. Jenni, M. Kiczka, U. Mäder, M. Mazurek, D. Rufer, H.N. Waber, P. Wersin, C. Zwahlen & D. Traber |
| IX | TBO Stadel-3-1: Rock-mechanical and Geomechanical Laboratory Testing | E. Crisci, L. Laloui & S. Giger |
| X | TBO Stadel-3-1: Petrophysical Log Analysis | S. Marnat & J.K. Becker |
| | TBO Stadel-3-1: Summary Plot | Nagra |

## 1.4 Scope and objectives of this dossier

The dossier at hand summarises the laboratory work of the Rock-Water Interaction Group (RWI) of the University of Bern, Institute of Geological Sciences, dedicated to rock and porewater characterisation of core materials obtained from the STA3-1 borehole. The level of ambition is to document observations and measurements and to provide a quality-assured dataset. Closely related data obtained by other laboratories (e.g. CEC data by PSI) are integrated with our data.

Data are evaluated and discussed to some degree, including consistency and plausibility checks. An in-depth discussion, sophisticated modelling efforts and regional comparisons with data from other sites are beyond the scope of this report. Additional data obtained by other groups (e.g. hydraulic tests, groundwater sampling, geophysical borehole and core logging, structural logging) are considered in several cases but not in a comprehensive way. An integrated interpretation of all available data is deferred to a later stage of the TBO programme, when results from several boreholes can be synthesised for a siting region.

Throughout this report, rock samples used for analysis are identified by their mid-sample depth in m.

Note that in this report «Brauner Dogger» is used for the Dogger units overlying the Opalinus Clay. In the Sectoral Plan Stages 1 and 2, «Brauner Dogger» is referred to the clay-rich rock sequence east of the lower Aare valley only (Nagra 2008).

# 2 Geoscientific data of interest and drilling conditions for the STA3-1 borehole

*Lukas Aschwanden, Martin Mazurek, Eric Gaucher*

## 2.1 Geological information

The STA3-1 borehole is located in the central part of the siting region Nördlich Lägern southwest of the village of Glattfelden (Canton Zürich; Fig. 1-1). Nördlich Lägern lies in the Deformed Eastern Tabular Jura between the autochtonous Tabular Jura in the NW and the Folded Jura in the SW. The siting area is delineated by some major tectonic structures, the Siglistorf Anticline and the Eglisau Fault in the north and the Baden – Irchel – Herdern Lineament and the Jura Main Thrust to the south. Tectonically, the Deformed Tabular Jura is compressively overprinted by the alpine forefront. This is for example manifested by the thrust of the Mesozoic sediments about 200 m to the north assumed to have occurred in the Triassic salt layers of the Zeglingen Formation (Nagra 2014). However, according to seismic interpretations, no relevant faults were identified in the Mesozoic sediment stack at the borehole location. The regional dip of the bedding is subhorizontal towards SE.

## 2.2 Structural logging

The results of the structural core logging are documented in Dossier V, where the following types of structural features are distinguished:

- Fault planes and fault zones (shear structures); mainly oriented bedding-subparallel and S-dipping (average at 177/06).
- Brittle extensional fractures (structures without shear or slip indication, e.g., joints, veins, tension gashes); these exhibit large variation in orientation and dip (1 – 90°), however, a poorly defined cluster showing mean orientations of 276/80 is identified.
- Stylolites; two classes with different orientation and dipping trend: 1) parallel or subparallel to bedding (SE- to S-dipping) and 2) subvertical, NNE or SSW dipping.
- Larger open pores

The interpreted structures are unevenly distributed among the stratigraphic units. Highest frequencies of structures are observed in the carbonates of the Malm and the Schinznach Formation but also of the Bänkerjoch Formation. The Dogger and the Liassic show distinctly less structures, especially the Opalinus Clay shows only few. However, a prominent deformed interval (850.20 – 851.80 m log depth) was identified in the Opalinus Clay, characterised by disturbed bedding and numerous fault planes forming a distinct fault zone (Fig. 2-1). All fault planes are mineralised (i.e. closed) with synkinematic calcite, generally < 2 mm thick and NE-SW striking.


Fig. 2-1: Illustration of a distinct fault zone at 851.38 – 851.77 m within the deformed interval of the Opalinus Clay (850.20 – 851.80 m)

360° core photograph of the drill core. The width of the image is 31 cm.

Another deformed interval (1135.77 – 1185.57 m; log depth) was identified in the halite- and anhydrite-rich lithologies of the lower part of the Zeglingen Formation («Salzlager») and the upper part of the Kaiseraugst Formation («Orbicularismergel»). Deformation structures include shape-preferred orientation of recrystallised salt crystals, sigma-clasts, salt veins, a fault zone with isoclinally folded anhydrite, a dilation breccia, deformed dolomitic intra-clasts in anhydrite beds, boudinage of dolomitic beds, mm – cm thick tension gashes filled with anhydrite and a dense network of sub-horizontal to steeply dipping fault planes with synkinematic calcite fibres at the base of the interval. Tension gashes and fault planes generally strike NW-SE, thus showing a distinctly different orientation compared to fault planes in the deformed interval of the Opalinus Clay (850.20 – 851.80 m).

A compilation of all individual fault zones and mirror-like fault zones encountered at STA3-1 is provided in Tab. 2-1.

Tab. 2-1: List of interpreted fault zones, mirror-like fault planes (MirFP), stylolitic fault planes (StylFP) and shear bands (SB)

From Dossier V

| **Fault zones** | | | |
|---|---|---|---|
| **Top** [m MD log depth] | **Bottom** [m MD log depth] | **Thickness** [m] | **Type** |
| 472.19 | 472.24 | 0.05 | FP zone |
| 518.67 | 518.83 | 0.16 | Fault zone |
| 570.09 | 570.14 | 0.05 | Fault zone |
| 577.43 | 577.47 | 0.04 | StylFP zone |
| 612.17 | 612.72 | 0.55 | Fault zone |
| 678.65 | 678.88 | 0.23 | Fault zone |
| 699.86 | 699.90 | 0.04 | Fault zone |
| 774.65 | 774.82 | 0.17 | Fault zone |
| 800.89 | 800.90 | 0.01 | Fault zone |
| 851.38 | 851.77 | 0.39 | Fault zone |
| 892.80 | 894.71 | 1.91 | Fault zone |
| 921.61 | 921.83 | 0.22 | Fault zone |
| 921.72 | 921.73 | 0.01 | SB zone |
| 942.09 | 942.50 | 0.41 | MirFP zone |
| 943.03 | 943.37 | 0.34 | MirFP zone |
| 944.55 | 944.68 | 0.13 | MirFP zone |
| 945.74 | 946.97 | 1.23 | MirFP zone |
| 948.62 | 948.77 | 0.15 | MirFP zone |
| 951.10 | 951.20 | 0.10 | MirFP zone |
| 951.38 | 951.54 | 0.16 | MirFP zone |
| 951.67 | 951.77 | 0.10 | MirFP zone |
| 951.99 | 952.06 | 0.07 | MirFP zone |
| 952.89 | 953.97 | 1.08 | MirFP zone |
| 1'002.09 | 1'002.39 | 0.30 | MirFP zone |
| 1'017.69 | 1'017.72 | 0.03 | MirFP zone |
| 1'108.60 | 1'108.88 | 0.28 | MirFP zone |
| 1'144.71 | 1'158.60 | 13.89 | SB zone |
| 1'162.98 | 1'165.18 | 2.20 | SB zone |
| 1'175.33 | 1'185.57 | 10.24 | Fault zone |
| 1'209.77 | 1'209.78 | 0.01 | MirFP zone |
| 1'228.25 | 1'228.37 | 0.12 | Fault zone |

## 2.3 Hydrogeological conditions

Twelve hydraulic packer tests were conducted in the STA3-1 borehole (Dossier VII), and selected results for the more permeable Malm and Muschelkalk aquifer sections are summarised in Tab. 2-2. Hydraulic conductivities for the clay-rich section «Brauner Dogger» to Staffelegg Formation range from $1 \times 10^{-14}$ to $1 \times 10^{-12}$ m/s (best estimates). Enhanced hydraulic conductivities were identified in the Malm and Muschelkalk aquifers. Note that the test interval in the Malm aquifer was targeted at the major inflow detected by fluid logging at around 521 m depth. The Keuper section is of low transmissivity ($K = 1 \times 10^{-12}$ m/s) and did not yield any groundwater for sampling.

Tab. 2-2: Selected results from hydraulic packer tests for the more permeable sections of the STA3-1 borehole

The best estimates for transmissivity *T*, hydraulic conductivity *K* and hydraulic head are indicated. Data are from Dossier VII.

| **Top** [m MD] | **Bottom** [m MD] | **Length** [m] | **Geological unit** | ***T*** [$m^2/s$] | ***K*** [m/s] | **Head** [m asl] |
|---|---|---|---|---|---|---|
| 499.20 | 527.81 | 28.61 | «Felsenkalke» + «Massenkalk» (Malm aquifer) | $3 \times 10^{-07}$ | $1 \times 10^{-08}$ | 361 |
| 1054.50 | 1101.00 | 46.50 | Schinznach Fm. (Muschelkalk aquifer) | $5 \times 10^{-06}$ | $1 \times 10^{-07}$ | 353 |

## 2.4 Groundwater samples

Groundwater samples with variable degrees of drilling-fluid contamination were obtained from the Malm and Muschelkalk aquifers. For the present report, values for the chemically conservative parameters Cl and Br and the water-isotope ratios $\delta^{18}O$ and $\delta^{2}H$ are of major interest, as these serve as boundary conditions for the porewater data. These values were corrected by Lorenz (*in prep.*) for (minor) drilling-fluid contamination and are reproduced in Tab. 2-3 along with information on the chemical water type and mineralisation of the groundwaters.

Tab. 2-3: Conservative parameters for groundwater from the Malm and Muschelkalk aquifer in borehole STA3-1 corrected for drilling-fluid contamination

| **Parameter** | **Unit** | **Malm aquifer** | **Muschelkalk aquifer** |
|---|---|---|---|
| Chemical type | | Na-Cl * | Na-Cl * |
| Mineralisation (TDS) | [g/L] | 11.3 – 11.9 * | 10.0 * |
| Chloride (Cl) | [mg/L] | 6731 **/ 7602 *** | 4235 **/ 4234 *** |
| Bromide (Br) | [mg/L] | 22 * | 0.49 **/ 0.37 *** |
| 1000·Br/Cl | [molal] | 1.45 **/ 1.28 *** | 0.05 **/ 0.04 *** |
| $\delta^{18}O$ of water | [‰$_{VSMOW}$] | –1.25 **/ –1.33 *** | –11.93 **/ –11.98 *** |
| $\delta^{2}H$ of water | [‰$_{VSMOW}$] | –48.8 **/ –49.1 *** | –85.2 **/ –86.0 *** |
| Test interval | [m MD] | 499.20 – 527.81 | 1'054.50 – 1'101.00 |

* Corrected based on preliminary extrapolation
** Corrected based on uranine (Lorenz *in prep.*)
*** Corrected based on $^{3}H$-$H_2O$ (Lorenz *in prep.*)

## 2.5 Drilling conditions and drilling fluids

During drilling of STA3-1 four different drilling muds werer used: Pure-Bore®, Pure-Bore® plus NaCl, potassium silicate and sodium chloride brine (Dossier I). Key information is listed in Tab. 2-4. No major mud losses were observed during the drilling operations. Minor losses occurred in the Villigen Formation (4 $m^3$) at 563 – 587 m depth and in the Muschelkalk (8 $m^3$) at 1'070 – 1190 m depth (base Schinznach Formation – top Kaiseraugst Formation).

Detailed information on the composition of the drilling muds used at STA3-1 is only available for the Malm and the Muschelkalk. These are listed in Tab. 2-5. Besides K silicate, the mud used in the Dogger – Keuper section also contains Flowzan, soda ash and other conditioners for achieving the desired density and viscosity / rheology.

Tab. 2-4: Drilling muds and main mud loss events

Based on Dossier I.

| **Depth interval** [m] | **Geological unit** | **Drilling mud** | **Comments** |
|---|---|---|---|
| 0 – 438.5 | Quaternary – «Felsen-kalke» + «Massenkalk» | Pure-Bore® | Destructive drilling |
| 438.5 – 563.0 | «Felsenkalke» + «Massen-kalk» – Villigen Fm. | Pure-Bore® + NaCl | Mud treated with 150 kg/m$^3$ NaCl for protection against freezing |
| 563.0 – 587.0 | Villigen Fm. | Pure-Bore® + NaCl | Dynamic seepage losses at 100 – 150 L/min (4 m$^3$) |
| 587.0 – 640.0 | Villigen Fm. – Wildegg Fm. | Pure-Bore® + NaCl | At 640 m exchange of Pure-Bore® + NaCl by freshwater, then by K-silicate |
| 640.0 – 1035.0 | Wildegg – Schinznach Fm. | Potassium silicate, polymers | |
| 1'035.0 – 1'101.0 | Schinznach Fm. – Zeglingen Fm. | Freshwater, polymers | Seepage losses (350 l) in the interval 1'070 – 1'090 m |
| 1'101.0 – 1'280.9 | Zeglingen Fm. – Weitenau Fm. | NaCl brine, polymers | Continued seepage losses at 1'090 – 1'190 m (8 m$^3$) |

Tab. 2-5: Composition of drilling mud used in the Malm and Muschelkalk

From Lorenz et al. (*in prep.*)

| **Parameter** | **Units** | **Malm: Pure-Bore® + NaCl** | **Muschelkalk: Freshwater + polymers** |
|---|---|---|---|
| pH | | 9.7 | 10.6 |
| EC | [µS/cm] | 118'750 | 6'910 |
| uranine | [ppb] | 1'107 | 1'359 |
| $^3$H-$H_2O$ | [TU] | 5.7 | 5.2 |
| Alk (pH 8.2) | [meq/L] | 20.7 | 25.3 |
| DOC | [mg/L] | 5'108 | 3'084 |
| Na | [mg/L] | 64'850 | 1'308 |
| K | [mg/L] | 251 | 1'265 |
| $NH_4$ | [mg/L] | < 1 | < 1 |
| Ca | [mg/L] | 3.7 | 34.5 |
| Mg | [mg/L] | 1.9 | 8.6 |
| Si | [mg/L] | 12.1 | 411 |
| Cl | [mg/L] | 78'450 | 183 |
| $SO_4$ | [mg/L] | 337 | 400 |
| $NO_3$ | [mg/L] | 2.5 | 12.6 |
| Br | [mg/L] | 2.3 | 0.16 |
| F | [mg/L] | 19.1 | < 1 |
| Sr | [mg/L] | 0.33 | 0.63 |
| Ba | [mg/L] | 0.50 | 0.93 |
| $\delta^{18}$O of water | [‰VSMOW] | -5.66 | -9.69 |
| $\delta^2$H of water | [‰VSMOW] | -61.1 | -69.3 |

The values are the mean of 8 analyses of samples taken in the suction pit and in the shaker for the mud monitoring. First Malm sample: 03/01/2021 15:30, last Malm sample 09/01/2021 15:30. First Muschelkalk sample: 16/05/2021 01:00, last Muschelkalk sample 19/05/2021 10:00.

# 3 Sampling and applied methods

## 3.1 Sampling strategy

*Lukas Aschwanden, Martin Mazurek*

A suite of 6 different sample types were investigated (Tab. 3-1). Sample types and the general procedures of core sampling, sample conditioning and storage are described by Rufer (2019).

Tab. 3-1: Sample types and sampling strategy

This Table includes on-site conditioned samples relevant for the present report.

| **Sample type** | **Main study targets** | **Sampling (by on-site team)** |
|---|---|---|
| RP (various rock properties), PW (porewater chemistry) | Characterisation of rock and porewater chemistry | Sample lithology representative of the current lithofacies and the sampled core section (usually 3 m). Sampling with a regular spacing in order to obtain a representative dataset |
| SQ (squeezing) | Characterisation of porewater chemistry | Focussed on clay-rich lithologies due to methodological constraints |
| AD (advective displacement) | Characterisation of porewater chemistry | Focussed on clay-rich lithologies due to methodological constraints |
| DI (diffusion experiments) | Diffusion coefficients, cation exchange & sorption parameters at PSI | Coverage of a wide range of lithologies (in particular clay-mineral contents) |
| NG (noble gas analysis) | Concentrations and isotopic compositions of dissolved noble and reactive gases | Sampling with a regular spacing, with situational tightening of the sampling interval close to potentially water-conducting features |
| GM (geomechanics) | Mineralogy and grain density of samples studied for their geomecha-nical properties by other laboratories | Representative sampling of the most relevant lithologies within the Opalinus Clay |

## 3.2 Laboratory programme

*Lukas Aschwanden*

A total of 164 core segments were prepared on-site and designated for our studies, not including samples for geomechanical tests (5 GM samples) and diffusion experiments (10 DI samples) for which the main studies were performed by other laboratories (see Tab. 3-3) but some supporting measurements were performed in our laboratories (e.g. mineralogy, water content, density).

A substantial subset of theses 164 samples were analysed for geochemical and petrophysical characterisation (porewater: PW, RP), squeezing (SQ) and advective displacement (AD). In total, 179 samples were investigated in the RWI laboratories as part of the standard programme, and Tab. 3-2 provides an overview. In Tab. 3-3, the analytical programme for the various sample types is shown in more detail.

Tab. 3-2: Number of samples analysed for the different geological units

For NG samples, the number refers to the number of samples for which samples had to be prepared for outgassing.

| **Unit** | **RP, PW** | **SQ** | **AD** | **DI** | **NG** | **GM** | **Total** |
|---|---|---|---|---|---|---|---|
| Malm | 22 | | | 2 | 13 | | 37 |
| «Brauner Dogger» | 26 | 1 | 1 | 5 | 7 | | 40 |
| Opalinus Clay | 19 | 2 | 2 | | 7 | 5 | 35 |
| Staffelegg Formation | 11 | 1 | 1 | 2 | 3 | | 18 |
| Klettgau Formation | 8 | | | | 2 | | 10 |
| Bänkerjoch Formation | 6 | | | 1 | 5 | | 12 |
| Schinznach Formation | 7 | | | | 4 | | 11 |
| Zeglingen Formation | 6 | | | | 4 | | 10 |
| Kaiseraugst Formation | | | | | 2 | | 2 |
| Dinkelberg Formation | | | | | 1 | | 1 |
| Weitenau Formation | | | | | 3 | | 3 |
| **All** | **105** | **4** | **4** | **10** | **51** | **5** | **179** |

Tab. 3-3: Analytical programme performed for the different sample types

×× = standard programme, × = selected samples only, calc. = calculated.

| **Method** | **RP, PW** | **SQ** | **AD** | **DI** | **NG** | **GM** |
|---|---|---|---|---|---|---|
| Bulk mineralogical composition including CNS analysis | ×× | ×× | ×× | ×× | | ×× |
| Clay mineralogy | × | | ×× | × | | |
| Bulk wet density | ×× | | calc. | ×× | calc. | |
| Grain density | ×× | | calc. | × | | ×× |
| Water content | ×× | ×× | ×× | ×× | ×× | |
| BET surface area | | | | × | | |
| Cation-exchange properties (Ni-en method) | ×* | | × | | | |
| Aqueous extraction | ×× | ×× | ×× | | | |
| Cl isotopes in aqueous extracts | ×** | | | | | |
| Cl isotopes of rock salt | ×** | | | | | |
| Pore-water squeezing | | ×× | | | | |
| Advective displacement of porewater | | | ×× | | | |
| Stable water isotopes | ×× | ×× | ×× | | | |
| Dissolved noble gases | | | | | ×*** | |
| Dissolved reactive gases | | | | | ×*** | |

* Subsamples collected during sample preparation, re-packed and sent to PSI for analysis

** Samples sent to Hydroisotop GmbH for analysis

*** Results will be documented in dedicated reports at a later stage

## 3.3 Analytical methods and methods of raw-data processing

*Lukas Aschwanden*

Experimental procedures and associated analytical methods, formalisms to process measured data and quantification of propagated errors are documented in Waber (ed.) (2020) and are not repeated here. Moreover, Mazurek et al. (2021) provide additional information for situations where the current practice is not documented or deviates from that described in Waber (ed.) (2020).

# 4 Results

## 4.1 Documentation of measured and calculated data

*Martin Mazurek*

Raw data collected in the framework of the analytical programme of STA3-1 are organised in a FileMaker database, including raw-data files (e.g. XRD quantification not corrected for C/N/S analysis), graphics (e.g. XRD patterns) and photographs. The main purpose of this database is to ensure the full documentation and traceability of original and derived data presented in this report. From this database, the relevant data were exported into a comprehensive Excel sheet, which is attached as Appendix A (Excel file). The full dataset for advective-displacement experiments is provided as Appendix B (Excel file).

The objective of the Excel summary sheet is not to fully document all analyses made but, per parameter and sample, to indicate the "best" or most representative value in case multiple measurements were made, and to list parameters calculated from the original measurements. For example, only one composition is given for squeezed and advectively displaced porewaters in a sample, even though multiple aliquots were collected and analysed. Explanatory notes for this sheet follow here.

Measurements on cation exchange capacity and selectivity were mostly performed by PSI. These data are partially integrated into Section 5.6, with reference to a stand-alone data report issued by PSI, and along with our own measurements on few selected samples. These data are also integrated in the Excel summary sheet in Appendix A.

### Bulk mineralogy (X-ray diffraction and CNS analysis)

- Contents of minerals not detected by X-ray diffraction are set to 0, as the actual detection limits are difficult to quantify. 'tr' = present in trace amounts.
- Clay-mineral content is not measured directly but is calculated by difference to 100%.
- Pyrite content is calculated from the measured S content, assuming that pyrite is the main S reservoir in the rock. This is not the case in anhydrite-bearing rocks, which are typically free of pyrite. Here, the S is used to calculate the content of anhydrite.
- Column 'Füchtbauer name' refers to the nomenclature of clastic rocks as defined in Naef et al. (2019). Names are listed only for rock compositions that have < 10 wt.-% minerals not represented in the Füchtbauer triangle (i.e. minerals other than clays, calcite, dolomite/ ankerite, siderite, quartz, K-feldspar, plagioclase). In particular, this means that evaporitic rocks are not given a Füchtbauer name. If a rock contains ≥ 90 wt.-% minerals represented in the Füchtbauer triangle but also contains anhydrite, this is stated in brackets.
- The Füchtbauer triangle does not distinguish between limestones and dolostones. When the content of calcite exceeds that of dolomite/ankerite, the terms "limestone" or "calcareous" are used in this report, and "dolostone" or "dolomitic" are used if the opposite applies.

### Clay mineral groups

- All data refer to wt.-% of the total rock.
- Illite/smectite ML (85-90) refers to a mixed-layer phase with 85 – 90% illite layers, Chl/Sm ML (85-95) designates a chlorite-smectite mixed-layer phase with 85 – 95% chlorite (analogous for the other listed mixed-layer phases).

### End-member clays

- All data refer to wt.-% of the total rock.
- Illite, smectite and chlorite partially occur in mixed-layer phases. Here, the respective total contents of the end-members are calculated. For example, if a sample contains 10 wt.-% illite and 8 wt.-% illite/smectite mixed layers containing 75% illite, the end-member illite content would be 16 wt.-%.

### Petrophysical parameters

- Bulk wet density was measured, and bulk dry density was calculated using equation 5-14 in Waber (ed.) (2020).
- Pycnometer porosity was calculated from densities using equation 5-16 in Waber (ed.) (2020).
- Water content (dry) was calculated from water content (wet) using $w_d = w_w/(1-w_w)$.
- Water-loss porosity was calculated using bulk wet density (equation 5-9 in Waber ed. 2020) or grain density (equation 5-7 in Waber ed. 2020).
- The formalisms to calculate water content from isotope diffusive-exchange experiments are given in equation 76 of Appendix A of Waber (ed.) (2020) and are detailed in Mazurek et al. (2021).

### Chloride and bromide from aqueous extracts recalculated to porewater concentrations using water content

- Concentrations are given relative to bulk porewater as well as relative to various assumptions regarding anion accessibility in the pore space. The calculation is made using equation 6-1 in Waber (ed.) (2020). The variants pertaining to the dependence of anion accessibility on the clay-mineral content are discussed in Chapter 5.

### Errors

- The error columns refer to analytical uncertainty or instrument precision for measured parameters and to propagated errors for calculated parameters, following the formalisms documented in Waber (ed.) (2020).

## 4.2 Mineralogical composition

*Martin Mazurek*

### 4.2.1 Whole rock data

A total of 103 mineralogical analyses were performed in the section «Felsenkalke» + «Massenkalk» (Malm) – Zeglingen Formation (Triassic). The full dataset is documented in Appendix A, and Tab. 4.2-1 provides formation-specific summaries. Plots against depth for the most relevant minerals are shown in Fig. 4.2-1, and a representation in the Füchtbauer triangle is given in Fig. 4.2-3.

The Triassic section is lithologically heterogeneous, mainly due to the variable contents of dolomite, calcite and anhydrite. Systematic depth trends cannot be resolved. The overlying Dogger – Lias section is discussed in detail further below. In the lower part of the Wildegg Formation, an upward trend of increasing clay-mineral contents and decreasing calcite contents is seen, which is the opposite of the trends identified in the BUL1-1 core (Mazurek et al. 2021).

Minor or trace amounts of the following phases have been identified:

- Celestite in the Bänkerjoch Formation
- Fluorite in the Zeglingen Formation
- Haematite in the Ergolz Member of the Klettgau Formation.

The depth profiles of the contents of S and N (based on CNS analysis) are shown in Fig. 4.2-2. Variable but often high S contents, mostly related to the presence of pyrite, are seen in the Dogger – Lias section. In the Triassic, high S contents are related to anhydrite. N contents above the quantification limit of 0.01 wt.-% are only found in the Dogger, Lias and in the underlying Klettgau Formation. The highest N content is observed in the Staffelegg Formation, likely related to the presence of abundant organic matter.

Tab. 4.2-1: Bulk-rock mineralogy: formation-specific means, medians, standard deviations and ranges [wt.-%]

For the calculation of statistical parameters, values below the limit of quantification were set to 0. One sample from the Klettgau Formation contains small amounts of haematite (not listed). [1] Variansmergel Formation + «Parkinsoni-Württembergica-Schichten».

| **Formation** (number of analyses) | **Member** | | **S** [wt.-%] | **N** [wt.-%] | **C(inorg)** [wt.-%] | **C(org)** [wt.-%] | **Quartz** [wt.-%] | **K-feldspar** [wt.-%] | **Plagioclase** [wt.-%] | **Calcite** [wt.-%] | **Dolomite / Ank.** [wt.-%] | **Siderite** [wt.-%] | **Anhydrite** [wt.-%] | **Celestite** [wt.-%] | **Fluorite** [wt.-%] | **Pyrite** [wt.-%] | **Clay minerals** [wt.-%] |
|---|---|---|---|---|---|---|---|---|---|---|---|---|---|---|---|---|---|
| «Felsenkalke» + «Massenkalk» (8) | | Mean | 0.00 | 0.00 | 11.74 | 0.07 | 0.0 | 0.0 | 0.0 | 97.9 | 0.0 | 0.0 | 0.0 | 0.0 | 0.0 | 0.0 | 2.1 |
| | | Median | 0.00 | 0.00 | 11.78 | 0.06 | 0.0 | 0.0 | 0.0 | 98.2 | 0.0 | 0.0 | 0.0 | 0.0 | 0.0 | 0.0 | 1.8 |
| | | Stdev | 0.00 | 0.00 | 0.18 | 0.04 | 0.0 | 0.0 | 0.0 | 1.5 | 0.0 | 0.0 | 0.0 | 0.0 | 0.0 | 0.0 | 1.5 |
| | | Min | 0.00 | 0.00 | 11.40 | 0.05 | 0.0 | 0.0 | 0.0 | 95.0 | 0.0 | 0.0 | 0.0 | 0.0 | 0.0 | 0.0 | 0.5 |
| | | Max | 0.00 | 0.00 | 11.94 | 0.15 | 0.0 | 0.0 | 0.0 | 99.5 | 0.0 | 0.0 | 0.0 | 0.0 | 0.0 | 0.0 | 4.9 |
| Schwarzbach Fm. (2) | | Mean | 0.02 | 0.00 | 9.65 | 0.24 | 3.4 | 0.0 | 0.0 | 76.9 | 3.2 | 0.0 | 0.0 | 0.0 | 0.0 | 0.0 | 16.2 |
| | | Median | 0.02 | 0.00 | 9.65 | 0.24 | 3.4 | 0.0 | 0.0 | 76.9 | 3.2 | 0.0 | 0.0 | 0.0 | 0.0 | 0.0 | 16.2 |
| | | Stdev | 0.03 | 0.00 | 0.63 | 0.04 | 0.3 | 0.0 | 0.0 | 4.0 | 1.2 | 0.0 | 0.0 | 0.0 | 0.0 | 0.1 | 4.9 |
| | | Min | 0.00 | 0.00 | 9.20 | 0.21 | 3.2 | 0.0 | 0.0 | 74.0 | 2.4 | 0.0 | 0.0 | 0.0 | 0.0 | 0.0 | 12.7 |
| | | Max | 0.05 | 0.00 | 10.09 | 0.27 | 3.6 | 0.0 | 0.0 | 79.7 | 4.1 | 0.0 | 0.0 | 0.0 | 0.0 | 0.1 | 19.7 |
| Villigen Fm. (6) | | Mean | 0.01 | 0.00 | 11.14 | 0.25 | 0.9 | 0.0 | 0.0 | 92.4 | 0.3 | 0.0 | 0.0 | 0.0 | 0.0 | 0.0 | 6.1 |
| | | Median | 0.00 | 0.00 | 11.46 | 0.24 | 0.4 | 0.0 | 0.0 | 95.5 | 0.0 | 0.0 | 0.0 | 0.0 | 0.0 | 0.0 | 4.3 |
| | | Stdev | 0.03 | 0.00 | 0.73 | 0.08 | 1.2 | 0.0 | 0.0 | 6.9 | 0.8 | 0.0 | 0.0 | 0.0 | 0.0 | 0.1 | 4.9 |
| | | Min | 0.00 | 0.00 | 9.72 | 0.17 | 0.0 | 0.0 | 0.0 | 78.9 | 0.0 | 0.0 | 0.0 | 0.0 | 0.0 | 0.0 | 2.9 |
| | | Max | 0.08 | 0.00 | 11.62 | 0.38 | 2.8 | 0.0 | 0.0 | 96.8 | 1.9 | 0.0 | 0.0 | 0.0 | 0.0 | 0.1 | 15.9 |
| Wildegg Fm. (8) | | Mean | 0.14 | 0.00 | 8.32 | 0.36 | 5.7 | 1.6 | 0.1 | 67.5 | 1.7 | 0.0 | 0.0 | 0.0 | 0.0 | 0.3 | 22.9 |
| | | Median | 0.12 | 0.00 | 8.30 | 0.35 | 5.7 | 1.2 | 0.0 | 67.4 | 1.9 | 0.0 | 0.0 | 0.0 | 0.0 | 0.2 | 22.1 |
| | | Stdev | 0.10 | 0.00 | 1.37 | 0.05 | 1.9 | 1.7 | 0.4 | 12.4 | 1.3 | 0.0 | 0.0 | 0.0 | 0.0 | 0.2 | 9.3 |
| | | Min | 0.00 | 0.00 | 6.65 | 0.29 | 2.2 | 0.0 | 0.0 | 52.9 | 0.0 | 0.0 | 0.0 | 0.0 | 0.0 | 0.0 | 9.0 |
| | | Max | 0.29 | 0.00 | 10.62 | 0.42 | 8.1 | 3.8 | 1.1 | 87.4 | 3.9 | 0.0 | 0.0 | 0.0 | 0.0 | 0.5 | 38.1 |
| VPW [1] (1) | | Mean | 0.76 | 0.04 | 1.98 | 0.52 | 15.3 | 4.9 | 1.2 | 16.5 | 0.0 | 0.0 | 0.0 | 0.0 | 0.0 | 1.4 | 60.1 |
| «Herrenwis Unit» (8) | | Mean | 0.03 | 0.00 | 9.76 | 0.19 | 5.2 | 1.2 | 0.2 | 79.6 | 1.7 | 0.0 | 0.0 | 0.0 | 0.0 | 0.1 | 11.9 |
| | | Median | 0.00 | 0.00 | 10.11 | 0.18 | 4.3 | 1.2 | 0.0 | 82.3 | 0.8 | 0.0 | 0.0 | 0.0 | 0.0 | 0.0 | 9.1 |
| | | Stdev | 0.07 | 0.00 | 1.88 | 0.13 | 4.0 | 1.4 | 0.7 | 15.6 | 2.0 | 0.0 | 0.0 | 0.0 | 0.0 | 0.1 | 10.2 |
| | | Min | 0.00 | 0.00 | 5.61 | 0.07 | 0.0 | 0.0 | 0.0 | 46.7 | 0.0 | 0.0 | 0.0 | 0.0 | 0.0 | 0.0 | 2.1 |
| | | Max | 0.19 | 0.00 | 11.74 | 0.44 | 12.1 | 4.2 | 1.9 | 97.8 | 5.0 | 0.0 | 0.0 | 0.0 | 0.0 | 0.4 | 34.3 |
| Wedelsandstein Fm. (10) | | Mean | 0.41 | 0.03 | 2.13 | 0.55 | 27.1 | 4.9 | 3.0 | 16.4 | 0.0 | 1.5 | 0.0 | 0.0 | 0.0 | 0.8 | 45.8 |
| | | Median | 0.38 | 0.04 | 1.72 | 0.54 | 26.9 | 5.0 | 3.0 | 12.7 | 0.0 | 0.9 | 0.0 | 0.0 | 0.0 | 0.7 | 49.7 |
| | | Stdev | 0.27 | 0.03 | 1.15 | 0.13 | 6.6 | 1.0 | 0.6 | 10.0 | 0.0 | 2.0 | 0.0 | 0.0 | 0.0 | 0.5 | 12.8 |
| | | Min | 0.00 | 0.00 | 0.78 | 0.28 | 18.2 | 2.6 | 2.4 | 6.5 | 0.0 | 0.0 | 0.0 | 0.0 | 0.0 | 0.0 | 24.8 |
| | | Max | 0.86 | 0.08 | 4.32 | 0.79 | 36.8 | 6.1 | 4.4 | 34.4 | 0.0 | 6.0 | 0.0 | 0.0 | 0.0 | 1.6 | 61.5 |

Tab. 4.2-1: (continued)

| **Formation** (number of analyses) | **Member** | | **S** [wt.-%] | **N** [wt.-%] | **C(inorg)** [wt.-%] | **C(org)** [wt.-%] | **Quartz** [wt.-%] | **K-feldspar** [wt.-%] | **Plagioclase** [wt.-%] | **Calcite** [wt.-%] | **Dolomite / Ank.** [wt.-%] | **Siderite** [wt.-%] | **Anhydrite** [wt.-%] | **Celestite** [wt.-%] | **Fluorite** [wt.-%] | **Pyrite** [wt.-%] | **Clay minerals** [wt.-%] |
|---|---|---|---|---|---|---|---|---|---|---|---|---|---|---|---|---|---|
| «Murchisonae-Oolith Fm.» (3) | | Mean | 0.45 | 0.00 | 1.12 | 0.46 | 42.1 | 4.3 | 2.2 | 8.7 | 0.0 | 0.7 | 0.0 | 0.0 | 0.0 | 0.8 | 40.7 |
| | | Median | 0.47 | 0.00 | 0.99 | 0.50 | 39.4 | 4.3 | 2.5 | 8.3 | 0.0 | 0.0 | 0.0 | 0.0 | 0.0 | 0.9 | 44.7 |
| | | Stdev | 0.04 | 0.00 | 0.26 | 0.09 | 21.1 | 0.2 | 0.5 | 1.1 | 0.0 | 1.3 | 0.0 | 0.0 | 0.0 | 0.1 | 18.8 |
| | | Min | 0.40 | 0.00 | 0.94 | 0.35 | 22.4 | 4.2 | 1.6 | 7.8 | 0.0 | 0.0 | 0.0 | 0.0 | 0.0 | 0.7 | 20.2 |
| | | Max | 0.47 | 0.00 | 1.42 | 0.52 | 64.4 | 4.5 | 2.5 | 9.9 | 0.0 | 2.2 | 0.0 | 0.0 | 0.0 | 0.9 | 57.2 |
| Opalinus Clay (27) | All | Mean | 0.59 | 0.04 | 1.42 | 0.99 | 21.6 | 4.1 | 2.7 | 8.4 | 0.0 | 4.0 | 0.0 | 0.0 | 0.0 | 1.1 | 57.1 |
| | | Median | 0.30 | 0.06 | 1.33 | 1.00 | 20.4 | 4.4 | 2.7 | 7.9 | 0.0 | 3.4 | 0.0 | 0.0 | 0.0 | 0.6 | 60.4 |
| | | Stdev | 0.77 | 0.03 | 0.50 | 0.13 | 5.6 | 1.2 | 0.5 | 3.9 | 0.0 | 2.8 | 0.0 | 0.0 | 0.0 | 1.4 | 8.2 |
| | | Min | 0.00 | 0.00 | 0.67 | 0.71 | 11.0 | 2.2 | 1.2 | 0.0 | 0.0 | 0.0 | 0.0 | 0.0 | 0.0 | 0.0 | 35.0 |
| | | Max | 3.32 | 0.08 | 3.19 | 1.30 | 31.9 | 5.8 | 3.7 | 17.0 | 0.0 | 11.1 | 0.0 | 0.0 | 0.0 | 6.2 | 69.8 |
| Opalinus Clay (5) | Sub-unit with silty calc. beds | Mean | 1.00 | 0.04 | 1.74 | 0.97 | 22.1 | 4.1 | 2.2 | 10.9 | 0.0 | 4.1 | 0.0 | 0.0 | 0.0 | 1.9 | 53.7 |
| | | Median | 0.47 | 0.05 | 1.53 | 1.02 | 18.5 | 3.9 | 2.3 | 11.3 | 0.0 | 2.4 | 0.0 | 0.0 | 0.0 | 0.9 | 58.0 |
| | | Stdev | 1.31 | 0.03 | 0.99 | 0.18 | 5.7 | 1.0 | 0.6 | 6.0 | 0.0 | 3.9 | 0.0 | 0.0 | 0.0 | 2.4 | 12.4 |
| | | Min | 0.25 | 0.00 | 0.67 | 0.71 | 17.8 | 2.7 | 1.2 | 3.0 | 0.0 | 1.8 | 0.0 | 0.0 | 0.0 | 0.5 | 35.0 |
| | | Max | 3.32 | 0.07 | 3.19 | 1.19 | 30.6 | 5.4 | 2.9 | 17.0 | 0.0 | 11.1 | 0.0 | 0.0 | 0.0 | 6.2 | 65.7 |
| Opalinus Clay (6) | Upper silty sub-unit | Mean | 0.63 | 0.02 | 1.44 | 0.98 | 27.8 | 3.4 | 2.6 | 9.9 | 0.0 | 2.4 | 0.0 | 0.0 | 0.0 | 1.2 | 51.7 |
| | | Median | 0.28 | 0.00 | 1.50 | 0.99 | 29.4 | 2.5 | 2.3 | 11.2 | 0.0 | 2.8 | 0.0 | 0.0 | 0.0 | 0.5 | 51.3 |
| | | Stdev | 0.97 | 0.03 | 0.43 | 0.16 | 4.5 | 1.6 | 0.7 | 3.6 | 0.0 | 1.2 | 0.0 | 0.0 | 0.0 | 1.8 | 8.0 |
| | | Min | 0.05 | 0.00 | 0.94 | 0.76 | 22.2 | 2.2 | 1.9 | 5.1 | 0.0 | 0.0 | 0.0 | 0.0 | 0.0 | 0.1 | 42.2 |
| | | Max | 2.61 | 0.06 | 1.90 | 1.18 | 31.9 | 5.5 | 3.7 | 13.2 | 0.0 | 3.3 | 0.0 | 0.0 | 0.0 | 4.9 | 63.9 |
| Opalinus Clay (13) | Mixed clay-silt-carbonate sub-unit | Mean | 0.41 | 0.05 | 1.33 | 1.01 | 20.5 | 4.3 | 2.9 | 6.7 | 0.0 | 5.0 | 0.0 | 0.0 | 0.0 | 0.8 | 58.8 |
| | | Median | 0.21 | 0.07 | 1.29 | 1.00 | 20.3 | 4.9 | 3.0 | 6.6 | 0.0 | 4.7 | 0.0 | 0.0 | 0.0 | 0.4 | 60.5 |
| | | Stdev | 0.44 | 0.03 | 0.26 | 0.11 | 3.0 | 1.2 | 0.4 | 2.9 | 0.0 | 2.6 | 0.0 | 0.0 | 0.0 | 0.8 | 4.7 |
| | | Min | 0.00 | 0.00 | 1.02 | 0.86 | 16.9 | 2.3 | 2.2 | 0.0 | 0.0 | 0.0 | 0.0 | 0.0 | 0.0 | 0.0 | 50.3 |
| | | Max | 1.28 | 0.07 | 1.99 | 1.30 | 25.4 | 5.8 | 3.3 | 11.7 | 0.0 | 10.5 | 0.0 | 0.0 | 0.0 | 2.4 | 63.8 |
| Opalinus Clay (3) | Clay-rich sub-unit | Mean | 0.64 | 0.07 | 1.28 | 0.97 | 13.1 | 4.7 | 2.7 | 8.7 | 0.0 | 2.3 | 0.0 | 0.0 | 0.0 | 1.2 | 66.3 |
| | | Median | 0.43 | 0.07 | 1.33 | 1.00 | 13.9 | 4.8 | 2.7 | 8.6 | 0.0 | 3.4 | 0.0 | 0.0 | 0.0 | 0.8 | 64.7 |
| | | Stdev | 0.38 | 0.01 | 0.24 | 0.14 | 1.9 | 0.4 | 0.2 | 0.6 | 0.0 | 2.0 | 0.0 | 0.0 | 0.0 | 0.7 | 3.1 |
| | | Min | 0.42 | 0.07 | 1.03 | 0.81 | 11.0 | 4.3 | 2.5 | 8.2 | 0.0 | 0.0 | 0.0 | 0.0 | 0.0 | 0.8 | 64.4 |
| | | Max | 1.08 | 0.08 | 1.49 | 1.09 | 14.5 | 5.0 | 2.8 | 9.3 | 0.0 | 3.7 | 0.0 | 0.0 | 0.0 | 2.0 | 69.8 |
| Staffelegg Fm. (10) | | Mean | 0.51 | 0.03 | 3.87 | 1.32 | 25.1 | 3.8 | 1.9 | 31.3 | 0.8 | 0.0 | 0.0 | 0.0 | 0.0 | 1.0 | 34.7 |
| | | Median | 0.36 | 0.00 | 1.62 | 0.64 | 25.9 | 3.4 | 2.4 | 12.1 | 0.0 | 0.0 | 0.0 | 0.0 | 0.0 | 0.7 | 34.6 |
| | | Stdev | 0.48 | 0.05 | 3.57 | 1.84 | 18.0 | 1.6 | 1.5 | 30.1 | 1.1 | 0.0 | 0.0 | 0.0 | 0.0 | 0.9 | 15.5 |
| | | Min | 0.03 | 0.00 | 0.94 | 0.27 | 3.8 | 2.0 | 0.0 | 5.9 | 0.0 | 0.0 | 0.0 | 0.0 | 0.0 | 0.1 | 13.2 |
| | | Max | 1.46 | 0.16 | 9.68 | 6.18 | 47.8 | 6.5 | 3.4 | 80.7 | 2.5 | 0.0 | 0.0 | 0.0 | 0.0 | 2.7 | 68.3 |

Tab. 4.2-1: (continued)

| **Formation** (number of analyses) | **Member** | | **S** [wt.-%] | **N** [wt.-%] | **C(inorg)** [wt.-%] | **C(org)** [wt.-%] | **Quartz** [wt.-%] | **K-feldspar** [wt.-%] | **Plagioclase** [wt.-%] | **Calcite** [wt.-%] | **Dolomite / Ank.** [wt.-%] | **Siderite** [wt.-%] | **Anhydrite** [wt.-%] | **Celestite** [wt.-%] | **Fluorite** [wt.-%] | **Pyrite** [wt.-%] | **Clay minerals** [wt.-%] |
|---|---|---|---|---|---|---|---|---|---|---|---|---|---|---|---|---|---|
| Klettgau Fm. (5) | | Mean | 0.34 | 0.01 | 5.76 | 0.10 | 11.9 | 5.7 | 4.4 | 4.4 | 40.2 | 0.0 | 0.0 | 0.0 | 0.0 | 0.6 | 32.7 |
| | | Median | 0.09 | 0.00 | 6.99 | 0.11 | 9.5 | 5.6 | 2.6 | 0.0 | 49.5 | 0.0 | 0.0 | 0.0 | 0.0 | 0.2 | 29.9 |
| | | Stdev | 0.49 | 0.02 | 3.60 | 0.06 | 6.6 | 1.8 | 3.4 | 6.0 | 27.6 | 0.0 | 0.0 | 0.0 | 0.0 | 0.9 | 17.3 |
| | | Min | 0.00 | 0.00 | 0.00 | 0.01 | 7.8 | 3.2 | 1.6 | 0.0 | 0.0 | 0.0 | 0.0 | 0.0 | 0.0 | 0.0 | 12.9 |
| | | Max | 1.14 | 0.04 | 9.32 | 0.17 | 23.5 | 8.1 | 9.9 | 11.7 | 71.5 | 0.0 | 0.0 | 0.0 | 0.0 | 2.1 | 58.5 |
| Bänker-joch Fm. (7) | | Mean | 11.73 | 0.00 | 1.42 | 0.27 | 6.3 | 2.8 | 0.7 | 3.1 | 8.1 | 0.0 | 49.5 | 0.4 | 0.0 | 0.0 | 28.9 |
| | | Median | 14.00 | 0.00 | 1.31 | 0.20 | 7.5 | 0.0 | 0.0 | 1.0 | 0.0 | 0.0 | 58.4 | 0.0 | 0.0 | 0.0 | 26.8 |
| | | Stdev | 8.56 | 0.00 | 1.23 | 0.21 | 4.7 | 3.8 | 1.2 | 4.2 | 11.2 | 0.0 | 36.4 | 0.7 | 0.0 | 0.1 | 22.5 |
| | | Min | 0.00 | 0.00 | 0.00 | 0.14 | 0.0 | 0.0 | 0.0 | 0.0 | 0.0 | 0.0 | 0.0 | 0.0 | 0.0 | 0.0 | 4.2 |
| | | Max | 21.00 | 0.00 | 3.59 | 0.73 | 12.6 | 8.7 | 2.6 | 10.9 | 27.5 | 0.0 | 89.4 | 1.4 | 0.0 | 0.2 | 65.6 |
| Schinz-nach Fm. (7) | All | Mean | 0.43 | 0.00 | 11.72 | 0.31 | 1.5 | 1.8 | 0.0 | 18.5 | 72.9 | 0.0 | 1.8 | 0.0 | 0.0 | 0.0 | 3.3 |
| | | Median | 0.41 | 0.00 | 11.80 | 0.30 | 1.6 | 1.8 | 0.0 | 0.4 | 90.2 | 0.0 | 1.7 | 0.0 | 0.0 | 0.0 | 2.5 |
| | | Stdev | 0.46 | 0.00 | 0.46 | 0.06 | 0.6 | 2.2 | 0.0 | 25.7 | 25.4 | 0.0 | 2.0 | 0.0 | 0.0 | 0.0 | 1.7 |
| | | Min | 0.00 | 0.00 | 10.82 | 0.25 | 0.7 | 0.0 | 0.0 | 0.0 | 35.0 | 0.0 | 0.0 | 0.0 | 0.0 | 0.0 | 1.8 |
| | | Max | 1.20 | 0.00 | 12.22 | 0.45 | 2.2 | 6.1 | 0.0 | 58.7 | 93.8 | 0.0 | 5.1 | 0.0 | 0.0 | 0.1 | 6.7 |
| Schinz-nach Fm. (3) | Stamberg Mb. | Mean | 0.74 | 0.00 | 12.07 | 0.35 | 0.9 | 0.7 | 0.0 | 0.0 | 92.6 | 0.0 | 3.1 | 0.0 | 0.0 | 0.0 | 2.3 |
| | | Median | 0.60 | 0.00 | 11.99 | 0.32 | 0.9 | 0.0 | 0.0 | 0.0 | 92.0 | 0.0 | 2.5 | 0.0 | 0.0 | 0.0 | 2.5 |
| | | Stdev | 0.41 | 0.00 | 0.14 | 0.09 | 0.3 | 1.3 | 0.0 | 0.0 | 1.0 | 0.0 | 1.8 | 0.0 | 0.0 | 0.0 | 0.4 |
| | | Min | 0.41 | 0.00 | 11.99 | 0.28 | 0.7 | 0.0 | 0.0 | 0.0 | 92.0 | 0.0 | 1.7 | 0.0 | 0.0 | 0.0 | 1.8 |
| | | Max | 1.20 | 0.00 | 12.22 | 0.45 | 1.3 | 2.2 | 0.0 | 0.0 | 93.8 | 0.0 | 5.1 | 0.0 | 0.0 | 0.0 | 2.5 |
| Schinz-nach Fm. (3) | Lied. + Leu-tschenb. + Kienb. Mb. | Mean | 0.01 | 0.00 | 11.34 | 0.30 | 1.9 | 2.6 | 0.0 | 43.0 | 47.4 | 0.0 | 0.0 | 0.0 | 0.0 | 0.0 | 4.7 |
| | | Median | 0.00 | 0.00 | 11.59 | 0.30 | 2.0 | 1.8 | 0.0 | 50.1 | 42.8 | 0.0 | 0.0 | 0.0 | 0.0 | 0.0 | 4.0 |
| | | Stdev | 0.02 | 0.00 | 0.45 | 0.01 | 0.3 | 3.1 | 0.0 | 20.1 | 15.2 | 0.0 | 0.0 | 0.0 | 0.0 | 0.0 | 1.8 |
| | | Min | 0.00 | 0.00 | 10.82 | 0.29 | 1.6 | 0.0 | 0.0 | 20.3 | 35.0 | 0.0 | 0.0 | 0.0 | 0.0 | 0.0 | 3.4 |
| | | Max | 0.04 | 0.00 | 11.61 | 0.32 | 2.2 | 6.1 | 0.0 | 58.7 | 64.3 | 0.0 | 0.0 | 0.0 | 0.0 | 0.1 | 6.7 |
| Zeglingen Fm. (1) | | Mean | 0.06 | 0.00 | 8.99 | 0.27 | 25.2 | 0.0 | 0.0 | 0.7 | 68.3 | 0.0 | 0.0 | 0.0 | 0.9 | 0.1 | 4.5 |

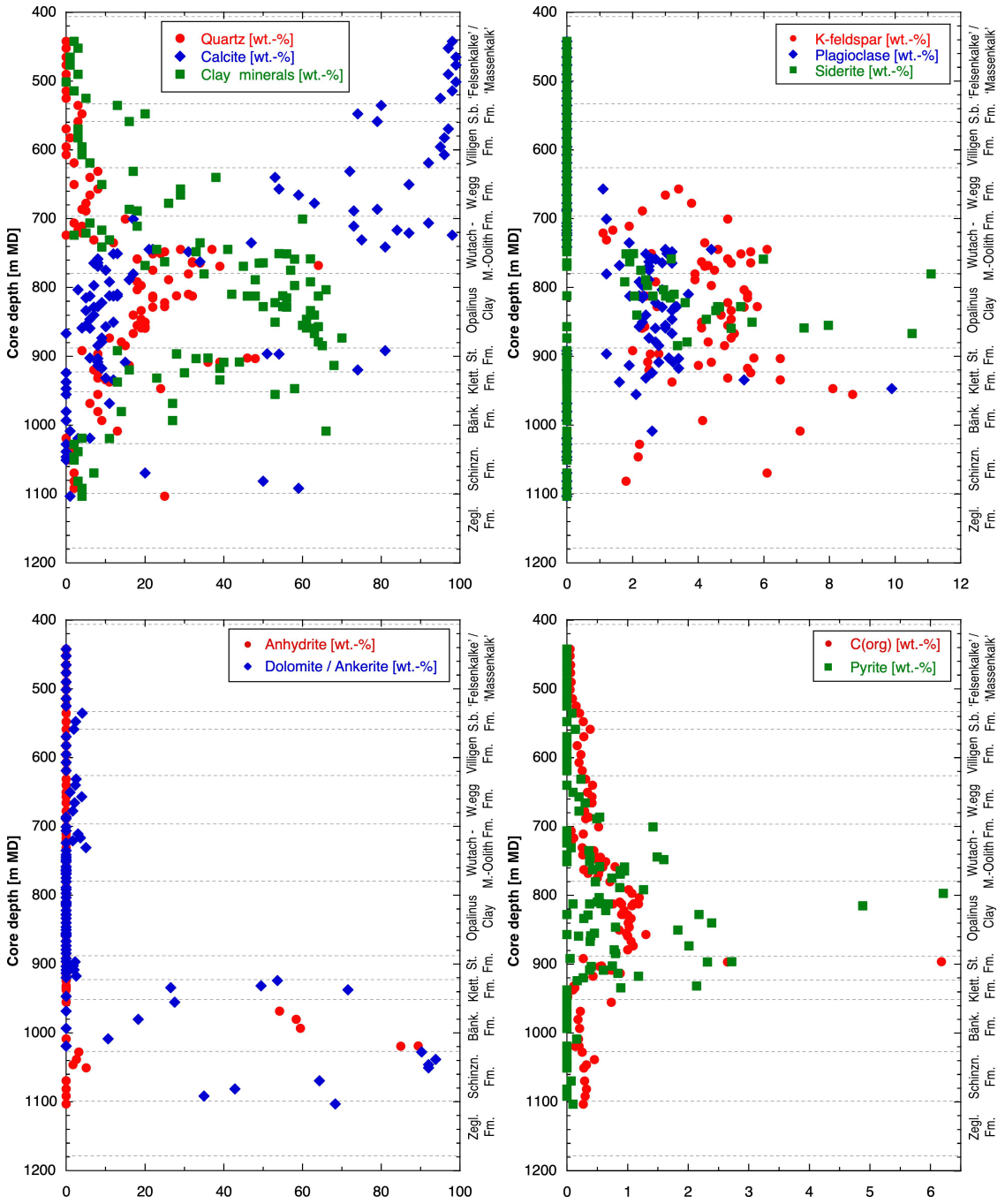


Fig. 4.2-1: Mineral contents in the bulk rock as a function of depth

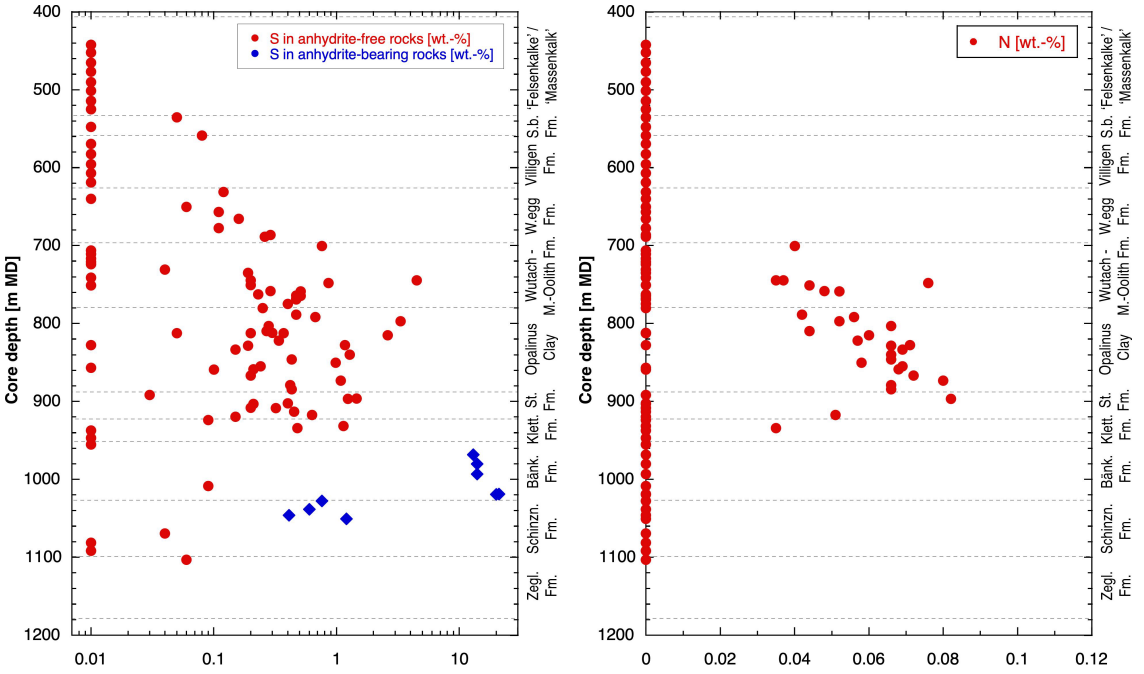


Fig. 4.2-2: Contents of S and N in the bulk rock as a function of depth

S contents below the detection limit of 0.05 wt.-% are represented by data points shown at 0.01 wt.-%. N contents below the detection limit of 0.01 wt.-% are represented by data points shown at 0 wt.-%.

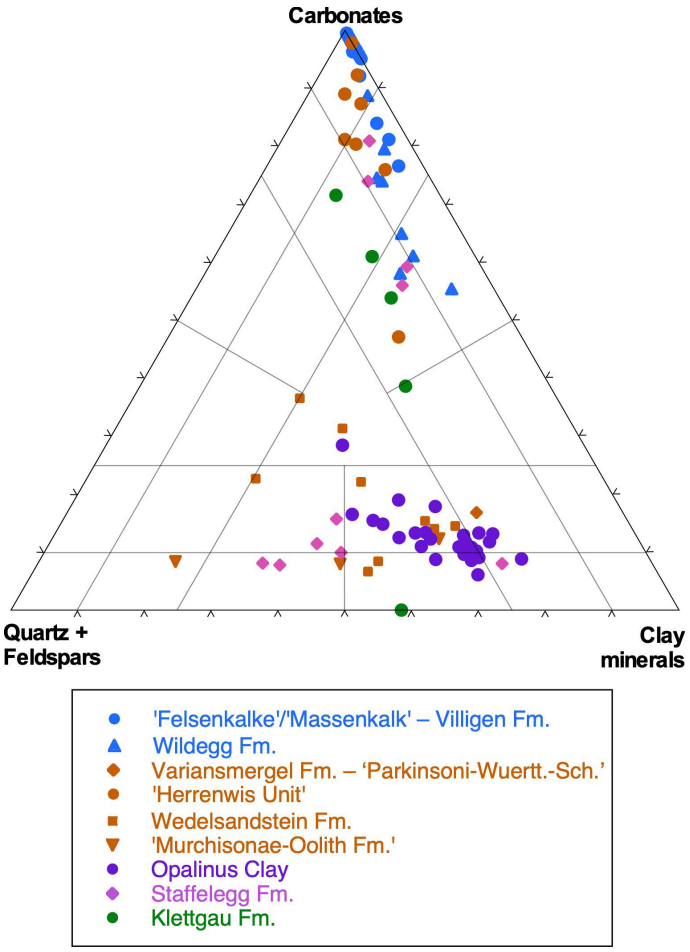


Fig. 4.2-3: Mineralogical composition of studied samples in the Füchtbauer triangle

Samples containing > 50% minerals other than those represented by the Füchtbauer triangle (which are clays, calcite, dolomite/ankerite, siderite, magnesite, quartz, K-feldspar, plagioclase) are excluded.

## A closer look at the section Staffelegg Formation – Opalinus Clay – «Brauner Dogger»

The graphs shown in Fig. 4.2-4 indicate systematic depth trends of the contents of quartz, clay minerals, calcite and C(org), whereas other minerals show no evident systematic variability.

### *Staffelegg Formation*

Lithological heterogeneity is a characteristic in the Staffelegg Formation, which, according to the Füchtbauer nomenclature, contains claystone, marl, limestone and sandstone/siltstone. Within the Frick Member (901.53 – 913.47 m), clay-mineral contents decrease sharply towards the top, while quartz contents (and therefore the quartz/clay ratio) increase. The decrease of clay minerals continues to the top of the Staffelegg Formation, while calcite contents become high. High contents of pyrite and C(org) are observed in some samples from the Rietheim Member (892.79 – 899.30 m).

### *Opalinus Clay*

Informal sub-units within the Opalinus Clay were defined by Mazurek & Aschwanden (2020) on a regional basis, and this scheme was successfully applied to several TBO boreholes. In borehole STA3-1, however, mineralogical trends are less well expressed, in particular when compared to the findings from the BUL1-1 profile (Mazurek et al. 2021). The subdivision of the 'Mixed clay-silt-carbonate sub-unit' in two sections with distinct trends is weakly defined. The 'Sub-unit with silty calcareous beds' at the top of the Opalinus Clay is the only one with clear trends, with increasing quartz and calcite and decreasing clay-mineral contents. Note that in the BUL1-1 profile, the same trends can be seen in the upper part of this sub-unit, while the lower part tends to indicate different trends. This sub-division is not evident in STA3-1.

Samples with high pyrite contents in the Opalinus Clay contain pyrite-rich concretions.

### *«Murchisonae-Oolith Formation»*

A distinct cycle of increasing quartz and decreasing clay-mineral and calcite contents is seen, resulting in a massive upward increase of the quartz/clay-mineral ratio.

### *Wedelsandstein Formation*

Clear trends of increasing quartz and calcite and decreasing clay minerals are found above about 760 m, whereas no systematic evolution is seen at the base of the formation.

### *Conclusion*

A number of mineralogical discontinuities and changes in depth trends were identified and generally correlate well with the lithostratigraphic subdivision defined in Dossier III.

Quartz, clay-mineral and calcite contents show the most pronounced trends and discontinuities in their depth profiles. In the Opalinus Clay, mineralogical trends are less well expressed than in other TBO boreholes.

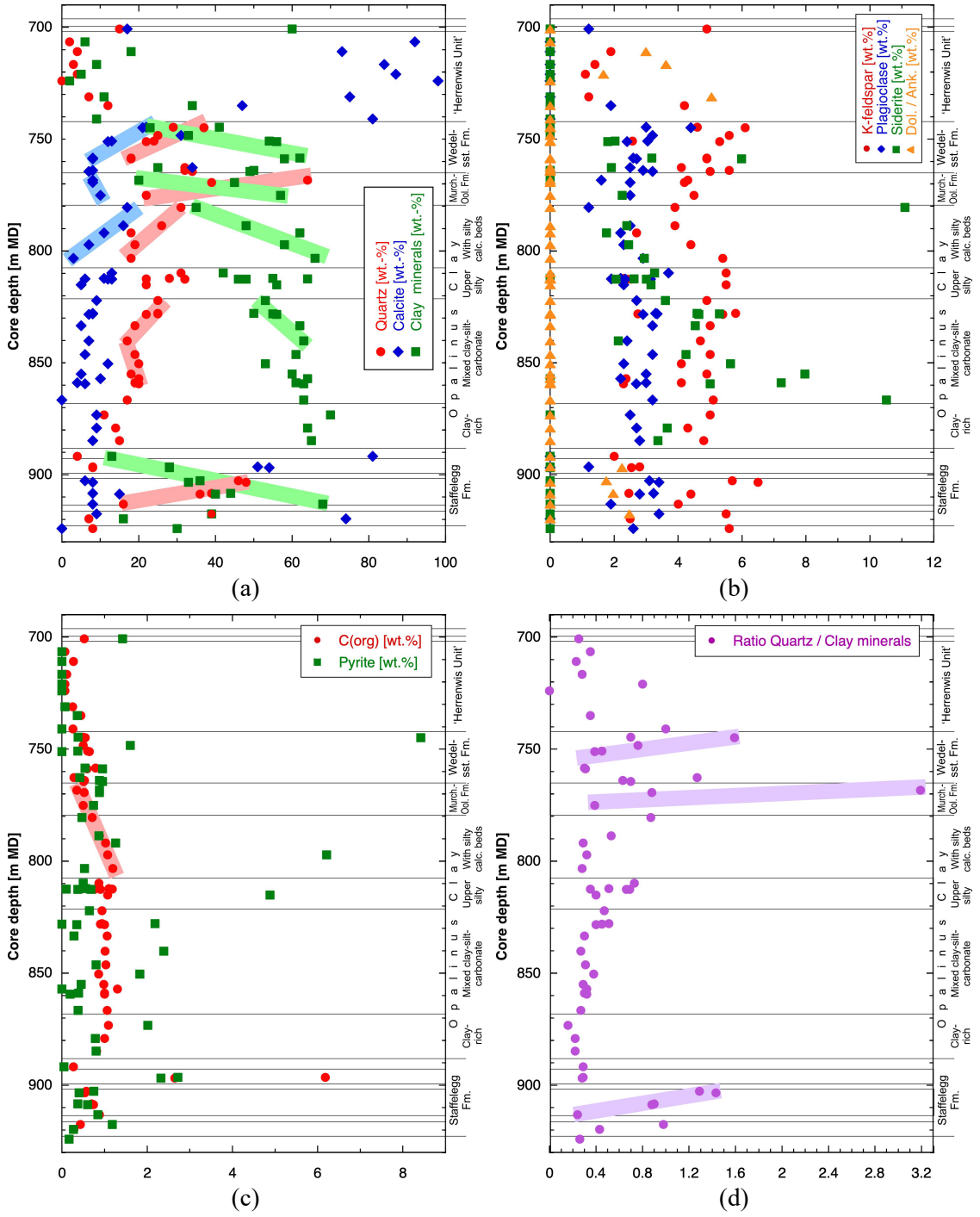


Fig. 4.2-4: Depth trends of mineral contents in the bulk rock in the Lias – Dogger interval

Coloured bars highlight systematic trends. Dolomite in sample 924.15 (54 wt.-%) is out of the range shown in (b).

### 4.2.2 Clay minerals

A total of 31 mineralogical analyses of the clay fraction were performed in the section Wildegg Formation – Klettgau Formation. The full dataset is documented in Appendix A. Tab. 4.2-2 provides formation-specific summaries, normalising the contents of individual clay phases to the sum of all clay minerals.

The identified clay-mineral species include illite, smectite, illite/smectite mixed layers, kaolinite, chlorite and chlorite/smectite mixed layers. The identification of chlorite/smectite mixed layers in all samples is in contrast with previous data from northern Switzerland where this mineral was rarely reported (Mazurek 2017). However, this is not a real difference but due to the improved methodology of the evaluation of X-ray patterns that was applied for the TBO campaign (details in Waber ed. 2020). Because the chlorite/smectite mixed-layer phase contains 85 – 95% chlorite layers, its XRD reflections are close to those of pure chlorite. The new methodology also allows to better resolve the fraction of smectite layers in the illite/smectite mixed-layer phase. As seen in Tab. 4.2-2, illite-rich mixed layers dominate, but minor amounts of illite-poorer mixed layers also occur. Given the fact that the contents of mixed-layer phases and the smectite fractions in these are known, the end-member compositions of illite, smectite, chlorite and kaolinite (whether in mixed layers or as a discrete phase) can be calculated and are also listed in Tab. 4.2-2.

Depth trends of the relative proportions of clay minerals are shown graphically in Fig. 4.2-5 for individual clay phases (a) and end-member clays (b). The depth plot of the latter is less noisy than that of the individual clay minerals. Smectite as a discrete phase occurs only infrequently (e.g. in the «Herrenwis Unit») and is quantitatively subordinate. Most smectite is found in illite/smectite mixed-layer minerals. Variability of the smectite end-member is limited, with highest proportions in the uppermost part of the Wedelsandstein Formation and in the «Herrenwis Unit», as well as in the Klettgau and Staffelegg Formations. Chlorite also varies only weakly. In contrast, the relative proportions of the two main end-member clays, namely illite and kaolinite, vary substantially over the profile (Figs. 4.2-5 and 4.2-6). The Klettgau Formation is characterised by the dominance of the illite end member, while the proportions of kaolinite are low (illite/kaolinite ratios are in the range 21 – 61). The overlying Dogger – Lias interval will be explored in more detail below.

Tab. 4.2-2: Mineralogical composition of the clay fraction: formation-specific means, medians, standard deviations and ranges

[a] VPW = Variansmergel Formation + «Parkinsoni-Württembergica-Schichten».

| **Formation** (number of analyses) | **Mem-ber** | | **Individual clay phases** [wt.-% of clay fraction] | | | | | | | | | | **End-member clays** [wt.-% of clay fraction] | | | |
|---|---|---|---|---|---|---|---|---|---|---|---|---|---|---|---|---|
| | | | **Illite** | **Ill/Sm ML (85-90)** | **Ill/Sm ML (75-80)** | **Ill/Sm ML (50-70)** | **Ill/Sm ML (20-40)** | **Total Ill/Sm** | **Smectite** | **Kaolinite** | **Chlorite** | **Chl/Sm ML (85-95)** | **Illite** | **Smectite** | **Kaolinite** | **Chlorite** |
| Wildegg Fm. (1) | | Mean | 23.1 | 12.7 | 17.6 | 0.0 | 0.0 | 30.3 | 0.0 | 33.0 | 4.8 | 8.6 | 48.1 | 6.3 | 33.0 | 12.6 |
| VPW [a] (1) | | Mean | 38.5 | 1.5 | 24.3 | 2.3 | 0.2 | 28.3 | 0.0 | 24.2 | 2.5 | 6.5 | 60.7 | 6.9 | 24.2 | 8.2 |
| «Herrenwis Unit» (4) | | Mean | 48.8 | 11.0 | 20.4 | 6.8 | 0.0 | 38.2 | 0.9 | 2.8 | 3.1 | 6.3 | 78.1 | 10.3 | 2.8 | 8.8 |
| | | Median | 48.3 | 8.8 | 12.8 | 6.5 | 0.0 | 40.5 | 1.0 | 1.5 | 2.6 | 7.5 | 78.8 | 10.5 | 1.5 | 9.2 |
| | | Stdev | 14.6 | 13.2 | 21.0 | 7.0 | 0.0 | 13.0 | 0.6 | 3.6 | 1.6 | 3.1 | 4.1 | 2.4 | 3.6 | 1.3 |
| | | Min | 33.0 | 0.0 | 5.5 | 0.0 | 0.0 | 21.5 | 0.1 | 0.2 | 1.8 | 1.7 | 73.1 | 7.5 | 0.2 | 6.9 |
| | | Max | 65.7 | 26.5 | 50.3 | 14.3 | 0.0 | 50.3 | 1.5 | 8.2 | 5.3 | 8.5 | 81.9 | 12.6 | 8.2 | 9.9 |
| Wedelsandstein Fm. (5) | | Mean | 30.0 | 9.4 | 25.3 | 3.4 | 0.1 | 38.2 | 0.0 | 20.3 | 2.8 | 7.5 | 60.3 | 10.0 | 20.3 | 9.5 |
| | | Median | 29.0 | 6.1 | 27.1 | 2.7 | 0.0 | 39.5 | 0.0 | 23.7 | 3.0 | 6.7 | 60.7 | 9.0 | 23.7 | 9.2 |
| | | Stdev | 3.2 | 7.1 | 10.3 | 3.7 | 0.3 | 8.0 | 0.0 | 12.0 | 0.9 | 2.7 | 7.7 | 4.6 | 12.0 | 2.6 |
| | | Min | 26.9 | 2.1 | 11.1 | 0.0 | 0.0 | 27.8 | 0.0 | 0.8 | 1.9 | 4.9 | 50.0 | 6.4 | 0.8 | 6.7 |
| | | Max | 34.5 | 19.5 | 36.0 | 9.3 | 0.7 | 48.5 | 0.0 | 31.2 | 4.0 | 11.2 | 69.5 | 17.8 | 31.2 | 12.4 |
| «Murchisonae-Oolith Fm.» (2) | | Mean | 27.0 | 8.0 | 18.9 | 0.0 | 0.0 | 26.9 | 0.0 | 34.2 | 3.5 | 8.5 | 48.7 | 6.0 | 34.2 | 11.2 |
| | | Median | 27.0 | 8.0 | 18.9 | 0.0 | 0.0 | 26.9 | 0.0 | 34.2 | 3.5 | 8.5 | 48.7 | 6.0 | 34.2 | 11.2 |
| | | Stdev | 6.4 | 11.2 | 5.1 | 0.0 | 0.0 | 6.2 | 0.0 | 0.1 | 0.7 | 0.6 | 0.6 | 0.3 | 0.1 | 0.2 |
| | | Min | 22.4 | 0.0 | 15.3 | 0.0 | 0.0 | 22.5 | 0.0 | 34.1 | 3.0 | 8.0 | 48.2 | 5.8 | 34.1 | 11.0 |
| | | Max | 31.5 | 15.9 | 22.5 | 0.0 | 0.0 | 31.2 | 0.0 | 34.3 | 4.0 | 8.9 | 49.1 | 6.2 | 34.3 | 11.3 |
| Opalinus Clay (10) | All | Mean | 28.4 | 6.3 | 15.4 | 2.1 | 0.0 | 23.7 | 0.2 | 36.0 | 2.4 | 9.3 | 46.9 | 6.3 | 36.0 | 10.8 |
| | | Median | 28.7 | 4.6 | 18.6 | 0.6 | 0.0 | 22.0 | 0.0 | 36.5 | 2.5 | 9.0 | 46.1 | 5.9 | 36.5 | 10.8 |
| | | Stdev | 3.1 | 7.4 | 8.5 | 4.4 | 0.0 | 5.2 | 0.5 | 3.4 | 1.0 | 2.0 | 3.2 | 1.5 | 3.4 | 0.9 |
| | | Min | 23.3 | 0.0 | 2.7 | 0.0 | 0.0 | 17.1 | 0.0 | 28.8 | 0.0 | 6.9 | 43.7 | 5.1 | 28.8 | 9.6 |
| | | Max | 33.4 | 22.5 | 26.7 | 14.4 | 0.0 | 32.2 | 1.5 | 40.1 | 3.9 | 14.4 | 54.1 | 10.1 | 40.1 | 12.6 |
| Opalinus Clay (2) | Sub-unit with silty calcareous beds | Mean | 29.3 | 2.6 | 23.5 | 0.6 | 0.0 | 26.6 | 0.0 | 32.6 | 3.2 | 8.5 | 50.2 | 6.5 | 32.6 | 10.8 |
| | | Median | 29.3 | 2.6 | 23.5 | 0.6 | 0.0 | 26.6 | 0.0 | 32.6 | 3.2 | 8.5 | 50.2 | 6.5 | 32.6 | 10.8 |
| | | Stdev | 0.9 | 3.6 | 4.6 | 0.8 | 0.0 | 7.4 | 0.0 | 5.3 | 1.0 | 2.2 | 5.5 | 0.8 | 5.3 | 1.0 |
| | | Min | 28.6 | 0.0 | 20.2 | 0.0 | 0.0 | 21.3 | 0.0 | 28.8 | 2.5 | 6.9 | 46.3 | 5.9 | 28.8 | 10.1 |
| | | Max | 29.9 | 5.1 | 26.7 | 1.1 | 0.0 | 31.8 | 0.0 | 36.3 | 3.9 | 10.0 | 54.1 | 7.0 | 36.3 | 11.5 |
| Opalinus Clay (1) | Upper silty | Mean | 23.9 | 11.0 | 21.2 | 0.0 | 0.0 | 32.2 | 0.0 | 33.6 | 2.1 | 8.1 | 49.9 | 6.9 | 33.6 | 9.6 |

Tab. 4.2-2: (continued)

| **Formation** (number of analyses) | **Mem-ber** | | **Individual clay phases** [wt.-% of clay fraction] | | | | | | | | | | **End-member clays** [wt.-% of clay fraction] | | | |
|---|---|---|---|---|---|---|---|---|---|---|---|---|---|---|---|---|
| | | | **Illite** | **Ill/Sm ML (85-90)** | **Ill/Sm ML (75-80)** | **Ill/Sm ML (50-70)** | **Ill/Sm ML (20-40)** | **Total Ill/Sm** | **Smectite** | **Kaolinite** | **Chlorite** | **Chl/Sm ML (85-95)** | **Illite** | **Smectite** | **Kaolinite** | **Chlorite** |
| Opalinus Clay (6) | Mixed clay-silt-carbonate sub-unit | Mean | 28.7 | 7.8 | 10.8 | 3.3 | 0.0 | 21.9 | 0.3 | 37.3 | 2.1 | 9.9 | 45.5 | 6.3 | 37.3 | 10.9 |
| | | Median | 28.6 | 5.6 | 9.8 | 1.3 | 0.0 | 21.9 | 0.0 | 37.7 | 2.4 | 9.3 | 45.0 | 5.6 | 37.7 | 10.8 |
| | | Stdev | 3.5 | 8.7 | 7.8 | 5.5 | 0.0 | 3.7 | 0.6 | 2.5 | 1.0 | 2.3 | 1.9 | 1.9 | 2.5 | 0.9 |
| | | Min | 23.3 | 0.0 | 2.7 | 0.0 | 0.0 | 17.1 | 0.0 | 33.6 | 0.0 | 8.2 | 43.7 | 5.1 | 33.6 | 9.9 |
| | | Max | 33.4 | 22.5 | 22.6 | 14.4 | 0.0 | 28.2 | 1.5 | 40.1 | 2.9 | 14.4 | 48.9 | 10.1 | 40.1 | 12.6 |
| Opalinus Clay (1) | Clay-rich | Mean | 29.4 | 0.0 | 21.0 | 0.0 | 0.0 | 21.0 | 0.0 | 37.9 | 3.0 | 8.7 | 45.9 | 5.4 | 37.9 | 10.9 |
| Staffelegg Fm. (5) | | Mean | 32.8 | 10.9 | 16.2 | 6.0 | 0.0 | 33.1 | 0.3 | 20.2 | 3.0 | 10.5 | 58.5 | 8.7 | 20.2 | 12.6 |
| | | Median | 30.3 | 13.5 | 9.2 | 4.3 | 0.0 | 32.0 | 0.0 | 16.2 | 2.6 | 9.2 | 58.0 | 7.0 | 16.2 | 12.4 |
| | | Stdev | 11.9 | 10.4 | 20.0 | 6.2 | 0.0 | 12.7 | 0.5 | 5.9 | 1.4 | 2.7 | 4.4 | 2.7 | 5.9 | 2.0 |
| | | Min | 21.2 | 0.0 | 0.0 | 0.0 | 0.0 | 16.1 | 0.0 | 15.6 | 1.5 | 8.0 | 53.7 | 6.3 | 15.6 | 9.7 |
| | | Max | 52.9 | 21.1 | 51.0 | 16.2 | 0.0 | 51.0 | 1.1 | 27.7 | 5.0 | 14.6 | 63.8 | 12.1 | 27.7 | 15.3 |
| Klettgau Fm. (3) | | Mean | 39.7 | 26.0 | 16.1 | 7.7 | 0.0 | 49.8 | 0.5 | 2.5 | 0.5 | 6.9 | 79.6 | 11.1 | 2.5 | 6.7 |
| | | Median | 40.2 | 28.5 | 11.5 | 11.5 | 0.0 | 49.6 | 0.5 | 2.3 | 0.3 | 6.5 | 79.4 | 13.3 | 2.3 | 6.9 |
| | | Stdev | 2.5 | 23.4 | 18.8 | 6.7 | 0.0 | 1.8 | 0.6 | 1.4 | 0.7 | 0.9 | 2.3 | 3.8 | 1.4 | 0.7 |
| | | Min | 37.0 | 1.4 | 0.0 | 0.0 | 0.0 | 48.0 | 0.0 | 1.3 | 0.0 | 6.4 | 77.4 | 6.8 | 1.3 | 6.0 |
| | | Max | 42.0 | 48.0 | 36.7 | 11.6 | 0.0 | 51.7 | 1.1 | 4.0 | 1.3 | 7.9 | 81.9 | 13.3 | 4.0 | 7.3 |

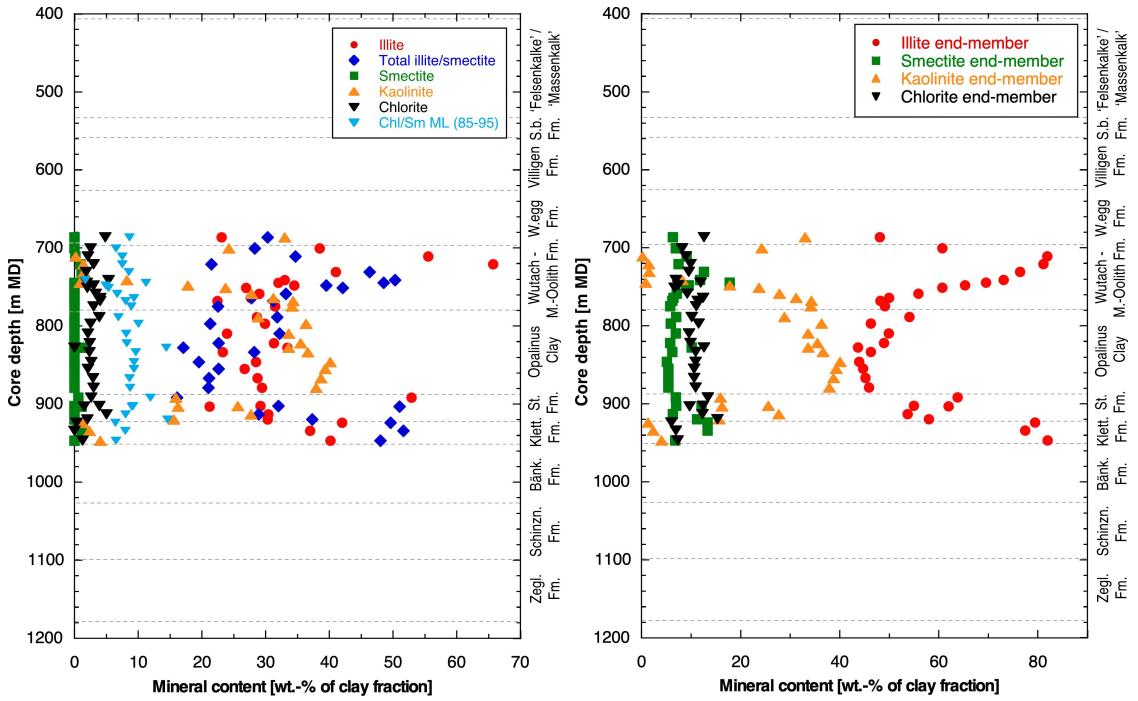


Fig. 4.2-5: Mineralogical composition of the clay fraction as a function of depth; (a) individual clay minerals, (b) end-member clays

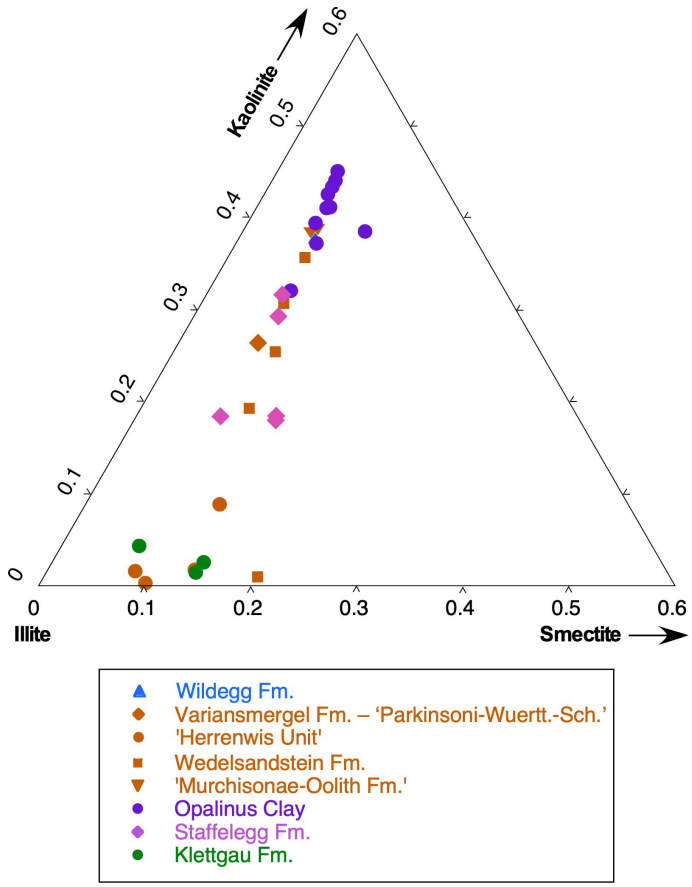


Fig. 4.2-6: Relative mass proportions of illite, smectite and kaolinite end-member clays

## A closer look at the section Staffelegg Formation – Opalinus Clay – «Brauner Dogger»

The composition of the clay fraction in this interval shows some distinct depth trends (Figs. 4.2-7 and 4.2-8). The ratio illite to kaolinite end member is low and remarkably constant in the Opalinus Clay and in the «Murchisonae-Oolith Formation» when compared to the underlying Staffelegg Formation. The Wedelsandstein Formation is characterised by a distinct trend of upwards decreasing kaolinite and increasing illite fractions. In the «Herrenwis Unit», the illite end-member keeps increasing, whereas kaolinite contents are close to 0 throughout this unit. These trends are similar to those observed in the BUL1-1 core.

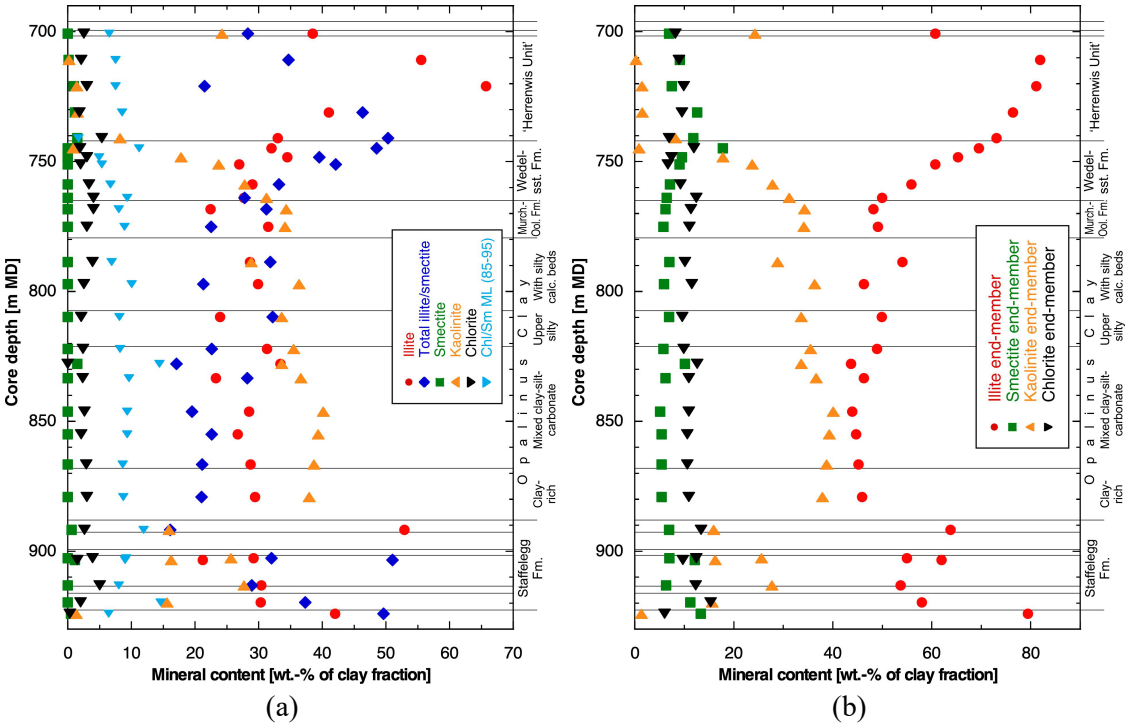


Fig. 4.2-7: Mineralogical composition of the clay fraction as a function of depth in the Lias – Dogger interval; (a) individual clay minerals, (b) end-member clays

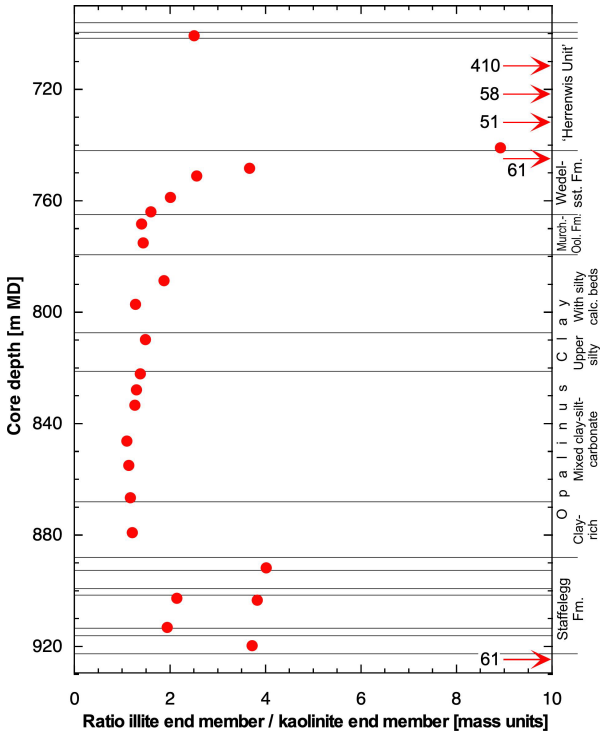


Fig. 4.2-8: Ratio of the illite to kaolinite end-member clays as a function of depth

Arrows indicate values outside the plotted range.

## 4.3 Petrophysical parameters

*Martin Mazurek & Lukas Aschwanden*

All petrophysical measurements were performed at the University of Bern, and the acquired parameters are listed in Tab. 4.3-1. The formalisms to calculate additional parameters from measured data (such as porosity) are detailed in Waber (ed.) (2020). Formation-specific statistical data are summarised in Tab. 4.3-2, and the full dataset is documented in Appendix A. In cases where gravimetric water content was available but density data were missing, water-loss porosity was calculated assuming a grain density of 2.7 g/cm$^3$. The uncertainty related to this assumption is small.

Tab. 4.3-1: Analytical programme for petrophysical measurements

| | **Number of samples** |
|---|---|
| Bulk wet density | 114 |
| Grain density | 92 |
| Gravimetric water content | 118 |
| Water content from isotope mass balance | 97 |
| $N_2$ adsorption<br>(BET external surface + full isotherm) | 7 |

Tab. 4.3-2: Summary of measured and calculated petrophysical data

Listed water contents (wet) are averages of measurements performed on typically 3 sub-samples. n = number of samples per geological unit.

| Formation | Member / Sub-unit | | Bulk wet density [g/cm³] | Bulk dry density, calculated [g/cm³] | Grain density [g/cm³] | Pycnometer porosity [–] | Gravimetry: Water content (wet) (105 °C) [wt.-%] | Gravimetry: Water content (dry) (105 °C) [wt.-%] | Gravimetry: Water-loss porosity using bulk wet density [–] | Gravimetry: Water-loss porosity using grain density [–] | Isotope mass balance: Water content (wet) based on isotope diff. exch. [wt.-%] | Isotope mass balance: Porosity based on isotope diff. exch. using bulk wet density [–] | Isotope mass balance: Porosity based on isotope diff. exch. using grain density [–] | External surface area (BET) [m²/g dry rock] |
|---|---|---|---|---|---|---|---|---|---|---|---|---|---|---|
| «Felsen-kalke» / «Massen-kalk» | | Mean | 2.683 | 2.675 | 2.714 | 0.015 | 0.315 | 0.316 | 0.008 | 0.008 | 0.353 | 0.009 | 0.009 | |
| | | Median | 2.686 | 2.676 | 2.714 | 0.015 | 0.286 | 0.287 | 0.008 | 0.008 | 0.302 | 0.008 | 0.008 | |
| | | Stdev | 0.011 | 0.014 | 0.004 | 0.005 | 0.170 | 0.171 | 0.005 | 0.005 | 0.202 | 0.005 | 0.005 | |
| | | Min | 2.664 | 2.646 | 2.710 | 0.009 | 0.148 | 0.148 | 0.004 | 0.004 | 0.173 | 0.005 | 0.005 | |
| | | Max | 2.696 | 2.691 | 2.722 | 0.024 | 0.665 | 0.669 | 0.018 | 0.018 | 0.778 | 0.021 | 0.021 | |
| | | n | 8 | 8 | 8 | 8 | 8 | 8 | 8 | 8 | 7 | 7 | 7 | 0 |
| Schwarz-bach Fm. | All | Mean | 2.647 | 2.595 | 2.713 | 0.044 | 1.957 | 1.999 | 0.052 | 0.051 | 2.357 | 0.062 | 0.061 | |
| | | Median | 2.647 | 2.595 | 2.713 | 0.044 | 1.957 | 1.999 | 0.052 | 0.051 | 2.357 | 0.062 | 0.061 | |
| | | Stdev | 0.057 | 0.074 | 0.010 | 0.024 | 0.678 | 0.706 | 0.017 | 0.017 | 0.597 | 0.014 | 0.015 | |
| | | Min | 2.606 | 2.542 | 2.706 | 0.027 | 1.478 | 1.500 | 0.040 | 0.039 | 1.935 | 0.052 | 0.051 | |
| | | Max | 2.687 | 2.647 | 2.721 | 0.061 | 2.437 | 2.498 | 0.064 | 0.063 | 2.779 | 0.072 | 0.072 | |
| | | n | 2 | 2 | 2 | 2 | 2 | 2 | 2 | 2 | 2 | 2 | 2 | 0 |
| Villigen Fm. | | Mean | 2.661 | 2.635 | 2.708 | 0.027 | 0.985 | 0.997 | 0.026 | 0.026 | 1.131 | 0.030 | 0.030 | |
| | | Median | 2.667 | 2.647 | 2.707 | 0.022 | 0.761 | 0.767 | 0.020 | 0.020 | 0.849 | 0.023 | 0.023 | |
| | | Stdev | 0.023 | 0.038 | 0.006 | 0.013 | 0.570 | 0.584 | 0.015 | 0.015 | 0.689 | 0.018 | 0.018 | |
| | | Min | 2.627 | 2.577 | 2.702 | 0.015 | 0.508 | 0.511 | 0.014 | 0.014 | 0.586 | 0.016 | 0.016 | |
| | | Max | 2.682 | 2.667 | 2.716 | 0.046 | 1.902 | 1.939 | 0.050 | 0.050 | 2.298 | 0.060 | 0.060 | |
| | | n | 6 | 6 | 6 | 6 | 6 | 6 | 6 | 6 | 6 | 6 | 6 | 0 |
| Wildegg Fm. | | Mean | 2.614 | 2.546 | 2.711 | 0.061 | 2.593 | 2.668 | 0.068 | 0.067 | 3.280 | 0.085 | 0.084 | 8.78 |
| | | Median | 2.610 | 2.538 | 2.711 | 0.063 | 2.752 | 2.832 | 0.072 | 0.071 | 3.657 | 0.095 | 0.093 | 8.78 |
| | | Stdev | 0.029 | 0.049 | 0.002 | 0.018 | 0.811 | 0.853 | 0.021 | 0.020 | 0.717 | 0.018 | 0.018 | 3.71 |
| | | Min | 2.575 | 2.489 | 2.707 | 0.032 | 1.350 | 1.368 | 0.036 | 0.036 | 2.345 | 0.062 | 0.061 | 6.16 |
| | | Max | 2.658 | 2.622 | 2.714 | 0.082 | 3.382 | 3.500 | 0.088 | 0.087 | 3.863 | 0.100 | 0.098 | 11.40 |
| | | n | 8 | 8 | 8 | 8 | 8 | 8 | 8 | 8 | 6 | 6 | 6 | 2 |
| Variansmergel Fm. + «Park.-Württ.-Sch.» | | Mean | 2.495 | 2.343 | 2.716 | 0.137 | 6.092 | 6.488 | 0.152 | 0.150 | 7.128 | 0.178 | 0.172 | |
| | | n | 1 | 1 | 1 | 1 | 1 | 1 | 1 | 1 | 1 | 1 | 1 | 0 |
| «Herrenwis Unit» | | Mean | 2.647 | 2.595 | 2.717 | 0.051 | 2.005 | 2.081 | 0.052 | 0.051 | 2.076 | 0.054 | 0.053 | |
| | | Median | 2.663 | 2.631 | 2.717 | 0.033 | 1.271 | 1.288 | 0.034 | 0.034 | 1.164 | 0.031 | 0.031 | |
| | | Stdev | 0.070 | 0.109 | 0.004 | 0.043 | 1.876 | 2.001 | 0.048 | 0.046 | 2.150 | 0.054 | 0.052 | |
| | | Min | 2.440 | 2.305 | 2.710 | 0.019 | 0.496 | 0.498 | 0.013 | 0.013 | 0.393 | 0.011 | 0.011 | |
| | | Max | 2.703 | 2.683 | 2.722 | 0.152 | 5.707 | 6.052 | 0.151 | 0.140 | 7.009 | 0.171 | 0.170 | |
| | | n | 12 | 12 | 8 | 8 | 12 | 12 | 12 | 12 | 12 | 12 | 12 | 0 |
| Wedel-sandstein Fm. | | Mean | 2.516 | 2.394 | 2.710 | 0.118 | 4.881 | 5.135 | 0.122 | 0.121 | 5.643 | 0.142 | 0.139 | 35.02 |
| | | Median | 2.516 | 2.383 | 2.711 | 0.121 | 4.899 | 5.152 | 0.121 | 0.120 | 5.800 | 0.145 | 0.142 | 35.02 |
| | | Stdev | 0.020 | 0.033 | 0.015 | 0.014 | 0.614 | 0.677 | 0.015 | 0.015 | 0.737 | 0.018 | 0.017 | 4.83 |
| | | Min | 2.490 | 2.348 | 2.692 | 0.102 | 3.621 | 3.757 | 0.093 | 0.092 | 4.841 | 0.122 | 0.121 | 31.61 |
| | | Max | 2.557 | 2.464 | 2.738 | 0.137 | 5.686 | 6.029 | 0.142 | 0.140 | 6.480 | 0.163 | 0.158 | 38.43 |
| | | n | 13 | 13 | 7 | 7 | 14 | 14 | 13 | 13 | 7 | 7 | 7 | 2 |
| «Murchi-sonae-Oolith Fm.» | | Mean | 2.495 | 2.375 | 2.685 | 0.115 | 4.794 | 5.039 | 0.120 | 0.119 | 5.529 | 0.138 | 0.136 | 13.67 |
| | | Median | 2.501 | 2.372 | 2.682 | 0.123 | 4.695 | 4.926 | 0.117 | 0.117 | 5.658 | 0.142 | 0.139 | |
| | | Stdev | 0.029 | 0.031 | 0.016 | 0.016 | 0.678 | 0.751 | 0.017 | 0.016 | 0.918 | 0.023 | 0.021 | |
| | | Min | 2.446 | 2.335 | 2.672 | 0.096 | 4.039 | 4.209 | 0.102 | 0.101 | 4.416 | 0.112 | 0.110 | |
| | | Max | 2.526 | 2.424 | 2.703 | 0.126 | 5.912 | 6.283 | 0.148 | 0.145 | 6.710 | 0.168 | 0.163 | |
| | | n | 6 | 6 | 3 | 3 | 6 | 6 | 6 | 6 | 5 | 5 | 5 | 1 |

Tab. 4.3-2: (continued)

| Formation | Member / Sub-unit | | Bulk wet density [g/cm³] | Bulk dry density, calculated [g/cm³] | Grain density [g/cm³] | Pycnometer porosity [–] | Gravimetry: Water content (wet) (105 °C) [wt.-%] | Gravimetry: Water content (dry) (105 °C) [wt.-%] | Gravimetry: Water-loss porosity using bulk wet density [–] | Gravimetry: Water-loss porosity using grain density [–] | Isotope mass balance: Water content (wet) based on isotope diff. exch. [wt.-%] | Isotope mass balance: Porosity based on isotope diff. exch. using bulk wet density [–] | Isotope mass balance: Porosity based on isotope diff. exch. using grain density [–] | External surface area (BET) [m²/g dry rock] |
|---|---|---|---|---|---|---|---|---|---|---|---|---|---|---|
| Opalinus Clay | All | Mean | 2.527 | 2.413 | 2.711 | 0.110 | 4.513 | 4.728 | 0.114 | 0.113 | 4.942 | 0.125 | 0.123 | |
| | | Median | 2.524 | 2.414 | 2.699 | 0.110 | 4.564 | 4.782 | 0.115 | 0.114 | 5.020 | 0.127 | 0.125 | |
| | | Stdev | 0.019 | 0.026 | 0.024 | 0.011 | 0.395 | 0.432 | 0.010 | 0.009 | 0.539 | 0.013 | 0.012 | |
| | | Min | 2.490 | 2.368 | 2.684 | 0.083 | 3.527 | 3.656 | 0.089 | 0.092 | 3.523 | 0.089 | 0.092 | |
| | | Max | 2.561 | 2.464 | 2.766 | 0.132 | 5.055 | 5.325 | 0.126 | 0.126 | 5.705 | 0.143 | 0.140 | |
| | | n | 21 | 21 | 21 | 21 | 23 | 23 | 21 | 21 | 19 | 19 | 19 | 0 |
| Opalinus Clay | Sub-unit with silty calc. beds | Mean | 2.512 | 2.399 | 2.720 | 0.118 | 4.501 | 4.717 | 0.113 | 0.113 | 4.956 | 0.124 | 0.124 | |
| | | Median | 2.506 | 2.384 | 2.699 | 0.120 | 4.858 | 5.106 | 0.122 | 0.122 | 5.456 | 0.137 | 0.137 | |
| | | Stdev | 0.019 | 0.033 | 0.033 | 0.012 | 0.643 | 0.702 | 0.015 | 0.015 | 0.919 | 0.022 | 0.021 | |
| | | Min | 2.490 | 2.368 | 2.695 | 0.098 | 3.527 | 3.656 | 0.089 | 0.092 | 3.523 | 0.089 | 0.092 | |
| | | Max | 2.536 | 2.438 | 2.766 | 0.132 | 5.055 | 5.325 | 0.126 | 0.126 | 5.705 | 0.143 | 0.140 | |
| | | n | 5 | 5 | 5 | 5 | 5 | 5 | 5 | 5 | 5 | 5 | 5 | 0 |
| Opalinus Clay | Upper silty sub-unit | Mean | 2.547 | 2.444 | 2.721 | 0.102 | 4.047 | 4.219 | 0.103 | 0.103 | 4.473 | 0.114 | 0.113 | |
| | | Median | 2.547 | 2.444 | 2.721 | 0.102 | 4.047 | 4.219 | 0.103 | 0.103 | 4.473 | 0.114 | 0.113 | |
| | | Stdev | 0.020 | 0.028 | 0.049 | 0.026 | 0.344 | 0.374 | 0.008 | 0.010 | 0.060 | 0.001 | 0.003 | |
| | | Min | 2.533 | 2.424 | 2.687 | 0.083 | 3.804 | 3.954 | 0.097 | 0.096 | 4.430 | 0.113 | 0.111 | |
| | | Max | 2.561 | 2.464 | 2.756 | 0.120 | 4.290 | 4.483 | 0.109 | 0.110 | 4.515 | 0.114 | 0.115 | |
| | | n | 2 | 2 | 2 | 2 | 2 | 2 | 2 | 2 | 2 | 2 | 2 | 0 |
| Opalinus Clay | Mixed clay-silt-carbonate sub-unit | Mean | 2.530 | 2.415 | 2.709 | 0.108 | 4.528 | 4.744 | 0.114 | 0.114 | 4.910 | 0.124 | 0.123 | |
| | | Median | 2.524 | 2.414 | 2.703 | 0.108 | 4.536 | 4.751 | 0.115 | 0.114 | 4.942 | 0.125 | 0.123 | |
| | | Stdev | 0.017 | 0.021 | 0.018 | 0.006 | 0.279 | 0.305 | 0.007 | 0.007 | 0.332 | 0.008 | 0.007 | |
| | | Min | 2.503 | 2.382 | 2.684 | 0.101 | 3.926 | 4.086 | 0.100 | 0.100 | 4.384 | 0.112 | 0.111 | |
| | | Max | 2.561 | 2.447 | 2.745 | 0.122 | 4.921 | 5.175 | 0.124 | 0.123 | 5.361 | 0.135 | 0.133 | |
| | | n | 11 | 11 | 11 | 11 | 13 | 13 | 11 | 11 | 9 | 9 | 9 | 0 |
| Opalinus Clay | Clay-rich sub-unit | Mean | 2.526 | 2.405 | 2.696 | 0.108 | 4.778 | 5.019 | 0.121 | 0.119 | 5.329 | 0.135 | 0.132 | |
| | | Median | 2.523 | 2.402 | 2.699 | 0.110 | 4.781 | 5.021 | 0.121 | 0.119 | 5.411 | 0.136 | 0.133 | |
| | | Stdev | 0.017 | 0.021 | 0.007 | 0.006 | 0.209 | 0.231 | 0.005 | 0.005 | 0.171 | 0.004 | 0.004 | |
| | | Min | 2.511 | 2.386 | 2.688 | 0.101 | 4.568 | 4.786 | 0.116 | 0.114 | 5.132 | 0.131 | 0.127 | |
| | | Max | 2.544 | 2.428 | 2.701 | 0.112 | 4.986 | 5.248 | 0.125 | 0.124 | 5.444 | 0.137 | 0.134 | |
| | | n | 3 | 3 | 3 | 3 | 3 | 3 | 3 | 3 | 3 | 3 | 3 | 0 |
| Staffelegg Fm. | | Mean | 2.523 | 2.436 | 2.672 | 0.085 | 3.483 | 3.616 | 0.087 | 0.088 | 3.926 | 0.098 | 0.098 | 14.83 |
| | | Median | 2.557 | 2.465 | 2.689 | 0.087 | 3.573 | 3.705 | 0.090 | 0.090 | 3.968 | 0.101 | 0.100 | 14.83 |
| | | Stdev | 0.096 | 0.105 | 0.074 | 0.016 | 0.885 | 0.945 | 0.022 | 0.022 | 1.094 | 0.025 | 0.026 | 5.47 |
| | | Min | 2.263 | 2.160 | 2.492 | 0.062 | 1.626 | 1.653 | 0.042 | 0.043 | 1.565 | 0.041 | 0.041 | 10.96 |
| | | Max | 2.594 | 2.552 | 2.732 | 0.116 | 5.115 | 5.391 | 0.130 | 0.128 | 5.536 | 0.140 | 0.137 | 18.69 |
| | | n | 14 | 14 | 9 | 9 | 15 | 15 | 14 | 14 | 11 | 11 | 11 | 2 |
| Klettgau Fm. | | Mean | 2.580 | 2.457 | 2.764 | 0.107 | 4.747 | 4.989 | 0.122 | 0.120 | 5.096 | 0.131 | 0.128 | |
| | | Median | 2.575 | 2.438 | 2.772 | 0.111 | 5.220 | 5.508 | 0.133 | 0.130 | 5.405 | 0.138 | 0.135 | |
| | | Stdev | 0.049 | 0.064 | 0.039 | 0.015 | 0.788 | 0.865 | 0.019 | 0.018 | 0.806 | 0.019 | 0.018 | |
| | | Min | 2.501 | 2.370 | 2.706 | 0.090 | 3.600 | 3.734 | 0.095 | 0.095 | 3.665 | 0.097 | 0.097 | |
| | | Max | 2.641 | 2.546 | 2.811 | 0.125 | 5.426 | 5.737 | 0.139 | 0.137 | 5.834 | 0.150 | 0.146 | |
| | | n | 8 | 8 | 5 | 5 | 8 | 8 | 8 | 8 | 8 | 8 | 8 | 0 |

Tab. 4.3-2: (continued)

| Formation | Member / Sub-unit | | Bulk wet density [g/cm³] | Bulk dry density, calculated [g/cm³] | Grain density [g/cm³] | Pycnometer porosity [–] | Gravimetry: Water content (wet) (105 °C) [wt.-%] | Gravimetry: Water content (dry) (105 °C) [wt.-%] | Gravimetry: Water-loss porosity using bulk wet density [–] | Gravimetry: Water-loss porosity using grain density [–] | Isotope mass balance: Water content (wet) based on isotope diff. exch. [wt.-%] | Isotope mass balance: Porosity based on isotope diff. exch. using bulk wet density [–] | Isotope mass balance: Porosity based on isotope diff. exch. using grain density [–] | External surface area (BET) [m²/g dry rock] |
|---|---|---|---|---|---|---|---|---|---|---|---|---|---|---|
| Bänkerjoch Fm. | | Mean | 2.730 | 2.669 | 2.830 | 0.072 | 2.345 | 2.451 | 0.061 | 0.061 | 2.736 | 0.071 | 0.070 | |
| | | Median | 2.750 | 2.704 | 2.841 | 0.057 | 1.660 | 1.688 | 0.046 | 0.046 | 1.750 | 0.048 | 0.048 | |
| | | Stdev | 0.158 | 0.213 | 0.079 | 0.047 | 2.297 | 2.453 | 0.057 | 0.056 | 2.832 | 0.070 | 0.068 | |
| | | Min | 2.496 | 2.340 | 2.736 | 0.016 | 0.333 | 0.334 | 0.010 | 0.009 | 0.286 | 0.008 | 0.008 | |
| | | Max | 2.916 | 2.906 | 2.939 | 0.147 | 6.249 | 6.665 | 0.156 | 0.155 | 7.367 | 0.184 | 0.179 | |
| | | n | 7 | 7 | 6 | 6 | 7 | 7 | 7 | 7 | 5 | 5 | 5 | 0 |
| Schinznach Fm. | All | Mean | 2.641 | 2.565 | 2.824 | 0.091 | 2.960 | 3.124 | 0.076 | 0.077 | 2.939 | 0.075 | 0.076 | |
| | | Median | 2.687 | 2.645 | 2.845 | 0.067 | 1.859 | 1.894 | 0.050 | 0.051 | 1.944 | 0.052 | 0.054 | |
| | | Stdev | 0.109 | 0.172 | 0.038 | 0.066 | 2.749 | 3.036 | 0.065 | 0.067 | 2.714 | 0.065 | 0.066 | |
| | | Min | 2.415 | 2.207 | 2.768 | 0.039 | 0.992 | 1.002 | 0.027 | 0.027 | 0.983 | 0.026 | 0.027 | |
| | | Max | 2.730 | 2.667 | 2.860 | 0.225 | 8.611 | 9.423 | 0.208 | 0.212 | 8.463 | 0.204 | 0.208 | |
| | | n | 7 | 7 | 7 | 7 | 7 | 7 | 7 | 7 | 7 | 7 | 7 | 0 |
| Schinznach Fm. | Stamberg Mb. | Mean | 2.567 | 2.443 | 2.851 | 0.143 | 4.961 | 5.311 | 0.124 | 0.126 | 4.976 | 0.125 | 0.127 | |
| | | Median | 2.590 | 2.476 | 2.847 | 0.130 | 4.412 | 4.616 | 0.114 | 0.116 | 4.522 | 0.117 | 0.119 | |
| | | Stdev | 0.141 | 0.221 | 0.008 | 0.076 | 3.409 | 3.812 | 0.079 | 0.081 | 3.283 | 0.076 | 0.078 | |
| | | Min | 2.415 | 2.207 | 2.845 | 0.075 | 1.859 | 1.894 | 0.050 | 0.051 | 1.944 | 0.052 | 0.054 | |
| | | Max | 2.695 | 2.645 | 2.860 | 0.225 | 8.611 | 9.423 | 0.208 | 0.212 | 8.463 | 0.204 | 0.208 | |
| | | n | 3 | 3 | 3 | 3 | 3 | 3 | 3 | 3 | 3 | 3 | 3 | 0 |
| Schinznach Fm. | Lied. + Leu-tschenb. + Kienb. Mb. | Mean | 2.685 | 2.654 | 2.786 | 0.047 | 1.171 | 1.185 | 0.031 | 0.032 | 1.175 | 0.032 | 0.032 | |
| | | Median | 2.687 | 2.660 | 2.783 | 0.050 | 1.165 | 1.179 | 0.031 | 0.032 | 1.006 | 0.027 | 0.028 | |
| | | Stdev | 0.019 | 0.017 | 0.019 | 0.008 | 0.182 | 0.186 | 0.005 | 0.005 | 0.313 | 0.009 | 0.009 | |
| | | Min | 2.665 | 2.634 | 2.768 | 0.039 | 0.992 | 1.002 | 0.027 | 0.027 | 0.983 | 0.026 | 0.027 | |
| | | Max | 2.703 | 2.666 | 2.806 | 0.054 | 1.355 | 1.374 | 0.037 | 0.037 | 1.536 | 0.042 | 0.042 | |
| | | n | 3 | 3 | 3 | 3 | 3 | 3 | 3 | 3 | 3 | 3 | 3 | 0 |
| Zeglingen Fm. | | Mean | 2.598 | 2.485 | 2.813 | 0.117 | 4.360 | 4.559 | 0.113 | 0.114 | 4.398 | 0.114 | 0.115 | |
| | | n | 1 | 1 | 1 | 1 | 1 | 1 | 1 | 1 | 1 | 1 | 1 | 0 |

### 4.3.1 Water content

The distribution of gravimetric water content in the studied section Malm – Triassic is shown in Fig. 4.3-1. Note that the error bars on gravimetric water content reflect the variability among 3 aliquots of the samples, i.e. they are a measure of the lithological heterogeneity of the sample on the cm-scale. The following systematics of water content can be observed in the Triassic and in the Malm (the Dogger – Lias section is detailed further below):

- In the lower part of the Schinznach Formation, an upwards increasing trend is identified. High and scattered values are found in the uppermost part of this unit.
- Water content varies widely in the Bänkerjoch Formation, reflecting the lithological heterogeneity in this unit.
- Water content is high in the Klettgau Formation, without evident depth trends.

- In the Wildegg Formation, water content varies widely but not systematically. Starting in the uppermost part of the Wildegg Formation, a decreasing trend is identified towards the top of the Villigen Formation.
- The Schwarzbach Formation shows distinctly higher water contents in comparison to its neighbouring units.
- Low and upwards decreasing water content is found in the «Felsenkalke» + «Massenkalk».

Water contents from gravimetry and from isotope diffusive exchange correlate well (Fig. 4.3-2), but the latter show values that are consistently higher, about 12%$_{rel}$ on the average.

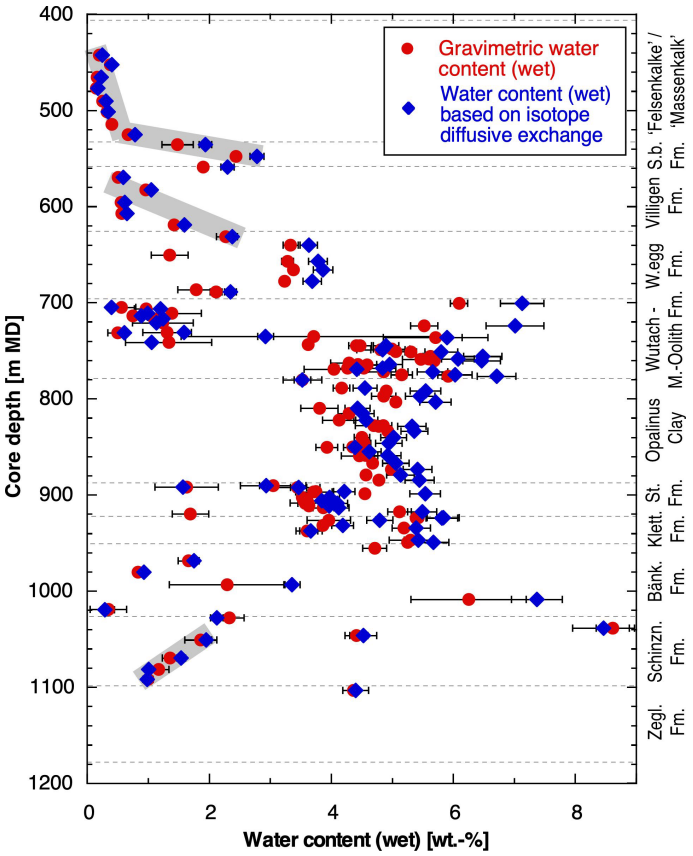


Fig. 4.3-1: Water content as a function of depth

Trends (thick grey bars) are only indicated for the Malm and Triassic sections, the Dogger and Lias are detailed in Fig. 4.3-3. Black bars for gravimetric water content indicate 1σ variability among 3 aliquots of the same sample. Black bars for water content from isotope diffusive exchange represent the propagated analytical error.

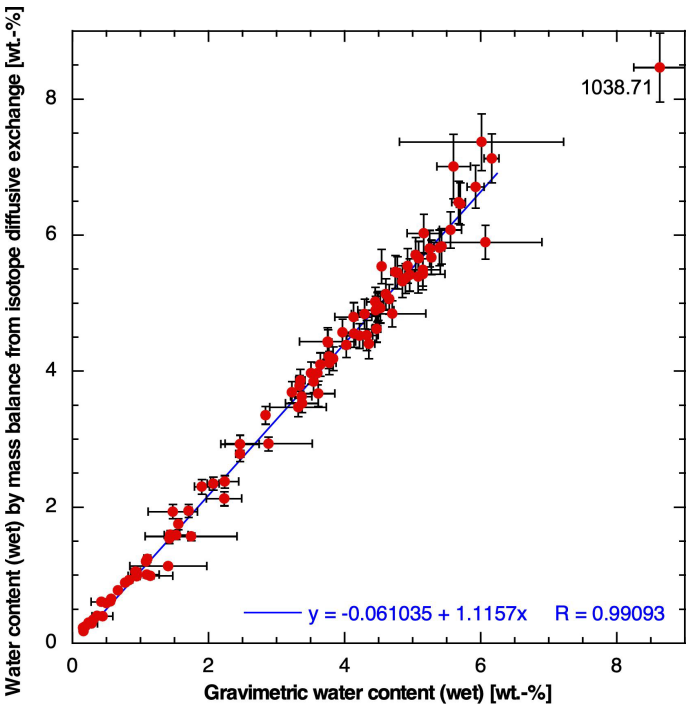


Fig. 4.3-2: Correlation of water contents based on gravimetry and on isotope diffusive exchange

Black bars for gravimetric water content indicate 1σ variability among 2 aliquots of the same sample. Black bars for water content from isotope diffusive exchange represent the propagated analytical error. Note that only the 2 gravimetric water contents obtained from the aliquots used for the isotope diffusive-exchange experiments were considered in this graph, so the correlation refers to identical sample materials. This is particularly important for anhydrite-bearing samples, given the fact that only the anhydrite-poorest portions of such samples were used for diffusive-exchange experiments. Sample 1'038.71 from the Schinznach Formation (porous dolostone) falls off the trend and was not considered for the linear regression line.

## A closer look at the clay-rich Lias – Dogger section

As shown in Fig.4.3-3, water contents in the Lias – Dogger section show several systematic trends with depth. These are similar for gravimetric water content and that obtained from isotope mass balance:

- In the Frick Member section (901.53 – 913.47 m) of the Staffelegg Formation, a slight upward trend towards lower values is evident.
- In the overlying Rietheim and Gross Wolf Members (887.94 – 899.30 m), a distinct cycle of strongly decreasing water content is observed.
- A sharp discontinuity towards higher values is observed at the base of the Opalinus Clay. Then the values decrease to reach a minimum in the centre of the 'Mixed clay-silt-carbonate sub-unit', from where an increase towards the top of this sub-unit is observed.

- The 'Silty sub-unit' has slightly lower water content, while the overlying 'Sub-unit with silty calcareous beds' represents a cycle starting with high values that decrease upwards.
- Two similar cycles of decreasing water content are observed in the «Murchisonae-Oolith Formation» and the Wedelsandstein Formation.

Overall, the observed trends show many similarities (and a few differences) to the profile of the BUL1-1 borehole (Mazurek et al. 2021). The observed trends of the water content correlate reasonably well with those identified for clay-mineral contents (Section 4.2.1, Fig. 4.2-4), and tend to be even clearer.

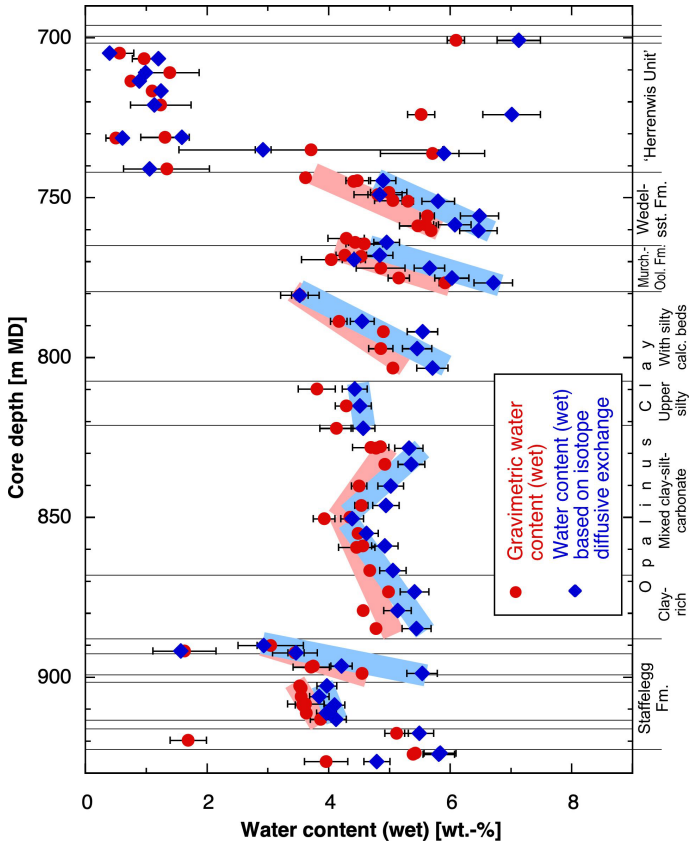


Fig. 4.3-3: Water content (wet) as a function of depth in the Lias – Dogger interval

Black bars for gravimetric water content indicate 1σ variability among 3 aliquots of the same sample. Black bars for water content from isotope diffusive exchange represent the propagated analytical error.

### 4.3.2 Grain density

The grain-density profile is shown in Fig. 4.3-4. Throughout the Malm, Dogger and Lias units, values are around 2.7 g/cm$^3$, with only limited scatter. Outliers towards higher values in the Opalinus Clay and in the Wedelsandstein Formation correlate with elevated contents of pyrite or siderite. The only other conspicuous excursion is identified in the Rietheim Member of the Staffelegg Formation ('Posidonienschiefer'), where high contents of organic matter ($C_{org}$ = 6.1 – 6.8 wt.-%) lead to markedly lower grain-density values.

In the underlying Triassic section, values become higher, as does variability. This reflects the lithological heterogeneity, in particular the variable contents of dolomite and anhydrite with their high mineral densities (2.85 and 2.97 g/cm$^3$, respectively). Fig. 4.3-5 shows the correlation between grain density and dolomite/ankerite contents. Grain density increases linearly with dolomite concentration, and outliers are due to the presence of anhydrite or organic carbon.

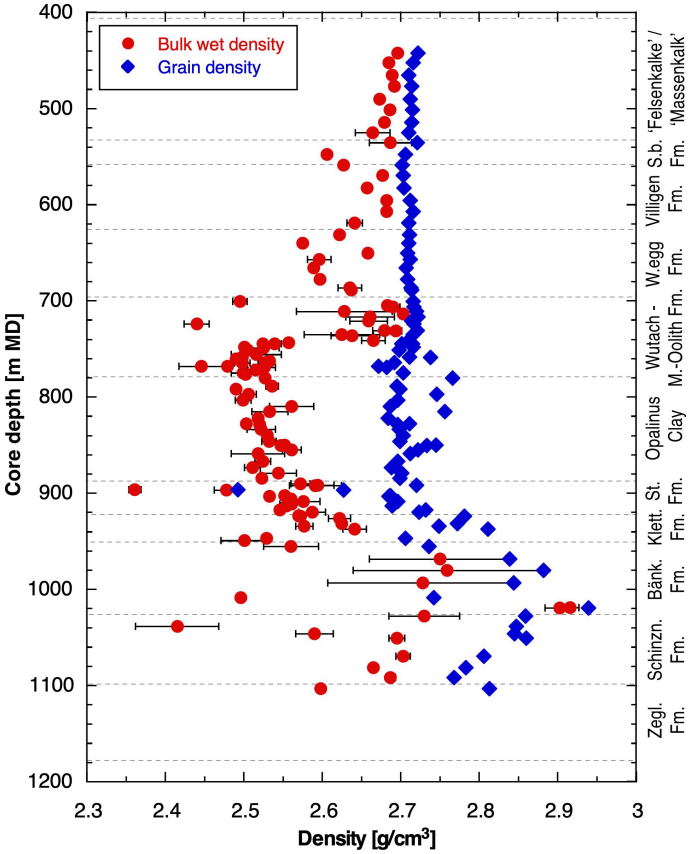


Fig. 4.3-4: Depth profile of bulk wet and grain densities

Black bars for bulk wet density indicate 1σ variability among 3 pieces of the same sample. Analytical error bars for grain density are smaller than the symbol size.

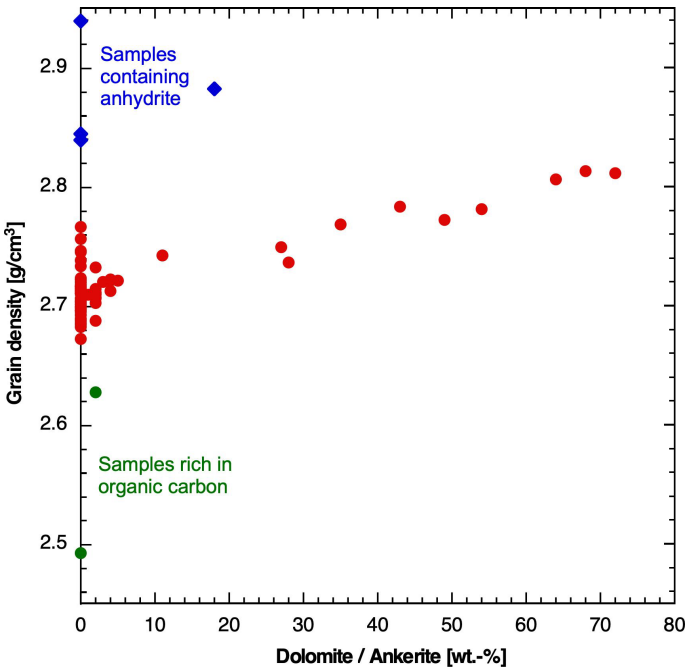


Fig. 4.3-5: Grain density as a function of the contents of dolomite/ankerite

Blue points are from the Schinznach and Bänkerjoch Formations. Green points are from the Rietheim Member of the Staffelegg Formation.

### 4.3.3 Bulk wet density

Data are shown in Fig. 4.3-4 as a function of depth. Large error bars for some samples reflect heterogeneity on the cm scale.

### 4.3.4 Porosity

Three different approaches were used to constrain rock porosity (for details see Waber ed. 2020):

- *Water-loss porosity:* calculation from the gravimetric water content using either bulk wet or grain density.
- *Porosity from isotope diffusive exchange:* calculation from the water content obtained by mass balance using either bulk wet or grain density.
- *Pycnometer porosity:* calculation from bulk dry and grain densities; bulk dry density is calculated from bulk wet density and water content.

Water-loss porosity and porosity from isotope diffusive exchange were calculated using bulk wet density by default. If the latter was not available, grain density was used, by which full water saturation of the pore space was assumed. The graphic in Fig. 4.3-6 shows that the two densities yield near-identical porosities, so the choice of the type of density for the calculation incurs no additional uncertainty.

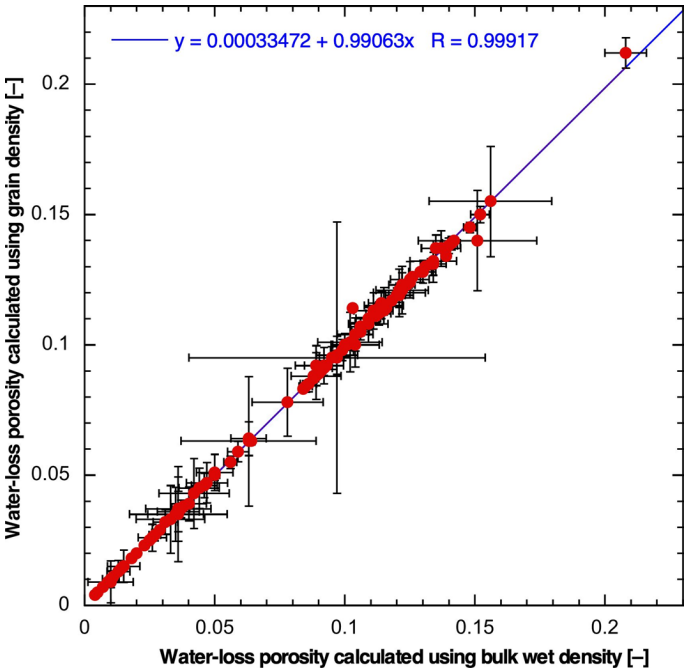


Fig. 4.3-6: Water-loss porosity calculated from gravimetric water content using either bulk wet or grain density

Bars indicate propagated errors which are dominated by local heterogeneity of water content.

## Comparison of porosities obtained by different methods

- An excellent linear correlation is observed between water-loss porosity and porosity from isotope diffusive exchange (Fig. 4.3-7). The latter yields about 10% higher values. Only sample 1'038.71 from the Schinznach Formation (a porous dolostone) falls off the general trend.
- A slightly less good linear correlation is found between pycnometer porosity and porosity from isotope diffusive exchange (Fig. 4.3-8). The latter yields about 19% higher values. Two outliers are explained by sample heterogeneity (see illustrations in Fig. 4.3-9).
- The correlation between water-loss and pycnometer porosity is shown in Fig. 4.3-10. Again, the same samples fall off the trend (see illustrations in Fig. 4.3-9). Excluding these outliers yields a slope for the regression line of about 0.89.

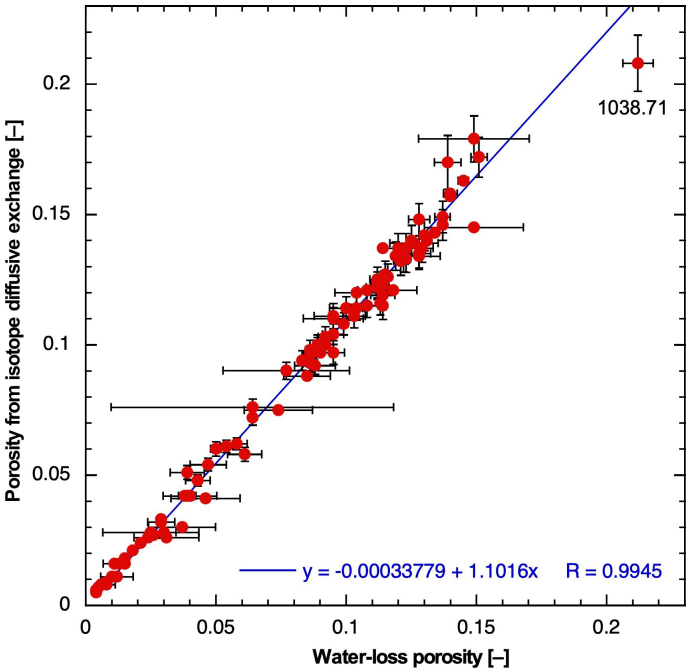


Fig. 4.3-7: Correlation of water-loss porosity and porosity from isotope diffusive exchange

Bars indicate propagated errors. Note that only the gravimetric water contents obtained from the aliquots used for the isotope diffusive-exchange experiments were considered for the x-axis of this graph, so the correlation refers to identical sample materials. Sample 1'038.71 was ignored for the calculation of the regression line.

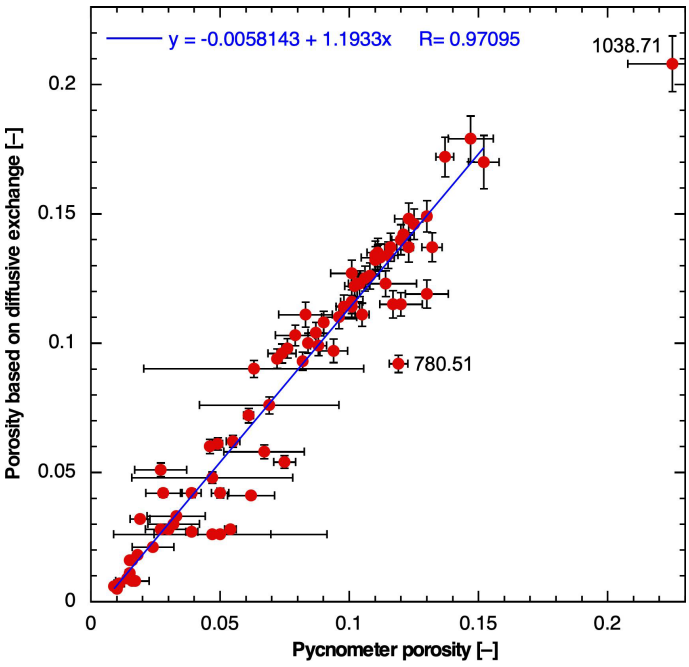


Fig. 4.3-8: Correlation of pycnometer porosity and porosity from isotope diffusive exchange

Bars indicate propagated errors. Indicated outliers were excluded from the regression line.

780.51 m
(Opalinus Clay)

1'038.71 m
(Schinznach Formation)

Fig. 4.3-9: Illustrations of heterogeneous samples

780.51 m: alternation of clay-rich and clay-poorer beds, with silty lenses and macrofossils; 1'038.71 m: dolostone with nodules and macroscopic dissolution vugs. Width of photographs is 10 cm.

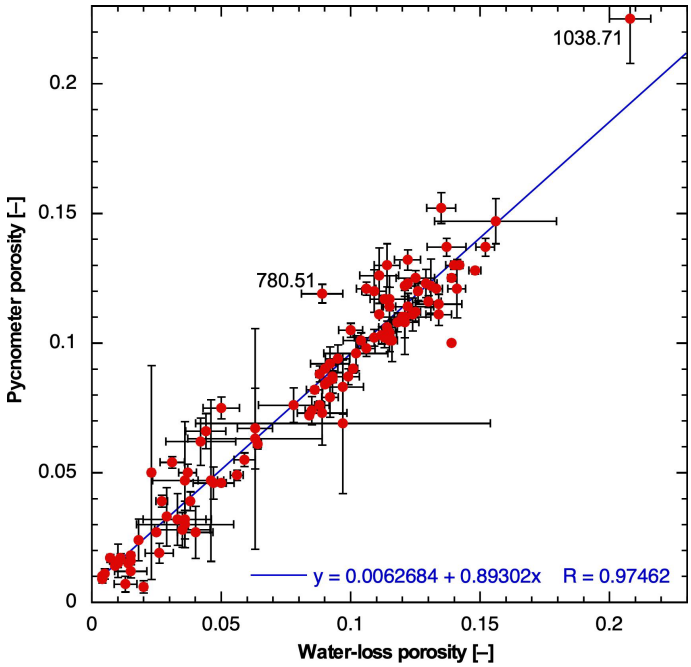


Fig. 4.3-10: Correlation of water-loss and pycnometer porosity

Bars indicate propagated errors. The indicated outliers were excluded from the regression line.

## Depth trends

In Fig. 4.3-11, porosity is shown as a function of depth. The shape of the profile is similar to that of water content (Figs. 4.3-1 and 4.3-3), including the systematic trends. The comments made on the distribution of water content with depth (Section 4.3.1) also apply to porosity.

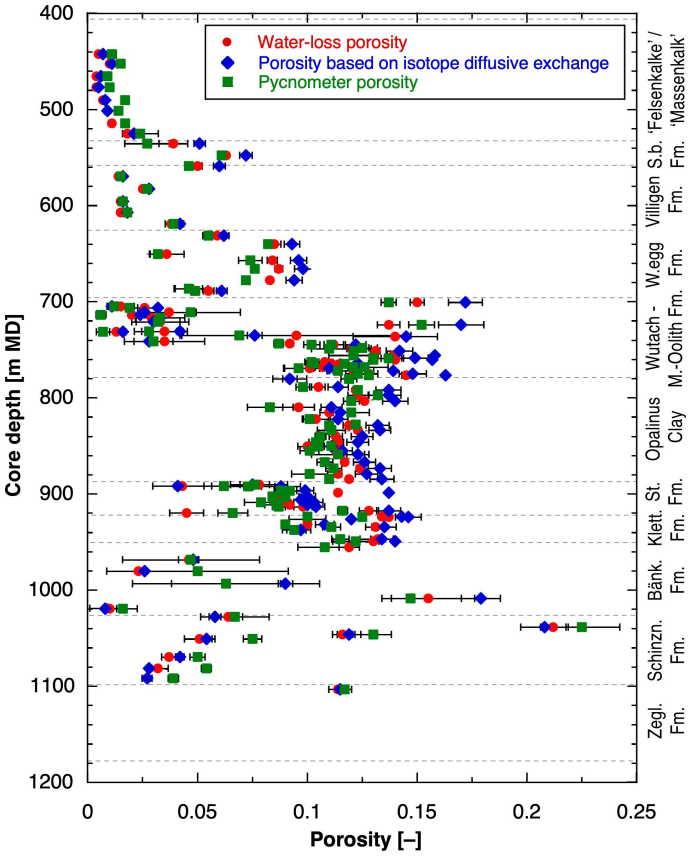


Fig. 4.3-11: Depth trends of porosities obtained by different methods

## Porosity as a function of mineralogical composition

The correlation of porosity with clay-mineral content is shown in Fig. 4.3-12. When considering all available data (Fig. 4.3-12a), a general positive correlation can be identified but scatter is substantial. Marked outliers towards high porosity at low clay-mineral content are dolostones of the Schinznach and Zeglingen Formations (except 723.96; see below). These were affected by diagenetic dissolution to some degree, either during the process of dolomitisation or at later stages. Thus, their porosity is not the result of compaction and cementation alone.

When only samples from the Malm – Dogger – Lias section are considered, i.e. when the mineralogically and texturally more heterogeneous samples from the Triassic are excluded, a more systematic correlation is obtained (Fig. 4.3-12b). Outliers include:

- 723.96 («Herrenwis Unit») – a highly porous limestone from the reef facies
- 768.34 («Murchisonae-Oolith Formation») and 917.60 (Schambelen Member of the Staffelegg Formation) – particularly quartz-rich samples (siltstones)
- 700.77 (Variansmergel Formation + «Parkinsoni-Württembergica-Schichten») and 913.19 (Frick Member of the Staffelegg Formation) – claystones; the reason for the deviation of these samples from the general trend is unclear.

The slope of the correlation in Fig. 4.3-12 is steeper for clay-mineral contents in the range of 0 – 30 wt.-% and becomes flatter at higher clay-mineral contents. The presence of anhydrite tends to reduce porosity for a given clay-mineral content. Fig. 4.3-13 illustrates that porosity tends to reach values < 0.02 for anhydrite-rich samples.

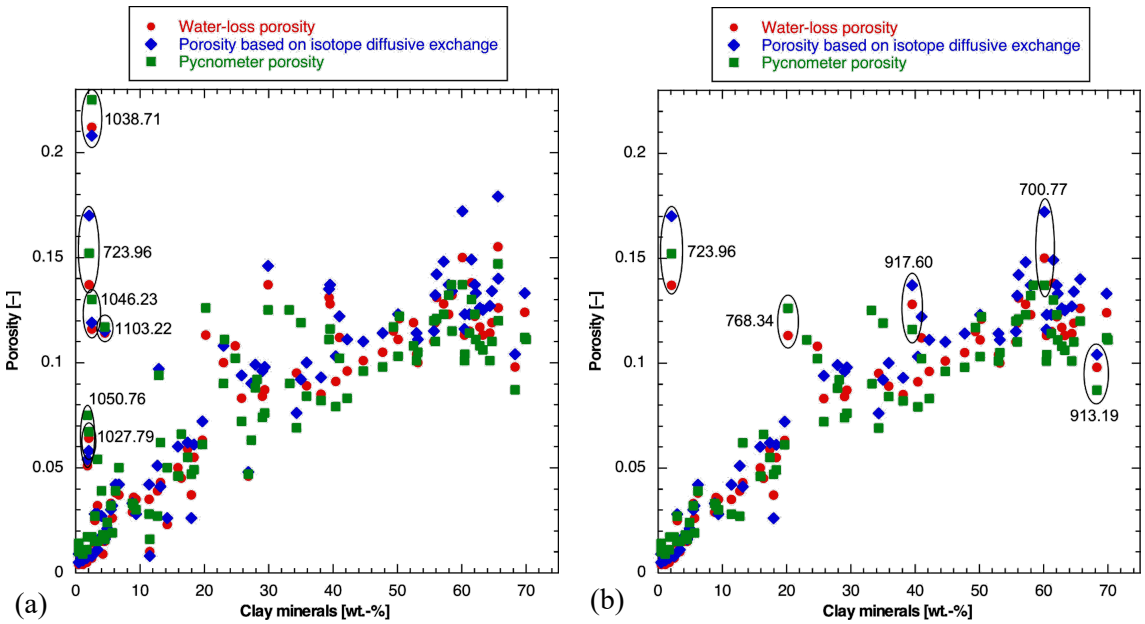


Fig. 4.3-12: Porosity as a function of clay-mineral content

(a) all data, (b) data from the section Malm – Dogger – Lias.

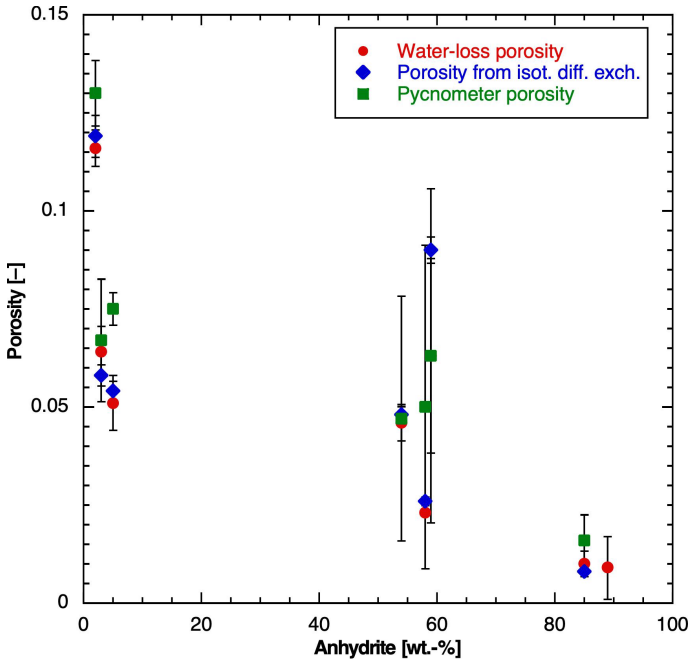


Fig. 4.3-13: Porosity of anhydrite-bearing samples

Bars indicate propagated errors.

### 4.3.5 Specific surface area and pore-size distributions from $N_2$ ad-/desorption

*Thomas Gimmi*

## Depth trends

Nitrogen adsorption data were only obtained for 7 of the 10 samples from the upper and lower confining units of Opalinus Clay on which through-diffusion experiments (PSI, Van Loon & Glaus *in prep.*) were performed (Tab. 4.3-2). Two samples are from the Wildegg Formation (650.49 m, 686.50 m), two from the Wedelsandstein (748.28 m and 758.65 m), one from the «Murchisonae-Oolith Formation» (768.24 m) and two from the Staffelegg Formation (896.72 m, 919.66 m). Their lithology is very different but claystone samples are underrepresented[7] (the lower Wedelsandstein sample only).

Due to the comparably small number of samples and the lack of data from the Opalinus Clay, the depth trends of the specific surface area $S_{BET}$ are not very clear (Fig. 4.3-14). However, a comparison with the data obtained from the BUL1-1 borehole (right plot in Fig. 4.3-14) shows that the variation with the rock formation is similar in both boreholes.

As $N_2$ cannot reach any interlayer pores of smectites, $S_{BET}$ represents surfaces of external (non-interlayer) pores. The largest values of about 30 – 40 $m^2/g$ were found for the two Wedelsandstein Formation samples with the largest clay-mineral contents in this series of samples (33 and 58 wt.-%, respectively). Lower values in the range of ~ 6 – 19 $m^2/g$ were found for the other samples, with the lower bound for the limestone in the Effingen Member of the Wildegg Formation, and the larger bound for the calcareous marl in the Rietheim Member of the Staffelegg Formation. As observed in other boreholes, notably in the BUL1-1 borehole or also in the BOZ2-1 borehole, the range of $S_{BET}$ values in the Staffelegg Formation appears to be considerable, probably due to heterogeneities regarding depositional environment and diagenesis.

The variation of the specific surface area $S_{BET}$ with depth is generally related to trends observed in other physical and mineralogical properties of samples from the STA3-1 borehole, such as the bulk dry density, the gravimetric water content, the water-loss porosity or the clay-mineral content. For comparison purposes, in some of the following plots the general trends seen for the larger dataset from BUL1-1 are also shown.

[7] The focus of this batch of diffusion samples was intentionally on less clay-rich samples of the confining units of Opalinus Clay.

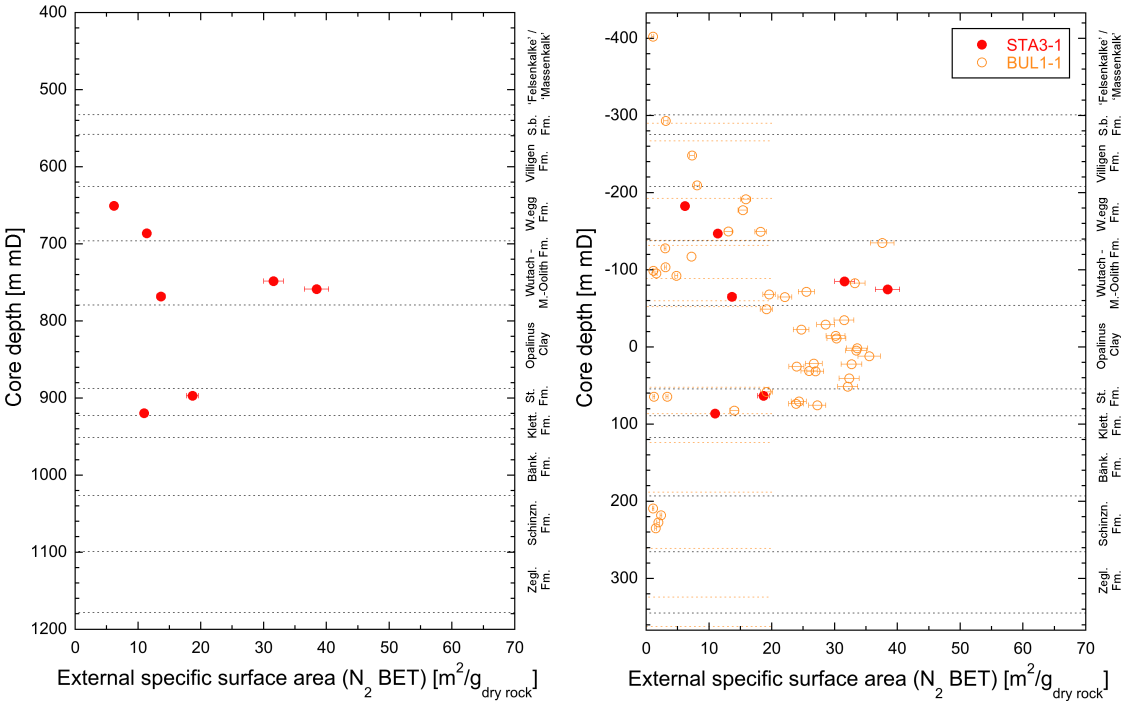


Fig. 4.3-14: Specific surface area ($S_{BET}$) derived from $N_2$ adsorption as a function of depth

Left: Data from STA3-1. Right: Comparison of data from STA3-1 with those from BUL1-1, with depth relative to center of Opalinus Clay. $S_{BET}$ represents external surfaces only. The total specific surface area, including interlayer surfaces, would be larger depending on the smectite content of the sample. Errors resulting from sample preparation and handling are estimated to be ± 5% in general and ± 10% for $S_{BET} < 2$ m$^2$ g$^{-1}$, as given by the error bars. In the right plot, the orange dashed lines show formation boundaries BUL1-1 (names not given).

## Correlation of $S_{BET}$ with water content and clay-mineral content

The $S_{BET}$ tends to increase with the gravimetric water content relative to the dry sample mass (Fig. 4.3-15). The correlation is, however, very weak, which is related to the small number and the lithological differences between the chosen samples from the confining units.

The largest $S_{BET}$ values for the sandy/silty marl and the very sandy/silty claystone in the Wedelsandstein Formation are related to large water contents, the low values in the limestones of the Wildegg Formation and in the lowest part of the Staffelegg Formation are related to small water contents. The sandstone/siltstone sample in the «Murchisonae-Oolith Formation» and the calcareous marl in the upper part of the Staffelegg Formation have a relatively small surface area compared to their medium to large water contents.

The specific surface area $S_{BET}$ is more clearly correlated with the total content of clay minerals (Fig. 4.3-16) than with the water content for the limited number of samples from the STA3-1 borehole. The single very sandy/silty claystone sample from the Wedelsandstein Formation (758.65 m) shows the largest $S_{BET}$ value, followed by a relatively large value (compared to its clay-mineral content of 33 wt.-%) for the sandy/silty marl.

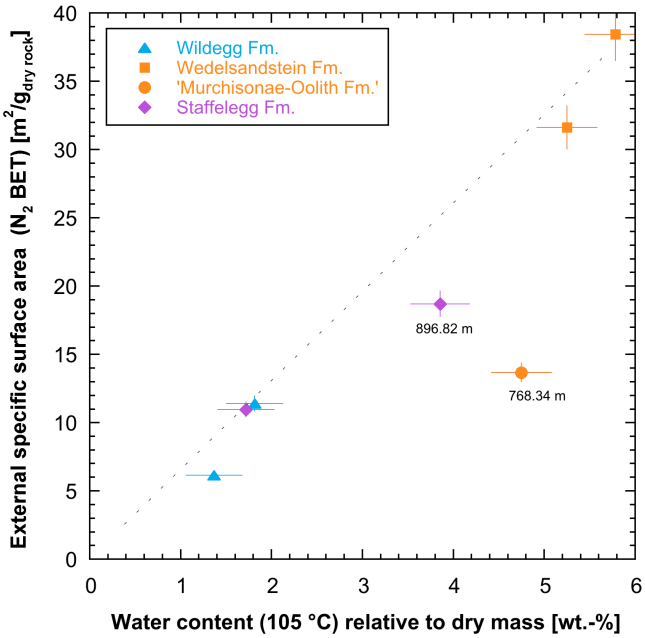


Fig. 4.3-15: Specific surface area ($S_{BET}$) derived from $N_2$ adsorption plotted against the gravimetric water content relative to the dry mass of the samples

Error bars show estimated errors for the water content (based on standard deviations of other samples) and estimated errors for $S_{BET}$. The dotted line shows the regression obtained for the BUL1-1 data which include samples from all formations. It is similar to a regression for the STA3-1 data when excluding the sample at 768.34 m (a regression for all speficially chosen samples from STA3-1 is considered as less meaningful).

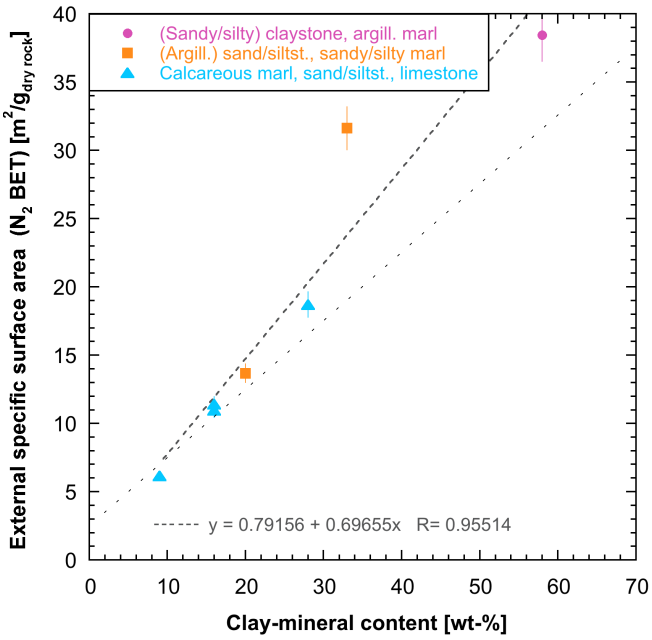


Fig. 4.3-16: Relation between external specific surface area ($S_{BET}$) derived from $N_2$ adsorption and content of clay minerals

The samples are assigned to three classes according to their positions in the Füchtbauer diagram (i.e., according to lithological rock types). The dashed line is a regression on the STA3-1 data which do not include any samples from the Opalinus Clay; the dotted line shows the regression obtained for the BUL1-1 data including samples from all formations.

A positive correlation of $S_{BET}$ exists also with the contents of the illite end-member (Fig. 4.3-17). The correlation with the few data points from the STA3-1 borehole (slope of 1.2) is similar to that obtained for the BUL1-1 data (slope of 1.1). A correlation seems also to exist with the smectite end-member content, similar as found for the BUL1-1 data (but not for other datasets, e.g., from BOZ2-1). No clear correlation with the kaolinite and chlorite end-member contents is visible for the limited dataset of STA3-1, but the individual data plot in a very similar range compared to the data from BUL1-1.

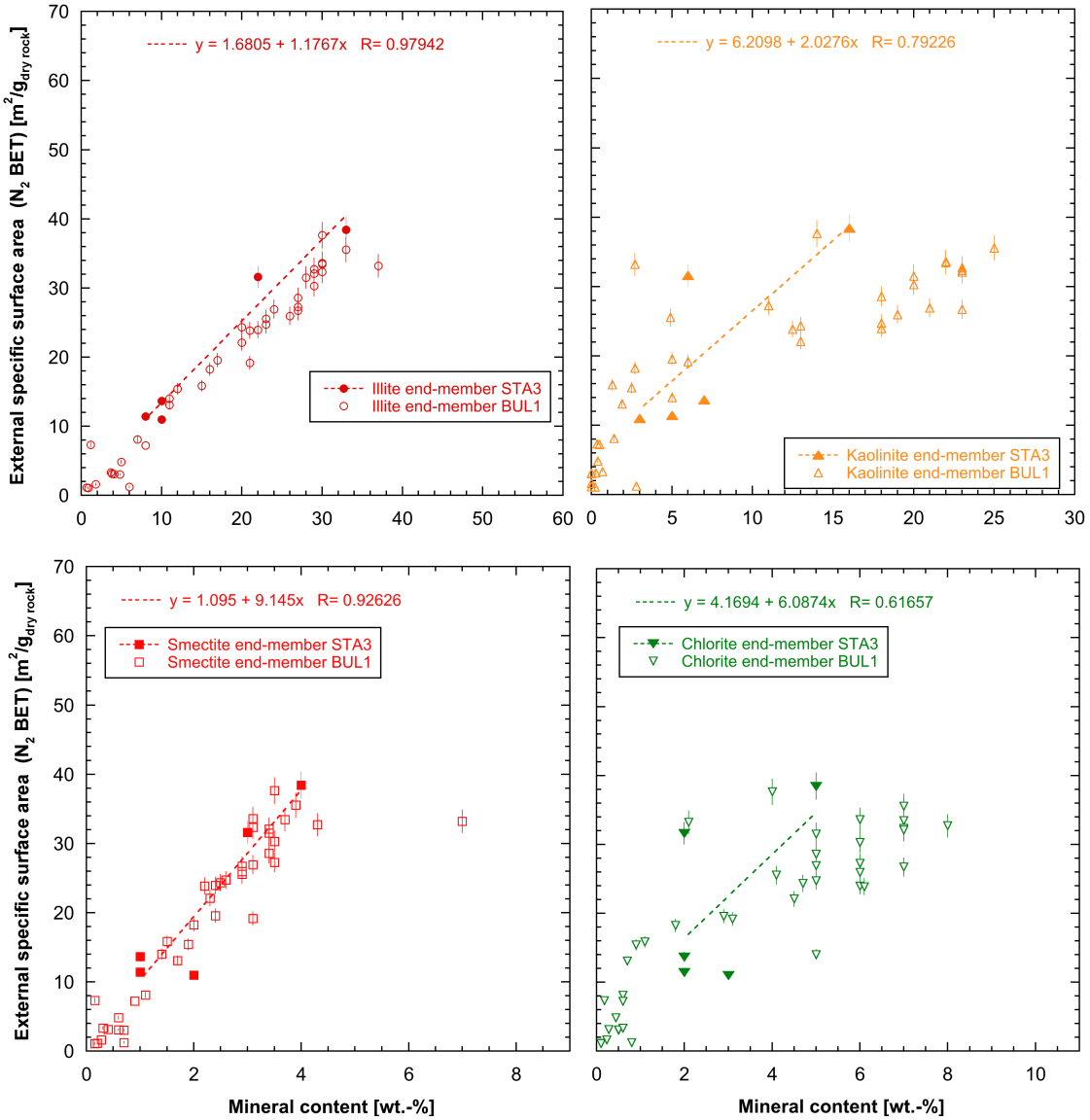


Fig. 4.3-17: Relation between external specific surface area ($S_{BET}$) derived from $N_2$ adsorption and contents of specific clay mineral end-members

The solid symbols and the regression line represent the STA3-1 data which do not include any samples from the Opalinus Clay; the open symbols show BUL1-1 data including samples from all formations

### Average sizes of external pores derived from $S_{BET}$

Average sizes of external pores were estimated from the specific surface area $S_{BET}$ and the water content per dry mass $WC_d$ as:

$$\overline{r_{ext}} = WC_d/(\rho_w\, S_{BET})$$

with $\rho_w$ the water density taken to be 1 g/mL. This calculation assumes negligible pore volumes in interlayer pores, i.e., it attributes the measured water content to external pores only (which is not appropriate for samples with relevant smectite end-member contents).

The slope of a linear relation in Fig. 4.3-15 represents $S_{BET}/WC_d$. From the inverse of this slope (6.49 $m^2\ g^{-1}$ wt.-$\%^{-1}$ when excluding the outlier at 768.34 m; slope is not shown in Fig. 4.3-15), we obtain an overall average layer thickness (or radius) of external pores for the six samples of 1.5 nm, which corresponds to about 5 to 6 water layers. A similar average value was obtained for the samples from BUL1-1, which included many claystone samples.

Instead of calculating an overall average from the linear regression, it is more interesting to derive an average layer thickness for each sample. Fig. 4.3-18 plots average external pore radii (attributing all water to external surfaces) for each sample as a function of the gravimetric water content per dry solid mass (a) and as a function of the total clay-mineral content (b). The lowest radius of 1.5 nm (diameter of ~ 3.0 nm) is obtained for the very sandy/silty claystone sample from the Wedelsandstein Formation, but similar values of 1.6 – 1.7 nm (diameter of ~ 3.1 – 3.3 nm) are obtained for two limestones and the sandy/silty marl sample, or of 2.1 – 2.2 nm (diameter of ~ 4.1 – 4.4 nm) for the other limestone and the calcareous marl. The largest value of 3.5 nm (diameter of 6.9 nm) is seen for the sandstone/siltstone sample from the «Murchisonae-Oolith Formation». As there were only few samples from STA3-1 analysed, no clear tendency with water contents or with clay-mineral contents are seen. However, when comparing with earlier data where a decrease with increasing clay-mineral contents or with increasing water contents was reported, the data from the STA3-1 borehole match approximately.

The very sandy/silty claystone sample at 758.75 m with a clay-mineral fraction of 58 wt.-% and a smectite end-member fraction of ~ 4 wt.-% will have some interlayer water. Accordingly, the calculated average external pore radius of ~ 1.5 nm represents a maximum value. A correction of average external pore size that accounts for the volume of interlayer water based on the smectite end-member content could be made assuming typical smectite particle geometries. However, in view of the involved uncertainties this is not done at present.

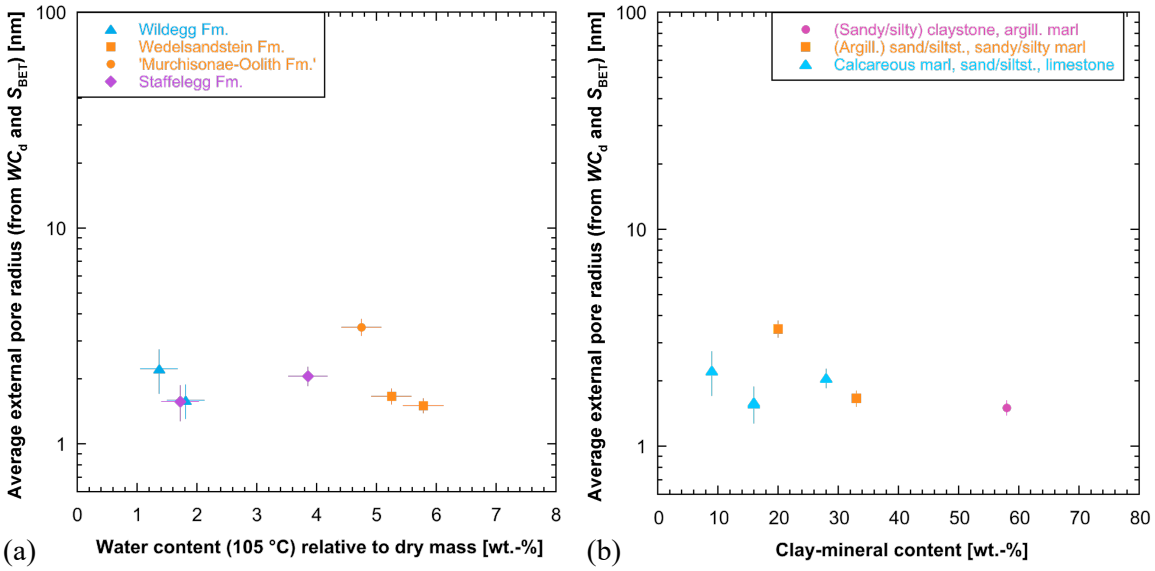


Fig. 4.3-18: Average external pore radius calculated from $S_{BET}$ and the gravimetric water content (assuming insignificant interlayer pore volume) plotted against the gravimetric water content per dry mass of the samples (a) and against the total clay-mineral content (b)

Samples are grouped according to geological units (a) or according to rock lithology (b). Error bars show estimated errors for the water content (based on standard deviations of other samples) and propagated errors for the average external pore radius.

## Distribution of external pore sizes derived from $N_2$ isotherms

Pore size distributions (diameters) of external pores were derived from $N_2$ ad- and desorption isotherms (using the standard BJH algorithm). Results from $N_2$ desorption for all samples are shown in Fig. 4.3-19, grouped according to rock lithology. All samples show a clear, partly prominent peak at a diameter of about 4 nm in these curves. These peaks are typically related to the closure of the hysteresis of the isotherm and are thus attributed to liquid instabilities (instability of the configuration of liquid nitrogen) rather than to a distinct pore volume in this size range. Hysteresis (and thus a clear closure peak) is generally interpreted as indicating a relatively complex pore architecture (e.g., Thommes et al. 2015).

Two of the three calcite-rich and clay-poor samples classified as limestones according to the Füchtbauer nomenclature (650.49 m and 686.50 m; Fig. 4.3-19a) have two distinct, comparably narrow peaks (in addition to the hysteresis peak) at ~ 10 – 20 nm and at ~ 100 nm, while the third limestone sample (919.66 m) has weaker peaks at ~ 10 nm and ~ 60 nm. The fourth sample in this figure, classified as calcareous marl, has a broad, important peak at ~ 7 nm and a less important peak at ~ 60 nm, in line with its lower calcite but comparably larger clay content. It also exhibits a strong hysteresis peak, indicating a more complex pore network compared to the limestone samples.

The sandy/silty marl sample according to the Füchtbauer nomenclature (748.38 m, Fig. 4.3-19b) shows also a strong hysteresis peak and then an important peak at ~ 10 nm and a second peak at ~ 100 nm. The sandstone/siltstone sample (768.34 m) is characterised by a broad diameter distribution peaking at ~ 20 nm and extending to values < 100 nm, but only a weak hysteresis peak.

The very sandy/silty claystone sample (758.75 m, Fig. 4.3-19c) has a complex pore architecture (strong hysteresis peak hinting), with a considerable amount of small pores (important peak at diameters of ~ 8 nm) as well as of larger pores (second peak at ~ 60 nm).

The reliability of the pore size distribution results was tested by comparing maximum adsorbed amounts of $N_2$ at highest $N_2$ pressures, expressed as wt.-% $H_2O$, with the samples' water contents (Fig. 4.3-20). The values scatter around the 1:1 line, lending generally confidence to the derived size distributions, but with some pronounced deviations. Notably, the total amounts of adsorbed $N_2$ clearly exceeds the water contents for the two limestone samples from the Wildegg Formation (650.49 m and 686.50 m), meaning that either some small-scale heterogeneity exists, or that some larger pores were overestimated. The difference can probably also explain their larger peak values compared to the limestone sample from the Staffelegg Formation (919.66 m), where the total amount of adsorbed $N_2$ is similar to or even somewhat smaller than the water content. The total adsorbed amount of $N_2$ for the sample from the «Murchisonae-Oolith Formation» (768.34 m) is clearly smaller than its water content, meaning that some (probably larger) pores were under-represented in Fig. 4.3-19.

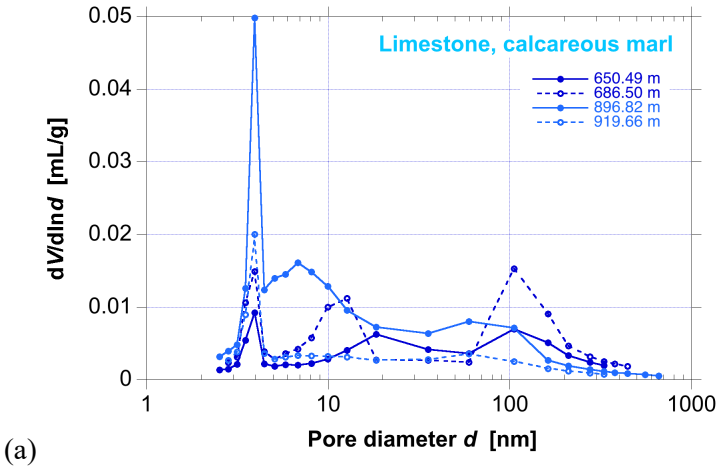


(a)

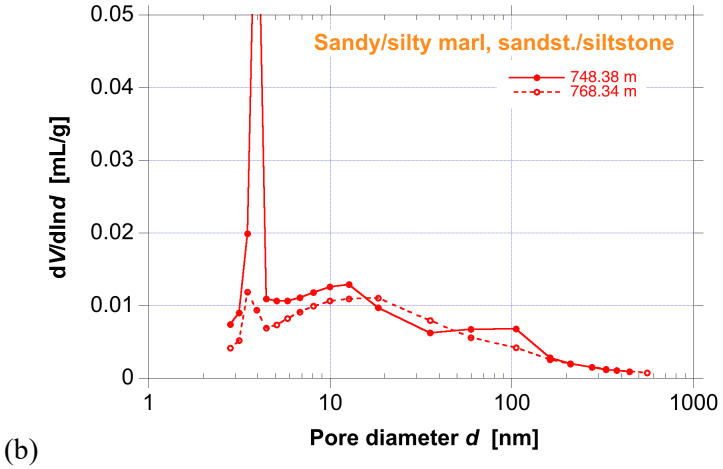


(b)

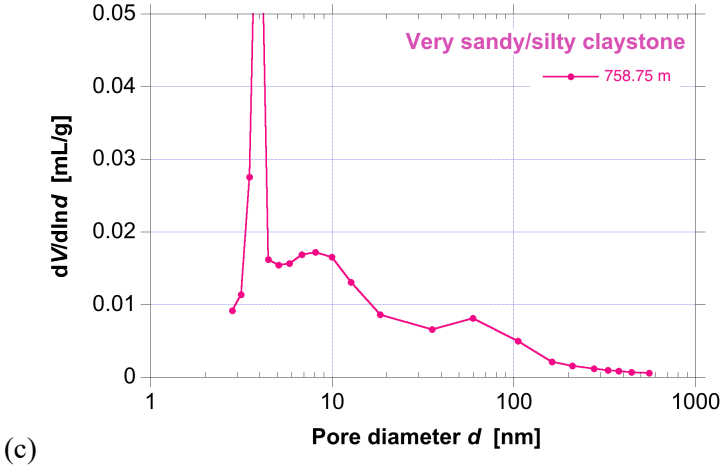


(c)

Fig. 4.3-19: Distribution of (external) pore diameters derived from $N_2$ desorption

(a) Limestones (650.49 m, 686.50 m, 919.66 m) and calcareous marl (896.82 m), (b) sandy/silty marl (748.38 m) and sandstone/siltstone (768.34 m), (c) very sandy/silty claystone (758.75 m).

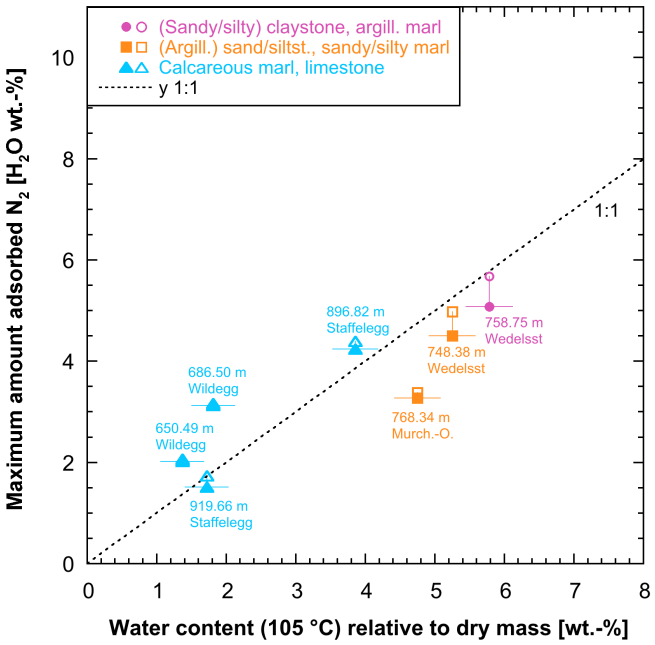


Fig. 4.3-20: Comparison of maximum amount of adsorbed $N_2$ (recalculated to $H_2O$ wt.-%) with water content per dry sample mass

Open symbols: adsorption, closed symbols: desorption.

## Average sizes of external pores based on pore size distributions calculated from the $N_2$ isotherms

Average sizes of external pores cannot only be derived from $S_{BET}$ and the water content as shown above but also from the pore size distribution derived from $N_2$ isotherms. In both cases, it is assumed that interlayer pore volumes (which are not probed by $N_2$ adsorption) are insignificant. Radii directly derived by averaging the BJH pore size distributions (Fig. 4.3-21) are larger by a factor 1.5 to 3.8 when compared with the average radii determined from $S_{BET}$ and the gravimetric water content (Fig. 4.3-18) but show the same tendencies: smaller radii (around 3 – 4 nm for the samples here) for the very sandy/silty claystone and larger radii, but with scatter, for the calcareous marl and the limestones (around 3 – 7 nm). The variation with lithology for the few samples from the STA3-1 borehole is somewhat smaller as that for the larger dataset from the BUL1-1 borehole.

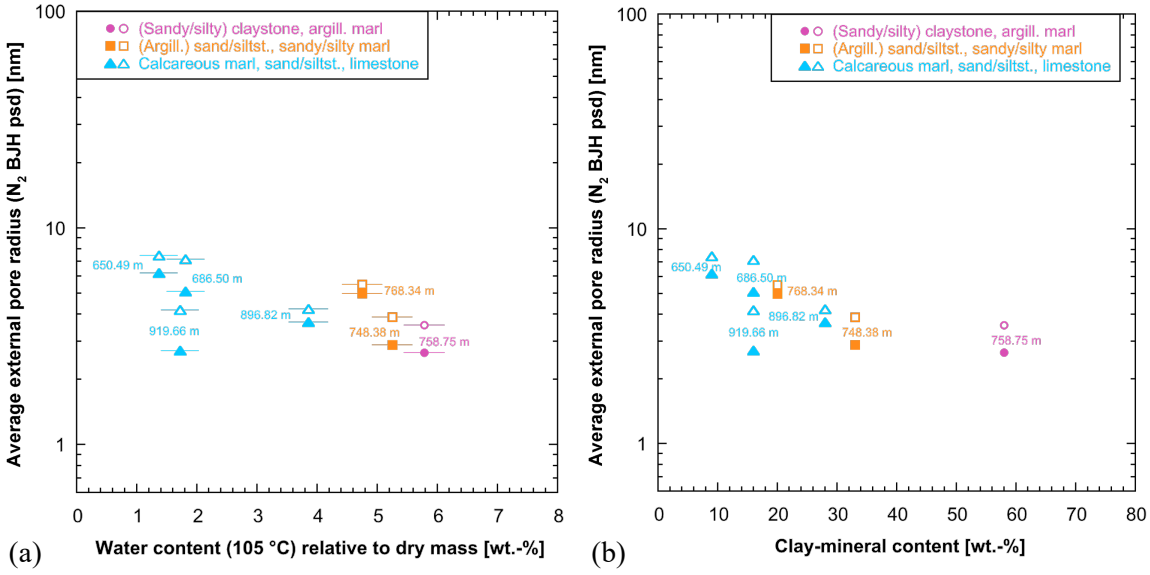


Fig. 4.3-21: Average external pore radius (assuming insignificant interlayer pore volume) based on the BJH pore size distribution from the $N_2$ isotherms (closed symbols: adsorption; open symbols: desorption) plotted against the gravimetric water content per dry mass of the samples (a) and against the total clay-mineral content (b)

Samples are grouped according to rock lithology. Error bars show estimated errors for the water content per dry mass (based on standard deviations of other samples)

## 4.4 Data from aqueous extraction tests

*Carmen Zwahlen*

Aqueous extraction (AqEx) tests are a simple but useful method to improve the understanding of the porewater – rock system across a sequence of sedimentary rocks if carried out at regular intervals. In this chapter, we present the data from aqueous extraction tests performed at a solid to liquid ratio of approximately 1. The data are discussed further in Chapter 5. The full dataset can be found in Appendix A, and details about the method are given in Waber (ed.) (2020).

### 4.4.1 Sample material and overview of analytical work

A total of 91 moisture-preserved drill core samples (PW, AD, SQ) from the Malm to the Zeglingen Formation were subjected to aqueous extraction tests. Additionally, the four SQ samples (cut-offs used for pre-characterisation) were also extracted after drying in order to compare the Cl and Br inventory pre and post drying.

Additionally, the chemical composition of the moisture-preserved samples, that includes analysis of cations, was used to model the mineral saturation states and the partial pressure of $CO_2$. These parameters were calculated with the PHREEQC Version 3 code (Parkhurst & Appelo 2013) and the PSI/Nagra thermodynamic database (Thoenen et al. 2014) assuming a temperature of 25 °C.

Tab. 4.4-1: Summary of analytical work performed on samples for aqueous extraction tests from the different geological formations (excluding duplicate and post-mortem extracts of AD and SQ experiments; *cf.* Sections 4.7.4 and 4.6.5)

Sample type: PW: porewater sample, AD: advective-displacement sample, SQ: squeezing sample, AqEx: aqueous extraction tests, *S/L*: solid to liquid ratio.

| **Group** | **Formation** | **Sample type** | **Lab** | **AqEx** at *S/L* 1, pH, Alkalinity, Anions only | **AqEx** at *S/L* 1, pH, Alkalinity, Anions & Cations |
|---|---|---|---|---|---|
| Malm | «Felsenkalke» + «Massenkalk» | PW | RWI | 8 | |
| Malm | Schwarzbach Formation | PW | RWI | 2 | |
| Malm | Villigen Formation | PW | RWI | 6 | |
| Malm | Wildegg Formation | PW | RWI | 6 | |
| Dogger | Variansm. Fm. + «Park.-Wütt.-Sch.» | PW | RWI | 1 | |
| Dogger | «Herrenwis Unit» | PW | RWI | 7 | 3 |
| Dogger | Wedelsandstein Formation | PW, AD, SQ | RWI | 4 | 2 |
| Dogger | «Murchisonae-Oolith Formation» | PW | RWI | 2 | |
| Dogger | Opalinus Clay | PW, AD, SQ | RWI | 19 | 4 |
| Lias | Staffelegg Formation | PW, AD, SQ | RWI | 6 | 2 |
| Keuper | Klettgau Formation | PW | RWI | 1 | 4 |
| Keuper | Bänkerjoch Formation | PW | RWI | | 6 |
| Muschelkalk | Schinznach Formation | PW | RWI | | 7 |
| Muschelkalk | Zeglingen Formation | PW | RWI | | 1 |
| **Total** | | **PW, AD, SQ** | **RWI** | **62** | **29** |

### 4.4.2 Aqueous extraction tests at a *S/L* of ~ 1

Ion concentrations in aqueous extracts have a limited significance if they are not recalculated to porewater concentrations. For cations possibly involved in reactions (ion exchange/sorption, dissolution/precipitation), this is not a simple task. For conservative anions, re-calculation to porewater concentrations can be based on the measured water content (leading to bulk porewater concentrations) or additionally corrected for anion exclusion (leading to concentrations in the anion-accessible porewater, here called 'free' porewater concentrations). For chemically conservative compounds, this recalculation is established in Chapter 5. Thus, in this section only ion ratios are presented, which are independent of the recalculation formalisms, as well as bulk porewater concentrations for Cl and Br.

#### 4.4.2.1 Contamination by drilling fluid

During sample preparation, approximately 1.5 cm of rim material was removed from the drill core samples to avoid contamination by the drilling fluid. However, in porous and permeable rocks such as e.g. dolostones or sandstones, the drilling fluid might reach the central parts of the drill core. This was already observed in a few samples from the BUL1-1, TRU1-1, MAR1-1 and BOZ1-1 boreholes (Mazurek et al. 2021, Aschwanden et al. 2021, Mäder et al. 2021, Wersin et al. 2022a).

The drilling fluid was a potassium silicate mud down to the upper part of the Schinznach Formation, a freshwater mud to the lower part of the Schinznach Formation and a NaCl drilling mud below (Tab. 2-4). The K-silicate drilling mud is highly alkaline, characterised by a high Si and K concentration (ca. 40 g/L Si, 70 g/L K, mostly balanced by OH), and only a small portion is required to significantly bias an aqueous extract.

In this borehole, we identified one sample at 723.96 m depth in the «Herrenwis Unit» that shows evidence for contamination by the K-silicate drilling fluid. This sample exhibits a high K concentration of 816 mg/L along with a low Na/K ratio of 0.5, which is difficult to reach through evolving marine porewater in the corresponding formation, or by later processes. This sample has an elevated alkalinity of 16.4 meq/L, a high pH of 9.9 and is highlighted with a red circle in all following figures.

#### 4.4.2.2 Anions

The Cl concentrations in the aqueous extracts range from 5.1 to 419 mg/L or 0.14 to 11.82 mmol/L and reach maximum values in the Zeglingen Formation (Figs. 4.4-1 and 4.4-7). The Br concentrations vary from 0.02 to 1.7 mg/L or 0.0003 to 0.0212 mmol/L with maximum values in the Bänkerjoch Formation (Figs. 4.4-1 and 4.4-8). More details on the Cl and Br bulk porewater concentrations are given in Section 4.4.3.

The depth profile of the Br/Cl ratio (Fig. 4.4-2) displays a trend with increasing Br/Cl ratios in the «Felsenkalke» + «Massenkalk» up to seawater ratios (although the scatter of the data is large) and remains close to seawater values down to the top of the Bänkerjoch Formation. All aqueous extracts from dry material (SQ) have systematically lower ratios compared to the corresponding wet extracts due to lower Br concentrations. This suggests that Br is not behaving conservatively after drying and that some Br is retained during subsequent extraction (e.g. binding with solid organic matter).

The Br/Cl ratios increase throughout the Bänkerjoch Formation. In the underlying Schinznach Formation the scatter in the data is large and no clear trends are evident. This might be due to variable contributions of fluid inclusions. During sample preparation, some fluid inclusion-rich crystals may break and mix with the porewater. This addition of fluid inclusions results in a higher Br/Cl ratio as shown for the STA2-1 borehole (Zwahlen et al. *in prep.*). The Br/Cl ratio of the sample from the Zeglingen Formation forms a minimum and fits well with the measured rock salt.

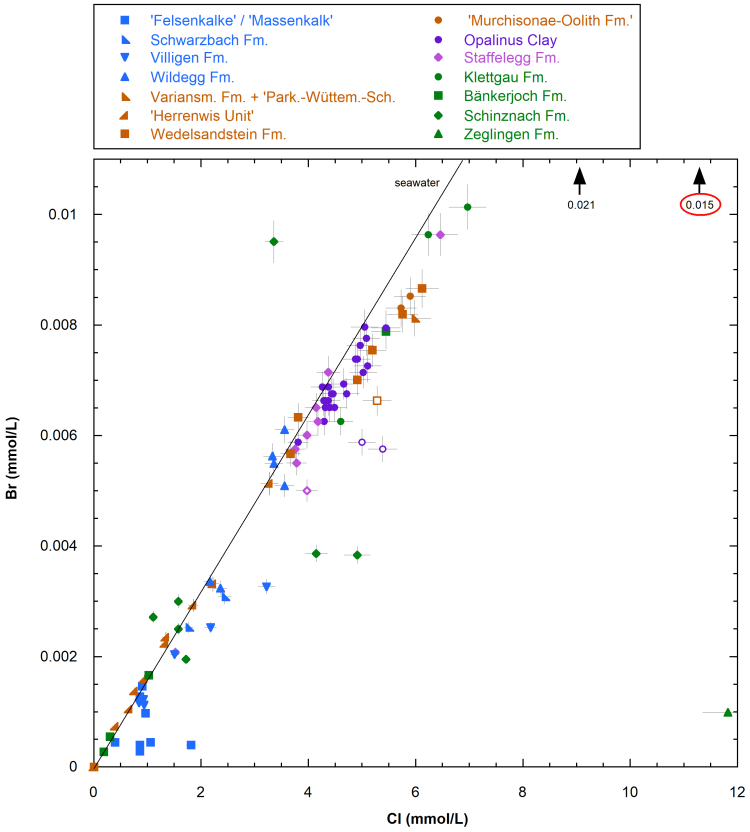


Fig. 4.4-1: Molar Br versus Cl concentrations in aqueous extracts at a *S/L* ratio of about 1

Empty symbols mark dry aqueous extracts of SQ samples. The sample with contamination by the drilling fluid is circled in red. The black arrows indicate samples that do not fit on the axes.

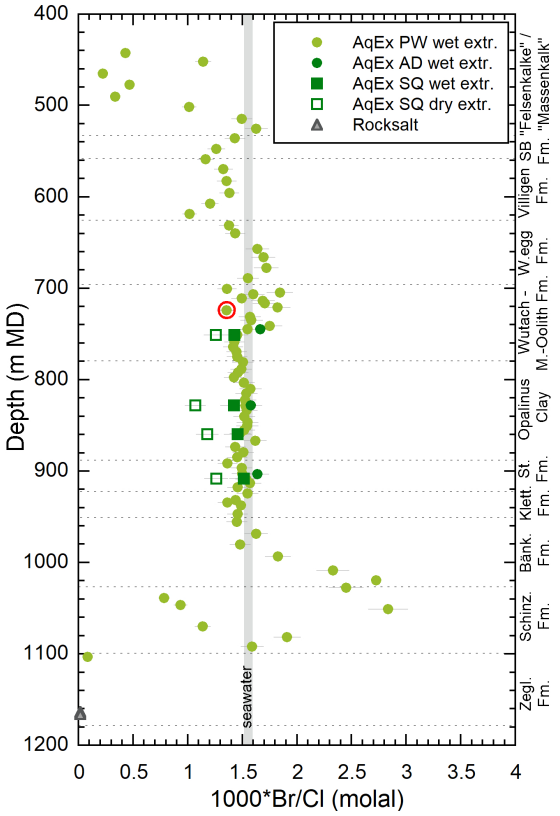


Fig. 4.4-2: Depth profile of the molar Br/Cl ratio in aqueous extracts at a *S/L* ratio of about 1
The sample with contamination by the drilling fluid is circled in red.

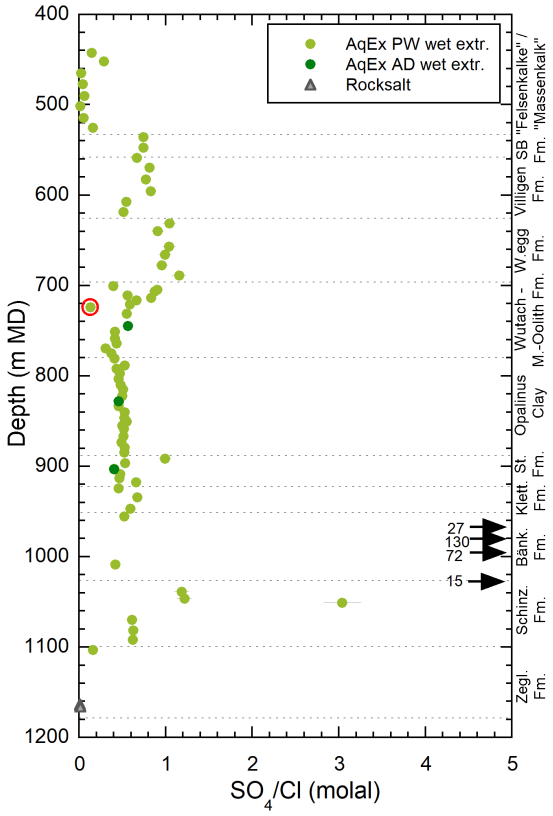


Fig. 4.4-3: Depth profile of $SO_4$/Cl molar concentration ratio in aqueous extracts at a *S/L* ratio of about 1

The sample with contamination by the drilling fluid is circled in red. The black arrows indicate samples that do not fit on the axes.

The $SO_4$ concentration varies between 1.4 and 397 mg/L with the exception of 8 anhydrite-bearing samples in the Bänkerjoch and Schinznach Formations where concentrations of 484 to 2'658 mg/L are reached, clearly a result of sulphate dissolution. The depth profile of the $SO_4$/Cl ratio in aqueous extract solutions presents low values in the «Felsenkalke» + «Massenkalk» and jumps to values close to 1 in the Schwarzbach, Villigen and Wildegg Formations (Fig. 4.4-3). The ratios decrease to around 0.5 across the «Brauner Dogger» and remain at this value down to the base of the Schinznach Formation except for one outlier in the top of the Staffelegg Formation and for the anhydrite-bearing samples in the Bänkerjoch Formation and the upper part of the Schinznach Formation, which show much higher $SO_4$/Cl ratios. The dolostone sample from the Zeglingen Formation exhibits a very low ratio, in agreement with the rock salt sample at the base of the Zeglingen Formation.

The F concentrations in aqueous extracts range between 0.3 and 6.9 mg/L across the whole depth profile (not shown) with the highest values in the «Herrenwis Unit», Variansmergel Formation and «Parkinsoni-Wüttembergica-Schichten». The $NO_3$ concentrations are between 0.08 and 0.7 mg/L with the maximum value reached in the Schinznach Formation. The alkalinity varies between 0.4 and 5.9 meq/L, disregarding the contaminated sample (16.4 meq/L). The pH (not shown) scatters from the «Felsenkalke» + «Massenkalk» to the top of the Bänkerjoch Formation between 8.0 and 9.6 with two pH values of 9.9 in the «Herrenwis Unit». In the Bänkerjoch, Schinznach and Zeglingen Formations, the pH values shift to lower values around between 7.2 and 8.2 with one outlier of 8.6 in the Bänkerjoch Formation.

### 4.4.2.3 Cations

The Na concentrations in the aqueous extracts vary between 24 and 447 mg/L with maximum values reached in the Bänkerjoch Formation. The Na/Cl ratios of the depth profile (Fig.4.4-4) show little variability from the Dogger to the top of the Bänkerjoch Formation beside two outliers in the «Herrenwis Unit» (one being contaminated with drilling fluid). The ratios reach a maximum in the centre of the Bänkerjoch Formation before dropping down to ratios around 1 from the bottom of the Bänkerjoch to the top of the Zeglingen Formation, which is in agreement with the ratios measured in the rock salt in the lower Zeglingen Formation.

The K concentrations range from 2.1 mg/L up to maximum values of 24.9 mg/L in the Bänkerjoch and Schinznach Formation, disregarding the contaminated sample with concentrations of 816 mg/L. The Na/K ratios sharply increase in the «Brauner Dogger», are nearly constant in the Opalinus Clay and reach maximum values in the Klettgau and top Bänkerjoch Formation (Fig. 4.4-5). The AD data plot close to neighbouring PW samples.

The Sr concentrations range from 0.05 to 7.4 mg/L with maximum values reached in the Bänkerjoch Formation. The Sr/Cl ratios plot in a narrow range of low ratios from the Dogger to the Zeglingen Formation with distinctly higher values reached in the Bänkerjoch Formation and the upper part of the Schinznach Formation (Fig. 4.4-6). These high values can be explained by the release of Sr from the dissolution of anhydrite or celestite during aqueous extraction. Celestite was detected by XRD in two of the anhydrite-bearing samples in the Bänkjoch Formation (at 980 m and 968 m depth).

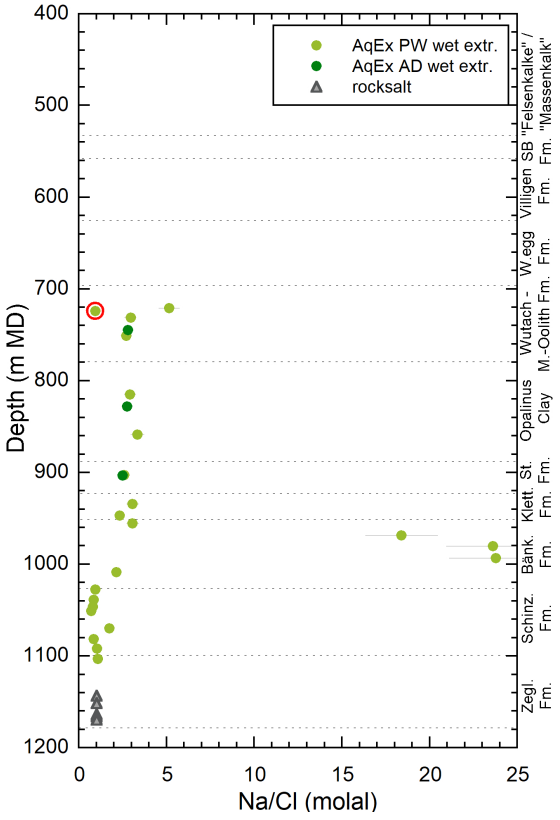


Fig. 4.4-4: Depth profile of the Na/Cl molar concentration ratio in aqueous extracts at a *S/L* ratio of about 1

The sample with contamination by the drilling fluid is circled in red.

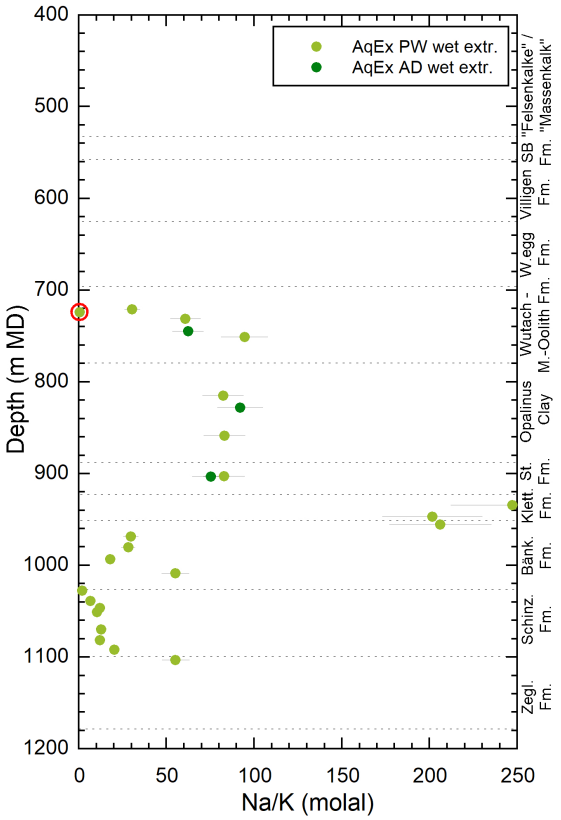


Fig. 4.4-5: Depth profile of the Na/K molar concentration ratio in aqueous extracts at a *S/L* ratio of about 1

The sample with contamination by the drilling fluid is circled in red.

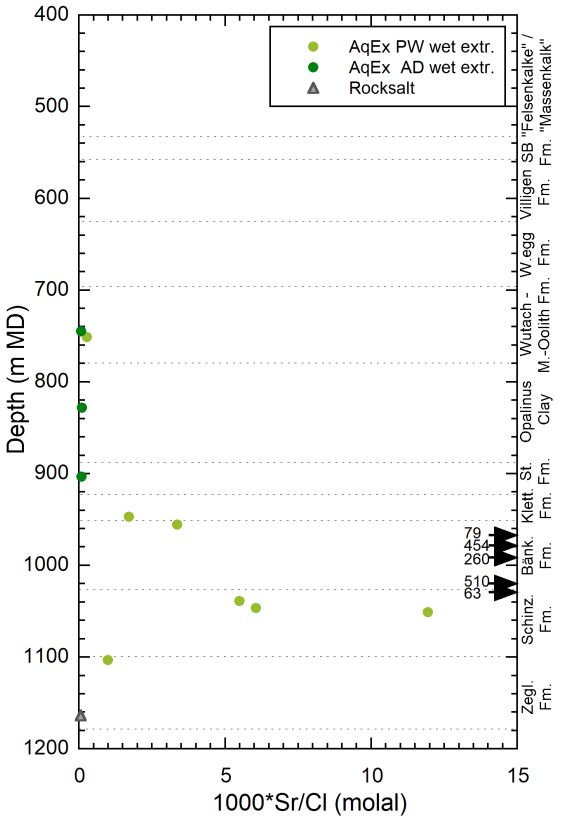


Fig. 4.4-6: Depth profile of the Sr/Cl molar concentration ratio in aqueous extracts at a *S/L* ratio of about 1

The black arrows indicate samples that do not fit on the axes.

### 4.4.2.4 Saturation indices

The saturation indices of calcite and dolomite of the aqueous extract solutions vary across the different formations (Tab. 4.4-2). In the «Herrenwis Unit» the solutions are saturated or oversaturated with respect to calcite and dolomite (ordered). The samples from the Wedelsandstein to the Zeglingen Formation are more diverse with half of the samples reaching saturation with respect to calcite (SI -0.9 to 0.6) but only some of those are also saturated with respect to dolomite (SI -3 to 1.5). Calcite oversaturation is expected for anhydrite-bearing samples where dissolution of Ca-sulphate is producing excess Ca that cannot be precipitated as calcite sufficiently fast. Most considerably undersaturated samples with respect to calcite contain detectable amounts of calcite. This might be caused by partial calcite dissolution during the aqueous extraction leading to a $pCO_2$ level below atmospheric concentrations and a subsequent decrease in pH due to $CO_2$ equilibration during filtration and titration.

The sulphate minerals gypsum, anhydrite and celestite are undersaturated by 1 to 3 orders of magnitude in all extract solutions with the exception of 4 samples from the Bänkerjoch Formation. These samples contain 54 to 85 wt% anhydrite, are saturated with respect to gypsum and not far from saturation with respect to anhydrite and celestite. Dolomite and celestite saturation indices are missing for some samples because the Mg and Sr concentrations are below the detection limit.

Tab. 4.4-2: Saturation indices for calcite, dolomite (disordered and ordered), gypsum, anhydrite and celestite at a *S/L* ~ 1, pH and partial pressure of $CO_2$

Mineral saturation indices were calculated with the PHREEQC Version 3 code (Parkhurst & Appelo 2013) and the PSI/Nagra thermodynamic database (Thoenen et al. 2014) assuming a temperature of 25 °C. Fm stands for Formation, He for «Herrenwis Unit», We for Wedelsandstein Formation, Opa for Opalinus Clay, Sta for Staffelegg, Kl for Klettgau, Bä for Bänkerjoch, Sch for Schinznach and Ze for Zeglingen Formations, *S/L* for solid/liquid, SI for saturation index, Cc for Calcite, Do for Dolomite ordered or disordered, Gy for gypsum, An for Anhydrite and Ce for Celestite. Empty cells in the SI Do and SI Ce columns are due to concentrations below the detection limit for Mg or Sr, respectively.

| **Fm.** | **Depth** [m] | ***S/L*** | **SI Cc** | **SI Do (dis)** | **SI Do (ord)** | **SI Gy** | **SI An** | **SI Ce** | **pH** | **$\log_{10} P_{CO2}$** [bar] |
|---|---|---|---|---|---|---|---|---|---|---|
| He | 721.0 | 0.91 | 0.23 | -0.32 | 0.23 | -3.72 | -3.95 | | 9.86 | -5.01 |
| He | 731.1 | 0.92 | 0.05 | -0.52 | 0.03 | -2.84 | -3.07 | | 9.05 | -3.91 |
| We | 744.9 | 0.97 | 0.06 | -0.95 | -0.40 | -2.76 | -2.98 | -2.81 | 9.05 | -3.91 |
| We | 751.1 | 0.90 | -0.28 | -1.39 | -0.84 | -2.77 | -2.99 | -2.44 | 8.50 | -3.17 |
| Opa | 815.2 | 0.97 | -0.41 | | | -2.69 | -2.91 | | 8.29 | -2.94 |
| Opa | 827.9 | 0.90 | 0.08 | -0.70 | -0.15 | -2.79 | -3.01 | -2.56 | 8.87 | -3.49 |
| Opa | 859.0 | 0.92 | -0.37 | -1.58 | -1.03 | -2.60 | -2.82 | | 8.06 | -2.54 |
| Sta | 902.7 | 0.91 | 0.17 | | | -2.88 | -3.10 | | 9.11 | -3.91 |
| Sta | 903.4 | 0.93 | -0.22 | -1.22 | -0.67 | -2.94 | -3.16 | -2.78 | 8.78 | -3.57 |
| Kl | 931.7 | 0.92 | 0.07 | -0.28 | 0.27 | -2.51 | -2.73 | -1.40 | 8.66 | -3.34 |
| Kl | 934.4 | 0.89 | 0.04 | -0.37 | 0.18 | -2.33 | -2.55 | | 8.61 | -3.36 |
| Kl | 937.6 | 0.94 | 0.50 | 0.66 | 1.21 | -2.36 | -2.58 | -1.06 | 8.98 | -3.77 |
| Kl | 947.0 | 0.89 | -0.32 | -1.18 | -0.63 | -2.03 | -2.26 | -1.30 | 8.46 | -3.61 |
| Bä | 955.4 | 0.90 | 0.61 | 0.92 | 1.47 | -2.33 | -2.55 | -1.27 | 8.94 | -3.50 |
| Bä | 968.4 | 0.95 | -0.50 | -2.46 | -1.91 | 0.13 | -0.09 | -0.17 | 7.18 | -2.85 |
| Bä | 980.2 | 0.98 | 0.35 | -1.53 | -0.98 | 0.19 | -0.04 | -0.18 | 7.82 | -3.40 |
| Bä | 993.2 | 0.95 | 0.00 | -2.39 | -1.84 | 0.11 | -0.11 | -0.21 | 7.71 | -3.47 |
| Bä | 1'008.6 | 0.89 | -0.06 | -0.90 | -0.35 | -2.30 | -2.52 | | 8.61 | -3.44 |
| Bä | 1'019.4 | 0.98 | -0.20 | -2.95 | -2.40 | 0.13 | -0.09 | -0.25 | 7.41 | -3.09 |
| Sch | 1'027.8 | 0.94 | 0.02 | -0.87 | -0.32 | -0.11 | -0.33 | -0.32 | 7.39 | -2.69 |
| Sch | 1'038.7 | 0.84 | 0.06 | -0.38 | 0.17 | -0.83 | -1.05 | -0.94 | 7.63 | -2.76 |
| Sch | 1'046.2 | 0.91 | -0.11 | -0.56 | -0.01 | -0.98 | -1.20 | -1.00 | 7.55 | -2.67 |
| Sch | 1'050.8 | 0.96 | 0.08 | -0.49 | 0.06 | -0.44 | -0.67 | -0.65 | 7.47 | -2.63 |
| Sch | 1'069.8 | 0.96 | -0.47 | -1.06 | -0.51 | -2.17 | -2.39 | | 7.76 | -2.77 |
| Sch | 1'081.6 | 0.97 | -0.90 | -2.19 | -1.64 | -1.98 | -2.20 | | 7.47 | -2.83 |
| Sch | 1'091.7 | 0.96 | -0.85 | -1.55 | -1.00 | -2.36 | -2.58 | | 7.74 | -2.94 |
| Ze | 1'103.2 | 0.91 | -0.06 | -0.23 | 0.32 | -1.90 | -2.12 | -1.63 | 8.22 | -3.39 |

### 4.4.3 Chloride and bromide concentrations in bulk porewater

The formalisms to recalculate Cl and Br concentrations in aqueous extracts to concentrations in bulk porewater are given in Waber (ed.) (2020). In clay-free rocks, this recalculation to bulk water content delivers the transport relevant porewater concentrations of Cl and Br directly. In clay-bearing rocks, the anion-exclusion effect has to be considered in the re-calculation of 'free' porewater concentrations. The derivation of the Cl and Br accessible porosity proportion and calculation of 'free' porewater concentrations is established in Chapter 5.

The recalculation of Cl and Br concentrations in aqueous extracts to concentrations in bulk porewater (Figs. 4.4-7 and 4.4-8) requires the knowledge of the water content of the rocks, which is obtained by calculating the average of three gravimetric water contents (one regular sample and two subsamples used for diffusive-exchange experiments; Section 4.3). Additional aqueous extraction tests were carried out on 4 dried water content subsamples (SQ) from the Dogger to the Lias in order to compare the concentration between dry and wet extracts.

The depth profiles of Cl and Br concentrations in bulk porewater cover a large range of 480 to 39'553 mg/L and 1.9 to 42 mg/L, respectively (Figs. 4.4-7 and 4.4-8). In the Br profile, the four aqueous extracts conducted on dried rock material show lower concentrations compared to the wet extracts. No such difference between dry and wet extracts is seen in the Cl data. The differences for Br may be related to drying process (e.g., attachment to organic matter), but this is not proven at this stage.

Both, the Cl and Br concentrations, show considerable scatter in the «Felsenkalke» + «Massenkalk», Villigen Formation and «Herrenwis Unit». The samples from the «Felsenkalke» + «Massenkalk» show signs of desaturation which equates to an underestimation of the water content and hence to an overestimation of the ion concentrations (see Fig. 4.3-10). The high values in the «Herrenwis Unit» might be overestimated due to contributions from fluid inclusions. The Villigen Formation forms a sharp positive excursion between the overlying Schwarzbach and the underlying Wildegg Formation, which both show distinctly lower and similar Cl concentrations of around 4 g/L. There is a general decreasing trend from the «Murchisonae-Oolith Formation» down to the base of the Opalinus Clay (Figs. 4.4-7 and 4.4-8). There is a sharp jump to higher concentrations in the top of the Staffelegg Formation with subsequent decrease to values slightly lower than at the base of the Opalinus Clay. There is substantial scatter in the Klettgau Formation. The Br and Cl concentrations decrease in the Bänkerjoch Formation and reach the lowest values of the profile before increasing again in the bottom of the Bänkerjoch Formation down to the top of the Zeglingen Formation (with a few of outliers showing higher concentrations). The sample in the Zeglingen Formation has a higher Cl and lower Br concentration than expected from the trend set out in the lower Bänkerjoch Formation. This might be related to an input from salt dissolution, which would yield higher Cl but lower Br concentrations in agreement with the observation in the Br/Cl ratio (Fig. 4.4-2).

At this stage, these observed trends should be treated with care because the recalculated Cl and Br concentrations still need to be corrected for anion accessibility, which is further investigated in Chapter 5.

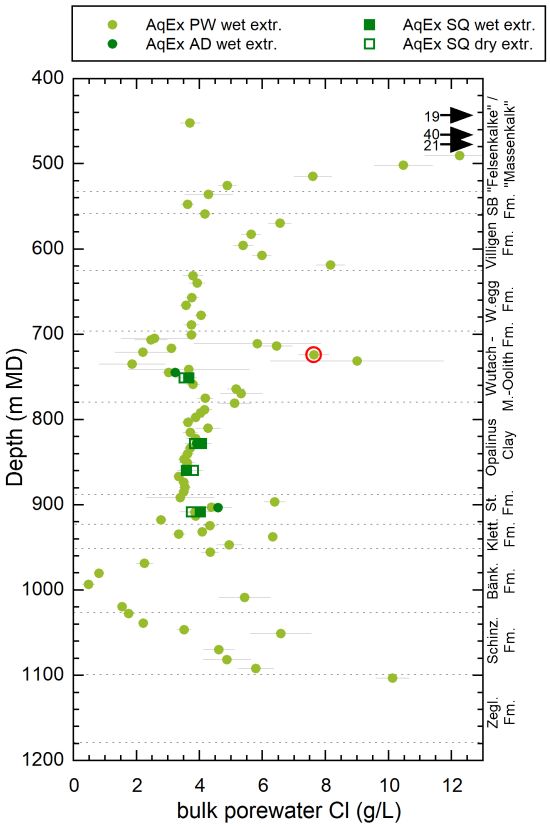


Fig. 4.4-7: Bulk porewater Cl concentrations versus depth from aqueous extracts of PW, AD and SQ samples

The sample with contamination by the drilling fluid is circled in red. The black arrows indicate samples that do not fit on the axes.

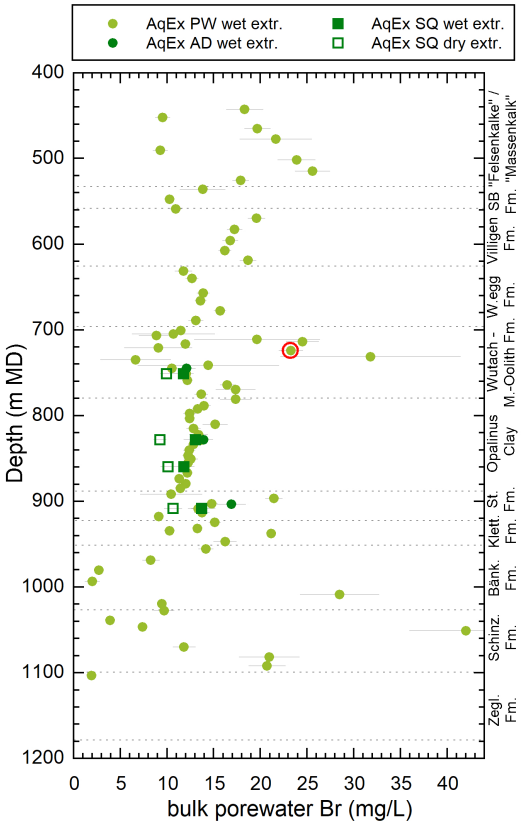


Fig. 4.4-8: Bulk porewater Br concentrations versus depth from aqueous extracts of PW, AD and SQ samples

The sample with contamination by the drilling fluid is circled in red.

### 4.4.4 Cl-isotopes in AqEx solutions

The stable isotopes signature of Cl in aqueous extract solutions, expressed as $\delta^{37}Cl$ relative to the SMOC standard, carries information about the origin of Cl. Thus, Cl isotope ratios may be used to some degree to discern the origin of Cl between seawater and rock salt dissolution. Over long periods of time, however, Cl-isotopes fractionate through Cl diffusion across low-permeability rocks (e.g., Gimmi & Waber 2004).

In the «Felsenkalke» + «Massenkalk», Schwarzbach and Villigen Formations, the $\delta^{37}Cl$ values of aqueous extract solutions scatter between -2 and -1.4 ‰ (Fig. 4.4-9). In the Wildegg Formation the $\delta^{37}Cl$ value increases sharply to a much higher value of -0.2‰ which is close to modern seawater values. Subsequently, there is a large spread in values in the «Herrenwis Unit» as observed in the bulk porewater profiles, continued by an increasing trend towards the top of the Opalinus Clay. The two high values from the Wildegg Formation (710.87 m) and «Herrenwis Unit» (720.97 m) are close to seawater values and might be influenced by fluid inclusions which record a marine signal. There is little variation from the top of the Opalinus Clay to the top of the Bänkerjoch Formation, which contrasts the trends seen in the bulk porewater profiles where sharp gradients are observed in the Staffelegg and Klettgau Formations. From the top of the Bänkerjoch Formation there is a continuous increasing trend down to the top of the Zeglingen Formation with some values exceeding rock salt values measured in the Zeglingen Formation.

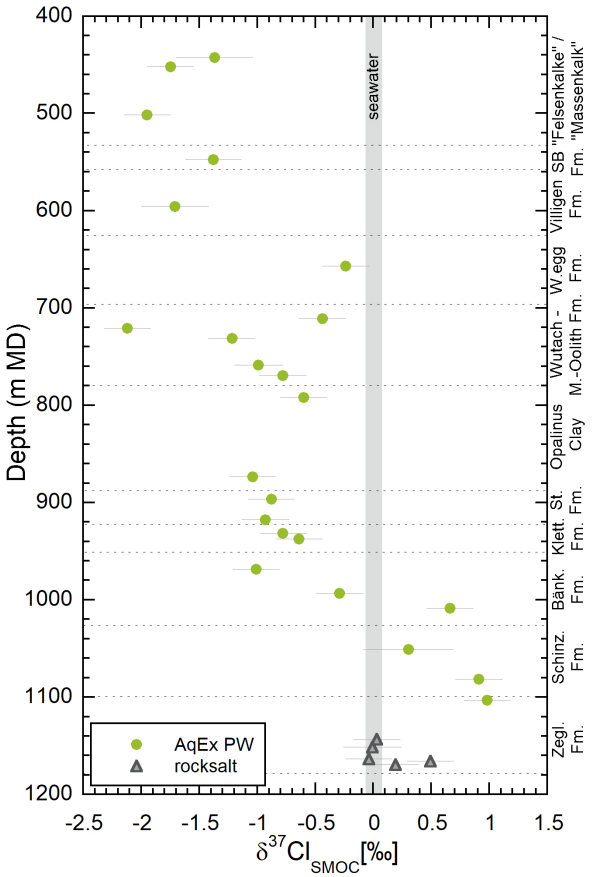


Fig. 4.4-9: Cl isotopes, expressed as $\delta^{37}Cl$, in AqEx solutions of rocks vs. depth from the Malm to the Muschelkalk and in rock salt samples from the Zeglingen Formation

## 4.5 Cation-exchange extraction data

*Paul Wersin*

Three samples used for advective-displacement experiments (AD samples) were analysed at Uni Bern with the nickel ethylenediamine (Ni-en) extraction method to determine the cation exchange capacity (CEC) and the composition of the clay exchanger (for methodology see Waber ed. 2020). Material from end pieces above and below the AD core was mixed to obtain a representative sample for Ni-en extraction. A larger number of samples were studied by the team at PSI using the CsCl extraction method (see Section 5.6 and Marques Fernandes & Baeyens *in prep.*). The objective of the Ni-en extraction study was (i) to help to analyse the AD data (Section 4.7) and (ii) to compare and verify the PSI study with an alternative method.

The CEC can be derived in two ways: (1) from the consumption of the index cation (Ni in this case) during extraction and (2) from the sum of extracted cations (ΣCAT). Note that the latter includes (i) the exchangeable cations, (ii) cations dissolved in the porewater and (iii) cations released from potentially dissolving minerals (e.g. carbonates, sulphates) during extraction, but (iv) misses any cations not analysed. Thus, in principle, the CEC derived from the sum of cations requires correction from contributions of (ii), (iii) and potentially (iv). Corrected CEC and

exchangeable cation data are discussed in Section 5.6, where the data from Uni Bern is also compared with that of PSI. The analysis does not include ammonium, $NH_4^+$, known to be present in small but usually measurable amounts (e.g., ~ 1.7 mg/L in aqueous extracts, at *S/L* ≈ 1, Appendix A).

Tab. 4.5-1 shows the Ni consumption and extracted cation data (Na, K, Ca, Mg, Sr, Ba) for solid/liquid ratios (*S/L*) around 1[8]. Anion data (F, Cl, Br, $SO_4$, $NO_3$) is depicted in Tab. 4.5-2. Note that Ni nitrate was added to the samples, which explains the high $NO_3$ contents.

Tab. 4.5-1: Cation data from Ni-en extracts at a *S/L* ratio near 1 (Uni Bern data)

Fe content: < 0.001 mg/kg

| Type | Depth | Formation | *S/L* | Na | K | Ca | Mg | Sr | Ba | ΣCAT | Ni cons. |
|---|---|---|---|---|---|---|---|---|---|---|---|
| | [m] | | [g/g] | [meq/kg] | | | | | | | |
| AD | 744.88 | Wedelsandstein | 0.888 | 60.2 | 6.0 | 40.0 | 14.2 | 0.6 | 0.003 | 121.1 | 121.5 |
| AD | 827.93 | Opalinus Clay | 0.890 | 60.3 | 5.0 | 31.4 | 11.3 | 0.5 | 0.008 | 108.5 | 111.1 |
| AD | 903.38 | Staffelegg | 0.909 | 39.2 | 4.2 | 21.8 | 7.1 | 0.4 | 0.021 | 72.7 | 70.0 |

Tab. 4.5-2: Anion data from Ni-en extracts at a *S/L* ratio near 1 (Uni Bern data)

| Type | Depth | Formation | *S/L* | F | Cl | Br | $NO_3$ [a] | $SO_4$ |
|---|---|---|---|---|---|---|---|---|
| | [m] | | [g/g] | [meq/kg] | | | | |
| AD | 744.88 | Wedelsandstein | 0.888 | 0.014 | 4.0 | 0.007 | 223.5 | 3.3 |
| AD | 827.93 | Opalinus Clay | 0.890 | 0.007 | 5.2 | 0.008 | 225.2 | 3.3 |
| AD | 903.38 | Staffelegg | 0.909 | 0.019 | 4.6 | 0.007 | 223.3 | 2.9 |

[a] Nitrate is part of the added Ni-en stock solution

The CEC derived from Ni consumption of the three AD samples lies in the range of 70 – 122 meq/$kg_{rock}$ and is very similar to the uncorrected sum of cations (73 – 121 meq/$kg_{rock}$).

The depth profiles of Ni consumption and ΣCAT data suggest a decreasing trend with depth (Fig. 4.5-1) but note that this trend is based on only three samples. No trend with clay-mineral content for the three samples, which vary between 30 and 52 wt.-%, is indicated (Fig. 4.5-2). This is further discussed in Section 5.6.

Na and Ca are the main extracted cations, followed by Mg and K (Tab. 4.5-1). The molar Ca/Na ratio is about 0.55 for the two lower samples from the OPA and Staffelegg Formation and slightly higher for the Wedelsandstein Formation sample (0.66). Mg correlates with Ca, thus the same trend is noted for the (Ca+Mg)/Na ratios (Fig. 4.5-3).

[8] A solution mass equal to the mass of the wet rock was added, leading to *S/L* (mass of dry rock / [mass of added solution + porewater]) slightly below 1.

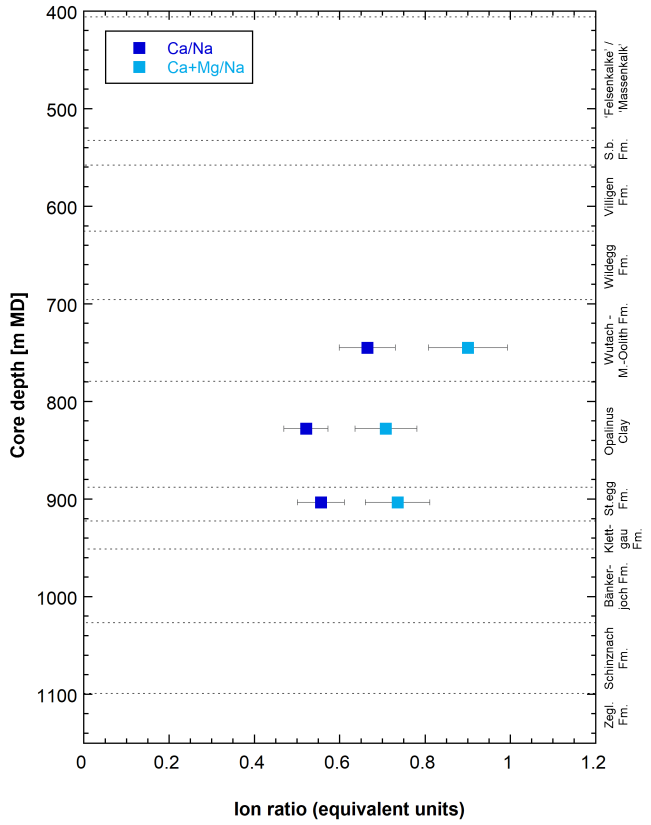


Fig. 4.5-1: Depth profile of Ni consumption and sum of cations (uncorrected, Uni Bern data)
Errors reflect propagated analytical uncertainties.

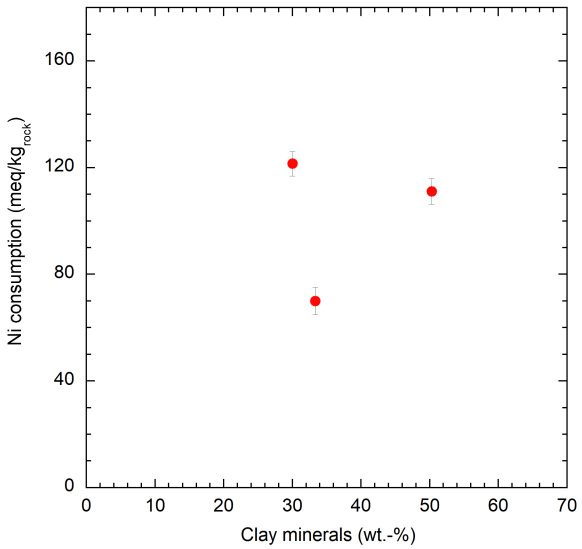


Fig. 4.5-2: Ni consumption vs. clay-mineral content (Uni Bern data)

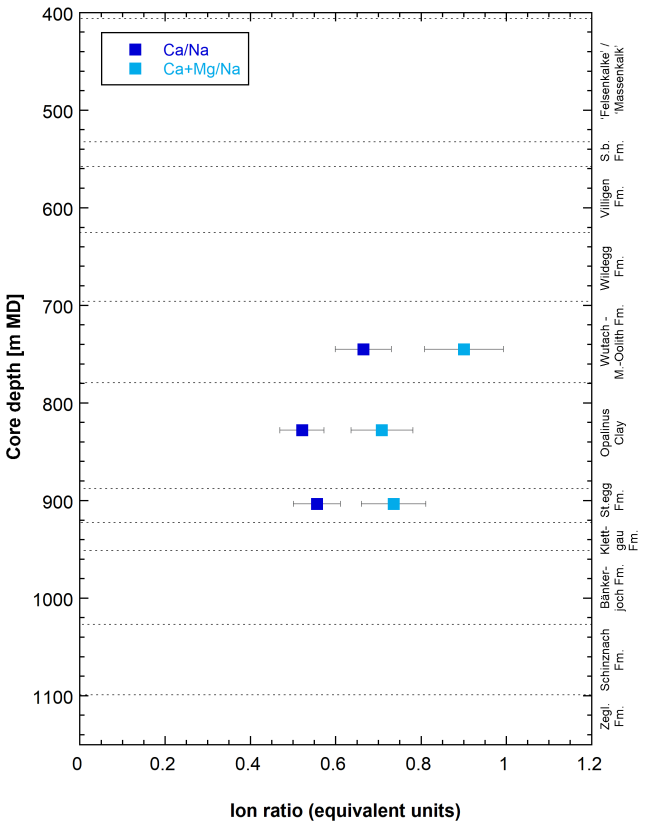


Fig. 4.5-3: Depth profiles of Ca/Na and (Ca+Mg)/Na ratios in Ni-en extracts (Uni Bern data)

Errors reflect propagated analytical uncertainties.

Speciation calculations on the Ni-en extracts were carried out with the PHREEQC Version 3 code (Parkhurst & Appelo 2013) and the PSI/Nagra thermodynamic database (Thoenen et al. 2014) assuming a temperature of 25 °C. The ethylene diamine complexes were taken from the MINTEC database (Allison et al. 1991) and are included in the calculations. The concentration of ethylene diamine in the extracts, which was not analysed, was constrained by charge balance. The dissolved carbonate concentration (not measured) was constrained by assuming calcite equilibrium. The calculated TIC values are low, in the range of 0.09 – 0.14 mM (Tab. 4.5-3). The calculated partial pressures of $CO_2$ ($pCO_2$) and saturation indices for selected minerals are depicted in Tab. 4.5-3. The Ni-en extracts are clearly undersaturated with regard to the carbonate minerals dolomite and strontianite. They are also undersaturated with regard to the sulphate minerals gypsum and celestite, but either close to saturation or oversaturated with regard to barite.

Tab. 4.5-3: Calculated saturation indices of selected minerals, TIC log($pCO_2$) for Ni-en extract solutions

Calcite saturation was assumed in the calculations.

| Type | Depth [m] | Formation | Log ($P_{CO2}$) [bar] | TIC [mmol/$kg_w$] | Gypsum | Celestite | Barite | Dolomite (ord) | Dolomite (dis) | Strontianite |
|---|---|---|---|---|---|---|---|---|---|---|
| AD | 744.88 | Wedelsandst. Fm. | -4.81 | 0.094 | -1.25 | -1.01 | 0.03 | -0.32 | -0.87 | -1.02 |
| AD | 827.93 | Opalinus Clay | -4.55 | 0.138 | -1.32 | -1.05 | 0.46 | -0.32 | -0.87 | -0.99 |
| AD | 903.38 | Staffelegg Fm. | -4.65 | 0.142 | -1.48 | -1.17 | 0.90 | -0.36 | -0.91 | -0.96 |

## 4.6 Data from squeezing experiments

*Martin Mazurek*

A small set of 4 samples from the interval Wedelsandstein-Formation – Staffelegg Formation were subjected to porewater squeezing. Photographs of the core samples are shown in Fig. 4.6-1. The mineralogical composition of the samples is listed in Tab. 4.6-1. Clay-mineral contents are ≥ 44 wt.-% for all samples.

Tab. 4.6-1: Mineralogical composition of samples subjected to squeezing experiments

Empty field = mineral not identified, "tr" = trace.

| Depth [m] | Formation | Member | S [wt.-%] | C(inorg) [wt.-%] | C(org) [wt.-%] | Quartz [wt.-%] | K-feldspar [wt.-%] | Plagioclase [wt.-%] | Calcite [wt.-%] | Dolomite / Ank. [wt.-%] | Siderite [wt.-%] | Magnesite [wt.-%] | Anhydrite [wt.-%] | Pyrite [wt.-%] | Clay minerals [wt.-%] |
|---|---|---|---|---|---|---|---|---|---|---|---|---|---|---|---|
| 750.86 | Wedelsandstein Fm. | | 0.2 | 1.8 | 0.6 | 24 | 3 | 3 | 13 | | 2 | | | 0.4 | 54 |
| 828.13 | Opalinus Clay | 'Mixed clay-silt-carbonate sub-unit' | < 0.1 | 1.5 | 0.9 | 25 | 3 | 3 | 8 | | 5 | | | < 0.1 | 55 |
| 859.37 | Opalinus Clay | 'Mixed clay-silt-carbonate sub-unit' | 0.1 | 1.2 | 1.0 | 20 | 2 | 3 | 6 | | 5 | | | 0.2 | 63 |
| 908.31 | Staffelegg Fm. | Frick Mb. | 0.2 | 1.2 | 0.7 | 39 | 2 | 3 | 8 | 2 | tr | | | 0.4 | 44 |

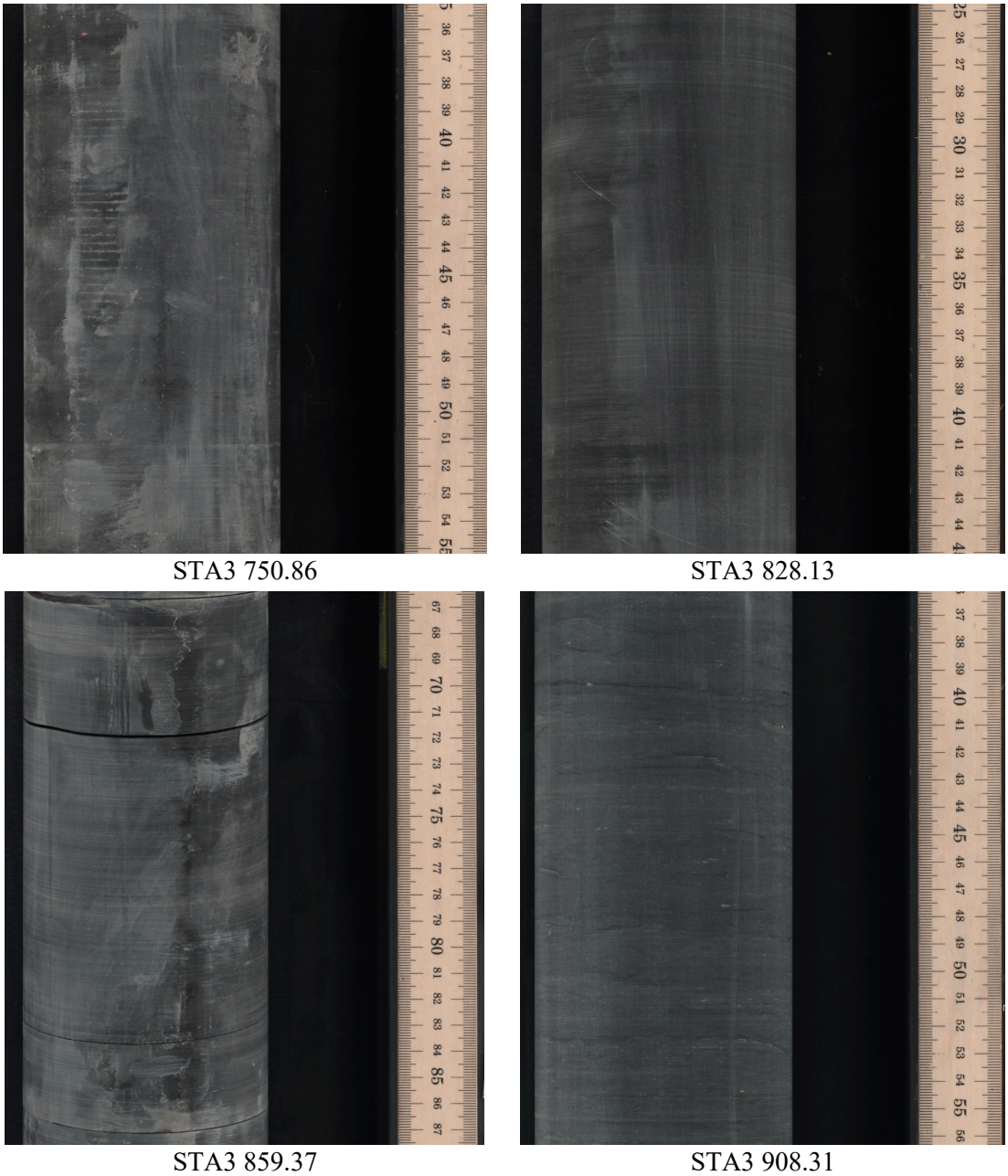

STA3 750.86 STA3 828.13

STA3 859.37 STA3 908.31

Fig. 4.6-1: Photographs of core samples subjected to squeezing

### 4.6.1 Mass recovery

The water masses obtained by squeezing are listed in Tab. 4.6-2 and shown graphically in Fig. 4.6-2 as a function of the squeezing pressure. Given the small number of samples, a correlation between the initial water content of the sample and the total mass recovery, as observed in other squeezing campaigns, is not well established (Fig. 4.6-3). Samples yielded first water aliquots at 200 MPa, except for the sample from the Staffelegg Formation where 500 MPa were required to extract porewater. Given the fact that for 3 samples a sufficient water mass was obtained in the pressure range 200 – 300 MPa, the experiments were terminated at this pressure, i.e. no waters were squeezed at higher pressures.

Tab. 4.6-2: Water masses squeezed at different pressure steps

The initial water content was reconstructed on the basis of the measured water content of the squeezed sample and the squeezed water mass (see Section 4.6.5), and this value was then used to calculate the initial mass of porewater in the sample. "-": pressure step not applied.

| **Depth** [m] | **Formation** | **Initial sample mass (CRIEPI)** [g] | **Initial wet water content** [wt.-%] | **Mass of porewater prior to squeezing** [g] | **Mass squeezed at P =** | | | | | | **Total mass squeezed** [g] |
|---|---|---|---|---|---|---|---|---|---|---|---|
| | | | | | **100 MPa** [g] | **150 MPa** [g] | **200 MPa** [g] | **300 MPa** [g] | **400 MPa** [g] | **500 MPa** [g] | |
| 750.86 | Wedelsandstein Fm. | 353.16 | 5.020 | 17.73 | 0 | - | 1.50 | 1.35 | - | - | 2.85 |
| 828.13 | Opalinus Clay | 381.91 | 4.655 | 17.78 | 0 | - | 1.21 | 1.76 | - | - | 2.97 |
| 859.37 | Opalinus Clay | 377.15 | 4.367 | 16.47 | 0 | - | 1.11 | 1.47 | - | - | 2.58 |
| 908.31 | Staffelegg Fm. | 349.65 | 3.324 | 11.62 | 0 | - | 0 | 0 | 0 | 1.12 | 1.12 |

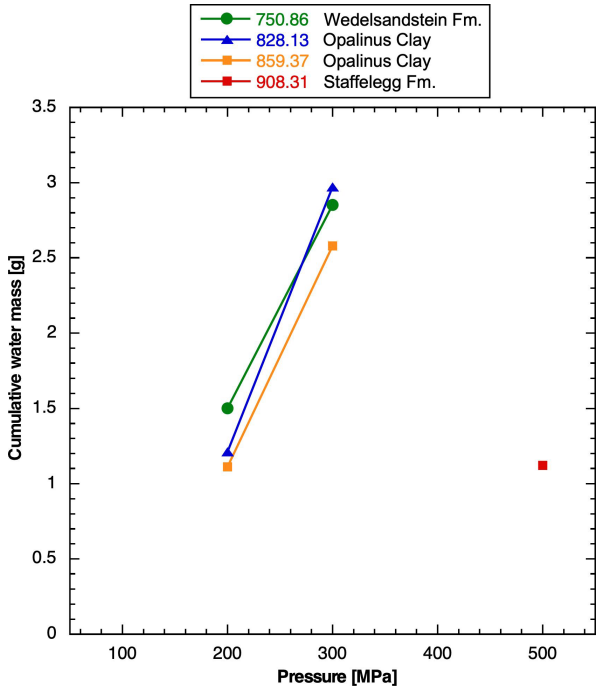


Fig. 4.6-2: Cumulative water masses obtained by squeezing as a function of the squeezing pressure

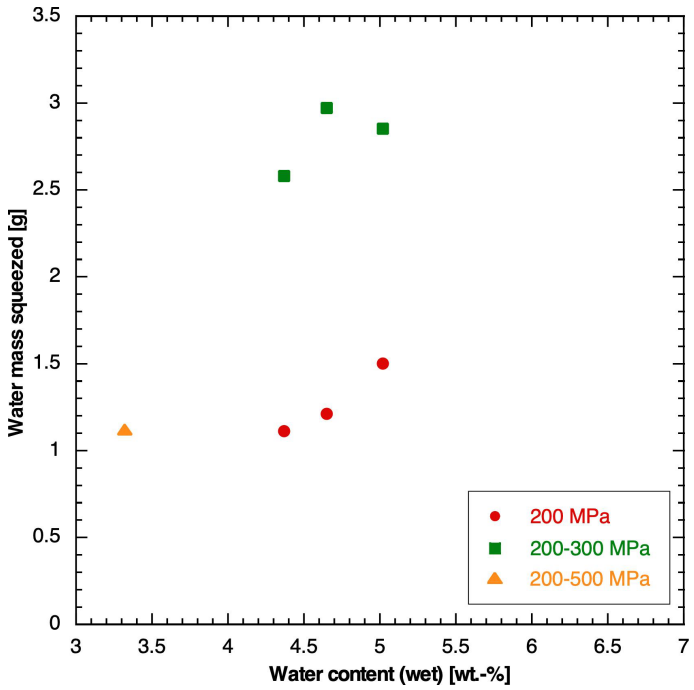


Fig. 4.6-3: Correlation of the original water content and the cumulative water mass obtained by squeeezing

### 4.6.2 Chemical composition of squeezed waters

The first squeezed aliquots yielded > 1.1 g water in all cases, from which a complete dataset (major-ion composition, TIC/TOC, pH, water isotopes) could be obtained. The chemical compositions of squeezed waters are listed in Tab. 4.6-3 and are shown graphically as a function of squeezing pressure in Fig. 4.6-4. Na is by far the most abundant cation, and Cl dominates the anions, followed by $SO_4$.

The concentrations of monovalent ions Na, K, Cl and Br decrease with squeezing pressure, likely due to ion-filtration effects that become important at higher pressures (Mazurek et al. 2015). Ca and Mg evolve slightly towards higher concentrations. As discussed in Mazurek et al. (2015) and Rufer & Mazurek (2018), the composition of the first water aliquot recovered from a sample is considered to be closest to that of the porewater, and these analyses are highlighted by bold print in Tab. 4.6-3. F concentrations, in particular in the first squeezed aliquots, are contaminated by F leached from the fiberglass filters and so are not representative of the porewater. For clarity, the subset of the data that is considered to be useful for further interpretation is summarised in Tab. 4.6-4.

Tab. 4.6-3: Chemical composition of squeezed waters: full dataset

Bold print indicates the selected ("best") aliquots. F concentrations, in particular in the first squeezed aliquots, are contaminated by F leached from the fiberglass filters and so are not representative of the porewater.

| **Depth** [m] | **Pressure** [MPa] | **Squeezing time** [d] | **Mass squeezed** [g] | **Na** [mg/L] | **$NH_4$** [mg/L] | **K** [mg/L] | **Ca** [mg/L] | **Mg** [mg/L] | **Sr** [mg/L] | **F** [mg/L] | **Cl** [mg/L] | **Br** [mg/L] | **$NO_3$** [mg/L] | **$SO_4$** [mg/L] | **pH** | **TIC** [mg/L] | **TOC** [mg/L] | **TDS** [mg/L] | **Charge balance** [%] |
|---|---|---|---|---|---|---|---|---|---|---|---|---|---|---|---|---|---|---|---|
| 750.86 | **200** | **3** | **1.50** | **4705** | **< 10** | **83.4** | **688** | **164** | **20.0** | **10.4** | **7049** | **21.6** | **9.18** | **2330** | **8.76** | **18.4** | **156.8** | **15334** | **-1.9** |
| | 300 | 3 | 1.35 | 3698 | < 10 | 43.9 | 695 | 180 | 19.4 | 6.9 | 5449 | 17.6 | 3.95 | 2094 | 8.58 | 16.5 | 89.7 | 12383 | -0.6 |
| 828.13 | **200** | **3** | **1.21** | **4931** | **< 10** | **83.5** | **697** | **169** | **20.6** | **9.2** | **7555** | **23.0** | **8.96** | **2421** | **8.54** | **23.0** | **215.0** | **16254** | **-2.9** |
| | 300 | 5 | 1.76 | 4181 | < 10 | 47.6 | 738 | 180 | 22.2 | 5.5 | 6027 | 20.0 | 4.55 | 2217 | 8.43 | 24.6 | 134.6 | 13705 | 0.5 |
| 859.37 | **200** | **3** | **1.11** | **4943** | **< 10** | **101.0** | **663** | **166** | **16.7** | **8.9** | **7488** | **21.5** | **10.02** | **2407** | **8.28** | **24.0** | **236.2** | **16188** | **-2.7** |
| | 300 | 5 | 1.47 | 4238 | < 10 | 63.9 | 698 | 174 | 14.9 | 5.7 | 6081 | 20.1 | 4.37 | 2395 | 8.31 | 29.3 | 148.3 | 13994 | -0.6 |
| 908.31 | **500** | **3** | **1.12** | **5650** | **< 10** | **91.2** | **809** | **125** | **18.2** | **10.5** | **7655** | **24.9** | **7.40** | **2936** | **8.69** | **17.1** | **157.2** | **17574** | **1.5** |

Tab. 4.6-4: Chemical composition of squeezed waters: summary of selected analyses to be used for interpretation

| **Depth** [m] | **Formation** | **Pressure** [MPa] | **Squeezing time** [d] | **Mass squeezed** [g] | **Na** [mg/L] | **K** [mg/L] | **Ca** [mg/L] | **Mg** [mg/L] | **Sr** [mg/L] | **Cl** [mg/L] | **Br** [mg/L] | **$NO_3$** [mg/L] | **$SO_4$** [mg/L] | **pH** | **TIC** [mg/L] | **TOC** [mg/L] |
|---|---|---|---|---|---|---|---|---|---|---|---|---|---|---|---|---|
| 750.86 | Wedelsst. Fm. | 200 | 3 | 1.50 | 4705 | 83.4 | 688 | 164 | 20.0 | 7049 | 21.6 | 9.18 | 2330 | 8.76 | 18.4 | 156.8 |
| 828.13 | Opalinus Clay | 200 | 3 | 1.21 | 4931 | 83.5 | 697 | 169 | 20.6 | 7555 | 23.0 | 8.96 | 2421 | 8.54 | 23.0 | 215.0 |
| 859.37 | Opalinus Clay | 200 | 3 | 1.11 | 4943 | 101.0 | 663 | 166 | 16.7 | 7488 | 21.5 | 10.02 | 2407 | 8.28 | 24.0 | 236.2 |
| 908.31 | Staffelegg Fm. | 500 | 3 | 1.12 | 5650 | 91.2 | 809 | 125 | 18.2 | 7655 | 24.9 | 7.40 | 2936 | 8.69 | 17.1 | 157.2 |

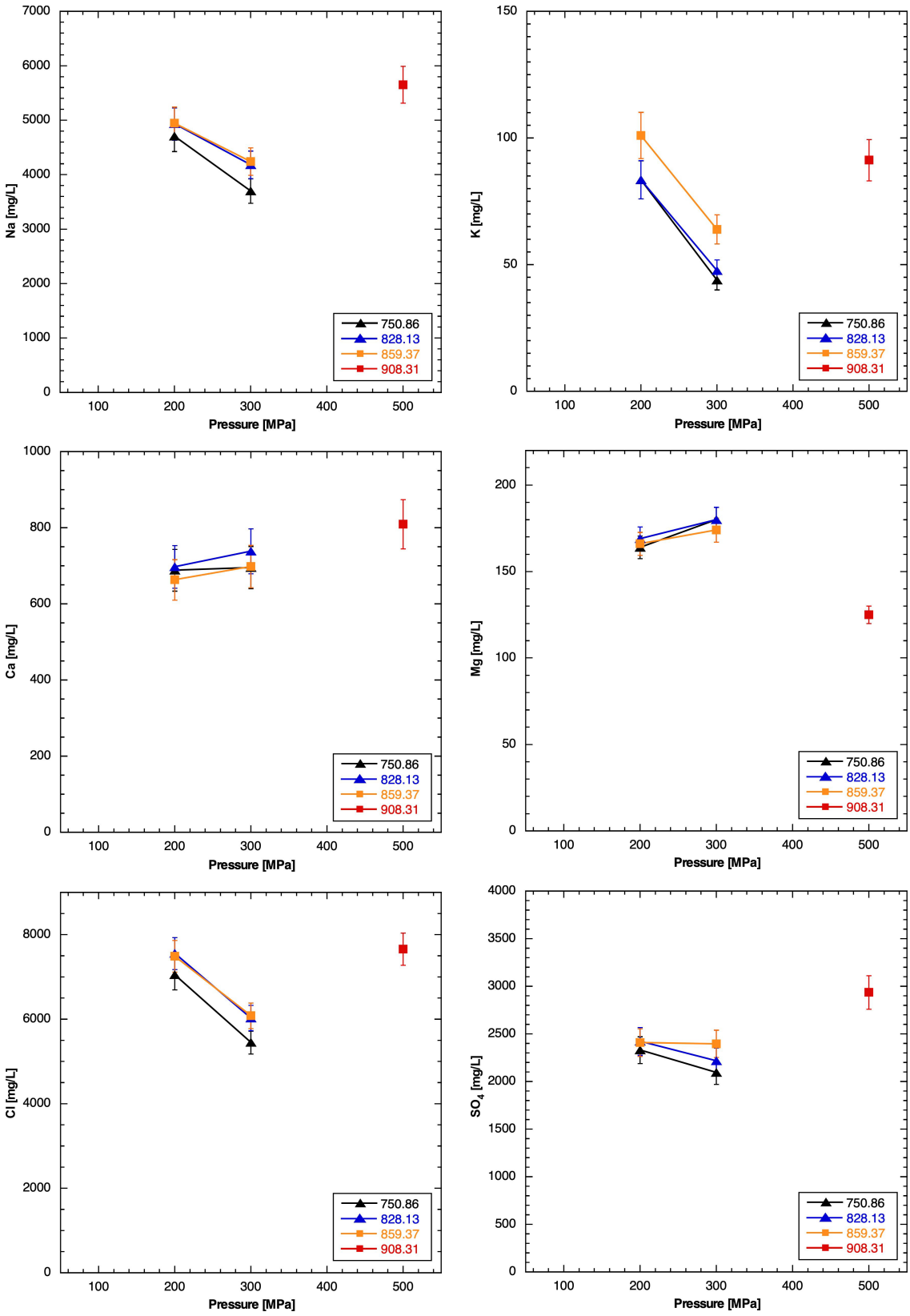


Fig. 4.6-4: Ion concentrations in squeezed waters as a function of squeezing pressure

Bars indicate analytical errors of ion-chromatography analysis.

### 4.6.3 Depth trends

Profiles with depth for various pore-water constituents are shown in Fig. 4.6-5. Given the fact that only 4 samples were studied, trends should preferably be studied in conjunction with data from other methods. Nevertheless, the following observations can be made:

- Na, Cl and $SO_4$ show limited variability with depth in the Dogger. In the Staffelegg Formation, Na and $SO_4$ as well as the Na/Cl and $SO_4$/Cl ratios increase markedly, and salinity increases slightly.
- Ca and Mg contents are constant in the Dogger, but Ca increases and Mg decreases in the Staffelegg Formation. Interestingly, the sample from the latter unit is the only one in which dolomite was identified (Tab. 4.6-1), indicating that the control of Mg in the porewater is complex.
- The Br/Cl ratio is slightly below that of current seawater and does not evolve with depth. It is markedly higher than that in the BUL1-1 profile.
- The $SO_4$/Cl ratio is higher than in seawater or in porewater from the BUL1-1 core at the same stratigraphic level.

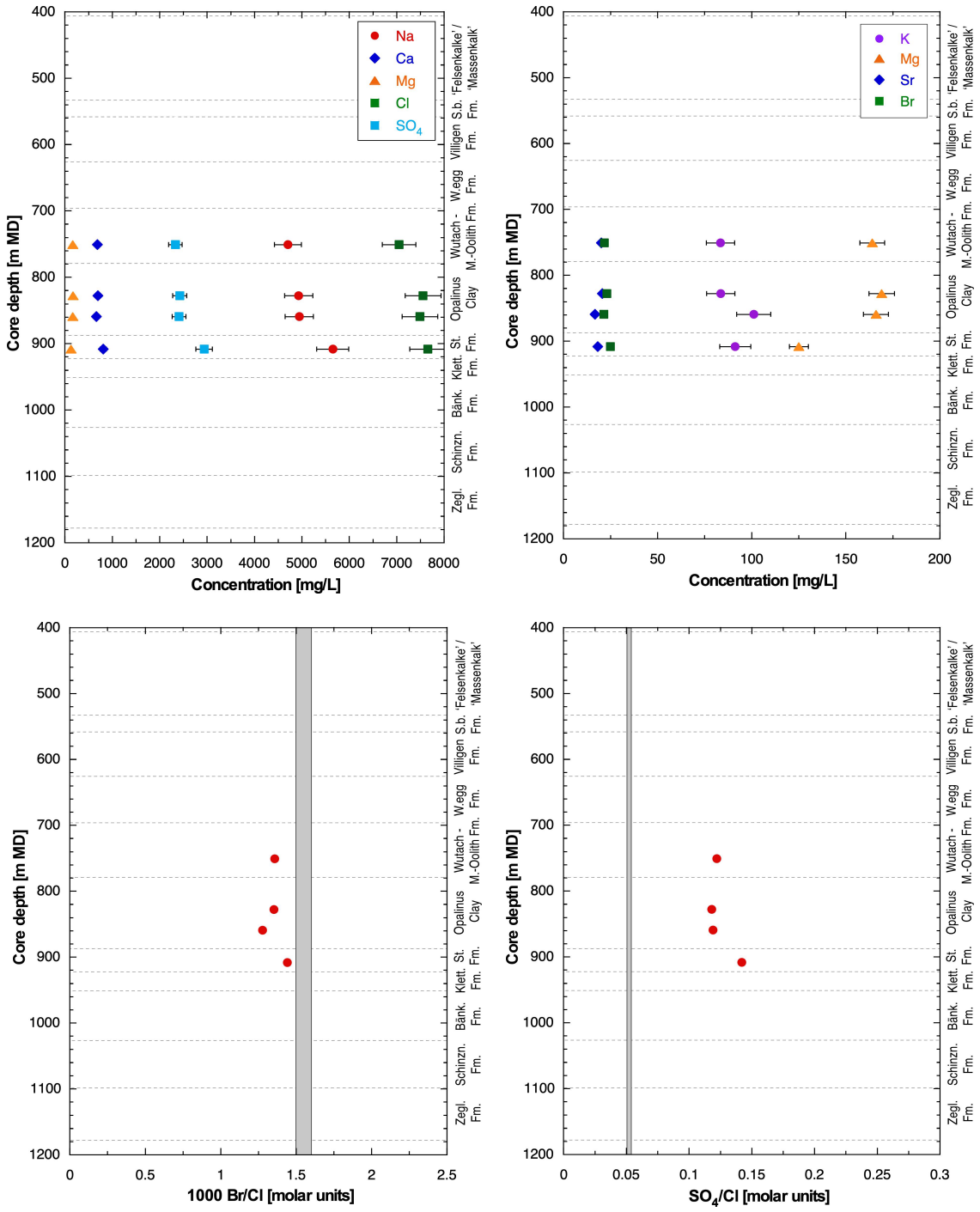


Fig. 4.6-5: Depth trends of ion concentrations and ion ratios in squeezed waters

Only the selected aliquots are shown for each sample. Bars indicate analytical errors of ion-chromatography analysis. Grey bars represent current seawater ratios.

### 4.6.4 Geochemical modelling and mineral saturation states

Mineral saturation indices for squeezed waters were calculated using PHREEQC V3 and the PSI/Nagra thermodynamic database at 25 °C (Thoenen et al. 2014) and are shown in Tab. 4.6-5.

- Squeezed waters are strongly oversaturated with respect to calcite, dolomite and magnesite, a feature already known from previous studies (e.g. Mazurek et al. 2015). The oversaturation is possibly due to the fact that carbonate mineral solubility at high pressures during squeezing is higher than at atmospheric pressure. Further, outgassing of $CO_2$ during the squeezing process increases the pH and the saturation indices of calcite and dolomite (Tournassat et al. 2015). Further outgassing my take place in the headspace of the sample vials during sample storage. The comparatively low calculated $P_{CO2}$ suggests that some outgassing may have taken place, which also affects pH. However, this nevertheless does not markedly affect the obtained major-ion composition due to the large buffering capacity of the rock – water system in clay-rich lithologies. Last, lattice defects in carbonate minerals induced by deformation during squeezing might increase the solubility of these minerals. On the other hand, outgassing into the external atmosphere during sample storage in glass vessels is not considered to contribute to the low $P_{CO2}$. Such a process should also be seen by higher δ values of water isotopes, which is not the case (see Section 4.8), but this depends on the mode of water loss (via a gas phase, or via a liquid film). In Section 5.5 below, an attempt is made to restore the outgassing by model calculations assuming equilibrium with calcite.
- A more limited oversaturation is seen for strontianite (except for sample 859.37 that is at equilibrium).
- The waters are close to saturation with respect to celestite and only marginally undersaturated with respect to gypsum.
- Using the data from Tab. 4.6-3, squeezed waters are strongly oversaturated with respect to fluorite, which is a consequence of the contamination of F concentrations by the filter material. Therefore, no F data are listed in Tab. 4.6-4.

Tab. 4.6-5: Mineral saturation indices for squeezed waters

Bold print indicates the selected ("best") aliquots.

| **Depth** [m] | **Formation** | **Pressure** [MPa] | **pH** | **TIC** [M] | **Log ($P_{CO2}$)** [bar] | **SI Calcite** | **SI Aragonite** | **SI Dolomite (ordered)** | **SI Dolomite (disordered)** | **SI Strontianite** | **SI Magnesite** | **SI Gypsum** | **SI Anhydrite** | **SI Celestite** | **SI Fluorite** |
|---|---|---|---|---|---|---|---|---|---|---|---|---|---|---|---|
| 750.86 | Wedelsst. Fm. | **200** | **8.76** | **1.56E-03** | **-4.04** | **1.41** | **1.27** | **2.54** | **1.99** | **0.33** | **0.80** | **-0.18** | **-0.40** | **0.01** | **1.27** |
| | | 300 | 8.58 | 1.39E-03 | -3.87 | 1.25 | 1.10 | 2.24 | 1.69 | 0.15 | 0.67 | -0.19 | -0.40 | -0.02 | 0.94 |
| 828.13 | Opalinus Clay | **200** | **8.54** | **1.95E-03** | **-3.68** | **1.33** | **1.18** | **2.37** | **1.82** | **0.25** | **0.72** | **-0.17** | **-0.38** | **0.02** | **1.16** |
| | | 300 | 8.43 | 2.08E-03 | -3.53 | 1.30 | 1.16 | 2.32 | 1.77 | 0.23 | 0.70 | -0.16 | -0.38 | 0.04 | 0.75 |
| 859.37 | Opalinus Clay | **200** | **8.28** | **2.03E-03** | **-3.38** | **1.10** | **0.95** | **1.92** | **1.37** | **-0.05** | **0.50** | **-0.19** | **-0.40** | **-0.07** | **1.11** |
| | | 300 | 8.31 | 2.47E-03 | -3.32 | 1.24 | 1.09 | 2.20 | 1.65 | 0.02 | 0.64 | -0.15 | -0.37 | -0.10 | 0.75 |
| 908.31 | Staffelegg Fm. | **500** | **8.69** | **1.45E-03** | **-3.99** | **1.36** | **1.22** | **2.25** | **1.70** | **0.17** | **0.56** | **-0.05** | **-0.27** | **0.03** | **1.33** |

### 4.6.5 Water content and aqueous extraction of squeezed and adjacent unsqueezed core material

For the calculation of the Cl-accessible porosity fraction $f_{Cl}$ (see below), the inventories of water and Cl in the rock prior to squeezing must be known. These data can be obtained by two alternative methods:

1. Measure the water content (by drying) and then the Cl content (by aqueous extraction) of the squeezed material (so-called POST data). From these data, the masses of water and Cl remaining in the sample after squeezing can be calculated. By adding the masses of squeezed water and Cl to these data, the respective contents prior to squeezing can be reconstructed.
2. Measure the water content (by drying) and Cl content (by aqueous extraction of wet material) of adjacent unsqueezed material some 10 cm away (so-called PRE data).

Both approaches have advantages and disadvantages:

- Method 1 has the advantage that all measurements are performed on the same material, so potential heterogeneity is not an issue. On the other hand, the reconstruction of the water and Cl inventories is less direct and assumes that the dead volume of the system is negligible (which is likely the case[9]). The results are listed in Tab. 4.6-6.
- Method 2 directly yields the desired data – no addition of two measurements is needed – but relies on the assumption that the measurement performed on adjacent material is also representative for the squeezed material itself. The assumption of homogeneity incurs some degree of uncertainty. Moreover, the material used for the PRE measurements (typically a 8 – 10 cm long piece of core) has been exposed to the atmosphere for a few minutes during sample preparation (dry sawing) prior to being re-sealed again. While this was the case for the squeezed material as well, the exposed surface area of the adjacent cutoff material is much larger. Results are shown in Tab. 4.6-7.

Tab. 4.6-6: Water contents and results of aqueous-extraction tests on previously squeezed samples (method 1, POST data)

| **Depth** [m] | **Formation** | **Water content (wet) of squeezed sample** [wt.-%] | **Mass of porewater in squeezed sample** [g] | **Aqueous extraction of squeezed sample** | | | | |
|---|---|---|---|---|---|---|---|---|
| | | | | **Mass of dry rock** [g] | **Mass of added water** [g] | ***S/L*** [g/g] | **Cl** [mg/$L_{extract\ solution}$] | **Br** [mg/$L_{extract\ solution}$] |
| 750.86 | Wedelsst. Fm. | 4.247 | 14.88 | 30.08 | 30.41 | 0.989 | 131 | 0.40 |
| 828.13 | Opalinus Clay | 3.907 | 14.81 | 30.45 | 30.31 | 1.004 | 128 | 0.38 |
| 859.37 | Opalinus Clay | 3.708 | 13.89 | 30.50 | 30.50 | 1.000 | 110 | 0.27 |
| 908.31 | Staffelegg Fm. | 3.013 | 10.50 | 30.64 | 30.34 | 1.010 | 107 | 0.34 |

[9] A sensitivity calculation was performed on the impact of dead volume. Assuming a dead volume of 1 mL results is an anion-accessible porosity fraction that is 0.01 – 0.04 higher than the value without consideration of a dead volume. The most strongly expressed shift is found in samples where only a small water volume was squeezed, while it becomes insignificant for samples with a good water yield.

Tab. 4.6-7: Water contents and results of aqueous-extraction tests on material adjacent to squeezed samples (method 2, PRE data)

| Depth [m] | Formation | Water content (wet) [wt.-%] | Aqueous extraction of virgin material adjacent to squeezed sample | | | | |
|---|---|---|---|---|---|---|---|
| | | | Mass of dry rock [g] | Mass of added water [g] | *S/L* [g/g] | Cl [mg/$L_{extract\ solution}$] | Br [mg/$L_{extract\ solution}$] |
| 750.86 | Wedelsst. Fm. | 5.055 | 28.59 | 30.42 | 0.895 | 174.1 | 0.56 |
| 828.13 | Opalinus Clay | 4.693 | 28.68 | 30.28 | 0.905 | 181.0 | 0.58 |
| 859.37 | Opalinus Clay | 4.459 | 28.90 | 30.46 | 0.909 | 152.2 | 0.50 |
| 908.31 | Staffelegg Fm. | 3.622 | 29.40 | 30.43 | 0.932 | 140.9 | 0.48 |

### 4.6.6 Chloride-accessible porosity

The Cl-accessible porosity fraction $f_{Cl}$ can be estimated from

$$f_{Cl} = \frac{C_{Cl\ in\ bulk\ porewater}}{C_{Cl\ in\ squeezed\ water}}$$

$C_{Cl\ in\ squeezed\ water}$ is taken from Tab. 4.6-4, assuming that these data represent the concentrations in the anion-accessible pore space. $C_{Cl\ in\ bulk\ porewater}$ can be obtained using the two alternative methods described in Section 4.6.5. According to method 1, the masses of Cl and water obtained by squeezing and by drying/aqueous extraction of the squeezed material are added. The formalism is documented in more detail in Mazurek et al. (2021), and the results are listed in Tab. 4.6-8.

Alternatively, applying method 2, $C_{Cl\ in\ bulk\ porewater}$ can be obtained directly by drying/aqueous extraction of adjacent, unsqueezed rock according to

$$C_{Cl\ in\ bulk\ porewater} = \frac{C_{Cl\ in\ extract\ solution}}{S/_L\ w_d}$$

using the data listed in Tab. 4.6-7 ($w_d$ = water content relative to dry rock). The results are shown in Tab. 4.6-9.

The resulting Cl-accessible porosity fractions obtained by the two methods are also listed in Tabs. 4.6-8 and 4.6-9. They are shown as a function of the clay-mineral content in Fig. 4.6-6. All values of $f_{Cl}$ lie in the narrow range 0.46 – 0.54. The results obtained by the two methods agree closely, as they already did for samples from BOZ2-2 (Gimmi et al. 2022). While the differences between the methods were not systematic in the case of BOZ2-2, method 2 yields slightly higher values for all samples from the STA3-1 borehole. Overall, method 1 is considered to be the preferred way to calculate $f_{Cl}$, given the fact that all measurements refer to identical materials and so heterogeneity plays no role.

Tab. 4.6-8: Cl-accessible porosity fractions derived from squeezing and aqueous-extraction experiments using method 1 to obtain $C_{Cl\ in\ bulk\ porewater}$.

| **Depth** [m] | **Formation** | **Total mass of squeezed Cl** [mg] | **Mass of Cl in aq. extract of squeezed core** [mg] | **Porewater mass squeezed** [g] | **Water mass remaining in squeezed core** [g] | **Cl in bulk porewater** [mg/L] | **Cl-accessible porosity fraction $f_{Cl}$** [-] |
|---|---|---|---|---|---|---|---|
| 750.86 | Wedelsst. Fm. | 17.93 | 44.5 | 2.85 | 14.88 | 3519 | 0.50 |
| 828.13 | Opalinus Clay | 19.75 | 46.6 | 2.97 | 14.81 | 3730 | 0.49 |
| 859.37 | Opalinus Clay | 17.25 | 39.6 | 2.58 | 13.89 | 3451 | 0.46 |
| 908.31 | Staffelegg Fm. | 8.57 | 35.8 | 1.12 | 10.50 | 3822 | 0.50 |

Tab. 4.6-9: Cl-accessible porosity fractions derived from squeezing and aqueous-extraction experiments, using method 2 to obtain $C_{Cl\ in\ bulk\ porewater}$

| **Depth** [m] | **Formation** | **Cl concentration in bulk porewater (in adjacent unsqueezed rock)** [mg/L] | **Cl-accessible porosity fraction $f_{Cl}$** [-] |
|---|---|---|---|
| 750.86 | Wedelsandstein Fm. | 3654 | 0.52 |
| 828.13 | Opalinus Clay | 4063 | 0.54 |
| 859.37 | Opalinus Clay | 3587 | 0.48 |
| 908.31 | Staffelegg Fm. | 4023 | 0.53 |

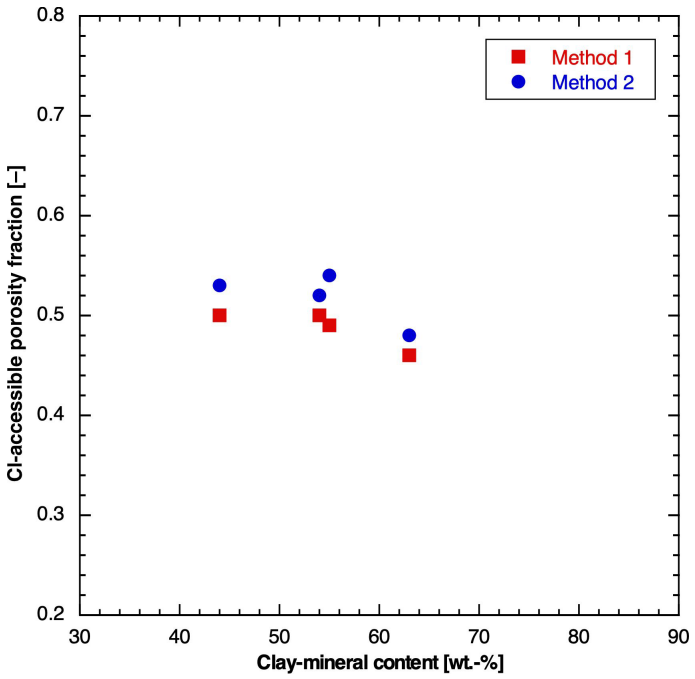


Fig. 4.6-6: Cl-accessible porosity fractions derived from squeezing experiments as a function of the clay-mineral content

See text for explanations regarding the two methods.

### 4.6.7 Composition of stable isotopes of squeezed water

Results of analyses of stable water isotopes are listed in Tab. 4.6-10 and shown as a function of depth in Fig. 4.6-7. The following observations can be made:

- Within any sample, the variation of the δ values with squeezing pressure is small (within analytical error).
- $\delta^{18}O$ shows a distinct trend of values decreasing downwards, whereas $\delta^{2}H$ shows no depth trend.
- In a plot $\delta^{18}O$ vs. $\delta^{2}H$ (Fig. 4.6-8), the shallower samples are located far on the right side of the global ($\delta^{2}H = 8\ \delta^{18}O + 10$; Craig 1961) and the local ($\delta^{2}H = 7.55\ \delta^{18}O + 4.8$; Kullin & Schmassmann 1991) meteoric water lines. The deeper samples come closer to these lines.
- The same information is illustrated in Fig. 4.6-9 by the depth trend of deuterium excess ($\delta^{18}O - 8 \times \delta^{2}H$), which increases systematically with depth.

Tab. 4.6-10: Composition of stable isotopes of squeezed waters

The aliquots selected for interpretation are shown in bold.

| **Depth** [m] | **Formation** | **Pressure** [MPa] | **$\delta^{18}O$** [‰ VSMOW] | **$\delta^{2}H$** [‰ VSMOW] | **D excess** [‰] |
|---|---|---|---|---|---|
| 750.86 | Wedelsandstein Fm. | **200** | **-3.31** | **-35.5** | **-9.0** |
| | | 300 | -3.48 | -36.2 | -8.4 |
| 828.13 | Opalinus Clay | **200** | **-3.99** | **-35.7** | **-3.8** |
| | | 300 | -4.05 | -35.8 | -3.4 |
| 859.37 | Opalinus Clay | **200** | **-4.48** | **-36.2** | **-0.4** |
| | | 300 | -4.49 | -36.3 | -0.4 |
| 908.31 | Staffelegg Fm. | **500** | **-4.73** | **-36.3** | **1.5** |

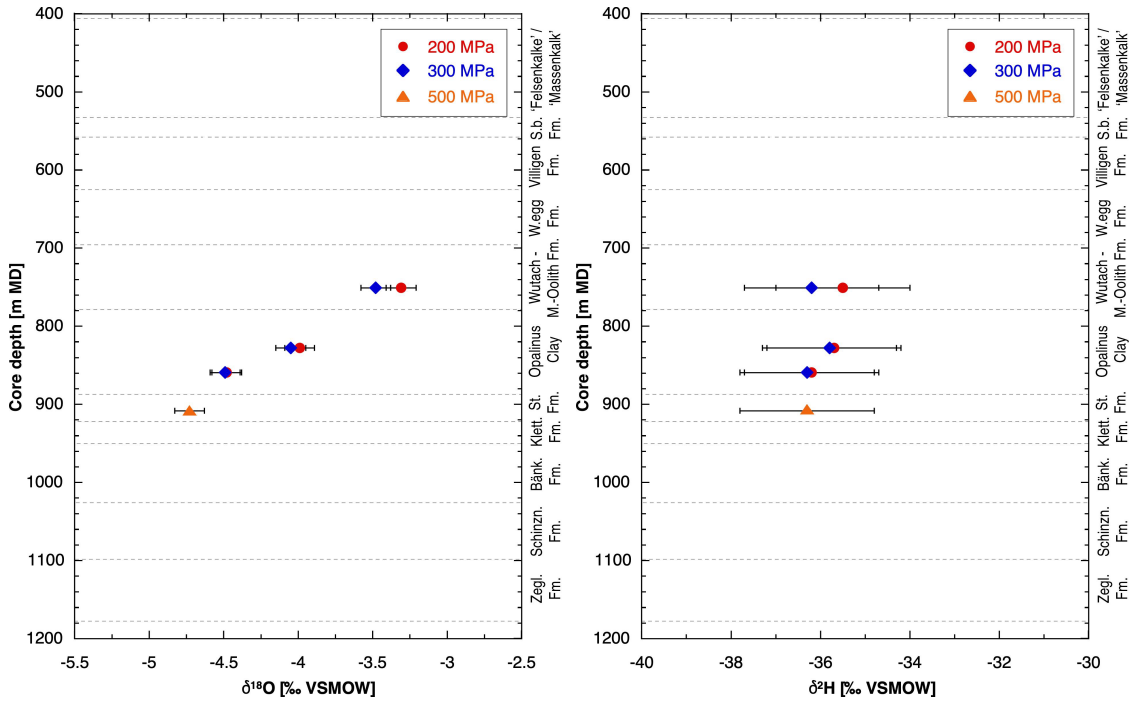


Fig. 4.6-7: Depth trends of $\delta^{18}O$ and $\delta^{2}H$ in squeezed waters

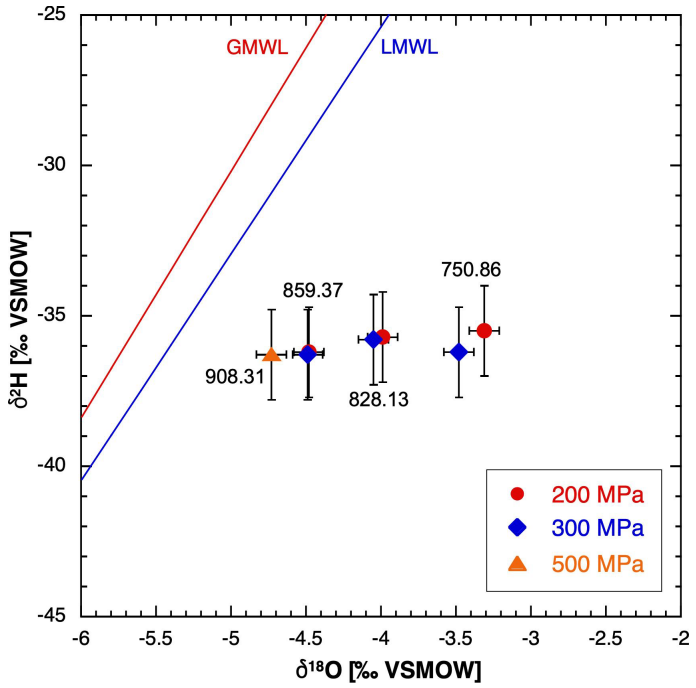


Fig. 4.6-8: Plot of $\delta^{18}O$ vs. $\delta^{2}H$ for squeezed waters

GMWL = Global Meteoric Water Line, LMWL = Local Meteoric Water Line. Numbers indicate sample depths in m.

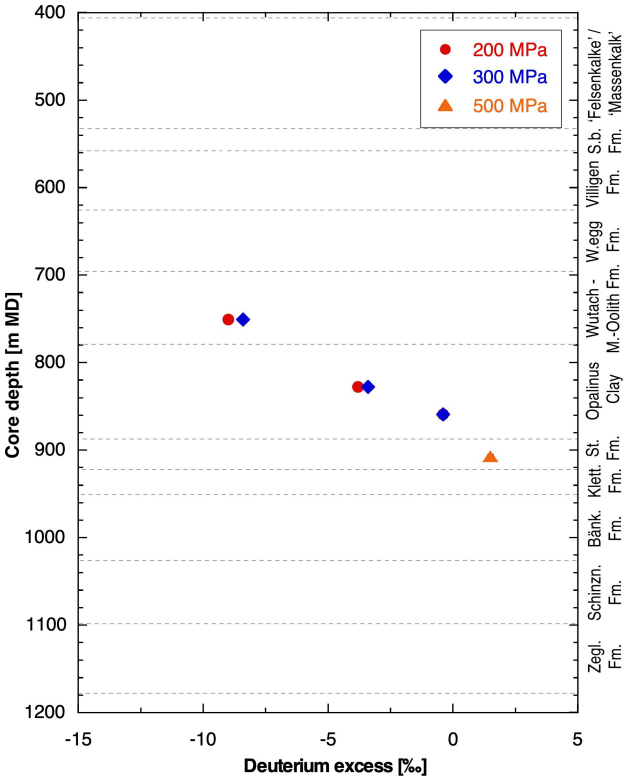


Fig. 4.6-9: Depth trend of deuterium excess in squeezed waters

## 4.7 Data from advective-displacement experiments

*Andreas Jenni, Mirjam Kiczka, Carmen Zwahlen, Urs Mäder & H. Niklaus Waber*

Advective-displacement (AD) experiments are a methodology for a comprehensive physico-chemical characterisation, including porewater chemistry and certain transport properties (details in method report, Waber ed. 2020). This section presents a data summary, more details where important, and short discussions where appropriate. The full datasets are provided in Appendix B. Integration of the data into context and depth profiles are included in Chapter 5.

Initially three samples from the Opalinus Clay and the clay-rich confining units were processed. These experiments were successful from a technical point of view, subjected to a similar analytical programme, with differences mainly related to the duration of each experiment (numbers of sampled fluid aliquots). However, during data inspection, some uncertainty regarding the early sampled porewaters in the STA3-2 (Opalinus Clay) and STA3-3 (Staffelegg Formation) cores arose due to high nitrate concentrations (discussed in Section 4.7.5.4). In addition, Ag filters replaced the PEEK filters used in earlier experiments with the intention to suppress microbial activity, but this led to lower Br in early aliquots, attributed to surface complexation on the filters. For these reasons, an additional experiment with a sample from the Opalinus Clay was started at a later time, for which sample preparation was improved as detailed in Section 4.7.2. This experiment was subjected to a shorter duration.

The extent of pre- and post-mortem characterisation of core material was optimised based on gained experience from former boreholes BUL1-1, TRU1-1, MAR1-1, BOZ1-1 and BOZ2-1 investigations. The programme fulfilled the planned work, but partially provided longer durations of advective displacement than requested. The duration of the percolation period was 56 – 258 days, transporting 0.4 – 3.6 pore volumes of fluid.

The salinity in this borehole is similar to the TRU1-1 and MAR1-1 boreholes, but significantly higher than in BOZ1-1 and BOZ2-1 (neglecting the nitrate contribution; see Section 4.7.5.4).

### 4.7.1 Sample material and overview of analytical work

The four sample cores (Fig. 4.7-1) span 160 m of clay-rich confining and host rock units (745 m – 903 m depth), from the Wedelsandstein Formation («Brauner Dogger») to the Staffelegg Formation and include two samples from the Opalinus Clay.

X-ray computed tomography (CT) was performed on a medical scanner (Waber ed. 2020) for sample selection (Fig. 4.7-2) and detection of disturbing features (fractures, pyrite accumulations, macro-fossils, etc.). Dry cutting with a mitre saw was used for obtaining a central core segment for AD experiments (yellow in Fig. 4.7-2), and adjacent 2 discs for accompanying characterisation (green in Fig. 4.7-2). In case of STA3-4, pre-existing cracks in the core only allowed for sampling discs below the core segment for the AD experiment. The central core segment was machined on a lathe from 95 mm to 80 mm in diameter. Tab. 4.7-1 lists all analytical work performed on the four samples.

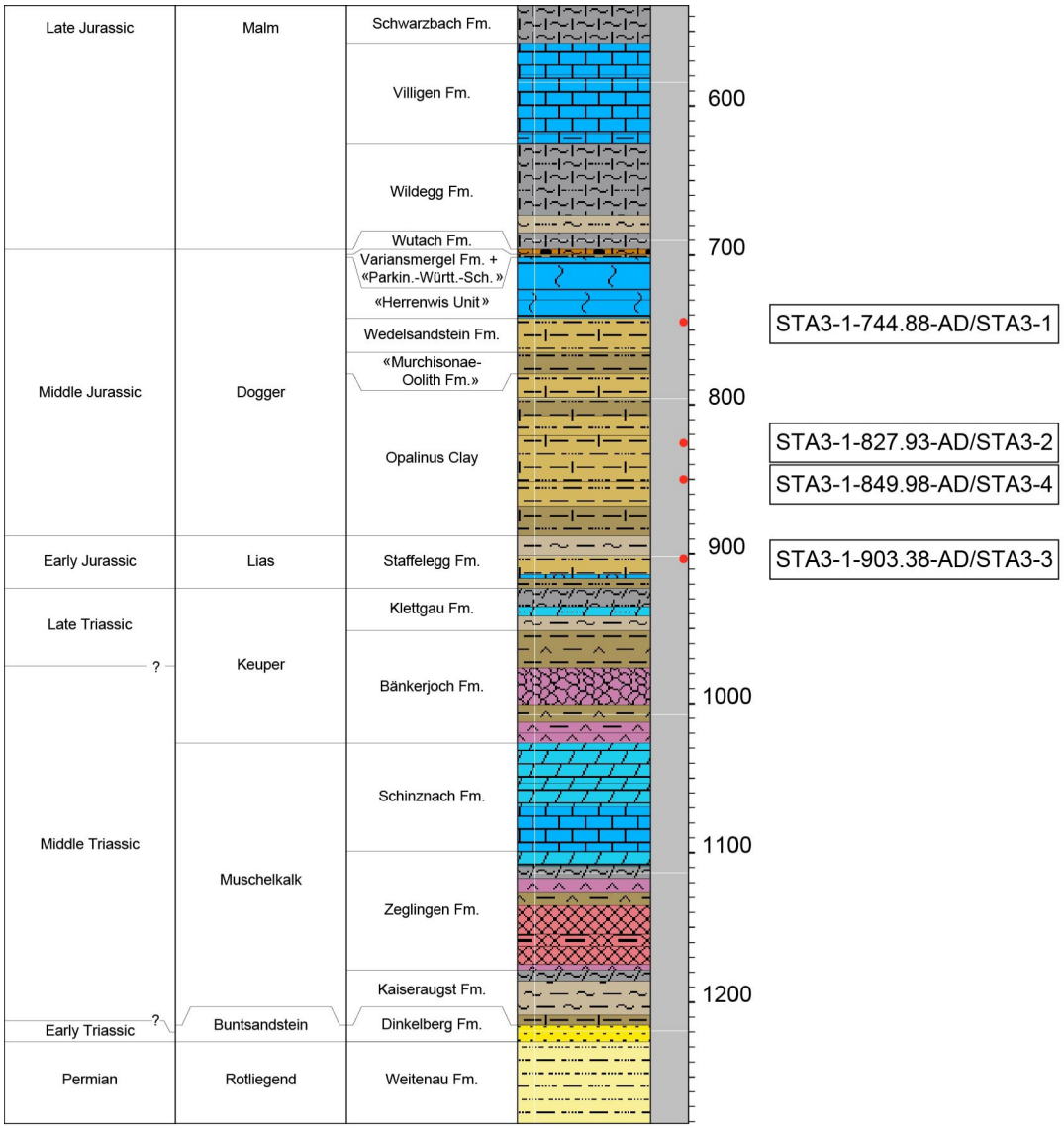


Fig. 4.7-1: Location of samples used for advective-displacement experiments (red dots)
Short labels are consecutively numbered laboratory abbreviations.

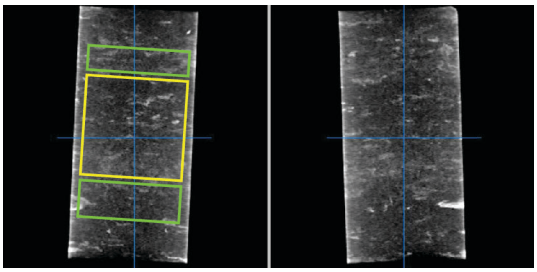

STA3-1-744.88-AD (Wedelsandstein Fm.)

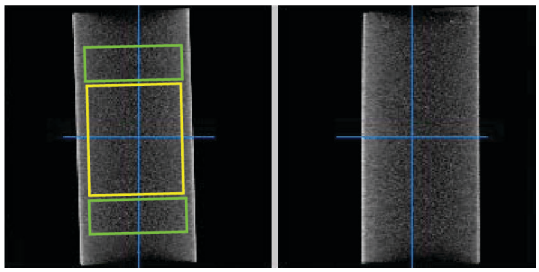

STA3-1-827.93-AD (Opalinus Clay)

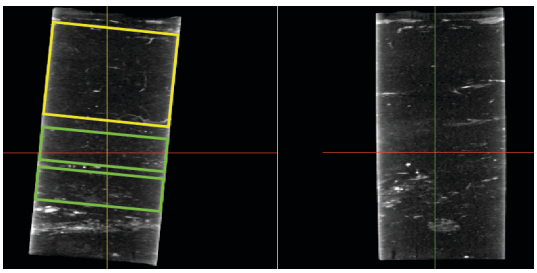

STA3-1-849.98-AD (Opalinus Clay)

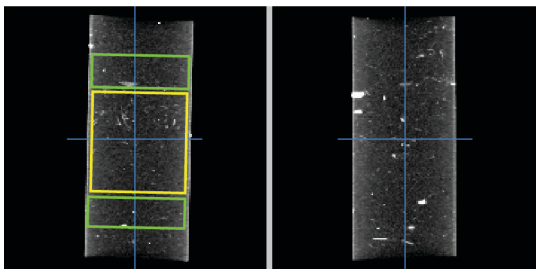

STA3-1-903.38-AD (Staffelegg Fm.)

Fig. 4.7-2: X-ray CT images of AD samples

Central sections parallel to core axis at right angle. Grey scale range setting is 1700-2500 HU. Yellow segments are used for advective displacement, green segments for pre-characterisation. Low X-ray absorbance represents clay/quartz-rich sections (darker grey), slightly lighter grey indicates carbonate-richer parts, siderite is brighter, and pyrite is white (strongest absorbance). Black lines/gaps represent fractures. Image base is downhole direction.

Tab. 4.7-1: Summary of analytical work perfomed on samples for advective-displacement experiments

| **Parameter** | **STA3-1** | **STA3-2** | **STA3-4** | **STA3-3** |
|---|---|---|---|---|
| Sample ID RWI | STA3-1-744.88-AD | STA3-1-827.93-AD | STA3-1-849.98-AD | STA3-1-903.38-AD |
| Lab sample ID | STA3-1xx-AD | STA3-2xx-AD | STA3-4xx-AD | STA3-3xx-AD |
| Depth [m] | 744.88 | 827.93 | 849.98 | 903.38 |
| Geological unit | Wedelsandstein Fm. | Opalinus Clay | Opalinus Clay | Staffelegg Fm. |
| Member | | | | Frick Mb. |
| AD_exp | y | y | y | y |
| Pre_WC | 1+1 | 1+1 | 2+0 | 1+1 |
| Pre_M | y | y | y | y |
| Pre_V,A,L | y | y | y | y |
| Pre_Min | 1 | 1 | 1 | 1 |
| Pre_Clay | 1 | 1 | 1 | 1 |
| Pre_AqEx | 1+1 | 1+1 | 2+0 | 1+1 |
| Pre_Ni-en | ave | ave | n | ave |
| Post_WC | 4 | 5 | 4 | 5 |
| Post_M | y | y | y | y |
| Post_V,A,L | y | y | y | y |
| Post_AqEx | 1+1 | 1+1 | 1+1 | 1+1 |
| Post_Ni-en | 1+1 | n | n | 1+1 |
| Abras_Drilling_Fl | n | n | n | n |
| Post_IsoEx | 1 | n | n | n |

y = yes = done; n = no = not done; integer numbers refer to the number of samples processed; +: samples from above (left number) and below (right number) the core were processed, or the sum of both samples (ave); 'above' and 'below' refer to the orientation in the infiltration apparatus, which is rotated by 180° in case of STA3-4 in Fig. 4.7-2 (see section below); Pre: sample pre-characterisation; Post: post-mortem characterisation; WC: water content; M: mass; V,A,L: core volume, sectional area and length; Min: mineralogy; Clay: clay mineralogy; AqEx: aqueous extracts; Ni-en: cation selectivity with Ni-en method; Post_WC: post-mortem water content determined along a profile with 5 segments; AD_exp: complete analysis of fluid sample aliquots collected during advective displacement; Post_IsoEx: Isotope exchange experiment on core material.

## 4.7.2 Conditions of advective-displacement experiments

Sample preparation was performed according to Waber (ed.) (2020). In addition to the description therein, the STA3-4 core was fully wrapped with elastic electric tape that was only applied to the ends of the latex rubber sleeves in previous sample preparations. Then, a cold-shrink tube (3M Kaltschrumpfschlauch 8430.9, EPDM, 93.7/42.6/229) was applied, overlapping the edges of the Ti head pieces. The ends are sealed with clear silicone sealant, as done with the latex rubber sleeves. Cores were infiltrated from the base upwards (Fig. 4.7-2), i.e., against downhole direction, except STA3-4: this core was flipped by 180° and was infiltrated parallel to the down-hole direction. The aqueous extract from the top of the core segment as mounted in the apparatus can be compared with the early exfiltrating chemistry to estimate anion accessibility. All figures or sample names refer to the orientation in the infiltration apparatus.

Ag filters replaced the PEEK filters used in earlier experiments as a measure to reduce any potential microbial activity. However, the first measured aliquots were lower in Br compared to later aliquots and had a lower Br/Cl ratio as obtained from aqueous extracts. This reduction of Br was attributed to surface complexation on the Ag filters to form AgBr. Ag filters were still implemented in experiments on samples from the STA2-1 borehole (Zwahlen et al. *in prep.*) but abandoned later as was done for the STA3-4 core for which again PEEK filters were used.

The overview table (Tab. 4.7-2) presents some experiment specific parameters such as variation in sample preparation, sample processing dates, storage time and other characteristic times like arrival of the first fluid drop and its electric conductivity. Numbers of samples taken and analysed are listed as well as average pressures for confining and injection. The number of percolated pore volumes is based on the water content determined from pre-characterisation. Infiltration pressure of the artificial porewater (APW) was on average 46 bar, pressurised by He. The hydraulic gradients are large, 5'000 – 6'000 $m_{H2O}$/m (sample dimensions are in Tab. 4.7-4). Experiments were started within 3 days of sample delivery and within 2 weeks after drilling, except the second OPA sample STA3-4 (1 year after delivery, 1.2 years after drilling). The time until arrival of a first fluid drop at the electric conductivity cell (outflow, before sampling syringe) was 6 – 9 days after start of infiltration.

Confining pressure was on average 58 – 61 bar, pressurised by Ar on water (Waber ed. 2020). For sample STA3-4, a piston pump was used to pressurise a diaphragm accumulator (Parker Membranspeicher MBSP 050-210/60 S ST NBR), where a sturdy NBR membrane separates the confining fluid from the pressurised gas. There is no gas-water interface in this set-up, and no gas is expected to dissolve in the confining fluid other than initially present.

Especially at early stages, gas exfiltrated the core (Tab. 4.7-2). The density of the gas was derived from high-precision weighing. These data, and gas characterisations as done for samples from boreholes BOZ1-1 and MAR1-1 (Wersin et al. 2022a and Mäder et al. 2021), indicated that the initial exfiltrating gas mainly consisted of air that is present at the core surface, in filters and in dead-space (entrapped during preparation). In addition, minor volumes of Ar from the confining system penetrated the core sealing layers and could be detected in the sampling syringe (STA3-1, STA3-2, STA3-3). At later stages, exfiltrating gas volumes decreased and were dominated by $N_2$ and, after APW breakthrough, contained some He (used to pressurise the APW infiltration tank). Cores with elevated nitrate concentration in exfiltrates showed ongoing enhanced gas exfiltration, presumably from microbial activity. The enhanced packing of the STA3-4 core, and of all cores processed thereafter, lead to a strong decrease in gas exfiltration.

The drop of the APW level in the infiltration tank below the capillary inlet led to He infiltration into core STA3-3 after 48 days (0.50 pore volumes percolated). On the 7.4.2021 at 15:45, the gas started to exfiltrate the core. Within 24 hours, the APW tank was refilled, and the gas injection stopped. In total approximately 440 $cm^3$ STP He infiltrated the core and exfiltrated within the following 25 days. Then, the exfiltrating gas volumes decreased, and the hydraulic conductivity increased to values similar as before the gas breakthrough. Evolutions of solute water tracer concentrations in the exfiltrate were not affected by the breakthrough of the inert gas (Section 4.7.5). These observations indicated that solute transport was only temporarily slowed down during a gas breakthrough across this confined core, and no preferential pathway for advective or diffusive transport persisted.

Tab. 4.7-2: Conditions of advective-displacement experiments

| **Parameter** | **STA3-1** | **STA3-2** | **STA3-4** | **STA3-3** |
|---|---|---|---|---|
| Depth [m] | 744.88 | 827.93 | 849.98 | 903.38 |
| Geol. unit | Wedelsandstein Fm. | Opalinus Clay | Opalinus Clay | Staffelegg Fm. |
| Drilled | 29.01.2021 | 03.02.2021 | 05.02.2021 | 08.02.2021 |
| Delivered | 08.02.2021 | 15.02.2021 | 15.02.2021 | 15.02.2021 |
| Prep_AD | 11.02.2021 | 18.02.2021 | 25.04.2022 | 18.02.2021 |
| Injection | 12.02.2021 | 19.02.2021 | 26.04.2022 | 19.02.2021 |
| First drop | 21.02.2021 | 28.02.2021 | 04.05.2022 | 25.02.2021 |
| Days to first drop | 8.6 | 8.5 | 7.7 | 6.4 |
| Initial gas [mL] | 6.9 | 3.5 | 0.2 | 20.5 |
| End_AD | 28.10.2021 | 28.10.2021 | 21.06.2022 | 26.08.2021 |
| Duration [d] | 257.8 | 250.7 | 55.9 | 187.7 |
| Pore-volumes | 3.6 | 0.4 | 0.5 | 2.1 |
| EC_initial (25 °C) [mS/cm] | 22.9 | 27.0 | 24.8 | 24.7 |
| Filter | Ag-Filter | Ag-Filter | PEEK | Ag-Filter |
| Core packing | Teflon tape, 2 latex sleeves | Teflon tape, 2 latex sleeves | Teflon tape, 2 latex sleeves, adhesive tape, cold-shrink tube | Teflon tape, 2 latex sleeves |
| Confining pressure | Ar on water | Ar on water | Piston pump on water, diaphragm accumulator | Ar on water |
| AD-samples | 23 | 10 | 7 | 21 |
| AD-samp_chem | 17 | 9 | 5 | 15 |
| AD-samp_isotopes | 17 | 9 | 5 | 15 |
| inline pH | 12 | 7 | 3 | 11 |
| P_Conf [bar] | 58 | 60 | 61 | 60 |
| P_Inf [bar] | 45 | 47 | 46 | 45 |
| Gradient [$mH_2O/m$] | 5'453 | 5'281 | 6'270 | 5'279 |

## 4.7.3 Mineralogy and petrophysical properties

For each core, the mineralogy was determined on the sum of subsamples cut adjacent to the core segment used for the AD experiments (Tab. 4.7-1). Results are summarised in Tab. 4.7-3 and plotted in Section 4.2. Samples cover a range of clay-mineral contents of 30 – 65 wt.-%, calcite contents of 6 – 21 wt.-%, and quartz contents of 20 – 48 wt.-%. The clay-mineral fraction is composed of variable amounts of illite (7 – 17 wt.-%), illite/smectite mixed layers (9 – 18 wt.-%), and kaolinite (0.2 – 21 wt.-%).

Carbon, sulphur and nitrogen analyses are also included. Pyrite contents are moderately low (0.4 – 2 wt.-%) because pyrite-rich lithologies were avoided based on X-ray CT characterisation (Fig. 4.7-2). More details, including end-member clays, are included in Appendix B.

Tab. 4.7-3: Mineralogy of advective-displacement samples, including C, S and N analyses

| **Parameter** | **Unit** | **STA3-1** | **STA3-2** | **STA3-4** | **STA3-3** |
|---|---|---|---|---|---|
| Depth | [m] | 744.88 | 827.93 | 849.98 | 903.38 |
| Geological unit | | Wedelsst. Fm. | Opalinus Clay | Opalinus Clay | Staffelegg Fm. |
| S | [wt.-%] | 0.8 | 1.2 | 0.5 | 0.2 |
| C(inorg) | [wt.-%] | 2.5 | 1.4 | 1.0 | 1.0 |
| C(org) | [wt.-%] | 0.6 | 0.9 | 1.3 | 0.5 |
| N | [wt.-%] | 0.0 | 0.1 | 0.1 | b.d. |
| Quartz | [wt.-%] | 37 | 25 | 20 | 48 |
| K-feldspar | [wt.-%] | 6 | 6 | 2 | 7 |
| Plagioclase | [wt.-%] | 4 | 3 | 2 | 3 |
| Calcite | [wt.-%] | 21 | 8 | 6 | 8 |
| Dolomite / Ankerite | [wt.-%] | b.d. | b.d. | b.d. | b.d. |
| Siderite | [wt.-%] | b.d. | 5 | 2 | b.d. |
| Anhydrite | [wt.-%] | b.d. | b.d. | b.d. | b.d. |
| Celestite | [wt.-%] | b.d. | b.d. | b.d. | b.d. |
| Pyrite | [wt.-%] | 1 | 2 | 0.9 | 0.4 |
| **Clay minerals** | **[wt.-%]** | **30** | **50** | **65** | **33** |
| Illite | [wt.-%] | 10 | 17 | 17 | 7 |
| Illite/smectite ML (85-90) | [wt.-%] | 6 | b.d. | 13 | b.d. |
| Illite/smectite ML (75-80) | [wt.-%] | 6 | 1 | b.d. | 17 |
| Illite/smectite ML (50-70) | [wt.-%] | 3 | 7 | 5 | b.d. |
| Illite/smectite ML (20-40) | [wt.-%] | 0.2 | b.d. | b.d. | b.d. |
| Smectite | [wt.-%] | 1.7 | 0.8 | 0.0 | 0.4 |
| Kaolinite | [wt.-%] | 0.2 | 16.9 | 20.8 | 5.4 |
| Chlorite | [wt.-%] | 0.6 | b.d. | 1.8 | 0.5 |
| Chl/Sm ML (85-95) | [wt.-%] | 3.4 | 7.2 | 7.6 | 3.0 |
| **Total illite/smectite** | [wt.-%] | **15** | **9** | **18** | **17** |
| (tot_ill/sm+sm)/(total_clay) | | 0.49 | 0.17 | 0.27 | 0.51 |
| (tot_ill+ill/sm+sm)/(total_clay) | | 0.80 | 0.50 | 0.53 | 0.72 |

b.d.: below detection

A plethora of petrophysical parameters can be derived from sample dimensions, mass, water content, and changes in these parameters determined before and after an AD experiment (Tab. 4.7-4). These quantities include porosity, bulk density, grain density, water uptake during the experiments, and unsaturated porosity (saturation ratio). The relationships are given in Waber (ed.) (2020). Note that the water content determined for pre-characterisation is based on 2 subsamples adjacent to the AD core segment, if sufficient material was available.

The corrected initial water content as well as the unsaturated (gas-filled) porosity fraction of the core used in the AD experiment can be derived from the post-mortem water content and the usually observed slight core volume expansion during the experiment. The core volume increases by 0.1 – 1.0% (Tab. 4.7-4), accompanied by a water uptake of 2.7 – 6.4 g. Accounting for volume expansion, there remains a small net water uptake of 0.1 – 3.1 g that must reflect an initially small volume of unsaturated porosity, ranging from 0.1 to 3.1 mL, corresponding to a saturation ratio in the range 0.93 – 1.00. This analysis is valid if significant drying of a sample core is avoided by minimising exposure times, as was done for AD experiments (Waber ed. 2020). The largest measurement uncertainty is associated with the measurement of the core dimensions using callipers. Although reading precision is in the order of 0.05 mm, using callipers on slightly uneven cores adds to the uncertainty, as do any small breakouts along edges. Assuming a practical accuracy of ± 0.1 mm for diameter and length, results in a typical error of approximately ± 1 mL in core volume (or ± 1 g in terms of porewater mass) for the core dimensions commonly used. Such an error would translate to an error in saturation ratio of approximately ± 0.045 at porewater contents of 40 – 50 g. Thus, the initial state can be assumed saturated for all samples with saturation ratios > 0.955. Two samples, STA3-1 and STA3-3, yield saturation ratios of 0.93 – 0.94 and may thus have been initially marginally desaturated, indicative of the presence of a gas phase (already in situ or after core retrieval). Note that these samples are still nearly saturated.

Tab. 4.7-4: Core dimensions and derived petrophysical parameters

| **Parameter** | **Unit** | **STA3-1** | **STA3-2** | **STA3-4** | **STA3-3** |
|---|---|---|---|---|---|
| Depth | [m] | 744.88 | 827.93 | 849.98 | 903.38 |
| Geological unit | | Wedelsst. Fm. | Opalinus Clay | Opalinus Clay | Staffelegg Fm. |
| **Pre_Core_M** | [g] | **1'054.02** | **1'096.28** | **945.56** | **1'091.56** |
| Pre_Core_DM | [cm] | 8.02 | 8.00 | 8.00 | 8.00 |
| Pre_Core_L | [cm] | 8.27 | 8.71 | 7.37 | 8.58 |
| Pre_Core_A | [$cm^2$] | 50.47 | 50.26 | 50.30 | 50.25 |
| Pre_Core_V | [$cm^3$] | 417.58 | 437.93 | 370.59 | 430.89 |
| **Post_Core_M** | [g] | **1'060.45** | **1'099.93** | **949.46** | **1'094.30** |
| Post_Core_DM | [cm] | 8.03 | 8.01 | 8.02 | 8.00 |
| Post_Core_L | [cm] | 8.31 | 8.74 | 7.42 | 8.59 |
| Post_Core_A | [$cm^2$] | 50.62 | 50.39 | 50.48 | 50.20 |
| Post_Core_V | [$cm^3$] | 420.92 | 440.57 | 374.39 | 431.29 |
| **Delta_M** | [g] | **6.43** | **3.65** | **3.90** | **2.74** |
| Delta_Core_DM | [cm] | 0.012 | 0.010 | 0.014 | -0.004 |
| Delta_Core_L | [cm] | 0.041 | 0.030 | 0.049 | 0.016 |
| Delta_Core_A | [$cm^2$] | 0.154 | 0.130 | 0.179 | -0.047 |
| **Delta_Core_V** | [$cm^3$] | **3.340** | **2.636** | **3.807** | **0.399** |
| Delta_Core_V-% | [%] | 0.800 | 0.602 | 1.027 | 0.093 |
| **Pre_Bulk_WD** | [$g/cm^3$] | **2.524** | **2.503** | **2.552** | **2.533** |
| **Post_Bulk_WD** | [$g/cm^3$] | **2.519** | **2.497** | **2.536** | **2.537** |
| Delta_Bulk_WD | [$g/cm^3$] | -0.005 | -0.007 | -0.016 | 0.004 |
| Delta_Bulk_WD-% | [%] | -0.188 | -0.267 | -0.609 | 0.159 |
| **Pre_GD** | [$g/cm^3$] | **2.715** | **2.711** | **2.745** | **2.685** |
| **Post_GD** | [$g/cm^3$] | **2.714** | **2.713** | **2.725** | **2.697** |
| Delta_GD | [$g/cm^3$] | -0.001 | 0.002 | -0.021 | 0.013 |
| **Corr_Pre_GD** | [$g/cm^3$] | **2.692** | **2.706** | **2.724** | **2.681** |
| **Pre_WCw** | | **0.0441** | **0.0485** | **0.0435** | **0.0355** |
| **Post_WCw** | | **0.0451** | **0.0506** | **0.0431** | **0.0372** |
| Delta_WCw | | 0.0010 | 0.0021 | -0.0004 | 0.0017 |
| **Corr_Pre_WCw** | | **0.0393** | **0.0474** | **0.0392** | **0.0348** |
| **Pre_$H_2O$_Core** | [g] | **46.52** | **53.16** | **41.13** | **38.73** |
| **Post_$H_2O$_Core** | [g] | **47.83** | **55.64** | **40.95** | **40.70** |
| Delta_$H_2O$_Core | [g] | 1.30 | 2.48 | -0.18 | 1.97 |
| **Corr_Pre_$H_2O$_Core** | [g] or [mL] | **41.40** | **51.99** | **37.05** | **37.96** |
| Unsat_Vol | [g] or [mL] | 3.09 | 1.01 | 0.09 | 2.34 |
| Pore_Vol_tot | [mL] | 44.49 | 53.00 | 37.15 | 40.30 |
| **Sat_ratio** | | **0.93** | **0.98** | **1.00** | **0.94** |
| **Pre_Poro_WL** | | **0.1114** | **0.1214** | **0.1110** | **0.0899** |
| **Post_Poro_WL** | | **0.1136** | **0.1263** | **0.1094** | **0.0944** |
| Delta_Poro_WL | | 0.0022 | 0.0049 | -0.0016 | 0.0045 |
| Delta_Poro_WL-% | [%] | 1.9874 | 4.0456 | -1.4399 | 4.9993 |
| **Corr_Pre_Poro_WL** | | **0.0991** | **0.1187** | **0.1000** | **0.0881** |
| **Corr_Pre_Poro_tot** | | **0.1065** | **0.1210** | **0.1002** | **0.0935** |
| Delta_Corr_Poro_WL-% | [%] | -11.02 | -2.19 | -9.91 | -1.99 |

_L = length; _A = area; _V = volume; _M = mass; WD = wet density; GD = grain density; WCw = water content rel. to wet mass; _WL = water loss

There are significant differences in water content measured in adjacent samples (pre-characterisation) and in the core itself (post-mortem), the latter showing 2 – 5%$_{rel.}$ higher values. This reduces to 2%$_{rel.}$ lower values (11% in case of STA3-1) when accounting for core expansion (Fig. 4.7-3). This leads to different values of bulk wet density, water-loss porosity and grain density (assuming saturated conditions) derived from pre-characterisation and post-mortem data. This spread is larger than measurement uncertainties and illustrates that the largest contribution to uncertainty is sample heterogeneity for parameters that depend on water content. Differences in water content commonly correlate with differences in clay-mineral content, such that this heterogeneity is mainly an issue of lamination in fine-grained sediments. In case of the STA3-1 core, a thin layer enriched in calcite at the bottom of the AD core (visible as bright band/laminae on the CT image, Fig. 4.7-2) is suspected to cause the low water content determined post-mortem for the bottom slice. Note, that for STA3-1, an additional water content was determined gravimetrically on two slices over the entire post-mortem core for the IsoEx experiments. This bulk value from IsoEx slices is slightly higher than the weighted average calculated from the different slices, pointing to some uncertainty introduced by the cutting and averaging procedure in case of high heterogeneity.

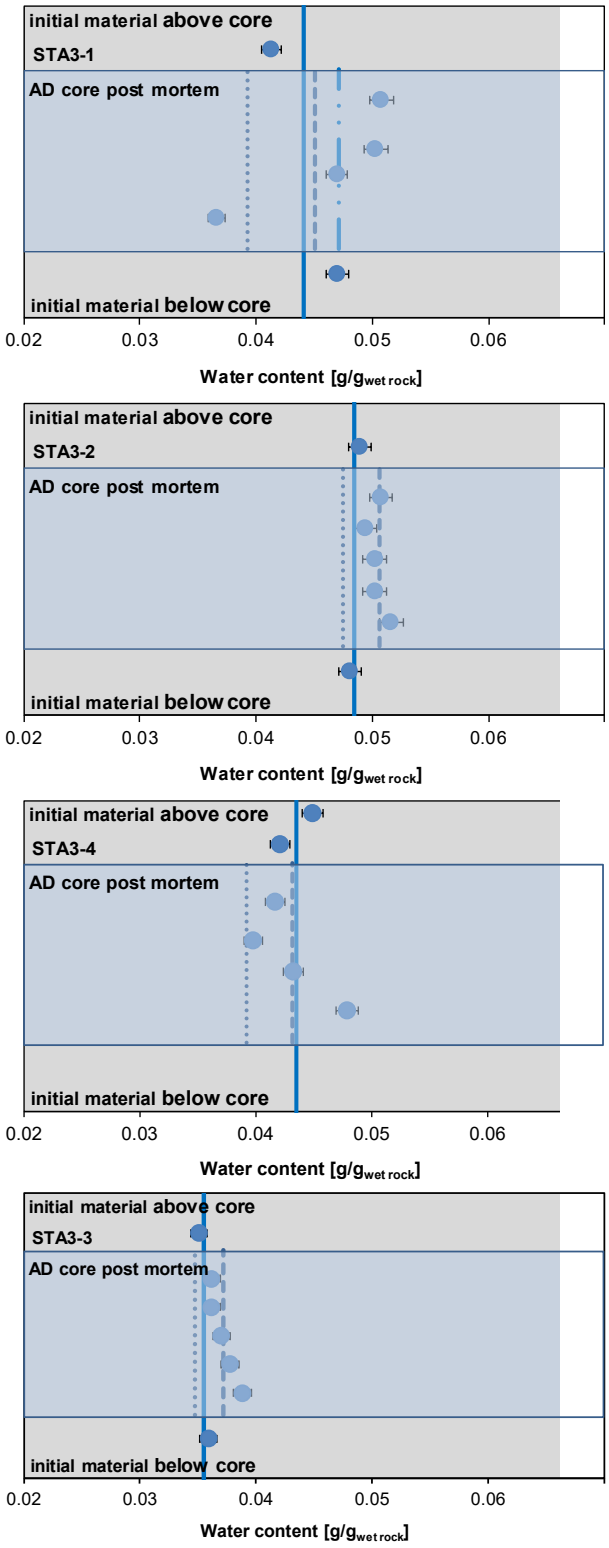


Fig. 4.7-3: Details of water content measurements before and after AD experiments

STA3-1 = STA3-1-744.88-AD (Wedelsandstein Formation); STA3-2 = STA3-1-827.93-AD (Opalinus Clay); STA3-4 = STA3-1-849.98-AD (Opalinus Clay); STA3-3 = STA3-1-903.38-AD (Staffelegg Formation). Vertical lines indicate the average value for pre-characterisation (solid line), average of post-mortem characterisation (dashed line) and the calculated corrected initial water content (dotted line). In STA3-1 the value obtained in the Iso-Ex experiment is indicated in addition (dash-dot-line). Error bars refer to measurement uncertainty of 2%.

### 4.7.4 Aqueous extracts, CEC and cation selectivity of AD samples

Aqueous extracts, CEC and cation selectivity determinations were carried out within the pre-characterisation and post-mortem analysis. Detailed analyses are provided in Appendix B. Methods are the same as used for other core samples (Waber ed. 2020), with the exception of sample masses for water content that may have been smaller than used for regular core sample analysis. Averaged data – also used for integrative data plots – are presented in this section. Averaging refers to aqueous extraction measurements of pieces above and below the segment used for the AD experiments (indicated in Fig. 4.7-2 and Tab. 4.7-5). For CEC / cation selectivity, the pieces were combined in equal proportions and analysed as a single sample.

All averaged aqueous extract solutions (Tab. 4.7-5) from pre-characterisation processed at *S/L* ≈ 1 contain low concentrations of $NH_4$ (up to 1.8 mg/L) and $NO_3$ (up to 0.36 mg/L). *S/L* ($S_d$/(L+PW)) refers to the exact *S/L* of the aqueous extract accounting for the porewater of the wet solid sample. The factor (1/WCw·L/Sw) refers to the scaling factor required to scale aqueous concentrations for conservative components to porewater concentrations (i.e., at water content).

Characteristic molar ion ratios (Tab. 4.7-6) do not follow a systematic trend with depth. Tab. 4.7-7 shows that the aqueous extract solutions are at or very close to calcite saturation. Extracts are distinctly undersaturated with respect to sulphates and strontianite, and slightly undersaturated with respect to dolomite (ordered). TIC was used as input for the carbon system because the titrated alkalinity would also include acetate. However, the calculated alkalinity agrees well with the measured one due to low relative acetate concentrations in samples from this borehole.

Tab. 4.7-5: Composition of aqueous extract solutions from pre-characterisation

| **Parameter** | **Unit** | **STA3-1** | **STA3-2** | **STA3-4** | **STA3-3** |
|---|---|---|---|---|---|
| Depth | [m] | 744.88 | 827.93 | 849.98 | 903.38 |
| Geological unit | | Wedelsandstein Fm. | Opalinus Clay | Opalinus Clay | Staffelegg Fm. |
| averaging | | top+base (1+1) | top+base (1+1) | top1+top2 (2+0) | top+base (1+1) |
| $1/WC_w*L/S_w$ | | 23.88 | 21.85 | 24.28 | 29.60 |
| Rock wet | [g] | 30.15 | 30.21 | 29.83 | 30.05 |
| Water | [g] | 30.31 | 30.54 | 30.17 | 30.49 |
| $WC_w$ | [$g/g_{wet}$] | 0.044 | 0.048 | 0.043 | 0.035 |
| $S/L$ ($S_d/(L+PW)$) | | 0.911 | 0.898 | 0.907 | 0.918 |
| pH at titration | | 9.05 | 8.87 | 8.48 | 8.78 |
| Na | [mg/L] | 245 | 319 | 283 | 250 |
| $NH_4$ | [mg/L] | 1.85 | 1.72 | 1.50 | 1.55 |
| K | [mg/L] | 6.69 | 5.90 | 9.48 | 5.65 |
| Ca | [mg/L] | 2.92 | 2.84 | 2.80 | 2.21 |
| Mg | [mg/L] | 0.403 | 0.574 | 0.529 | 0.622 |
| Sr (OES) | [mg/L] | 0.048 | 0.089 | < 0.1 | 0.060 |
| Ba (OES) | [mg/L] | < 0.025 | < 0.025 | < 0.025 | < 0.025 |
| F | [mg/L] | 5.01 | 2.10 | 2.17 | 4.26 |
| Cl | [mg/L] | 135 | 179 | 148 | 155 |
| Br | [mg/L] | 0.51 | 0.64 | 0.47 | 0.57 |
| $NO_3$ | [mg/L] | 0.36 | 0.12 | 0.29 | 0.14 |
| $SO_4$ | [mg/L] | 207 | 222 | 197 | 171 |
| Alk (tit) | [meq/L] | 2.77 | 4.68 | 4.17 | 3.08 |
| Alk as $HCO_3$ | [mg/L] | 168.7 | 285.6 | 254.6 | 187.6 |
| TOC | [mg/L] | 10.90 | 6.65 | 1.85 | 5.40 |
| TIC | [mg/L] | 32.0 | 54.1 | 51.9 | 33.3 |
| lactate | [mg/L] | < 0.2 | < 0.2 | < 2 | < 0.2 |
| acetate | [mg/L] | 4.00 | 8.41 | 5.48 | 3.94 |
| propionate | [mg/L] | 0.991 | < 0.2 | < 2 | < 0.2 |
| formate | [mg/L] | 0.282 | 0.258 | < 2 | 0.219 |

Tab. 4.7-6: Cation ratios and details of carbon system in aqueous extract solutions from pre-characterisation

| **Parameter** | **Unit** | **STA3-1** | **STA3-2** | **STA3-4** | **STA3-3** |
|---|---|---|---|---|---|
| Depth | [m] | 744.88 | 827.93 | 849.98 | 903.38 |
| Geol. unit | | Wedelsandstein Fm. | Opalinus Clay | Opalinus Clay | Staffelegg Fm. |
| Br/Cl*1'000 | [mol/mol] | 1.66 | 1.58 | 1.41 | 1.64 |
| $SO_4$/Cl | [mol/mol] | 0.56 | 0.46 | 0.49 | 0.41 |
| Ca/Mg | [mol/mol] | 4.39 | 3.00 | 3.21 | 2.15 |
| Ca/Sr | [mol/mol] | 134 | 70 | Sr < 0.1 | 81 |
| (Ca+Mg)/(Na+K) | [eq/eq] | 0.013 | 0.010 | 0.011 | 0.010 |
| Alk (tit) | [meq/L] | 2.77 | 4.68 | 4.17 | 3.08 |
| TIC | [meq/L] | 2.66 | 4.50 | 4.32 | 2.77 |
| acetate | [meq/L] | 0.068 | 0.142 | 0.093 | 0.067 |
| TOC | [mg/L] | 10.9 | 6.7 | 1.8 | 5.4 |
| acetate (as C) | [mg/L] | 1.63 | 3.42 | 2.23 | 1.60 |

Tab. 4.7-7: Saturation indices calculated for aqueous extract solutions from pre-characterisation

| **Parameter** | **unit** | **STA3-1** | **STA3-2** | **STA3-4** | **STA3-3** |
|---|---|---|---|---|---|
| Depth | [m] | 744.88 | 827.93 | 849.98 | 903.38 |
| Geological unit | | Wedelsandstein Fm. | Opalinus Clay | Opalinus Clay | Staffelegg Fm. |
| Charge | [eq/$kg_w$] | -2.1E-04 | -2.6E-04 | 9.0E-06 | 1.9E-04 |
| %-Error | | -0.93 | -0.92 | 0.04 | 0.85 |
| Acetate | [eq/$kg_w$] | 6.8E-05 | 1.4E-04 | 9.3E-05 | 6.7E-05 |
| Ionic strength | [mol/$kg_w$] | 1.34E-02 | 1.67E-02 | 1.48E-02 | 1.29E-02 |
| tot_alk | [eq/kg] | 2.92E-03 | 4.79E-03 | 4.42E-03 | 2.92E-03 |
| pH | | 9.05 | 8.87 | 8.48 | 8.78 |
| Log $P_{CO2}$ | [bar] | -3.89 | -3.48 | -3.09 | -3.59 |
| SI(calcite) | | 0.08 | 0.10 | -0.26 | -0.25 |
| SI(dolomite) | | -0.35 | -0.15 | -0.90 | -0.70 |
| SI(gypsum) | | -2.76 | -2.79 | -2.80 | -2.93 |
| SI(celestite) | | -2.81 | -2.56 | -5.52 | -2.77 |
| SI(strontionaite) | | -1.23 | -0.93 | -4.25 | -1.35 |
| SI(anhydrite) | | -2.98 | -3.01 | -3.02 | -3.16 |

PSI/Nagra 2012 thermodynamic database (Thoenen et al. 2014), calculated in PHREEQC for 25°C, using ordered dolomite; kgw = kg water; charge = Σ(cation charge) – ׀Σ(anion charge)׀ ; %-error = 100*charge / (Σ(cation charge) + ׀Σ(anion charge)׀ ).

Aqueous extracts of all cores were also produced after termination of the experiments. A thin disc (13 – 24 mm) from the top and base of each core was processed according to the protocols used for pre-characterisation. The base of the core represents the inlet of the artificial porewater (APW), whereas the top represents the outflow to sampling. The two may yield different results depending on the overall progress of fluid percolation (different concentrations in inlet sample compared to outlet), and averaging is therefore meaningless, unless a full breakthrough was achieved, including equilibration with the exchanger.

Results (Tab. 4.7-8) show that Br (not present in the APW) was effectively flushed out of each core, whereas other minor anionic components were buffered to some extent (e.g., F, $NO_3$). Cores with excessive $NO_3$ exfiltration (STA3-2 and STA3-3) show high $NO_3$ concentrations in the aqueous extracts especially in the top (outflow side) of the core (post-mortem), which indicates nitrogen mobilisation in the core during infiltration (artefact, discussed in Section 4.7.5.4).

The initially observed elevated TOC and acetate were partially flushed out at the APW inlet side, except for cores with excessive $NO_3$ exfiltration: the mobilisation of $NO_3$ seems to correlate with TOC mobilisation and further seems to shift the composition of the TOC from low molecular organic acids to more complex organic molecules (both artefacts, Fig. 4.7-12). Ion-exchange processes must be considered to fully understand the changes in cation fractions. A more in-depth analysis will be required to reconcile differences between extracts from pre-characterisation and post-mortem analysis.

Calculation of post-mortem speciation and saturation indices (Tab. 4.7-9) of the aqueous extract solutions from Tab. 4.7-8 indicated no significant change compared to calculations based on core material before the experiment: post-mortem extracts are also close to calcite saturation and distinctly undersaturated with respect to sulphates and strontianite. TIC was used as input for the carbon system.

Cation exchange capacities and cation selectivities determined by the Ni-en method (Waber ed. 2020) were performed on one pre-combined sample for each core from the two samples used for aqueous extracts. The results are also presented and interpreted in Section 4.5. Tab. 4.7-10 shows uncorrected (for porewater contribution and mineral dissolution/precipitation) capacities of 73 – 121 meq/kg (dry rock) with errors of up to ~ ± 5%. Ni consumptions agree well with the sum of cations. Ammonium was not measured but is expected to be present on the exchanger judged by the presence of up to 2 mg/L of $NH_4$ in the aqueous extracts performed at the same *S/L* ratio (Tab. 4.7-5). The high nitrate concentrations derive from the Ni-en solution. The negative charge balance arises from the lack of incorporating ethylendiamine complexes from the Ni-en solution into the calculation (Tab. 4.7-10). The low Br concentrations agree with the Br concentrations in aqueous extracts, as well as the Br/Cl and $SO_4$/Cl ratios. The cation occupancies (selectivities) derived from Ni-en extracts and applying a correction for the porewater contribution are presented in Section 4.5.

Tab. 4.7-11 shows the results of post-mortem cation occupancy measurements performed on two AD cores using slices from the top (outflow) and the base (inflow) of the core. The sum of cations at the base of core STA3-1 is significantly lower than at the top and also lower than the pre-characterisation value. The low sum of cations indicates a lower clay content which coincides with the low water content at this location (Fig. 4.7-3). In addition, the Ni consumption is 20% below the sum of cations, suggesting mineral dissolution. STA3-3 material shows better agreement between top, bottom, pre- and post-characterisation values, in agreement with homogeneous water contents (Fig. 4.7-3). Cation occupancies at the core base are expected to be close to the equilibrium with the APW.

Tab. 4.7-8: Composition of aqueous extract solutions from post-mortem characterisation

| **Parameter** | **Unit** | **STA3-1** | | **STA3-2** | |
|---|---|---|---|---|---|
| Depth | [m] | 744.88 | | 827.93 | |
| Geological unit | | Wedelsandstein Formation | | Opalinus Clay | |
| averaging | | top post-mortem (outflow side) | base post-mortem (inflow side) | top post-mortem (outflow side) | base post-mortem (inflow side) |
| $1/WC_w*L/S_w$ | | 20.93 | 28.11 | 20.91 | 20.69 |
| Rock wet | [g] | 30.14 | 30.68 | 30.14 | 30.85 |
| Water | [g] | 30.50 | 30.44 | 30.45 | 30.51 |
| $WC_w$ | [$g/g_{wet}$] | 0.051 | 0.037 | 0.051 | 0.050 |
| $S/L$ ($S_d/(L+PW)$) | | 0.89 | 0.94 | 0.89 | 0.91 |
| pH at titration | | 9.48 | 9.09 | 8.56 | 8.53 |
| Na | [mg/L] | 222 | 238 | 295 | 291 |
| $NH_4$ | [mg/L] | 2.55 | 1.93 | 1.70 | 1.71 |
| K | [mg/L] | 4.43 | 6.68 | 5.78 | 6.10 |
| Ca | [mg/L] | 1.98 | 2.75 | 3.50 | 3.66 |
| Mg | [mg/L] | 0.28 | 0.64 | 0.59 | 0.61 |
| Sr (OES) | [mg/L] | 0.04 | 0.04 | 0.08 | 0.07 |
| Ba (OES) | [mg/L] | < 0.05 | < 0.05 | < 0.05 | < 0.05 |
| F | [mg/L] | 5.38 | 3.68 | 2.23 | 2.19 |
| Cl | [mg/L] | 107.0 | 107.0 | 131 | 138 |
| Br | [mg/L] | < 0.16 | < 0.16 | 0.20 | < 0.16 |
| $NO_3$ | [mg/L] | 0.7 | 0.5 | 17.60 | 5.62 |
| $SO_4$ | [mg/L] | 186 | 217 | 197 | 188 |
| I | [mg/L] | n.a. | n.a. | n.a. | n.a. |
| Alk (tit) | [meq/L] | 2.87 | 2.56 | 4.80 | 4.86 |
| Alk as $HCO_3$ | [mg/L] | 175.3 | 156.3 | 292.6 | 296.6 |
| TOC | [mg/L] | 12.9 | 7.1 | 11.1 | 8.1 |
| TIC | [mg/L] | 36.1 | 30.7 | 58.3 | 58.8 |
| lactate | [mg/L] | < 2 | < 2 | < 2 | < 2 |
| acetate | [mg/L] | < 2 | < 2 | < 2 | 2.38 |
| propionate | [mg/L] | < 2 | 2.11 | < 2 | < 2 |
| formate | [mg/L] | < 2 | < 2 | < 2 | < 2 |

n.a.: not analysed

Tab. 4.7-8: (continued)

| **Parameter** | **Unit** | **STA3-4** | | **STA3-3** | |
|---|---|---|---|---|---|
| Depth | [m] | 849.98 | | 903.38 | |
| Geological unit | | Opalinus Clay | | Staffelegg Formation | |
| averaging | | top post-mortem (outflow side) | base post-mortem (inflow side) | top post-mortem (outflow side) | base post-mortem (inflow side) |
| $1/WC_w*L/S_w$ | | 24.89 | 21.50 | 28.78 | 28.43 |
| Rock wet | [g] | 30.38 | 30.50 | 30.40 | 30.05 |
| Water | [g] | 30.23 | 29.93 | 30.56 | 30.52 |
| $WC_w$ | [$g/g_{wet}$] | 0.042 | 0.048 | 0.036 | 0.037 |
| $S/L$ ($S_d/(L+PW)$) | | 0.92 | 0.93 | 0.93 | 0.91 |
| pH at titration | | 8.56 | 8.56 | 9.16 | 8.92 |
| Na | [mg/L] | 271 | 253 | 209 | 214 |
| $NH_4$ | [mg/L] | 1.70 | 1.49 | < 1 | < 1 |
| K | [mg/L] | 11.10 | 9.62 | 5.16 | 6.35 |
| Ca | [mg/L] | 3.25 | 3.14 | 1.69 | 2.27 |
| Mg | [mg/L] | < 1 | < 1 | 0.31 | 0.53 |
| Sr (OES) | [mg/L] | < 1 | < 1 | 0.04 | 0.06 |
| Ba (OES) | [mg/L] | < 0.025 | < 0.025 | < 0.025 | 0.03 |
| F | [mg/L] | 2.05 | 2.26 | 4.15 | 3.96 |
| Cl | [mg/L] | 132 | 109 | 95 | 121 |
| Br | [mg/L] | 0.20 | < 0.16 | 0.02 | < 0.016 |
| $NO_3$ | [mg/L] | 0.26 | 0.36 | 8.66 | 2.17 |
| $SO_4$ | [mg/L] | 193 | 184 | 136 | 156 |
| I | [mg/L] | n.a. | n.a. | n.a. | n.a. |
| Alk (tit) | [meq/L] | 4.29 | 4.33 | 3.58 | 3.00 |
| Alk as $HCO_3$ | [mg/L] | 262.0 | 264.3 | 218.4 | 183.1 |
| TOC | [mg/L] | 3.8 | 1.2 | 7.9 | 4.3 |
| TIC | [mg/L] | 51.3 | 52.5 | 38.7 | 34.4 |
| lactate | [mg/L] | < 2 | < 2 | < 0.2 | < 0.2 |
| acetate | [mg/L] | 5.62 | 2.74 | 2.49 | 0.67 |
| propionate | [mg/L] | < 2 | < 2 | < 0.2 | < 0.2 |
| formate | [mg/L] | < 2 | < 2 | 0.21 | < 0.2 |

n.a.: not analysed

Tab. 4.7-9: Saturation indices calculated for aqueous extract solutions obtained post-mortem

| **Parameter** | **Unit** | **STA3-1** | **STA3-1** | **STA3-2** | **STA3-2** |
|---|---|---|---|---|---|
| Depth | [m] | 744.88 | | 827.93 | |
| Geological unit | | Wedelsandstein Formation | | Opalinus Clay | |
| Position | | top post-mortem | base post-mortem | top post-mortem | base post-mortem |
| Charge | [eq/$kg_w$] | -8.5E-04 | 2.5E-04 | 1.1E-04 | 1.1E-04 |
| %-Error | | -4.15 | 1.18 | 0.42 | 0.43 |
| Acetate | [eq/$kg_w$] | < 3E-05 | < 3E-05 | < 3E-05 | 4.0E-05 |
| Ionic strength | [mol/$kg_w$] | 1.26E-02 | 1.29E-02 | 1.52E-02 | 1.50E-02 |
| tot_alk | [eq/kg] | 3.70E-03 | 2.84E-03 | 4.99E-03 | 5.02E-03 |
| pH | | 9.48 | 9.09 | 8.56 | 8.53 |
| log$P(CO_2)$ | [bar] | -4.32 | -3.95 | -3.12 | -3.09 |
| SI(calcite) | | 0.29 | 0.07 | -0.05 | -0.05 |
| SI(dolomite) | | 0.10 | -0.14 | -0.52 | -0.52 |
| SI(gypsum) | | -3.03 | -2.77 | -2.71 | -2.71 |
| SI(celestite) | | -3.00 | -2.82 | -2.63 | -2.69 |
| SI(strontianite) | | -0.95 | -1.25 | -1.22 | -1.29 |
| SI(anhydrite) | | -3.25 | -2.99 | -2.94 | -2.93 |
| **Parameter** | **Unit** | **STA3-4** | **STA3-4** | **STA3-3** | **STA3-3** |
| Depth | [m] | 849.98 | | 903.38 | |
| Geological unit | | Opalinus Clay | | Staffelegg Formation | |
| Position | | top post-mortem | base post-mortem | top post-mortem | base post-mortem |
| Charge | [eq/$kg_w$] | 2.4E-04 | 1.3E-04 | -7.8E-05 | -3.1E-04 |
| %-Error | | 1.00 | 0.58 | -0.42 | -1.60 |
| Acetate | [eq/$kg_w$] | 9.5E-05 | 4.6E-05 | 4.2E-05 | 1.1E-05 |
| Ionic strength | [mol/$kg_w$] | 1.42E-02 | 1.34E-02 | 1.10E-02 | 1.15E-02 |
| tot_alk | [eq/kg] | 4.27E-03 | 4.37E-03 | 3.54E-03 | 3.04E-03 |
| pH | | 8.56 | 8.56 | 9.16 | 8.92 |
| log$P(CO_2)$ | [bar] | -3.19 | -3.18 | -3.92 | -3.72 |
| SI(calcite) | | -0.12 | -0.12 | 0.04 | -0.08 |
| SI(dolomite) | | -0.71 | -0.67 | -0.29 | -0.45 |
| SI(gypsum) | | -2.72 | -2.74 | -3.16 | -2.95 |
| SI(celestite) | | -5.49 | -5.50 | -3.02 | -2.82 |
| SI(strontianite) | | -4.17 | -4.15 | -1.08 | -1.22 |
| SI(anhydrite) | | -3.02 | -3.05 | -3.38 | -3.17 |

PSI/Nagra 2012 thermodynamic database, calculated in PHREEQC for 25 °C, using ordered dolomite; kgw = kg water; charge = Σ(cation charge) – ıΣ(anion charge)ı ; %-error = 100*charge / (Σ(cation charge) + ıΣ(anion charge)ı).

Tab. 4.7-10: Composition of Ni-en extract solutions and related parameters from pre-characterisation

| **Parameter** | **Unit** | **STA3-1** | **STA3-2** | **STA3-4** | **STA3-3** |
|---|---|---|---|---|---|
| Depth | [m] | 744.88 | 827.93 | 849.98 | 903.38 |
| Geological unit | | Wedelsandstein Fm. | Opalinus Clay | Opalinus Clay | Staffelegg Fm. |
| averaging | | 1 averaged sample | 1 averag. sample | No sample | 1 averag. sample |
| $1/WC_w*L/S_w$ | | 24.40 | 22.04 | | 29.90 |
| Rock wet | [g] | 30.04 | 30.34 | | 30.30 |
| Solution | [g] | 31.03 | 30.95 | | 31.07 |
| $WC_w$ | [$g/g_{wet}$] | 0.04 | 0.05 | | 0.04 |
| $S/L$ ($S_d/(L+PW)$) | | 0.89 | 0.89 | | 0.91 |
| pH (initial) | | 8.29 | 8.29 | | 8.29 |
| Ni (initial) | [mg/L] | 5'730 | 5'885 | | 5'885 |
| pH (final) | | 8.38 | 8.30 | | 8.43 |
| Na | [mg/L] | 1'229 | 1235 | | 820 |
| K | [mg/L] | 209 | 173 | | 149 |
| Mg | [mg/L] | 153 | 122 | | 78 |
| Ca | [mg/L] | 712 | 560 | | 397 |
| Sr | [mg/L] | 23.8 | 20.1 | | 15.4 |
| Ba | [mg/L] | 0.191 | 0.475 | | 1.328 |
| Fe | [mg/L] | < 0.05 | < 0.05 | | < 0.05 |
| Ni | [mg/L] | 2330 | 2714 | | 3821 |
| F | [mg/L] | 0.24 | 0.12 | | 0.33 |
| Cl | [mg/L] | 126 | 163 | | 147 |
| Br | [mg/L] | 0.47 | 0.58 | | 0.52 |
| $NO_3$ | [mg/L] | 12'306 | 12'424 | | 12'585 |
| $SO_4$ | [mg/L] | 139 | 140 | | 126 |
| TDS | [mg/L] | 17'228 | 17'552 | | 18'141 |
| Charge %-error | [%] | -4.62 | -4.74 | | -3.33 |
| Na | [meq/$kg_d$] | 60.2 | 60.3 | | 39.2 |
| K | [meq/$kg_d$] | 6.0 | 5.0 | | 4.2 |
| Mg | [meq/$kg_d$] | 14.2 | 11.3 | | 7.1 |
| Ca | [meq/$kg_d$] | 40.0 | 31.4 | | 21.8 |
| Sr | [meq/$kg_d$] | 0.61 | 0.52 | | 0.39 |
| Ba | [meq/$kg_d$] | 0.003 | 0.008 | | 0.021 |
| Fe | [meq/$kg_d$] | < 0.002 | < 0.002 | | < 0.002 |
| SumCat | [meq/$kg_d$] | 121.1 | 108.5 | | 72.7 |
| SumCat_err | [meq/$kg_d$] | 5.23 | 4.87 | | 3.21 |
| Ni_cons | [meq/$kg_d$] | 121.5 | 111.1 | | 70.0 |
| Ni_cons_err | [meq/$kg_d$] | 4.60 | 4.80 | | 5.10 |
| Br/Cl | [mol/mol*1000] | 1.66 | 1.58 | | 1.57 |
| $SO_4$/Cl | [mol/mol] | 0.41 | 0.32 | | 0.32 |

kgd = kg dry rock

Tab. 4.7-11: Composition of Ni-en extract solutions and related parameters from post-characterisation

| **Parameter** | **Unit** | **STA3-1** | | **STA3-3** | |
|---|---|---|---|---|---|
| Depth | [m] | 744.88 | | 903.38 | |
| Geological unit | | Wedelsandstein Formation | | Staffelegg Formation | |
| averaging | | top post-mortem | base post-mortem | top post-mortem | base post-mortem |
| $1/WC_w*L/S_w$ | | 19.99 | 28.97 | 29.32 | 27.55 |
| Rock wet | [g] | 30.34 | 30.16 | 30.31 | 30.14 |
| Solution | [g] | 30.82 | 30.87 | 31.06 | 31.08 |
| $WC_w$ | [$g/g_{wet}$] | 0.053 | 0.037 | 0.036 | 0.039 |
| *S/L* ($S_d/(L+PW)$) | | 0.89 | 0.91 | 0.91 | 0.90 |
| pH (initial) | | 8.25 | 8.25 | 8.25 | 8.25 |
| Ni (initial) | [mg/L] | 5'183 | 5'183 | 6'023 | 6'023 |
| pH (final) | | 8.55 | 8.41 | 8.38 | 8.37 |
| Na | [mg/L] | 1'193 | 852 | 756 | 725 |
| K | [mg/L] | 184 | 138 | 119 | 123 |
| Mg | [mg/L] | 129 | 134 | 72 | 98 |
| Ca | [mg/L] | 549 | 420 | 404 | 431 |
| Sr | [mg/L] | 22.3 | 10.8 | 12.1 | 9.9 |
| Ba | [mg/L] | 0.105 | 0.120 | 0.743 | 0.718 |
| Fe | [mg/L] | < 0.05 | < 0.05 | < 0.05 | < 0.05 |
| Ni | [mg/L] | 2'291 | 3'219 | 3'842 | 3'844 |
| F | [mg/L] | 0.46 | 0.50 | 0.85 | 0.89 |
| Cl | [mg/L] | 99 | 105 | 97 | 101 |
| Br | [mg/L] | < 0.16 | < 0.16 | < 0.16 | < 0.16 |
| $NO_3$ | [mg/L] | 12'574 | 13'060 | 12'697 | 12'521 |
| $SO_4$ | [mg/L] | 150 | 113 | 97 | 91 |
| TDS | [mg/L] | 17'193 | 18'051 | 18'097 | 17'946 |
| Charge %-error | [%] | -9.29 | -8.42 | -4.07 | -2.81 |
| Na | [$meq/kg_d$] | 58.3 | 41.9 | 36.2 | 35.1 |
| K | [$meq/kg_d$] | 5.3 | 4.0 | 3.4 | 3.5 |
| Mg | [$meq/kg_d$] | 11.9 | 12.4 | 6.5 | 9.0 |
| Ca | [$meq/kg_d$] | 30.8 | 23.7 | 22.2 | 23.9 |
| Sr | [$meq/kg_d$] | 0.57 | 0.28 | 0.30 | 0.25 |
| Ba | [$meq/kg_d$] | 0.002 | 0.002 | 0.010 | 0.010 |
| Fe | [$meq/kg_d$] | < 0.002 | < 0.002 | < 0.002 | < 0.002 |
| SumCat | [$meq/kg_d$] | 107.0 | 82.3 | 68.5 | 71.8 |
| SumCat_err | [$meq/kg_d$] | 4.70 | 3.55 | 2.98 | 2.98 |
| Ni_cons | [$meq/kg_d$] | 101.3 | 66.3 | 74.1 | 74.4 |
| Ni_cons_err | [$meq/kg_d$] | 4.20 | 4.50 | 5.20 | 5.30 |
| Br/Cl | [mol/mol*1'000] | - | - | - | - |
| $SO_4$/Cl | [mol/mol] | 0.56 | 0.40 | 0.37 | 0.33 |

### 4.7.5 Chemical and isotopic evolution of displaced porewater aliquots

An artificial porewater (APW) was injected to force advective displacement. The outflow of each experiment was continuously sampled in small syringes (Waber ed. 2020). These syringe aliquots were analysed for chemical and water isotopic composition. Hydraulic conductivity was evaluated for each sampled aliquot (Darcy's law), and any expelled gas was also recorded, although gas-tightness is commonly good, but cannot be ensured for a syringe sampling system. Most data for each experiment are included in tables and graphs in this section, and more details are provided in Appendix B.

According to the method of advective displacement (Mäder 2018), it is expected that the first few sampled aliquots are of similar composition and represent the displaced porewater from the sample core. After this, a gradual breakthrough of the injected APW should be observed, until full breakthrough of conservative components (e.g. Cl, Br), given enough time.

#### 4.7.5.1 Artificial porewater used for advective displacement

In the absence of constraining data, an artificial porewater (APW) composition (Tab. 4.7-12, details in text below) was chosen that was based on work performed for the deep geothermal well Schlattingen-1 (advective-displacement experiments detailed in Mäder & Waber 2017). The composition was calculated with PHREEQC for 25 °C, to be saturated with respect to calcite and dolomite, and a partial pressure of $CO_2$ of $10^{-2.2}$ bar. This partial pressure was imposed by bubbling with an $Ar/CO_2$ gas mixture during mixing and again when the fluid reservoir was filled before the experiments started. A recipe with the appropriate amounts of PA-grade chemicals is given in Tab. 4.7-13.

Deuterium was added as a water tracer for advective-diffusive transport, aiming for a $\delta^2H$ of approximately +100 ‰ (VSMOW). There is no Br contained in the APW and therefore bromide-breakout can be used as an anionic tracer in the case of significant Br concentrations in the porewater. If the Cl concentration in the APW is significantly different from the displaced early aliquots, Cl breakthrough forms an additional anionic tracer for transport.

Experiments STA3-1 to STA3-3 were fed from the same PFA-coated fluid tank containing the APW from batch3 (Tab. 4.7-12). On April 8, 2021, the infiltration tank had to be topped up with APW batch2, and the resulting mixture with the earlier batch was measured. This date corresponds to 0.57, 0.22 and 0.50 pore volumes, respectively (during syringes 10, 6, and 10, respectively). STA3-4 was infiltrated from a different tank containing APW batch2 exclusively. After every tank opening, the headspace was filled with He after bubbling with the $Ar/CO_2$ gas mixture mentioned above. The compositions of the different APW batches were designed to be identical and the analyses agree well within analytical uncertainties.

Tab. 4.7-12: Composition and recipe for the artificial porewater

* calculated from the weighed-in chemical compounds; pH measured; $CO_2$-Ar bubbling not taken into account; n.a.: not analysed.

| **Parameter** | **Unit** | **Recipe** | **Batch3 STA3-1 to STA3-3 initial** | | **Batch2 Top-up, STA3-4** | | **Mix (top up)** | **Compounds** |
|---|---|---|---|---|---|---|---|---|
| | | | **Calc.*** | **Meas.** | **Calc.*** | **Meas.** | **Meas.** | |
| pH | | 7.19 | | 7.38 | | 7.43 | 7.75 | |
| Na | [mg/L] | 3'989 | 3'988 | 4'059 | 3'988 | 4'009 | 4'013 | NaCl; $NaHCO_3$; $Na_2SO_4$ |
| $NH_4$ | [mg/L] | | | < 10 | | < 10 | < 10 | |
| K | [mg/L] | 79.4 | 79.3 | 78.7 | 79.4 | 78.4 | 78.8 | KCl |
| Ca | [mg/L] | 503 | 504 | 506 | 503 | 488 | 500 | $CaCl_2 \cdot 2H_2O$ |
| Mg | [mg/L] | 226 | 226 | 208 | 226 | 206 | 226 | $MgCl_2 \cdot 6H2O$ |
| Sr (OES) | [mg/L] | | | < 0.25 | | < 0.5 | < 10 | |
| Ba | [mg/L] | | | < 0.25 | | < 0.5 | n.m | |
| Si | [mg/L] | | | < 2.5 | | 9.04 | n.m | |
| Al | [mg/L] | | | 0.279 | | < 50 | n.m | |
| F | [mg/L] | | | < 1.6 | | < 1.6 | < 0.016 | |
| Cl | [mg/L] | 5'992 | 5'986 | 5'826 | 5'985 | 5'908 | 5'883 | $CaCl_2 \cdot 2H_2O$; KCl; $MgCl_2 \cdot 6H_2O$ |
| Br | [mg/L] | | | < 1.6 | | < 1.6 | < 0.016 | |
| $NO_3$ | [mg/L] | | | 5.25 | | 1.94 | 1.3 | |
| $SO_4$ | [mg/L] | 2'305 | 2'303 | 2'132 | 2'304 | 2'146 | 2'139 | $Na_2SO_4$ |
| I | [mg/L] | | | n.a. | | n.a | n.a | |
| TOC | [mg/L] | | | 7.4 | | < 5 | 112 | |
| TIC | [mg/L] | 29.3 | 29.32 | 28.0 | 29.33 | 33.9 | 34 | $NaHCO_3$ |
| lactate | [mg/L] | | | < 20 | | < 20 | < 20 | |
| acetate | [mg/L] | | | < 20 | | < 20 | < 20 | |
| propionate | [mg/L] | | | < 20 | | < 20 | < 20 | |
| formate | [mg/L] | | | < 20 | | < 20 | < 20 | |
| $\delta^{18}O$ | [‰ VSMOW] | | -11.43 | -11.52 | -11.43 | -11.24 | -11.34 | |
| $\delta^{2}H$ | [‰ VSMOW] | 100 | 91.9 | 90.8 | 110.9 | 113.3 | 111.2 | $D_2O$ |

Tab. 4.7-13: Recipe for the artificial porewater for a 2-litre batch

| **Chemical** | **Manufacturer** | **Grade** | **Recipe** | | **Batch3 STA3-1 to STA3-3** | **Batch2 STA3-4** |
|---|---|---|---|---|---|---|
| | | | [g/kg$_w$] | [g/2kg$_w$] | weighted in [g/2 L] | weighted in [g/2 L] |
| $NaHCO_3$ | Merck | p.a. | 0.2051 | 0.4101 | 0.4102 | 0.4103 |
| $CaCl_2 \cdot 2H_2O$ | Merck | p.a. | 1.8465 | 3.6930 | 3.6944 | 3.6922 |
| KCl | Merck | p.a. | 0.1514 | 0.3029 | 0.3026 | 0.3027 |
| $MgCl_2 \cdot 6H_2O$ | Merck | p.a. | 1.8907 | 3.7814 | 3.7827 | 3.7812 |
| NaCl | Merck | p.a. | 7.1916 | 14.3831 | 14.3838 | 14.3837 |
| $Na_2SO4$ | AnalaR NORMAPUR | Ph.Eur. | 3.4089 | 6.8177 | 6.8114 | 6.8121 |
| $D_2O$ (100%) | Roth | > 99.8% D | 0.0318 | 0.0635 | 0.0607 | 0.0673 |

### 4.7.5.2 Physical conditions, hydraulic conductivity, sampling, and pore volume equivalents

All core samples were subjected to 58 – 61 bar hydraulic confining pressure, and an infiltration pressure of initially around 48 bar set by a He headspace. The infiltration pressure was gradually decreasing with time (displaced APW, and any small He leak), and was replenished repeatedly until the end of the last experiments. The pressure range covered 44 – 48 bar.

Temperature conditions were stable without diurnal fluctuations, ranging seasonally from 21.5 to 25.5 °C. Critical temperature-sensitive measurements, such as electric conductivity, pH and hydraulic conductivity, were temperature-compensated, either intrinsically or explicitly (details in Waber ed. 2020).

Hydraulic conductivity referenced to 25 °C was evaluated for all sampled aliquots based on sample mass and Darcy's law (detailed data in Appendix B, method in Waber ed. 2020; Fig. 4.7-4). Observations in all AD experiments performed so far show initially lower apparent hydraulic conductivities due to the expulsion of gas from the dead volume in the outflow, and any small unsaturated volume in the sample core itself. Then, hydraulic conductivities increase, followed by a slight decrease to a steady-state value, if sufficient run-time was provided. However, some STA3 experiments behave differently: STA3-2 shows a distinct conductivity drop after the expected increasing trend at the beginning of the experiment (also observed in cores high in nitrate from the STA2-1 borehole; Zwahlen et al. *in prep.*), and STA3-3 a massive decrease after 1.5 pore volumes. The outflows of both cores contain large amounts of nitrate, and the Cl concentration in the outflow after 1.5 pore volumes of STA3-3 drops below the concentration in the infiltrating APW (Section 4.7.5.4). Especially at advanced decrease of hydraulic conductivity, increasing exfiltration of gas is observed. However, periods with low hydraulic conductivity and without gas exfiltration also occurred. All these unexpected observations are attributed to the interaction with the confining system and to microbial activity (discussed in the same section), which seems to affect conductivity. Also clogging in the filters or even in the inflow or outflow system cannot be ruled out. The increased water content in the core post-mortem compared to initial values indicates no clogging in the core itself. The graph in logarithmic scale better illustrates the differences between the early gas expulsion period, the period with the expected gradual conductivity increase, and the clogging period.

The early conductivities (after approximately 0.2 pore volumes, when gas exfiltration decreased, and conductivity increased linearly) and those measured towards the end of the experiments (Tab. 4.7-14) span a narrow range from 1.7 – 3.3 × $10^{-13}$ m/s (neglecting values attributed to clogging in the high nitrate cores). This conductivity refers to a direction perpendicular to bedding and a sample length of 8 – 9 cm, measured at very large hydraulic gradients (Tab. 4.7-2). A gradual but rather minor decrease after a maximum value (STA3-1) may be due to slow sample consolidation, and this was also observed in earlier work (Mäder 2018). These latter values are most representative for in situ conditions, although the confining stress of 60 bar (6 MPa) in the experiments is still considerably less than the lithostatic stresses at 426 – 598 m depth.

At 0.5 pore volumes, the APW level in the tank dropped below the feed capillary infiltrating the STA3-3 core. Subsequently, pressurised helium entered the core which led to faster fluid outflow, followed by a gas breakthrough (helium outflow into sampling syringe). After topping up the tank (Section 4.7.5.1) and re-establishment of the hydraulic head, helium gas contained in the sample core exfiltrated along with the porewater. This led to the visible low hydraulic conductivity shortly after 0.5 pore volumes (Fig. 4.7-7). Thereafter, the evolution of hydraulic conductivity continues as before the gas breakthrough. This suggests the closure of any potential preferential pathways after the gas breakthrough. The observed decrease in hydraulic conductivity after 1.5 pore volumes is likely not related to the gas event. The influence of the gas breakthrough on the evolution of the outflow chemistry is discussed in Section 4.7.5.4.

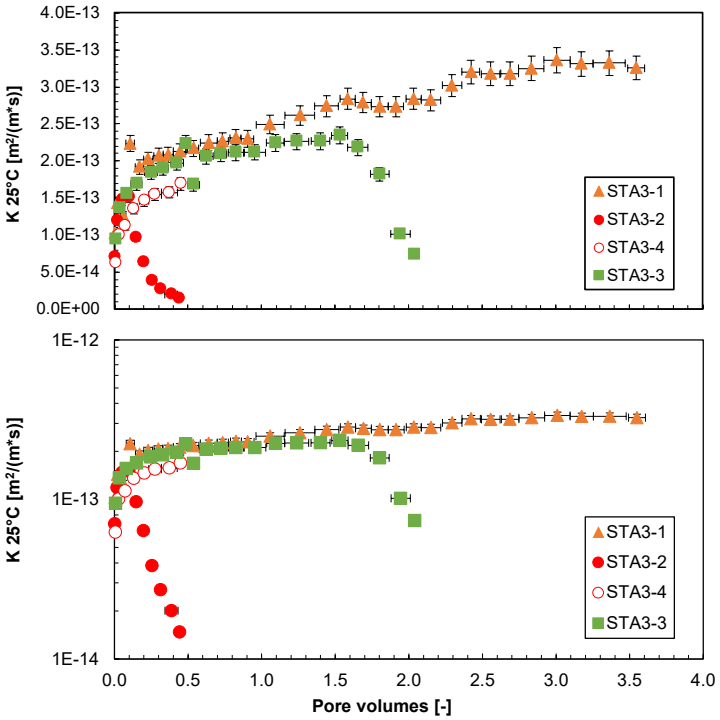


Fig. 4.7-4: Evolution of hydraulic conductivity during advective-displacement experiments

Linear scale (top) and logarithmic scale (bottom). STA3-1 = STA3-1-744.88-AD (Wedelsandstein Formation); STA3-2 = STA3-1-827.93-AD (Opalinus Clay); STA3-4 = STA3-1-849.98-AD (Opalinus Clay); STA3-3 = STA3-1-903.38-AD (Staffelegg Formation). Pore volume fractions relate to transport time based on water content. Experiment duration is 56 – 258 days. Horizontal length of symbol bar covers the sampling duration, vertical bars are an estimate of combined uncertainties.

Tab. 4.7-14: Hydraulic conductivity of AD samples

Defective values in *italics* (microbial activity, nitrate outflow, clogging).

| **Parameter** | **Unit** | **STA3-1** | **STA3-2** | **STA3-4** | **STA3-3** |
|---|---|---|---|---|---|
| Depth | [m] | 744.88 | 827.93 | 849.98 | 903.38 |
| Geological unit | | Wedelsandstein Fm. | Opalinus Clay | Opalinus Clay | Staffelegg Fm. |
| Early_K (25 °C) | [m/s] | $2.23 \times 10^{-13}$ | $1.52 \times 10^{-13}$ | $1.36 \times 10^{-13}$ | $1.69 \times 10^{-13}$ |
| Late_K (25 °C) | [m/s] | $3.27 \times 10^{-13}$ | *$1.47 \times 10^{-14}$* | $1.69 \times 10^{-13}$ | *$7.36 \times 10^{-14}$* |

The time axis for all data representations of sequential fluid aliquots is converted to pore volume fractions by dividing the cumulative sample mass (volume) by the water content of the core. In this way, experiments with very different hydraulic conductivities or different water contents can be represented in a meaningful way for transport. There may be some minor ambiguities in case where water contents from pre-characterisation deviate from the true water content of a sample core, or if a significant initial unsaturated porosity fraction would be present. The chosen approximation is sufficient for a visual presentation of data.

Sampled aliquots (mass) plotted versus pore volume fraction (time) provide an overview of all syringe samples taken for all three AD experiments (Fig. 4.7-5). For each experiment 8 to 33 samples were collected.

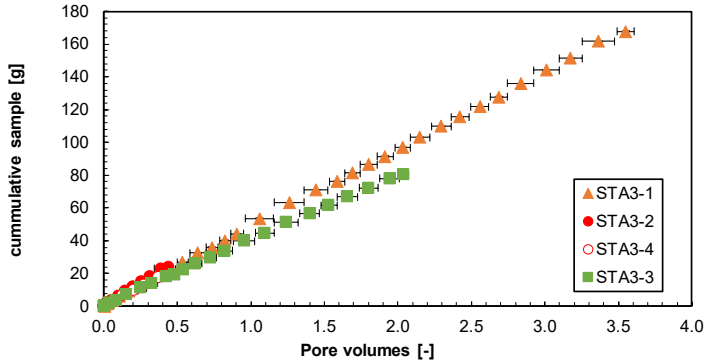


Fig. 4.7-5: Sampling schedule and sample volumes taken

STA3-1 = STA3-1-744.88-AD (Wedelsandstein Formation); STA3-2 = STA3-1-827.93-AD (Opalinus Clay); STA3-4 = STA3-1-849.98-AD (Opalinus Clay); STA3-3 = STA3-1-903.38-AD (Staffelegg Formation). Each data point represents a syringe aliquot taken, with the horizontal bar indicating the duration for sampling, here converted to pore volume fraction percolated. Different slopes reflect different volumetric flow rates scaled by porosity.

### 4.7.5.3 Inline measurement of electric conductivity and pH

Electric conductivity (EC) was continuously monitored in all experiments (Fig. 4.7-6, Waber ed. 2020, for method). Conductivity cells were initially calibrated but may show a drift to varying extent over time due to electrode corrosion, commonly resulting in low apparent readings. Therefore, electric conductivity values are only meant to provide an indication of salinity but are not used quantitatively.

The electric conductivities of STA3-1 and STA3-4 outflows show a similar evolution and follow in principle the major components. After a short plateau (barely visible at this scale) values decrease asymptotically and meet the expected APW value. The extremely high nitrate concentrations especially in the early outflow of the STA3-2 and STA3-3 lead to much higher electric conductivities compared to those of STA3-1 and STA3-4 (discussed in the section below).

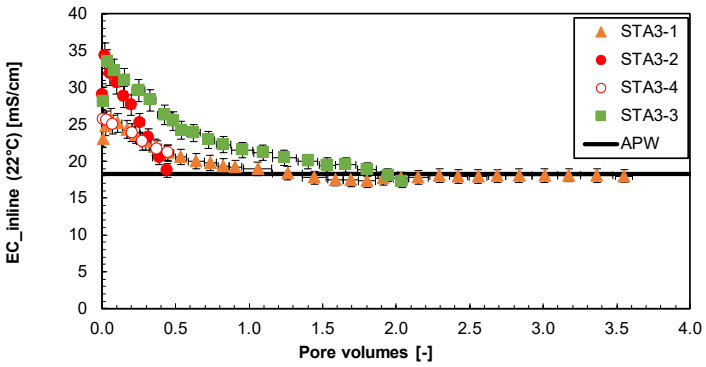


Fig. 4.7-6: Evolution of electric conductivity (22 °C) during advective-displacement experiments

STA3-1 = STA3-1-744.88-AD (Wedelsandstein Formation); STA3-2 = STA3-1-827.93-AD (Opalinus Clay); STA3-4 = STA3-1-849.98-AD (Opalinus Clay); STA3-3 = STA3-1-903.38-AD (Staffelegg Formation). Pore volume fractions relate to transport time based on water content. Experiment duration is 56 – 258 days days. Horizontal length of symbol bar covers the sampling duration, vertical bars are an estimate of combined uncertainties.

The aim was to measure pH inline three times before/after sampling of the first four aliquots, and less frequently at later times (method in Waber ed. 2020). Measurements took 12 – 24 hrs in most cases, to ensure that the dead volume of the very small flow-through pH cell was sufficiently flushed given the very slow flow rates of the experiments. The micro-electrode was left installed in the flow-through cell and was checked before and after each pH measurement period with a standard solution. The initial calibration was made at pH 7 and 9, and simple drift checks and corrections were made with a standard solution at pH 7. The electrode slope was checked from time to time and was found to remain remarkably stable. In most cases, drift corrections over 12 – 24 hrs were ≤ 0.1 pH units. The overall uncertainty is difficult to assess because these small electrodes may respond to manipulations at the flow-through cell (response to small strains), and also small gas bubbles temporarily affect readings. It is estimated that an error of ± 0.2 pH units is appropriate for most measurements. pH values of early aliquots are also tabulated below (Tab. 4.7-15).

These inline pH measurements (Fig. 4.7-7) are rather tricky and require careful handling of the equipment. Criteria to accept a value include a small drift and a reasonably well-defined pH-plateau, as well as a stable non-zero electric conductivity (no gas bubbles). It cannot be excluded that for long measurement durations some effect from outgassing or in-gassing of $CO_2$ may

influence the readings. pH measurements on small aliquots taken from the syringes are slightly shifted relative to the inline measurements but show comparable evolutions with progress of percolation. pH evolutions for each core are different and interpretation is not straightforward, especially in the light of the unknown mobilisation mechanism of nitrate.

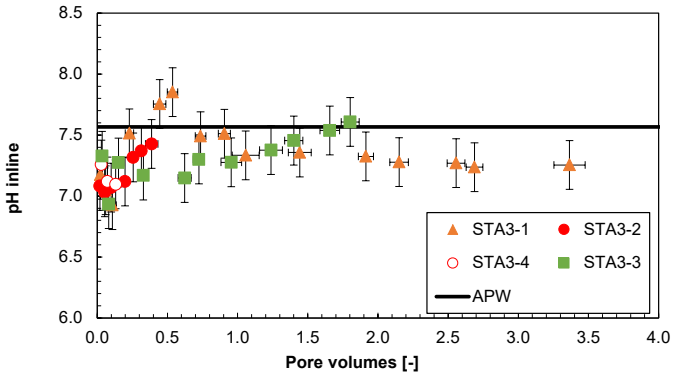


Fig. 4.7-7: Evolution of inline pH during advective-displacement experiments

STA3-1 = STA3-1-744.88-AD (Wedelsandstein Formation); STA3-2 = STA3-1-827.93-AD (Opalinus Clay); STA3-4 = STA3-1-849.98-AD (Opalinus Clay); STA3-3 = STA3-1-903.38-AD (Staffelegg Formation). Pore volume fractions relate to transport time based on water content. Experiment duration is 56 – 258 days. Horizontal length of symbol bar covers the sampling duration, vertical bars are an estimate of combined uncertainties.

### 4.7.5.4 Evolution of major and minor components

Evolution of concentrations with progress of percolation are shown in Figs. 4.7-8 to 4.7-13. Select analytical data for the first two aliquots sampled are summarised in Tab. 4.7-15 further below, with full details in Appendix B. The composition of the earliest aliquots displaced from the core samples are the most representative for the pore fluid extracted, and this is highlighted and interpreted in Section 4.7.5.5.

The displaced **major component Cl** presents a continuous decrease towards the APW, except in STA3-3: here, Cl drops below the APW concentration. This behaviour is only observed in cores with excessive nitrate exfiltration (especially in AD experiments on samples from the STA2-1 borehole; Zwahlen et al. *in prep.*) and might be caused by a connection between the confining fluid (diluted tap water, in contact with O-ring lubricant) and the core. The major component **$SO_4$** behaves as expected in all experiments: the $SO_4$ concentration starts above the APW and decreases smoothly towards APW values.

**The cations Na, Ca, Mg** are initially more concentrated in the outflow than in the injected APW and decrease steadily towards it (Fig. 4.7-8). In STA3-2 and STA3-3, Ca is expected to partly compensate for the exceptionally high nitrate, both decreasing with ongoing percolation (also see Fig. 4.7-10). In this case, nitrate forms a major component and is a carrier for anion charge along with chloride and sulphate.

The data gap in STA3-3 at 0.5 pore volumes represents the gas breakthrough (sample not measured, exposed to atmosphere) detailed in Section 4.7.5.2. The evolutions of major and minor compounds (Fig. 4.7-10) after the gas breakthrough follow the same trend as before the gas breakthrough. This indicates no substantial change in transport mechanisms due to the gas breakthrough, in line with no substantial change in hydraulic conductivity (Fig. 4.7-4).

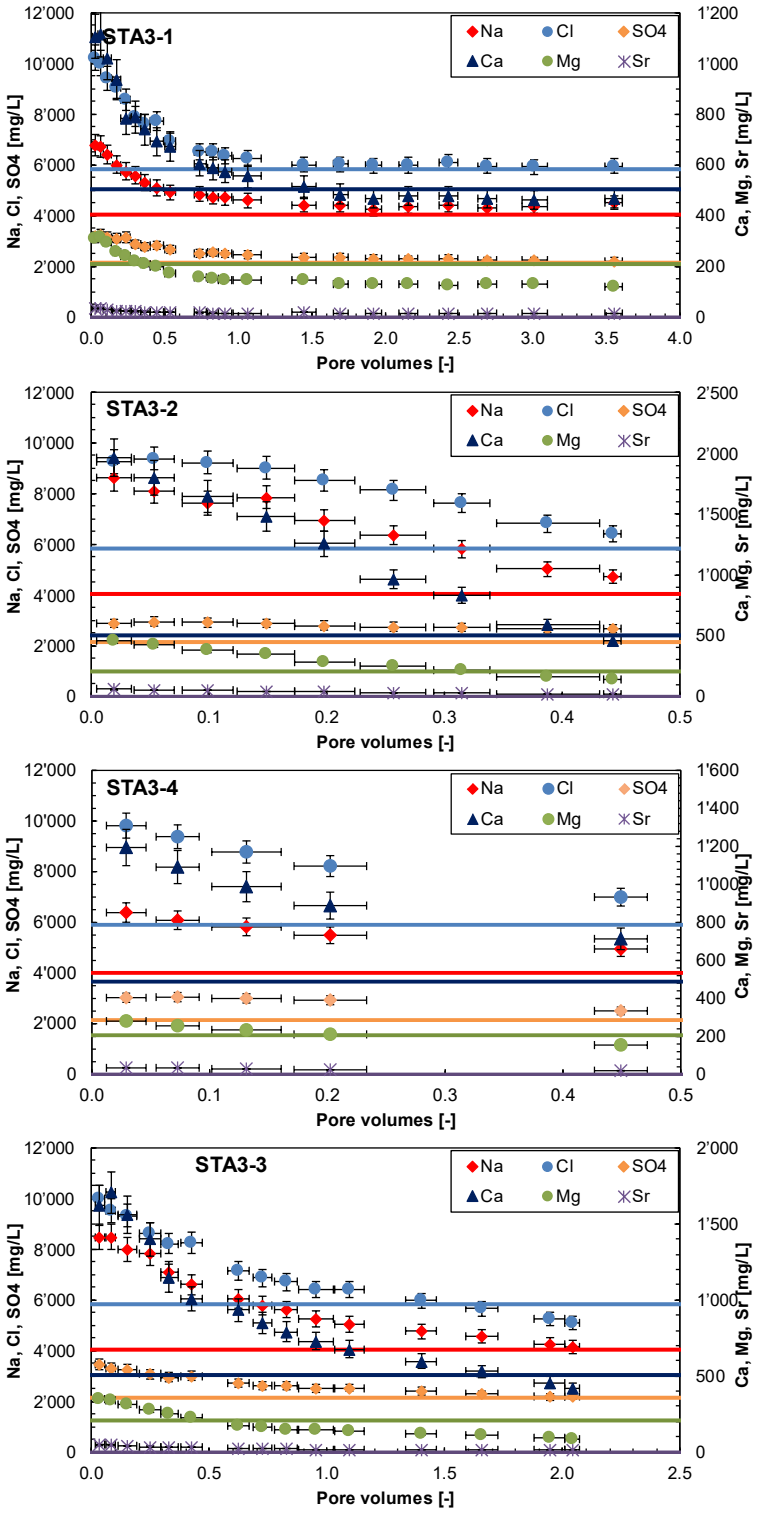


Fig. 4.7-8: Evolution of major components during advective-displacement experiments

STA3-1 = STA3-1-744.88-AD (Wedelsandstein Formation); STA3-2 = STA3-1-827.93-AD (Opalinus Clay); STA3-4 = STA3-1-849.98-AD (Opalinus Clay); STA3-3 = STA3-1-903.38-AD (Staffelegg Formation). Pore volume fractions relate to transport time based on water content. Experiment duration is 56 – 258 days. Horizontal length of symbol bar covers the sampling duration, vertical bars are an estimate of combined uncertainties. Horizontal lines represent the composition of the injected APW.

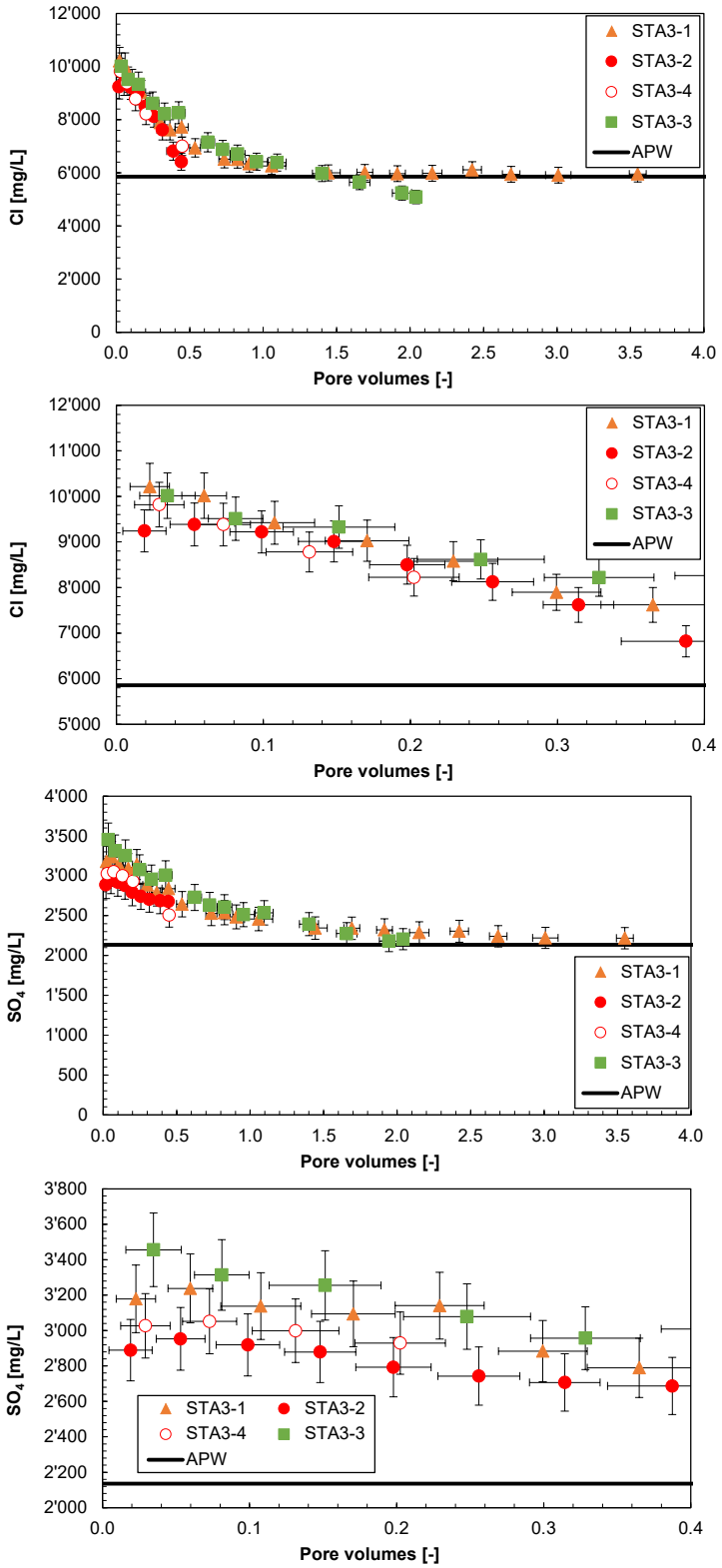


Fig. 4.7-9: Early evolution of Cl and $SO_4$ during advective-displacement experiments

STA3-1 = STA3-1-744.88-AD (Wedelsandstein Formation); STA3-2 = STA3-1-827.93-AD (Opalinus Clay); STA3-4 = STA3-1-849.98-AD (Opalinus Clay); STA3-3 = STA3-1-903.38-AD (Staffelegg Formation). Pore volume fractions relate to transport time based on water content. Experiment duration is 56 – 258 days. Horizontal length of symbol bar covers the sampling duration, vertical bars are an estimate of combined uncertainties. Horizontal lines represent the composition of the injected APW.

In STA3-2 most major ion concentrations form an early plateau, which is also the case in STA3-1 and STA3-3 (partially with an elevated first measurement due to minor drying of the sample surface; if plateaus not visible in Fig. 4.7-8, see enlarged Fig. 4.7-9). STA3-4 shows no plateau, possibly due to a sampling frequency slightly below that of the other experiments. A choice was made to use average compositions of the first two analysed aliquots to best represent the porewater composition. The resulting pore fluid compositions are summarised in Tab. 4.7-15 (Section 4.7.5.5) and are also used in the integrative plots in Chapter 5. The influence of the nitrate on the porewater composition is also discussed in Section 4.7.5.5.

Of the **minor components (Br, $NO_3$, K, Sr, Si)**, only potassium is present in the injected APW. Its concentration pattern is influenced by cation exchange reactions, whereby the outflow concentration only matches the APW concentration when the entire exchanger in the core is in equilibrium with the APW (Fig. 4.7-10). In STA3-1, STA3-2 and STA3-3, bromide is low in the first measurements due to complexation with the silver filters. The following maximum is most representative for the in situ porewater but must be seen as a minimum value. In case of PEEK filters (STA3-4), the very first measurement is the maximum. Bromide is then gradually decreasing in all experiments (details in Fig. 4.7-11) until flushed out completely. This can be used as a reversed break-through of an anionic tracer (see below). Dissolved silica elutes at 4 – 10 mg/L. Sr gradually decreases to a close to constant value at 11 – 14 mg/L in experiments with sufficient runtime, indicating some sort of buffering.

**Nitrate** is a major component in the early aliquots in experiments STA3-2 and STA3-3 (Opalinus Clay and Staffelegg Formation). For these samples, the maximum values reach up to 10 g/L already in the first couple of aliquots, followed by a regular decrease (Figs. 4.7-10 and 4.7-11, Tab. 4.7-15, Appendix B). In STA3-1, only the first 2 measurements are at ~ 600 mg/L, followed by values below 50 – 10 mg/L. In contrast, STA3-4 shows an initial $NO_3$ value of only 50 mg/L, decreasing to < 10 mg/L in the second sample and onwards. The origin of the extremely high nitrate concentrations is still unknown, but a reactive nitrogen phase in the cores is suspected (associated with solid organic matter, which is also mobilised and measured as TOC). This phase is not mobilised during comparably short and anaerobic aqueous extracts, neither during long-term aerobic extracts. These long-term aerobic extracts were conducted on original rock material mixed with Milli-Q water and left to react for more than 4 weeks, while opening the lid every few days to allow equilibration with oxygen. These aqueous extracts remained at low nitrogen concentrations of < 10 mg/L (Nitrat-Test MQuant®). But aqueous extracts of post-mortem samples from the Opalinus Clay (STA3-2) and Staffelegg Formation (STA3-3) show nitrate concentrations up to 18 mg/L (Tab. 4.7-8), generally higher at the outlet side than at the inlet of the core. This indicates a nitrogen mobilisation during the AD experiment. Other possible sources in the experimental set-up (APW tank, confining fluid, various materials in contact with the core) were measured by leaching and contain no nitrogen species. Ammonium ($NH_4$) is near or below the detection limit of 10 mg/L in all exfiltrated sample aliquots. Although the exact mechanism of nitrate mobilisation, presumably by oxidation from kerogen-bound nitrogen, is unclear, the substantial additional anion charge introduced must be balanced by cations (mainly Ca, interacting with the exchanger), as mentioned above. For STA3-4 and all later AD experiments, an additional sealing tube (a cold-shrink tube) was used to better isolate the core from the confining fluid, which stopped the excessive mobilisation of nitrogen, and all equipment including tanks, valves and pipes were thoroughly cleaned. Therefore, the mobilisation mechanism might involve interaction with the confining fluid possibly containing organics (lubricant), microbes, oxygen, hydrogen and Fe species from steel corrosion, under unknown redox conditions. It was shown earlier that (dissolved) Ar and Kr from the confining fluid can penetrate the core protected by the initial packing using a double layer of standard latex rubber sleeves used in geotechnical engineering tests. Increasing occurrence of nitrate in outflows while running AD experiments with partially reused confining water suggests bacterial growth therein.

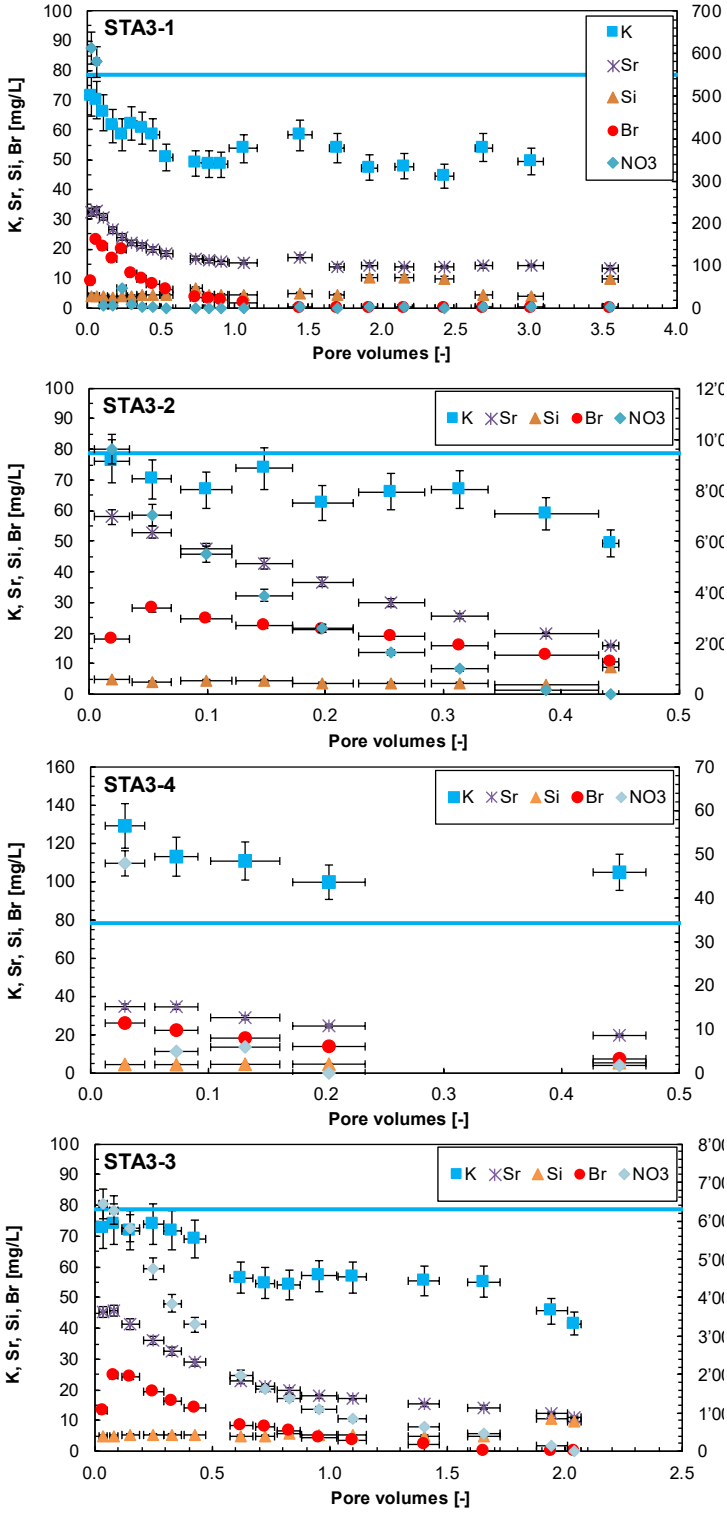


Fig. 4.7-10: Evolution of minor components during advective-displacement experiments

STA3-1 = STA3-1-744.88-AD (Wedelsandstein Formation); STA3-2 = STA3-1-827.93-AD (Opalinus Clay); STA3-4 = STA3-1-849.98-AD (Opalinus Clay); STA3-3 = STA3-1-903.38-AD (Staffelegg Formation). Pore volume fractions relate to transport time based on water content. Experiment duration is 56 – 258 days. Horizontal length of symbol bar covers the sampling duration, vertical bars are an estimate of combined uncertainties. Horizontal line represents the composition of the injected APW for K (0 for others).

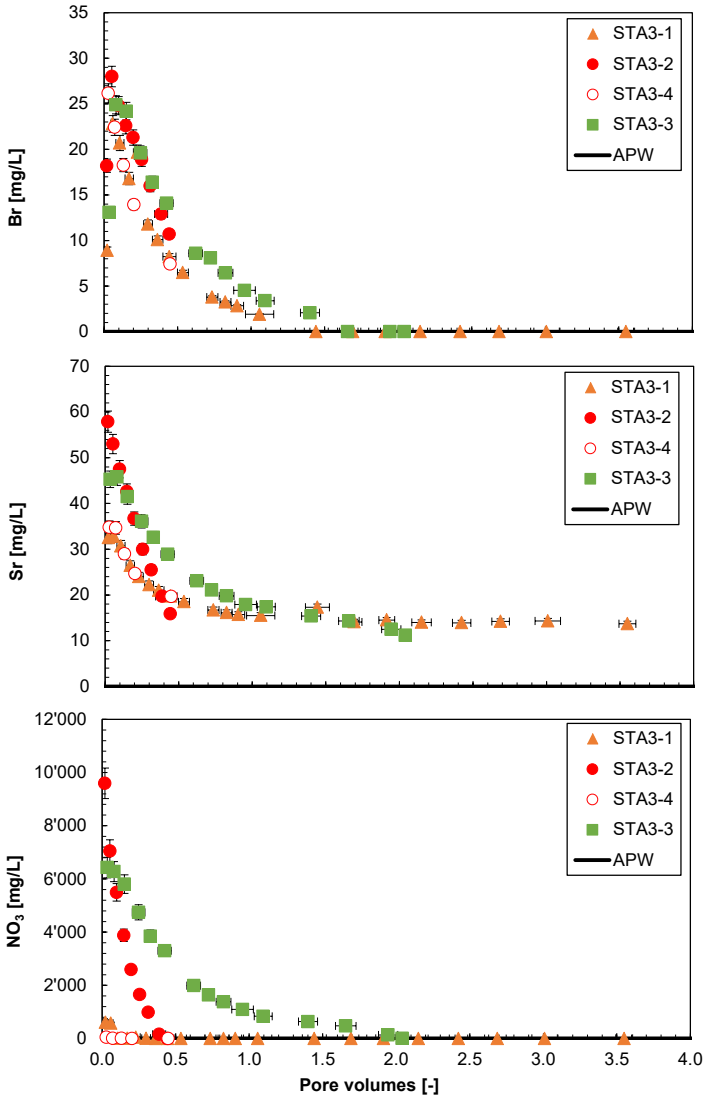


Fig. 4.7-11: Evolution of select minor components during advective-displacement experiments

STA3-1 = STA3-1-744.88-AD (Wedelsandstein Formation); STA3-2 = STA3-1-827.93-AD (Opalinus Clay); STA3-4 = STA3-1-849.98-AD (Opalinus Clay); STA3-3 = STA3-1-903.38-AD (Staffelegg Formation). Pore volume fractions relate to transport time based on water content. Experiment duration is 56 – 258 days. Horizontal length of symbol bar covers the sampling duration, vertical bars are an estimate of combined uncertainties. Br, Sr & $NO_3$ in the APW are 0. Br concentrations below detection are plotted at 0.

Ba and Al were measured by ICP-OES but remained below or, rarely, at detection limits. The detection limits depend on dilution factors and were 0.25 mg/L for Ba, and 0.25 – 5 mg/L for Al.

The **carbon system (TIC, TOC, TC, LMWOA)** shares as a common feature that relatively large TOC concentrations are eluted initially (260 – 400 mg/L, but 580 – 970 mg/L for cores with high nitrate) that gradually decrease to 20 – 40 mg/L with progressive percolation (Fig. 4.7-12, Tab. 4.7-15 shows averages of first 2 aliquots). TOC clearly dominates the dissolved carbon inventory (TC) at early times. The TOC can partly be explained by low-molecular-weight organic acids (LMWOA), mainly acetate, in case of STA3-1 and STA3-4 (Fig. 4.7-13). In STA3-2 and STA3-3 (high nitrate), all LMWOA concentrations are below detection, despite extremely high TOC. This indicates microbial activity, where preferentially LMWOA are consumed.

Aqueous extracts (Tab. 4.7-5) imply TOC values of 50 – 260 mg/L when scaled to porewater content, which partly covers the range observed in the early aliquots. Aqueous extracts carried out post-mortem (Tab. 4.7-8) show roughly similar TOC concentrations compared to the initial state, with consistently higher values at the top of the core (outflow) than at the base (inflow; TOC partly flushed out of cores). The former observations are similar to previous work, with samples from the Schlattingen-1 geothermal well (Mäder & Waber 2017) and also TBO borehole BUL1-1 (Mazurek et al. 2021), TRU1-1 (Aschwanden et al. 2021), MAR1-1 (Mäder et al. 2021) and BOZ1-1 (Wersin et al. 2022a).

TIC elutes initially at lower concentrations than TOC, covers a wide range of concentrations, but generally decreases to a close to constant concentration around 60 – 120 mg/L depending on the core (Figs. 4.7-12 and 4.7-13). Microbial activity might influence TIC/TOC, either in the syringe itself (i.e. during sampling/storage) or at the surface of the core sample, whereby a part of organic carbon might be oxidised to inorganic carbon, e.g. coupled with sulphate reduction.

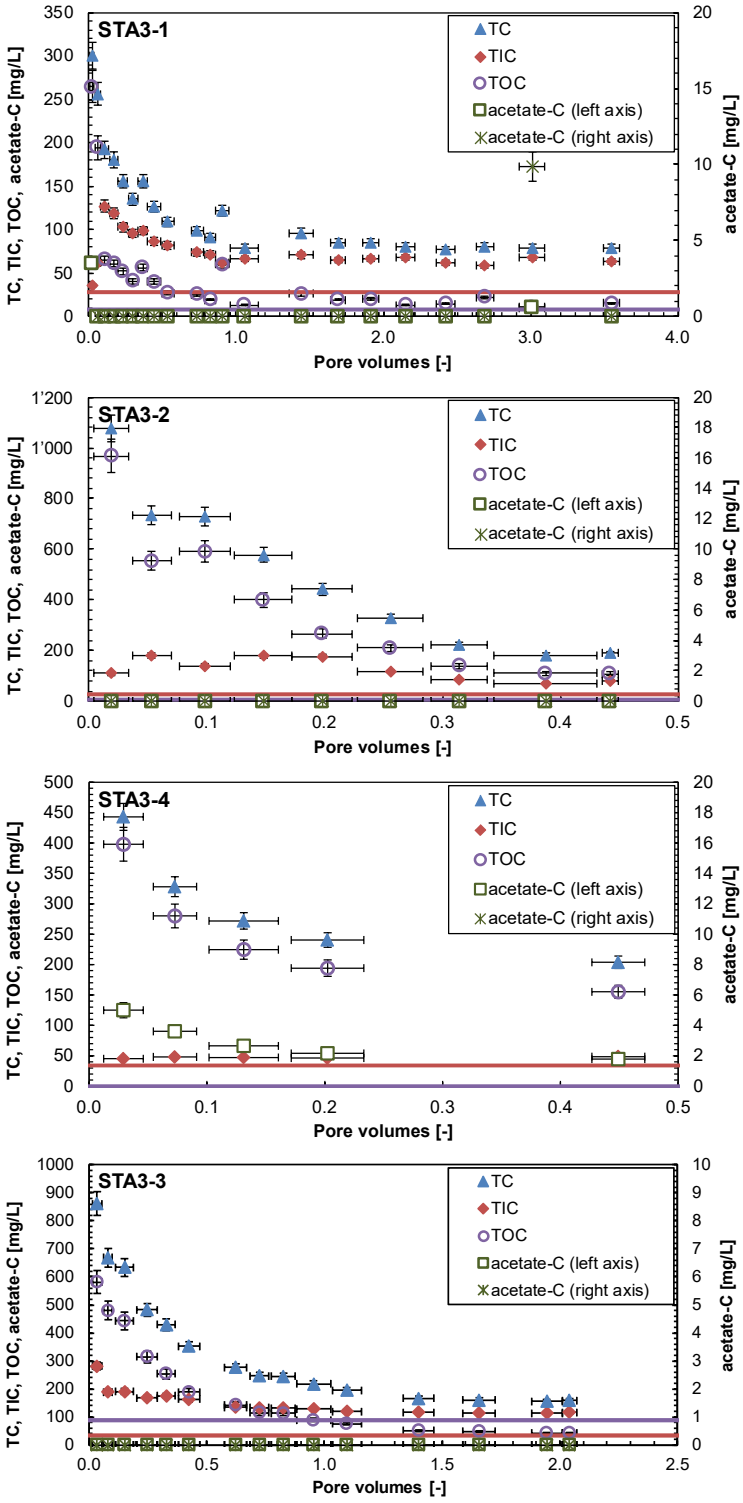


Fig. 4.7-12: Evolution of the carbon system during advective-displacement experiments

STA3-1 = STA3-1-744.88-AD (Wedelsandstein Formation); STA3-2 = STA3-1-827.93-AD (Opalinus Clay); STA3-4 = STA3-1-849.98-AD (Opalinus Clay); STA3-3 = STA3-1-903.38-AD (Staffelegg Formation). Pore volume fractions relate to transport time based on water content. Experiment duration is 56 – 258 days. Horizontal length of symbol bar covers the sampling duration, vertical bars are an estimate of combined uncertainties. Horizontal lines represent the composition of the injected APW.

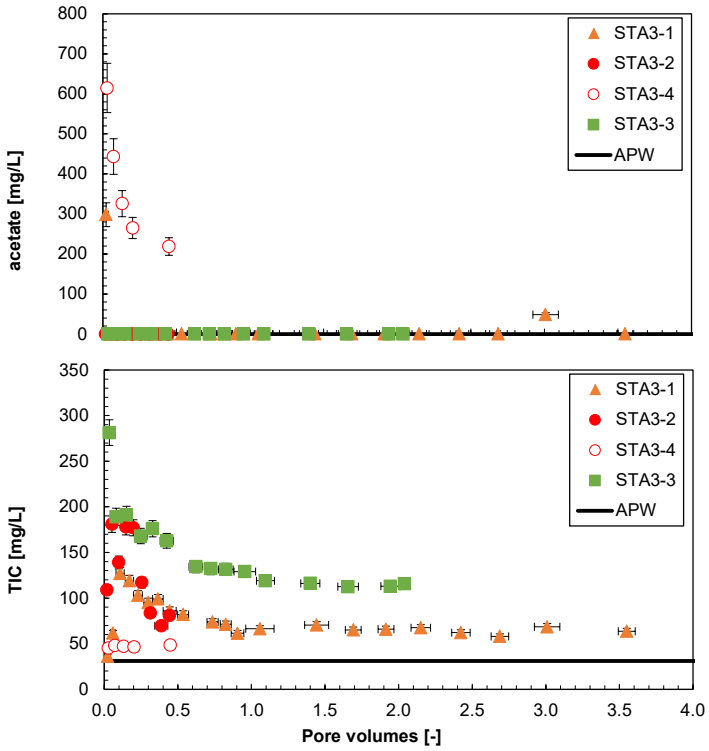


Fig. 4.7-13: Evolution of select carbon components during advective-displacement experiments

STA3-1 = STA3-1-744.88-AD (Wedelsandstein Formation); STA3-2 = STA3-1-827.93-AD (Opalinus Clay); STA3-4 = STA3-1-849.98-AD (Opalinus Clay); STA3-3 = STA3-1-903.38-AD (Staffelegg Formation). Pore volume fractions relate to transport time based on water content. Experiment duration is 56 – 258 days. Horizontal length of symbol bar covers the sampling duration, vertical bars are an estimate of combined uncertainties. Horizontal lines represent the composition of the injected APW. Concentrations below detection (acetate) are plotted at 0.

The **measurement of pH** was performed inline between some of the sampling intervals (set-up in Waber ed. 2020) and in the laboratory when syringe aliquots were prepared/preserved for analysis. The latter was done in most cases very shortly after sampling (one to a few hours), or after a few days of storage. The total range covered for all samples, inline and laboratory, is 6.9 – 7.9 (Fig. 4.7-14), both showing similar spreads. Values of both approaches either match within the error, or an early constant offset between the inline and laboratory measured pH is observed (systematically lower for inline pH). This can be explained by outgassing of $CO_2$ during the laboratory measured pH leading to higher values.

The pH series define relatively smooth trends with percolation progress but not a systematic behaviour in all experiments. The calculated partial pressure of $CO_2$ is larger than atmospheric in the aliquots, and this bears the potential for outgassing and resultant supersaturation with respect to calcite, and a possibility for some loss of Ca and TIC by precipitation.

It should be noted that in samples with the large initial nitrate concentrations (STA3-2 and STA3-3), there is some uncertainty regarding the generation of this dissolved nitrate. Depending on the processes, this could also affect pH values. While the pH may still be representative of the porewater of the experiment, it may deviate from the undisturbed state.

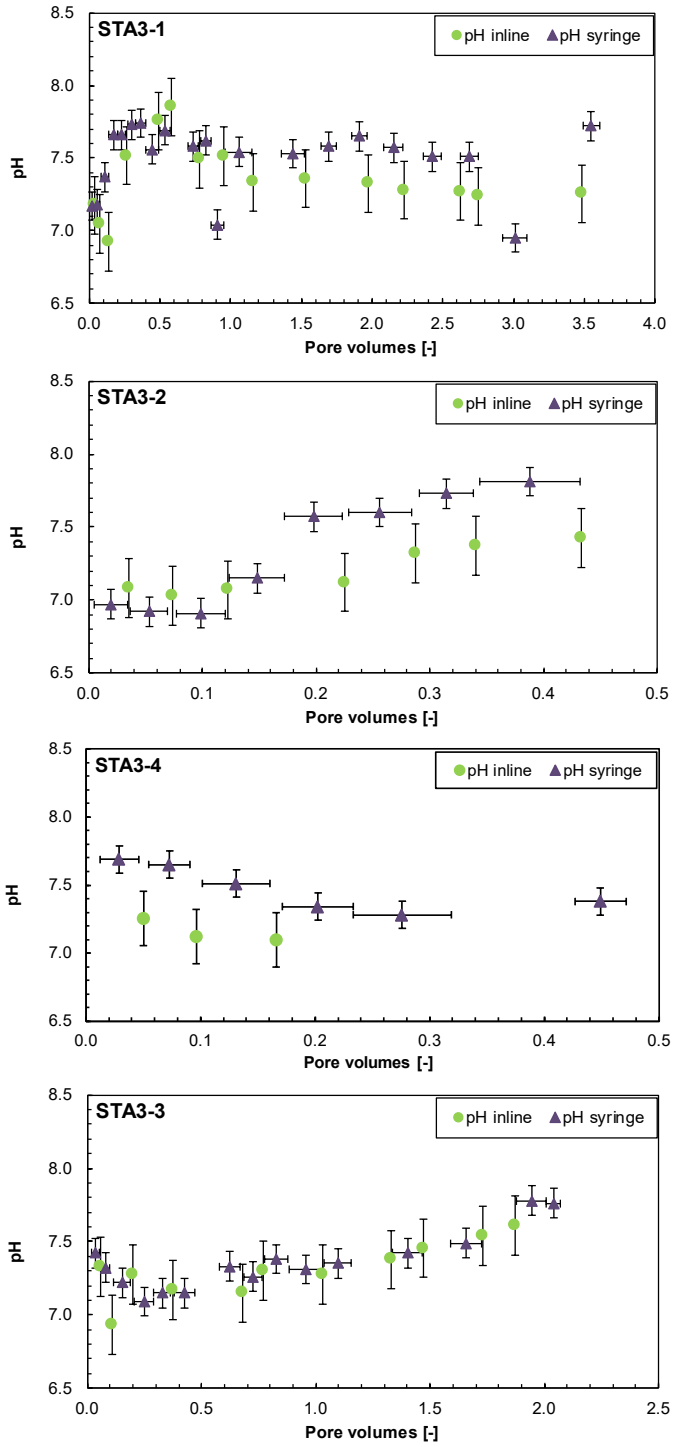


Fig. 4.7-14: Evolution of pH during advective-displacement experiments

STA3-1 = STA3-1-744.88-AD (Wedelsandstein Formation); STA3-2 = STA3-1-827.93-AD (Opalinus Clay); STA3-4 = STA3-1-849.98-AD (Opalinus Clay); STA3-3 = STA3-1-903.38-AD (Staffelegg Formation). Pore volume fractions relate to transport time based on water content. Experiment duration is 56 – 258 days. Horizontal length of symbol bar covers the sampling duration, vertical bars are an estimate of combined uncertainties.

#### 4.7.5.5 Early displaced aliquots representing the porewater composition

Early displaced aliquots were generally obtained by averaging the first two measured samples (Tab. 4.7-15). Interpretation of these early displaced aliquots as being representative of the in situ porewater, contained in the core at the time of the experiment, requires integration and interpretation of the entire dataset supported with geochemical calculations. Comprehensive reactive transport simulations are expected to further constrain the initial porewater compositions, as well as the transport properties of the cores. Only speciation calculations are included in this data report for the early compositions. Speciation calculations for all individual syringes are provided in Appendix B. The laboratory pH values were used for the speciation calculations. TIC was used as a constraint for inorganic carbon.

Experiments STA3-1, STA3-2, and STA3-3 were equipped with Ag filters, which led to decreased Br concentrations in the first aliquots (discussed in Section 4.7.5.4). Concentrations in the second aliquots are higher, but possibly still influenced by the not yet fully passivated filter surfaces. These Br concentrations are closest to the in situ porewater but must be seen as minimum concentrations, and thus also as minimum Br/Cl ratios.

In case of STA3-2 and STA3-3 there are high nitrate and TOC concentrations already in the first syringes, which is indicative for a disturbed porewater (Tab. 4.7-15). The additional anion charge leads to higher Ca concentrations, which equilibrate with the exchanger. Therefore, and as reasoned in Section 4.7.5.4, cations, nitrate and organics concentrations of these experiments are compromised. In AD experiment BOZ2-1 (Gimmi et al. 2022), the high nitrate concentration influenced visibly the anion concentrations throughout the experiment. In the STA3-1 borehole, however, the Cl concentration is significantly higher and early Cl concentrations of STA3-2 and STA3-3 experiments seem undisturbed when compared to the STA3-4 Cl concentrations (no disturbing nitrate) with differences within analytical uncertainty. This is additionally supported by the fact that the stable isotope data from all four AD experiments compare well with the isotope data from diffusive-exchange experiments (Section 5.7).

The speciation calculations (Tab. 4.7-16) reveal a cation charge surplus (positive 'Charge') that is not large and partially explained by significant TOC concentrations that were not included in the speciation. TIC was used as constraint for inorganic carbon. The aliquots are all significantly oversaturated with respect to calcite and also dolomite, as observed in earlier boreholes. Such oversaturation may result from shifts in pH linked to potential ingassing or outgassing of $CO_2$ during sampling and storage. Alternatively, the large TOC (and TC) contents pose analytical difficulties to obtain TIC, and associated errors may be larger than commonly assigned to TIC measurements.

Saturation is also reached or slightly exceeded for celestite and gypsum, equal to the BUL1-1 borehole. In contrast, earliest aliquots were generally slightly below gypsum saturation in the other earlier boreholes. The implication is that the ion-activity products ($[Sr]\cdot[SO_4]$) and ($[Ca]\cdot[SO_4]$) are controlling factors, but this does not necessarily mean that these minerals are also present in the core before the experiments. There are larger $SO_4$, Ca and Sr concentrations in the early aliquots than in the APW. The early aliquots are also close to saturation with respect to strontianite (implications above also apply).

In case of STA3-2 and STA3-3, saturation states are influenced by additional Ca from nitrate mobilisation and might be too high and not relevant in the context of the undisturbed state. A more in-depth analysis and interpretation will have to be carried out, including reconstructions by geochemical modelling to further understand and quantify the disturbing processes.

Tab. 4.7-15: Composition of earliest aliquots from advective-displacement experiments representing the best estimate of the in situ porewater chemistry

| **Parameter** | **Unit** | **STA3-1** | **STA3-2** | **STA3-4** | **STA3-3** |
|---|---|---|---|---|---|
| Depth | [m] | 744.88 | 827.93 | 849.98 | 903.38 |
| Geological unit | | Wedelsandstein Fm. | Opalinus Clay | Opalinus Clay | Staffelegg Fm. |
| pH inline | [-] | 7.11 | 7.06 | 7.19 | 7.13 |
| pH lab | [-] | 7.18 | 6.95 | 7.67 | 7.37 |
| Na | [mg/L] | 6'755 | *8'351* | 6'237 | *8'474* |
| $NH_4$ | [mg/L] | 10 | 16.95 | 15.35 | 16.9 |
| K | [mg/L] | 70.65 | *73.15* | 121.2 | *73.20* |
| Ca | [mg/L] | 1'110.5 | *1'877* | 1'143 | *1'663* |
| Mg | [mg/L] | 311 | *439* | 268 | *345* |
| Sr | [mg/L] | 32.65 | *55.45* | 34.72 | *45.55* |
| Ba | [mg/L] | < 0.25 | < 0.25 | < 0.25 | < 0.25 |
| Si | [mg/L] | 3.97 | 4.45 | 4.51 | 4.92 |
| Al | [mg/L] | < 5 | < 0.5 | < 2.5 | < 0.5 |
| F | [mg/L] | 8.35 | 6.30 | < 1.6 | 4.60 |
| Cl | [mg/L] | 10'115 | 9'313 | 9'601 | 9'764 |
| Br | [mg/L] | 22.8* | 28.0* | 24.3 | 24.9* |
| $NO_3$ | [mg/L] | 597 | *8'321* | 26.46 | *6'352* |
| $SO_4$ | [mg/L] | 3'209 | 2'921 | 3'039 | 3'385 |
| TOC | [mg/L] | 229 | *761* | 339 | *530* |
| TIC | [mg/L] | 48.8 | *145* | 46.6 | *235* |
| lactate | [mg/L] | < 20 | *31.4* | < 20 | *< 20* |
| acetate | [mg/L] | 298 | *< 20* | 529 | *< 20* |
| propionate | [mg/L] | < 20 | *40.6* | < 20 | *< 20* |
| formate | [mg/L] | < 20 | *53.3* | < 20 | *< 20* |
| $\delta^{18}O$ | [‰VSMOW] | -3.11 | -4.06 | -4.21 | -4.84 |
| $\delta^{2}H$ | [‰VSMOW] | -34.9 | -36.5 | -35.4 | -37.0 |

n.a.: not analysed; * only 2nd syringe, due to initial AgBr formation on Ag-filter; *italic*: compromised values due to nitrate mobilisation

Tab. 4.7-16: Saturation state of earliest aliquots from advective-displacement experiments

| **Parameter** | **Unit** | **STA3-1** | **STA3-2** | **STA3-4** | **STA3-3** |
|---|---|---|---|---|---|
| Depth | [m] | 744.88 | 827.93 | 849.98 | 903.38 |
| Geological unit | | Wedelsandstein Fm. | Opalinus Clay | Opalinus Clay | Staffelegg Fm. |
| Charge | [eq/$kg_w$] | 1.2E-02 | 2.8E-02 | 1.6E-02 | 1.6E-02 |
| %-Error | | 1.69 | 3.06 | 2.42 | 1.75 |
| Acetate | [eq/$kg_w$] | 5.0E-03 | < 3.4E-04 | 9.0E-03 | < 3.4E-04 |
| Ionic strength | [mol/$kg_w$] | 0.40 | 0.53 | 0.38 | 0.51 |
| tot_alk | [eq/$kg_w$] | 3.8E-03 | 1.1E-02 | 4.0E-03 | 1.9E-02 |
| pH (Lab) | | 7.18 | 6.95 | 7.67 | 7.37 |
| log$P(CO_2)$ | | -1.99 | -1.34 | -2.49 | -1.51 |
| SI(calcite) | | 0.48 | 0.93 | 0.99 | 1.53 |
| SI(dolomite-o) | | 0.74 | 1.57 | 1.68 | 2.71 |
| SI(dolomite-d) | | 0.19 | 1.02 | 1.13 | 2.16 |
| SI(gypsum) | | 0.06 | 0.19 | 0.06 | 0.20 |
| SI(celestite) | | 0.25 | 0.38 | 0.27 | 0.36 |
| SI(strontianite) | | -0.60 | -0.15 | -0.07 | 0.42 |
| SI(anhydrite) | | -0.15 | -0.02 | -0.15 | -0.01 |

PSI/Nagra 2012 thermodynamic database (Thoenen et al. 2014), calculated in PHREEQC for 25 °C; dolomite-o: ordered dolomite; dolomite-d: disordered dolomite; charge = Σ(cation charge) – ıΣ(anion charge)ı ; %-error = 100*charge/ (Σ(cation charge) + ıΣ(anion charge)ı ).

#### 4.7.5.6 Initial values and evolution of the composition of stable water isotopes

Common to all four experiments (Fig. 4.7-15) is a relatively smooth evolution of $\delta^{18}O$ towards the APW value with progress of percolation. Unlike some major chemical components (e.g. chloride), the breakthrough trend starts immediately with the second measured aliquot. The percolated pore volume is limited in all experiments, except in STA3-1, and therefore no complete breakthrough of the APW is reached.

$\delta^{2}H$ shows initially a slight trend against the breakthrough towards more negative values that goes through a minimum at 0.1 – 0.2 pore volumes for all cores (2nd syringe, and 3rd for STA3-3), except for STA3-4. The difference between the initial and minimum value is ≤ 1.0 ‰ and the disturbance of initial $\delta^{2}H$ values is therefore systematic (resolved by excellent precision) but within the error of the method (accuracy). An additional cold-shrink tube was applied to the STA3-4 core for enhanced separation from the confining fluid. This and all later experiments on cores equipped with this additional separation tube do not show an initial $\delta^{2}H$ evolution opposing the expected breakthrough trend. It must be kept in mind that the originally infiltrated APW used for STA3-1, STA3-2 and STA3-4 contained $\delta^{2}H$ = 90.8 ‰, which was then mixed with a slightly different batch (tank refill), resulting in $\delta^{2}H$ = 111.2 ‰ (Section 4.7.5.1). The actual breakthrough must be modelled taking into account the variable input conditions. The horizontal line represents the percolated pore volume – weighted average of the two tank compositions in Fig. 4.7-15. For experiment STA3-1, a post-mortem isotopic-exchange (IsoEx) experiment was done with granular material from the entire core, yielding the average isotopic composition of the porewater remaining in the core (neglecting an inhomogeneous water content distribution, see Fig. 4.7-3). While the $\delta^{2}H$ value plots between the last syringe and the APW composition as would be expected, the $\delta^{18}O$ value of the IsoEx is somewhat above both the final syringe and the APW composition. This reflects the tendency of IsoEx experiments to yield slightly heavier isotopic compositions compared to AD and SQ experiments, in particular for $\delta^{18}O$ (Section 5.7).

The stable isotopes composition in $\delta^{18}O$ versus $\delta^{2}H$ coordinates (Fig. 4.7-16) displays a slightly curved data array extending from the earliest and isotopically light ($\delta^{2}H$) or heaviest ($\delta^{18}O$) aliquot towards the APW isotopic composition (in case of sufficient runtime).

The observed differences between $\delta^{18}O$ and $\delta^{2}H$ concerning the extents of breakthrough are discussed in more detail in Section 4.7.7 and compared to other data sources in Chapter 5.

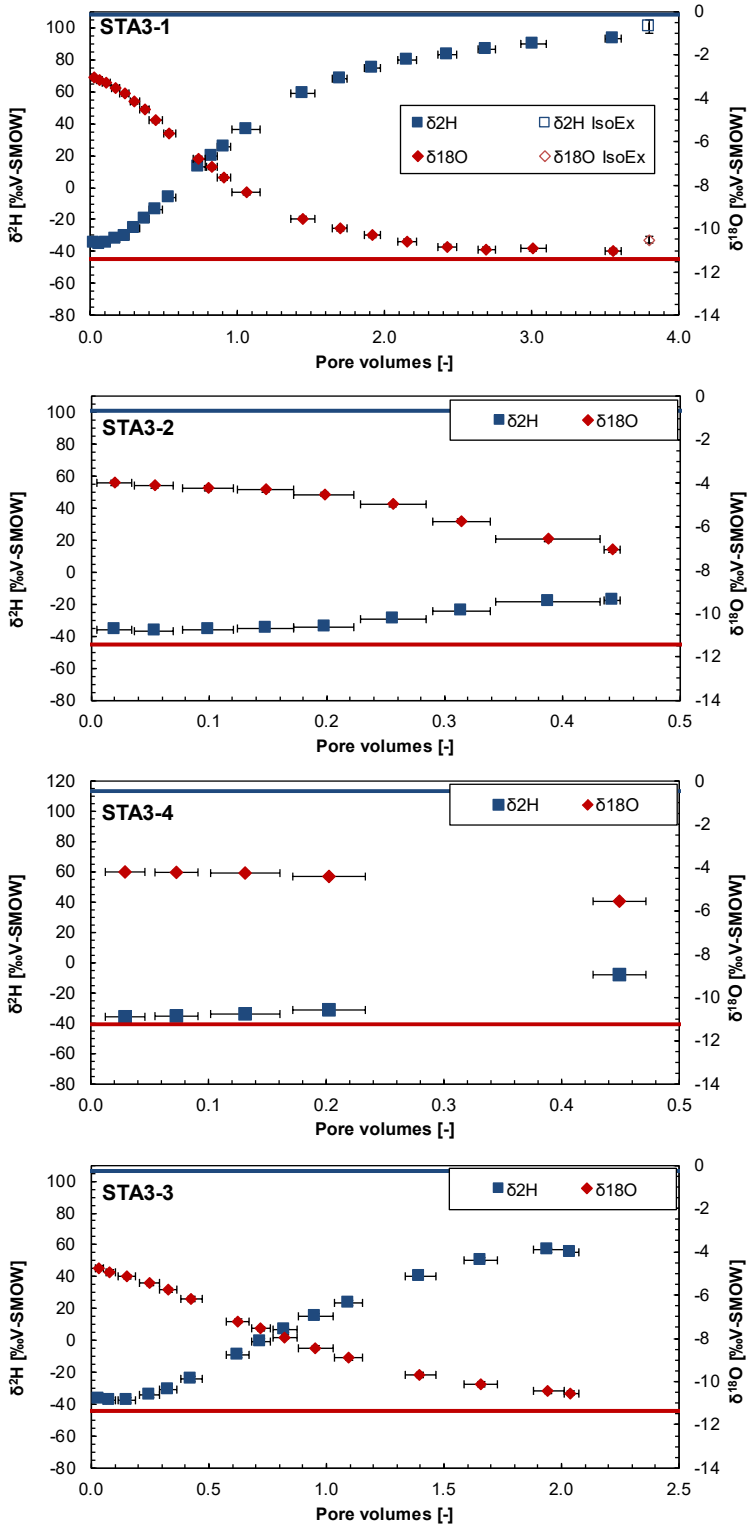


Fig. 4.7-15: Evolution of $\delta^2H$ and $\delta^{18}O$ during advective-displacement experiments

STA3-1 = STA3-1-744.88-AD (Wedelsandstein Formation); STA3-2 = STA3-1-827.93-AD (Opalinus Clay); STA3-4 = STA3-1-849.98-AD (Opalinus Clay); STA3-3 = STA3-1-903.38-AD (Staffelegg Formation). Pore volume fractions relate to transport time based on water content. Experiment duration is 56 – 258 days. Horizontal length of symbol bar covers the sampling duration. Measurement errors are 1.5 ‰ for $\delta^2H$ and 0.1 ‰ for $\delta^{18}O$.

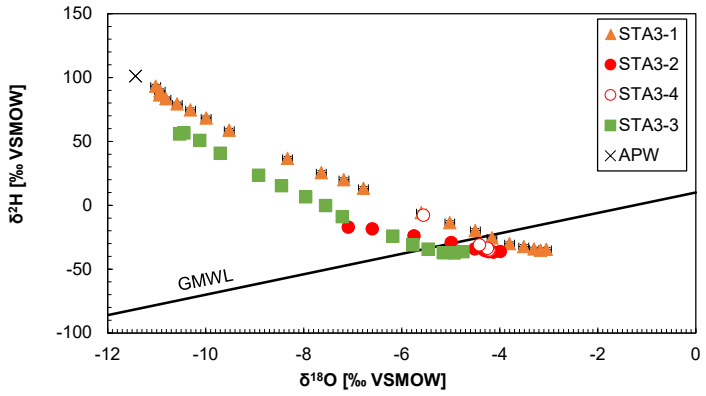


Fig. 4.7-16: Stable isotopes composition of aliquots from advective-displacement experiments

STA3-1 = STA3-1-744.88-AD (Wedelsandstein Formation); STA3-2 = STA3-1-827.93-AD (Opalinus Clay); STA3-4 = STA3-1-849.98-AD (Opalinus Clay); STA3-3 = STA3-1-903.38-AD (Staffelegg Formation). Pore volume fractions relate to transport time based on water content. Experiment duration is 56 – 258 days. Measurement errors are 1.5 ‰ for $\delta^2H$ and 0.1 ‰ for $\delta^{18}O$. GMWL is the global meteoric water line. 1st aliquots are located the furthest to the right and evolve towards the left.

### 4.7.6 Derivation of anion-accessible porosity

There are several ways by which chloride and bromide accessible porosity fractions may be obtained. The principle is the same: namely the ratio between the anion concentration obtained from aqueous extracts up-scaled to porewater content divided by that obtained from earliest aliquots from the advective-displacement experiments (discussion in Waber ed. 2020 and Mäder 2018). There are some variants depending on how water contents were measured and averaged, or how inferred water losses and volume changes may be corrected. In the case where a full or well-advanced breakthrough in chloride is captured, such a ratio may also be obtained by post-mortem aqueous extracts (top and base) and the latest aliquots sampled before the end of the experiments (for the outflow / top), or the injected APW (for the inflow / base). Normally, bromide drops below detection and only the chloride data can be evaluated for post-mortem data-sets. The bromide data commonly is more 'noisy'.

The top two data lines (lines 1 and 2 in Tab. 4.7-17) list the average concentrations (Cl, Br) for the first two displaced aliquots as shown in Tab. 4.7-15. Because Br complexation with the Ag filters massively decreased Br concentrations in the first aliquots, only the second value was used in experiments with Ag filters, which must be seen as a minimum value. Line 3 lists the concentration of Cl in the last syringe sampled (for post-mortem evaluation). The following three lines list different Cl concentrations in aqueous extracts, up-scaled to water content: for the sample from above the AD core (line 4), for the sample from below (line 5) and a corrected and averaged value (line 6). The correction compensates for a small amount of water loss (unsaturated volume) commonly observed and evaluated from a measured net water uptake. The net water uptake is the measured water uptake (mass gain of the core during the experiment) corrected for a commonly measured small volume increase during the experiment (Section 4.7.3 and Tab. 4.7-4). The correction hinges on the assumption that sample treatment for the AD core and the off-cuts share the same history (core handling, storage, sample preparation) and therefore also potentially underwent similar water losses. These corrections are rather small, with small net water uptakes. The following three lines (7 – 9) contain the same data for Br. The observed range in up-scaled concentrations is an indication of heterogeneity, mainly in the clay-mineral content. A homogeneous

sample with respect to the degree of anion-exclusion should yield the same up-scaled Cl and Br concentrations, despite differences in water content. A consistent proportion of anion-accessible porosity would then be evaluated regardless of choosing a sample from the top or from the base as a reference for the early displaced aliquots. The two data lines for Cl suffixed with _p-m (lines 10 and 11) are the up-scaled chloride concentrations evaluated post-mortem from aqueous extracts from the top of the core (outflow to sampling) and the base of the core (APW inflow).

The final data block (lines 12 – 19 in Tab. 4.7-17) lists the accessible porosity fraction obtained by various combinations and averaging. The first four lines 12 – 15 list values that are derived without knowledge of the net water uptake. The next two lines 16 and 17, including the suffix _corr, indicate values obtained after applying a correction for net water uptake as mentioned above. The last two data lines represent the post-mortem evaluations of the top of the core (outlet, line 18) and the base of the core (inlet, line 19).

Core STA3-1 contains a heterogeneous mineral composition along the core: Fig. 4.7-2 shows a bright band (high X-ray absorbance) at the core base, possibly related to an elevated calcite content. This core segment also shows a very low water content (Fig. 4.7-3), both indicating a low clay content. This leads to the high p-m_base chloride accessibility (0.51, line 19) compared to all other values from this sample. In contrast, the higher water content at the top of the core indicates a higher clay content, resulting in a lower post-mortem accessibility (0.38, line 19). The lowest accessibility (0.32) results from relating the chloride in the early outflow to aqueous extracts from material above and below the core, which has very likely a different smectite content than the actual core segment where the outflow originates (not measured). All these arguments suggest that the three different chloride accessibilities represent to a large extent the mineralogical variation within the 12 cm long segment. Due to this mineralogical heterogeneity, the water content correction cannot be applied to this sample, but in this case, the correction does not influence the accessibility within the displayed number of digits.

In case of STA3-1, 3-2 and 3-3, the experiments were equipped with Ag filters that complex with Br (and possibly some relatively minor Cl). The rapid surface passivation results in a much higher Br concentration already for the second aliquot measured (Fig. 4.7-8). To achieve a Br accessibility equal to Cl for STA3-1, 3-2 and 3-3, an in situ porewater concentration of 38, 33 and 36 mg/L, respectively, would be required. Replacing the beginning of the curves in Fig. 4.7-8 with these Br values would lead to a step at the beginning of the Br evolution that was not observed to this extent in previous experiments. Therefore, Cl-accessible porosity fractions are assumed to be more reliable than those derived from Br data.

Accessibilities of 0.41 and 0.35 calculated for the Opalinus Clay samples are below the range of 0.42 to 0.51 determined previously for Opalinus Clay with the same approach in the TBO boreholes BUL1-1 (Mazurek et al. 2021), MAR1-1 (Mäder et al. 2021) and BOZ1-1 (Wersin et al. 2022a). The low accessibility of 0.35 in the core STA3-4 might be related to the high clay content of 65 wt.-%. The AD experiment TRU1-4 (Aschwanden et al. 2021) resulted in a comparable Cl-accessibility fraction (0.37), also associated with a high CEC that is indicative of a high clay content (neighbouring samples show clay-mineral contents of 65 wt.-%).

In summary, the Cl accessibilities are considered reliable in all samples except for STA3-2 and STA3-3 top post-mortem. In these two experiments, processes presumably related to the high nitrate mobilisation induced a sudden drop in hydraulic conductivity and Cl concentrations falling below APW concentrations, both indicating a massive late disturbance of the pore structure and porewater chemistry. STA3-4 is the only sample with a reliable Br accessibility since no Ag filters were used in this sample.

Tab. 4.7-17: Chloride and bromide-accessible porosity fractions

| Line | Parameter | Unit | STA3-1 | STA3-2 | STA3-4 | STA3-3 |
|---|---|---|---|---|---|---|
| | Depth | [m] | 744.88 | 827.93 | 849.98 | 903.38 |
| | Geol. Unit | | Wedelsandst. Fm. | Opalinus Clay | Opalinus Clay | Staffelegg Fm. |
| 1 | Cl-AD_ave (1-2) | [mg/L] | 10'115 | 9'313 | 9'601 | 9'764 |
| 2 | Br-AD_ave(1-2) 2nd only (+) | [mg/L] | 22.80+ | 28.00+ | 24.29 | 24.90+ |
| 3 | Cl_AD_last | [mg/L] | 5'956 | 6'417 | 7'000 | 5'092 |
| 4 | Cl-AqEx-upscaled_top | [mg/L] | 3'217 | 3'934 | 3'656 | 4'663 |
| 5 | Cl-AqEx-upscaled_base | [mg/L] | 3'201 | 3'886 | 3'514 | 4'514 |
| 6 | Cl-AqEx-upscaled_ave_ corr | [mg/L] | **3'000** | **3'836** | **3'578** | **4'321** |
| 7 | Br-AqEx-upscaled_top | [mg/L] | 12.4 | 14.0 | 11.5 | 17.2 |
| 8 | Br-AqEx-upscaled_base | [mg/L] | 11.7 | 13.8 | 11.3 | 16.7 |
| 9 | Br-AqEx-upscaled_ave_ corr | [mg/L] | 11.2 | 13.6 | 11.4 | 15.9 |
| 10 | Cl-AqEx-upscaled_top_ p-m | [mg/L] | 2'240 | 2'739 | 3'292 | 2'734 |
| 11 | Cl-AqEx-upscaled_base_ p-m | [mg/L] | 3'008 | 2'856 | 2'351 | 3'440 |
| 12 | Cl-AqEx_top / Cl-AD_ave | | 0.32 | 0.42 | 0.38 | 0.48 |
| 13 | Br-AqEx_top / Br-AD_ave | | 0.54 | 0.50 | 0.47 | 0.69 |
| 14 | Cl-AqEx_ave / Cl-AD_ave | | 0.32 | 0.42 | 0.37 | 0.47 |
| 15 | Br-AqEx_ave / Br-AD_ave | | *0.53*** | *0.50*** | 0.47 | *0.68*** |
| 16 | Cl-AqEx_ave_corr / Cl-AD_ave | | *0.30**** | 0.41 | 0.37 | 0.44 |
| 17 | Br-AqEx_ave_corr / Br-AD_ave | | *0.49*** | *0.49*** | 0.47 | *0.64*** |
| 18 | Cl_AqEx_p-m_top / Cl_last_AD | | 0.38 | *0.43** | 0.47 | *0.54** |
| 19 | Cl_AqEx_p-m_base / Cl_APW | | 0.51 | *0.49** | 0.40 | *0.59** |

Preferred values are shaded in blue; values in *italic* are unreliable due to interferences with nitrate/clogging (*), Br interaction with the Ag-filter (**) or mineralogical heterogeneity (***).

### 4.7.7 Transport properties marked by breakthrough of $\delta^2H$, $\delta^{18}O$, Cl and Br

There are four components that can be used to elucidate on transport properties by their breakthrough behaviour, namely Cl, Br, and the water isotope ratios $\delta^2H$ and $\delta^{18}O$. Chloride is a good tracer in all four experiments, because the APW has a distinctly lower Cl concentration than the in situ porewater. The resolution towards a full breakthrough is diminished because small differences between large concentrations can no longer be resolved. Bromide is a break-out tracer that is gradually flushed out of the core (no Br in the APW). Again, as a full break-out is approached, bromide concentrations tend to fall below the detection limit. Water tracers also feature a considerable contrast between the in situ porewater (Tab. 4.7-15) and the APW and are therefore suitable to trace the APW breakthrough.

For comparison (Fig. 4.7-17) all breakthrough data are normalised to 1 and inverted in case of decreasing trends to mimic a breakthrough behaviour. The normalised breakthrough of chloride, for example, is given by $1-(Cl-Cl_{APW})/(Cl_{PW}-Cl_{APW})$, where $Cl_{PW}$ refers to the value of the early aliquots representing the in situ porewater composition (Tab. 4.7-15). In case of Br in experiments equipped with an Ag filter, the second sample better represents the in situ porewater and the first sample (low Br due to complexation on filter surface) mimics an apparent breakthrough. In all other cases, the average of the first and second measurement represents the in situ porewater. A slightly elevated first value (due to a potential drying of the surface) leads to a negative value for the first sample.

In general, Cl and Br breakthroughs behave as expected. Hydraulic conductivity of STA3-2 collapses early in the experiment (Fig. 4.7-4) in hand with an extremely high nitrate mobilisation, which seems to affect Br differently from Cl and might cause the difference in breakthrough behaviour. But also in STA3-4, without nitrate mobilisation and Br complexation on the Ag filter, a small but significant difference between Br and Cl breakthrough behaviour can be observed. This was also illustrated in earlier work by Mäder (2018). The gas breakthrough in STA3-3 at 0.5 pore volumes affects only the preceding Cl concentration, but not Br.

Fig. 4.7-18 illustrates the breakthrough behaviour of the Br/Cl molal ratio vs. time (pore volume fraction). Plotting the ratio removes some of the data scatter of the individual data series and illustrates similarities between the different experiments and thus also highlights any differences. The four experiments form a set of nearly parallel curves, neglecting initial low Br concentrations caused by complexation with the Ag filter. The trends of decreasing Br/Cl ratios are mainly caused by the washing out of bromide (no Br in the injected APW), the decrease in Cl concentrations towards the APW and to a minor extent by the small observed difference of Br transport vs. Cl transport properties. The offsets between the Br/Cl ratio in the AqEx and the early aliquot visualise a difference between Cl and Br accessible porosity fractions discussed in Section 4.7.6.

$\delta^{18}O$ and $\delta^2H$ break through more slowly compared to the anions Br and Cl, as expected in the presence of any anion-depleted porosity and under advective conditions. In STA3-4 and in all later AD experiments using an additional cold-shrink tube (BAC1-1 borehole), $\delta^{18}O$ and $\delta^2H$ breakthroughs match perfectly. Any mismatch observed in earlier AD experiments must be seen as artefact.

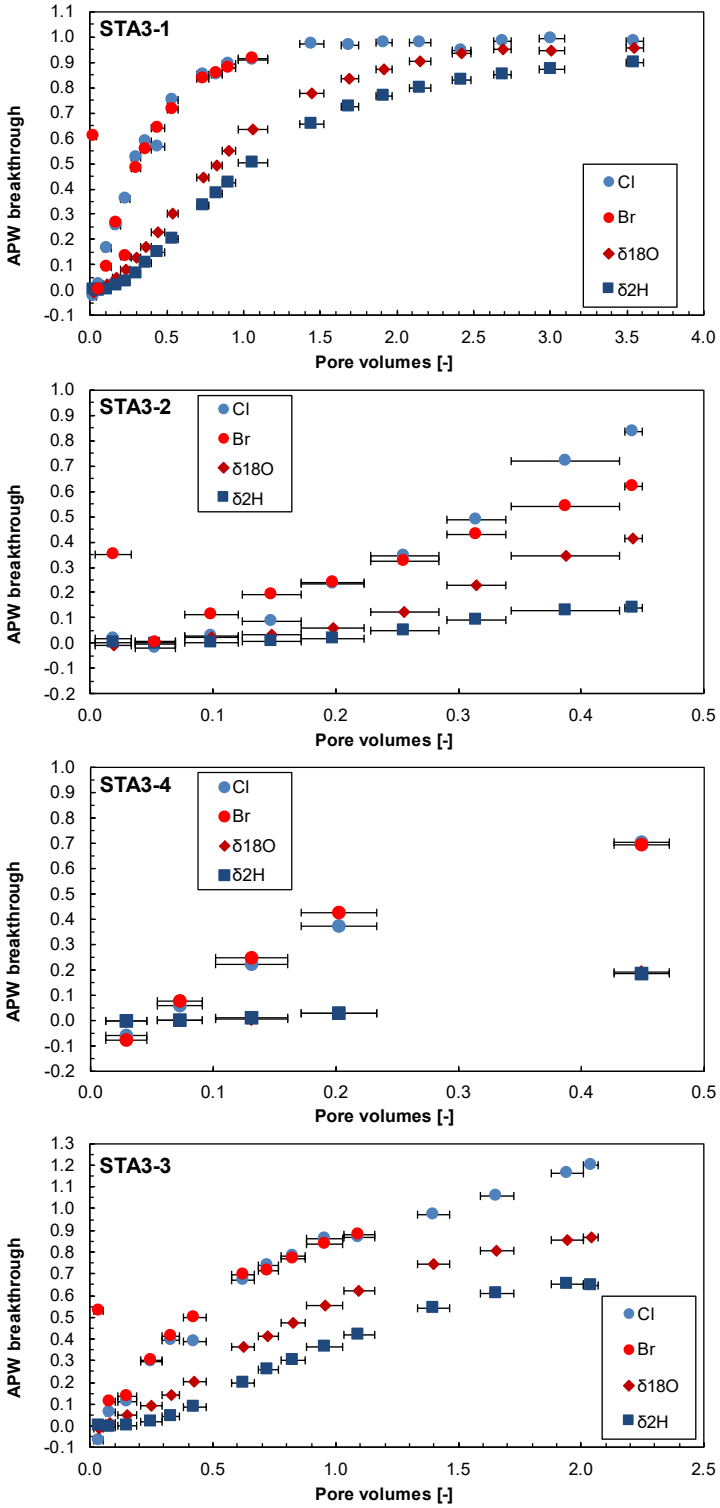


Fig. 4.7-17: Breakthrough of Cl, Br, $\delta^2H$ and $\delta^{18}O$ during advective-displacement experiments

STA3-1 = STA3-1-744.88-AD (Wedelsandstein Formation); STA3-2 = STA3-1-827.93-AD (Opalinus Clay); STA3-4 = STA3-1-849.98-AD (Opalinus Clay); STA3-3 = STA3-1-903.38-AD (Staffelegg Formation). Pore volume fractions relate to transport time based on water content. Experiment duration is 56 – 258 days. Horizontal length of symbol bar covers the sampling duration. The first Br values in STA3-1, STA3-2 and STA3-3 are compromised by the Ag filters.

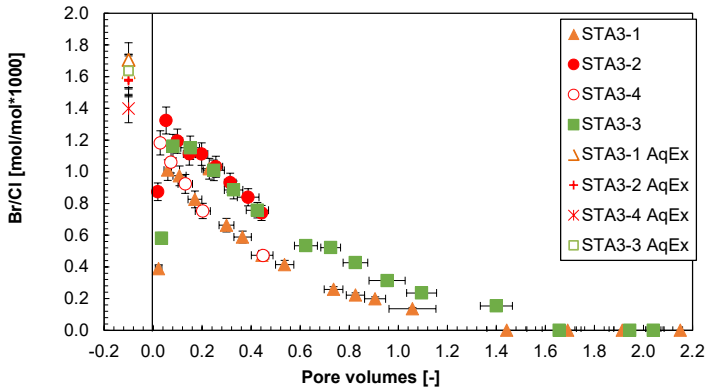


Fig. 4.7-18: Evolution of Br/Cl during advective-displacement experiments

Data on left side (top graph, 'AqEx') are the ratios measured in the aqueous extracts perfomed for pre-characterisation. Ratios plotted at 0 correspond to later aliquots where Br concentration drops below detection. STA3-1 = STA3-1-744.88-AD (Wedelsandstein Formation); STA3-2 = STA3-1-827.93-AD (Opalinus Clay); STA3-4 = STA3-1-849.98-AD (Opalinus Clay); STA3-3 = STA3-1-903.38-AD (Staffelegg Formation). Pore volume fractions relate to transport time based on water content. Experiment duration is 56 – 258 days. Pore volume fractions relate to transport time based on water content. Horizontal length of symbol bar covers the sampling duration.

## 4.7.8 Concluding remarks and open issues

Four advective-displacement experiments were conducted on samples from the clay-rich Dogger units and the Liassic, focussing on the derivation of constraints for a representative porewater composition, anion accessible porosity fractions and transport properties. A systematic and consistent dataset on petrophysical and geochemical properties was obtained not only of value for the specific site characterisation but also for interpretation of porewater chemistry and chloride / bromide accessible porosity fractions across all TBO drilling sites. Excessive nitrate was produced as an artefact in two of the experiments and this permitted only a limited data interpretation. Nevertheless, all experiments provided Cl and Br concentrations (minimum value of the latter) and compositions of stable water isotopes considered representative for the in situ porewater, as well as Cl-accessible porosity fractions.

Two cores (STA3-2 and STA3-3) from the Opalinus Clay and Staffelegg Formation show large nitrate concentrations (6 – 10 g/L) in the first two aliquots that gradually decrease at later sampling times, also observed in a limited number of previous AD experiments. Corresponding aqueous extracts from post-mortem samples show still increased nitrate concentrations not completely flushed out (or generated during extraction), but no anomalous nitrate was detected in the aqueous extracts from pre-characterisation. A second sample from the Opalinus Clay (STA3-4) was processed one year later using an improved set-up with an additional sealing layer consisting of a cold-shrink tube that solved this issue, also for later experiments (BAC1-1 borehole). The origin of this nitrate is likely kerogenous solid organic matter in the core samples, as no nitrogen source of any kind was detected in the experimental set-up. The mechanisms of its mobilisation or liberation during the experiment are not exactly known. While this artefact is unwanted, it indicates that the components from the kerogenous solid organic matter (nitrate and dissolved organic carbon species) present in many lithologies may be released at substantial concentrations via some disturbing process linked to redox reactions and microbial activity.

In STA3-2 (Opalinus Clay) and STA3-3 (Staffelegg Formation) the mobilisation of nitrate compromises the data of all cations and the carbon system, presumably including pH. The comparison with the unaffected STA3-4 experiment indicates that in the case of the STA3-1 borehole, the effect of elevated nitrate concentrations on the conservative tracers Cl and water isotopes is rather small and that calculated Cl-accessible porosity fractions are still representative.

The implementation of Ag filters (very thin, made of very fine-grained precipitated silver) at the base and top of the core, aimed to decrease any microbial activity. As a side effect, this drastically decreased Br concentrations in at least the first aliquot by formation of AgBr at the filter surface. Therefore, PEEK filters are used again in STA3-4 and later AD experiments, as was done earlier.

The sulphate system in all aliquots appears to be controlled by celestite equilibrium. This either implies that such a control is imposed by these minerals being initially present, or that a disturbance causes to reach such a solubility-product control. In the latter case, the reconstruction of the porewater-sulphate concentration is more challenging, and also influences the carbonate system and clay-exchanger complex by ways of interdependent thermodynamic mass-action equilibria.

Like in all earlier work, there are unusually high concentrations of TOC mobilised in the earliest aliquots, decreasing gradually to values more in line with aqueous extracts, but still at significant concentrations.

Nevertheless, all four advective-displacement experiments supplied systematic, consistent and plausible data on petrophysical and geochemical properties, albeit in three cores some artefacts are clearly identified. Samples covered a clay-mineral content of 30 – 65 wt.-%, with different proportions of illite/smectite + smectite compared to the total clay-mineral content. The mineralogically heterogeneous STA3-1 sample from the Wedelsandstein Formation shows Cl-accessible porosity fractions between 0.32 and 0.51, the two Opalinus Clay samples 0.35 and 0.41, and the Staffelegg Formation sample 0.44. The hydraulic conductivities are all in the range of 1.5 – $3.5 \times 10^{-13}$ m/s, except for STA3-2, where the flow decreased strongly before a stable value was reached (clogging in connection with nitrate mobilisation as a likely cause).

The data of this study, in combination with data from boreholes STA2-1 and BAC1-1, imply that the use of an additional separation layer in core packing in form of a cold shrink tube is an improvement. In addition, Ag filters are abandoned due to their complexation with Br. The mechanical, hydraulic and electronic or sensor aspects of the experimental set-up reliably performed for the duration of the experiments and even longer. Likewise, the analytical procedures were already optimised, naturally limited by very small sample volumes in some cases.

The gas volumes that exfiltrated mainly at the beginning of the experiments (Tab. 4.7-2), but in some cases continued throughout the entire percolation period, cannot be explained by initial dead volumes and initially unsaturated porosity in the core or He dissolved in the APW at infiltration pressure (45 – 49 bar) and outgassing due to a pressure decrease to 1 bar. During AD experiments on samples from boreholes MAR1-1 and BOZ1-1, selective gas analyses revealed considerable volumes of Ar and Kr (when substituted for Ar) in the exfiltrating gas, which originates from the core confinement water, where Ar (or Kr) was used in the pressurised headspace. Therefore, a gas-free confining-pressure system was installed starting with samples from the STA2-1 borehole. This new set-up was used for STA3-4, where, in combination with the cold-shrink tube core packing, the initial gas exfiltration decreased substantially and stayed low during the entire experiment. The general decrease in gas exfiltration was confirmed by all AD experiments with this improved set-up.

## 4.8 Water-isotope data from diffusive-exchange experiments

*Lukas Aschwanden & Thomas Gimmi*

The porewater isotope composition ($\delta^{18}O$, $\delta^{2}H$) was derived by isotope diffusive-exchange experiments conducted on core material of 100 samples collected across an interval of 442.5 – 1'103.2 m depth. The obtained highly resolved profiles for $\delta^{18}O$ and $\delta^{2}H$ cover the lithologies from the «Felsenkalke» + «Massenkalk» of the Malm to the Triassic Schinznach Formation. All experiments were conducted at the University of Bern. The relevant data are summarised in Appendix A.

### 4.8.1 Data evaluation

#### 4.8.1.1 Experimental and analytical data

All the isotope diffusive-exchange experiments followed the experimental and analytical protocol given in Waber (ed.) (2020). The evaluation of the experimental and analytical data underlying the derivation of the composition of stable water isotopes of the in situ porewater followed a standardised procedure as detailed below.

In order to qualify for a successful isotope diffusive-exchange experiment the following criteria had to be met (within the propagated analytical uncertainties) by the two experiments (so-called LAB[10] and NGW[11] experiments) conducted for one core sample:

- No severe leakage (evaporation). In most cases, the mass of experiment container including rock and test water before and after experiment remained constant (± 0.04 g). If the loss of mass was > 0.04 g, corrections were applied to the measured isotope value of the equilibrated test water by Rayleigh-distillation calculations before calculating the porewater isotope ratio, assigning the mass loss to evaporation of the initial test water. If the correction of the $\delta^{18}O$ value for evaporation was > 0.5 ‰ VSMOW (typically meaning that the mass loss of test water was > 5% of the initial mass of test water), the porewater isotope value was marked as less reliable.
- Reasonable mass ratio of porewater to test water yielding a change in the isotope signal of the test water after equilibration outside the propagated analytical uncertainty. Porewater to test water ratios as low as 0.1 – 0.2 were accepted but the calculated isotope composition of the porewater was marked as less reliable, whereas ratios < 0.1 lead to unreliable results that were rejected. The mass of porewater in an experiment is defined by the mass of rock and its gravimetric water content. The latter is not known when starting an experiment.

[10] LAB: Isotope diffusive-exchange experiments with laboratory tap water used as test water.

[11] NGW: Isotope diffusive-exchange experiments using test water depleted in $^{18}O$ and $^{2}H$ (melt water of Antarctic ice cores).

- Limited mass transfer between rock and test water, i.e. 1) limited transfer of test water to rock ($< 0.5\ m_{\text{test water}}$) caused either by high salinity of porewater compared to test water or hydrating mineral phases (e.g. anhydrite, halite) or 2) limited transfer of porewater to test water (< 0.02 g) caused by high salinity of test water compared to porewater. Such mass transfer between rock and test water may lead to isotope fractionation processes whose impacts on the experiments are poorly understood. Porewater isotope data not fulfilling these criteria are kept but classified as less reliable provided that the experiments do not show any further unconformities and that the calculated porewater isotope data and water contents derived from isotope mass balance agree well with those of neighbouring samples (i.e. within the propagated analytical uncertainty). If this is not the case (i.e. the data constitute outliers), the experiments are considered as failed.
- Analyses of stable isotopes of test water solutions within the required accuracy.

Of the 100 investigated samples (200 individual experiments) only 1 experiment couple did not pass these criteria, owing to severe leakage of the experiment container (STA3-1-743.76-RP). For two other samples the experiments failed owing to strong desiccation during sample preparation (STA3-1-514.50-PW) or accidental spillage of equilibrated testwater during termination of the experiment (STA3-1-955.40-PW). Porewater isotope compositions calculated from these experiments are unreliable and will not be shown in the following graphs.

For 10 samples the experimental data resulted in an elevated uncertainty of the calculated isotope composition of the in situ porewater. Two samples show minor evaporation of the test water (5 – 10%; corrected by Rayleigh-distillation calculations) during the experiments, three samples show low porewater to test-water ratios of 0.1 – 0.2 and five samples show minor transfer of porewater to test water. Porewater isotope compositions calculated from these experiments are afflicted by somewhat larger uncertainties. These data are shown but marked with open symbols in the following graphs.

#### 4.8.1.2 Calculation of porewater composition and water contents

Porewater $\delta^{18}O$ and $\delta^{2}H$-values were calculated using equation 76 in Appendix A in Waber (ed.) (2020) considering the ratio *q* of the gravimetric water contents of the individual subsamples used in the experiments (for details see Appendix A in Waber ed. 2020). Water contents could then also be calculated by mass balance from the porewater isotope values. The robustness of the calculated porewater $\delta^{18}O$ and $\delta^{2}H$-values was further tested according to the following criteria:

1. A relative difference of less than 20% between the water contents calculated from $\delta^{18}O$ and $\delta^{2}H$ data derived from the experiments with test water depleted in $^{18}O$ and $^{2}H$ (NGW subsamples).
2. A relative difference of less than 20% between the average water content calculated by isotope mass balance from $\delta^{18}O$ and $\delta^{2}H$ data and the average of the gravimetric water content of the two subsamples used in the experiments.

If the relative difference in the different water contents is larger than 20%, the calculated porewater $\delta^{18}O$ and $\delta^{2}H$-values are considered less reliable. Such data may still be used for further interpretation by accepting the larger propagated uncertainty; they are marked with open symbols in the following graphs.

Of the 97 samples that passed the experimental quality criteria (*cf.* Section 4.8.1.1; including samples with elevated experimental uncertainties), one sample does not pass criterion 1 above (Fig. 4.8-1), 6 samples do not pass criterion 2 (Fig. 4.8-2) and one sample fails both criteria. Four

of the samples that fail the comparison of the water contents are afflicted by larger uncertainties from the experiments themselves (*cf.* Section 4.8.1.1). In these cases, the failure of criterion 1 and/or criterion 2 is due to experimental artefacts. The remaining four samples that fail the comparison of the water contents exclusively fail criterion 2 and they do not show any experimental irregularities. In these cases, the differences between the average of the water contents derived by isotope mass balance and the average of the gravimetric water content of the two subsamples likely reflect lithological heterogeneity of the different subsamples used in the two experiments. Note that in anhydrite-bearing lithologies hydration of anhydrite during the isotope diffusive-exchange experiments also plays a role, although its extent and effect is unknown at this stage.

All samples that pass the above criterion 2 display a consistent, previously observed relationship between the average water content derived by isotope mass balance and the average of the gravimetric water content of the subsamples used in the experiments, the former being around 10% larger than the latter (Fig. 4.8-2). As the water content is generally well correlated with the clay-mineral content of the rocks (*cf.* Section 4.3), it was postulated that this difference might be associated with minor exchange with water of different isotope composition adsorbed on clay minerals (e.g. Pearson et al. 2003). However, no stringent explanation exists at this stage.

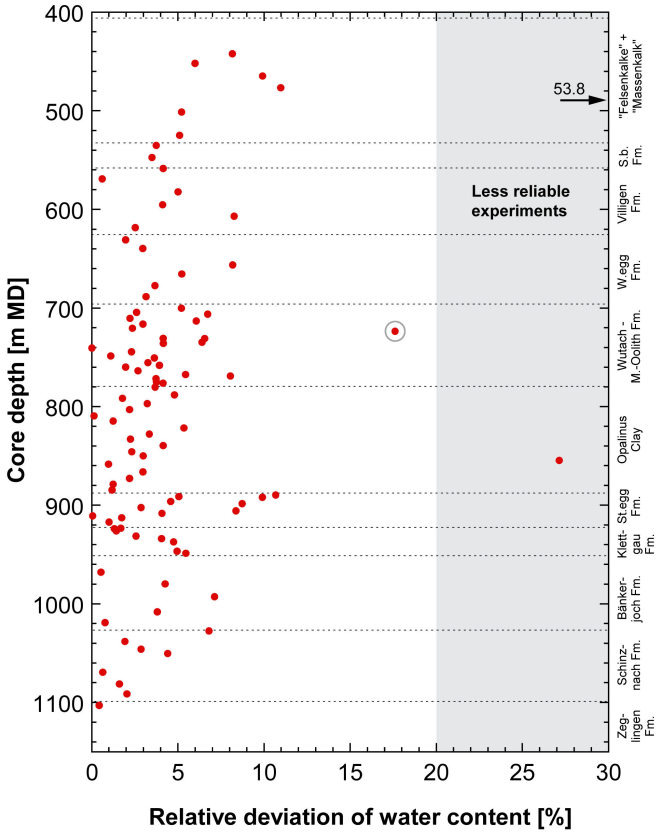


Fig. 4.8-1: Relative deviation of water contents obtained from $\delta^{18}O$ and $\delta^{2}H$ mass balance

The relative deviation is defined as the difference between the water contents calculated from the equilibrated $\delta^{18}O$ and $\delta^{2}H$ values, respectively, of the experiments with test water depleted in $^{18}O$ and $^{2}H$ (NGW) divided by the water content based on $\delta^{2}H$, expressed in %. Grey area: Relative deviation of water contents obtained from $\delta^{18}O$ and $\delta^{2}H$ mass balance is > 20%. For samples within this area the calculated porewater $\delta^{18}O$ and $\delta^{2}H$ values are considered less reliable. The sample with a grey circle shows some signs of contamination by drilling fluid (*cf.* Section 4.4).

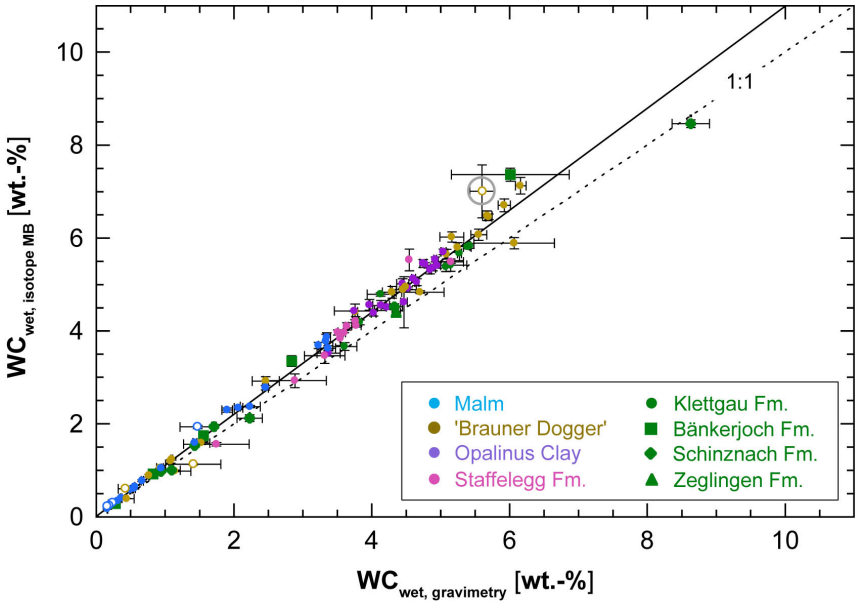


Fig. 4.8-2: Average water content obtained by water-loss at 105°C ($WC_{wet,\ gravimetry}$) of subsamples LAB and NGW vs. average water content calculated from $\delta^{18}O$ and $\delta^{2}H$ mass balance from NGW diffusive-exchange experiments ($WC_{wet,\ isotope\ MB}$)

Open symbols refer to samples showing differences larger than 20% between the average water content derived by isotope mass balance and the average gravimetric water content of the two subsamples used in the experiment. The sample with a grey circle shows signs of contamination by drilling fluid (*cf.* Section 4.4).

#### 4.8.1.3 Contamination by drilling fluid

For a limestone sample from the «Herrenwis Unit» (STA3-1-723.96-PW), contamination by drilling fluid – even in the central parts of the core material – was identified on the basis of aqueous extract solutions (*cf.* Section 4.4). This sample shows a rather high porosity (14 vol.-%) and likely elevated permeability allowing percolation of the drilling fluid to central parts of the drill core sample, which affected the porewater isotope composition derived from the isotope diffusive-exchange experiments to some degree. This sample is not excluded from the following graphs but marked with a grey circle being a less reliable datum.

### 4.8.2 $\delta^{18}O$ and $\delta^{2}H$-values of porewater

#### 4.8.2.1 Depth profiles of porewater isotope composition

All the porewater isotope data that pass the various quality criteria are illustrated in Fig. 4.8-3 as a function of depth. In the uppermost part of the investigated sequence in the «Felsenkalke» + «Massenkalk» no clear trends are indicated owing to the large scatter of the data. This is mainly related to experimental difficulties associated with these lithologies, e.g. very low water contents. Across the interval Schwarzbach Formation – Schinznach Formation both $\delta^{18}O$ and $\delta^{2}H$ values of the porewater show well defined, curved profiles. Although both tracers indicate the same general trends, some differences exist. The porewater $\delta^{18}O$ values cluster around a constant value of ca. –2.2‰ VSMOW across the Schwarzbach Formation down to the base of the Wildegg Formation. The same clustering is also observed for $\delta^{2}H$, however, an overall increasing trend is

indicated from the base of the Schwarzbach Formation (–48.7 ‰ VSMOW) down to the base of the Wildegg Formation (–42.1 ‰ VSMOW). In the underlying «Herrenwis Unit» (701.7 m – 742.0 m depth), the scatter of the data is again larger and a minor negative excursion of $\delta^{18}O$ and $\delta^{2}H$ is observed at 724.8 m depth indicated by three values considered as less reliable according to quality criteria (the most depleted value derived from a sample contaminated with drilling fluid; see Section 4.8.1.3). Across the remainder of the «Brauner Dogger» (note that the term «Brauner Dogger» is used for the Dogger units overlying the Opalinus Clay) and the Opalinus Clay porewater, $\delta^{18}O$ values constantly evolve towards more depleted values (from around –2.4 ‰ VSMOW to –4.7 ‰ VSMOW). At the base of the Opalinus Clay, this trend breaks and porewater $\delta^{18}O$ values remain constant across the Staffelegg Formation and the Klettgau Formation. In contrast, porewater $\delta^{2}H$ values remain remarkably constant (at around –35 ‰ VSMOW) across the lower half of the «Brauner Dogger» down to the base of the Klettgau Formation.

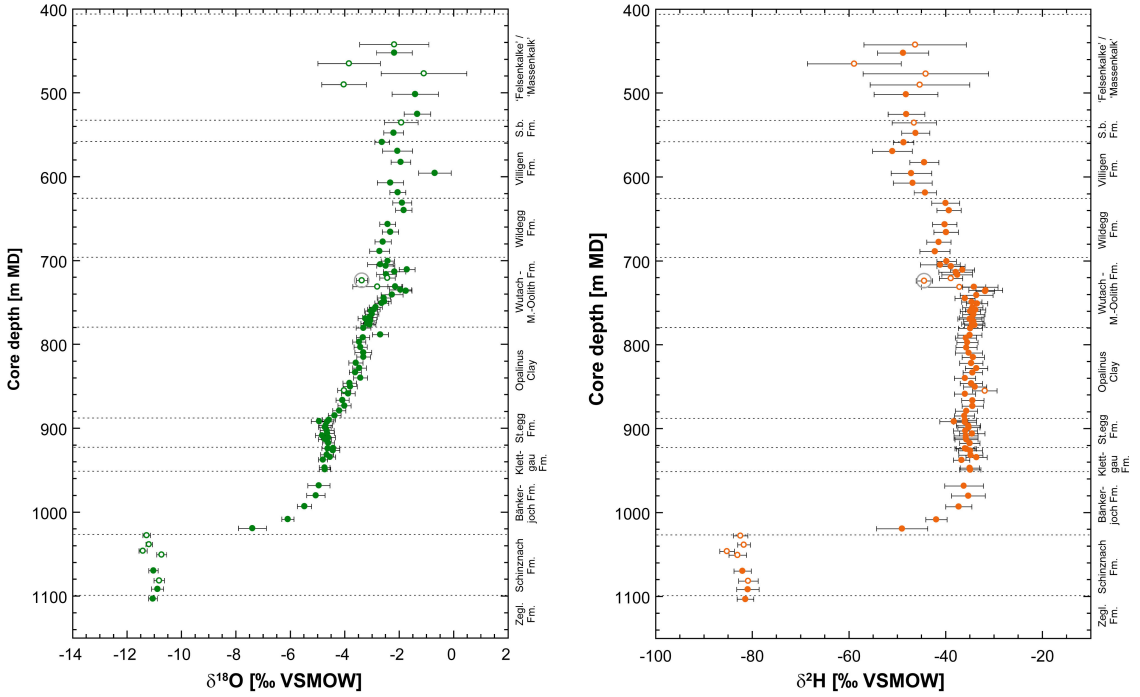


Fig. 4.8-3: Depth distribution of porewater $\delta^{18}O$ and $\delta^{2}H$-values obtained from isotope diffusive-exchange experiments

Open symbols refer to porewater isotope values which are less reliable owing to experimental artefacts (see text). The sample with a grey circle shows signs of contamination by drilling fluid (*cf.* Section 4.4).

The different shapes of the $\delta^{18}O$ and $\delta^{2}H$ profiles are also illustrated in Fig. 4.8-4, which shows the depth profile of deuterium excess (defined as $\delta^{2}H - 8 \times \delta^{18}O$; deuterium excess is +10 ‰ for a sample that lies on the GMWL, lower values of deuterium excess reflect sample positions to the right of the GMWL in a plot of $\delta^{18}O$ vs. $\delta^{2}H$). Note that the deuterium excess as used at this stage carries no direct implications about the palaeoclimate at the time of infiltration. As for $\delta^{18}O$ and $\delta^{2}H$, deuterium excess shows a large scatter in the «Felsenkalke» + «Massenkalk» and no clear trends are indicated. The underlying interval Schwarzbach Formation – Opalinus Clay is characterised by constantly increasing deuterium excess (from around –31.2 ‰ to +1.2 ‰). At the base of the Opalinus Clay this trend breaks, and the deuterium excess remains constant across the Staffelegg Formation and the Klettgau Formation.

Across the Bänkerjoch Formation, both $\delta^{18}O$ and $\delta^{2}H$ values of the porewater increasingly become more negative before they sharply evolve towards most negative values in the Schinznach Formation ($\delta^{18}O$ = –11.1 ‰ VSMOW; $\delta^{2}H$ = –82.5 ‰ VSMOW). Deuterium excess increases across the Bänkerjoch Formation (from 2.8 ‰ to 8.2 ‰), however, variability is within the propagated analytical uncertainty. In the Schinznach Formation, the deuterium excess remains at constant levels of around 6.6 ‰.

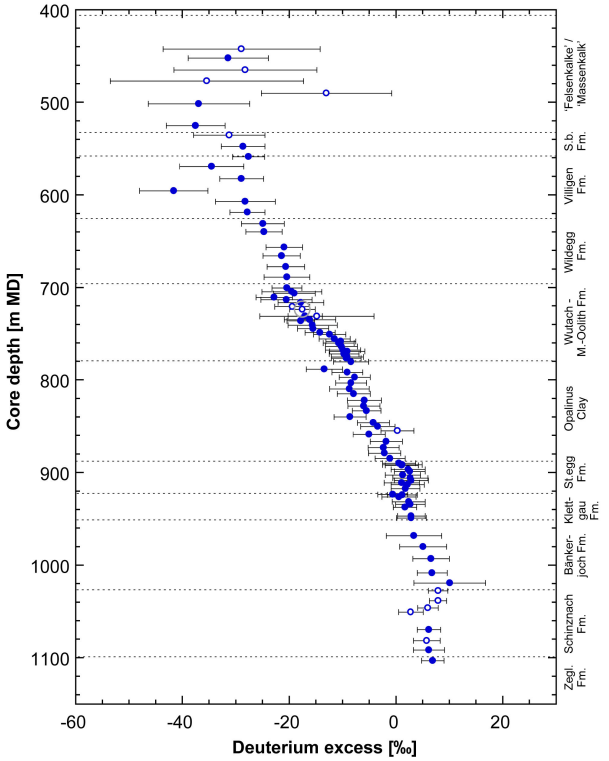


Fig. 4.8-4: Depth trend of deuterium excess in porewater based on the isotope diffusive-exchange technique

Deuterium excess is +10 ‰ for a sample that lies on the GMWL. Lower values of deuterium excess reflect sample positions to the right of the GMWL in a plot of $\delta^{2}H$ vs. $\delta^{18}O$. Note that the deuterium excess as used at this stage carries no genetic implications about the origin of $H_2O$, e.g. on palaeo-climate at the time of infiltration. Open symbols refer to samples which are less reliable owing to experimental artefacts (see text). The sample with a grey circle shows signs of contamination by drilling fluid (*cf.* Section 4.4).

### 4.8.2.2 $\delta^{18}O$ versus $\delta^{2}H$ and comparison with Global Meteoric Water Line

Porewater isotope signatures in the Malm fall to the right of the Global Meteoric Water Line (GMWL), same as porewaters in the underlying «Brauner Dogger», the latter being enriched in $^{2}H$ relative to Malm porewaters. From the «Brauner Dogger» across the Opalinus Clay down to the base of the Klettgau Formation, the porewater isotope composition continuously evolves towards values depleted in $^{18}O$ and approaching the GMWL, indicating a meteoric component in the latter porewaters. Similarly, the isotope composition of the porewaters in the Bänkerjoch Formation have a meteoric signature evolving – with increasing depth – along the GMWL towards values more depleted in $^{18}O$ and $^{2}H$. At the base of the Bänkerjoch Formation porewater $\delta^{18}O$ and $\delta^{2}H$ signatures sharply drop to distinctly more negative values across the water-conducting zone of the Muschelkalk (*cf.* Section 5.8 for further discussion) located on or slightly to the right of the GMWL.

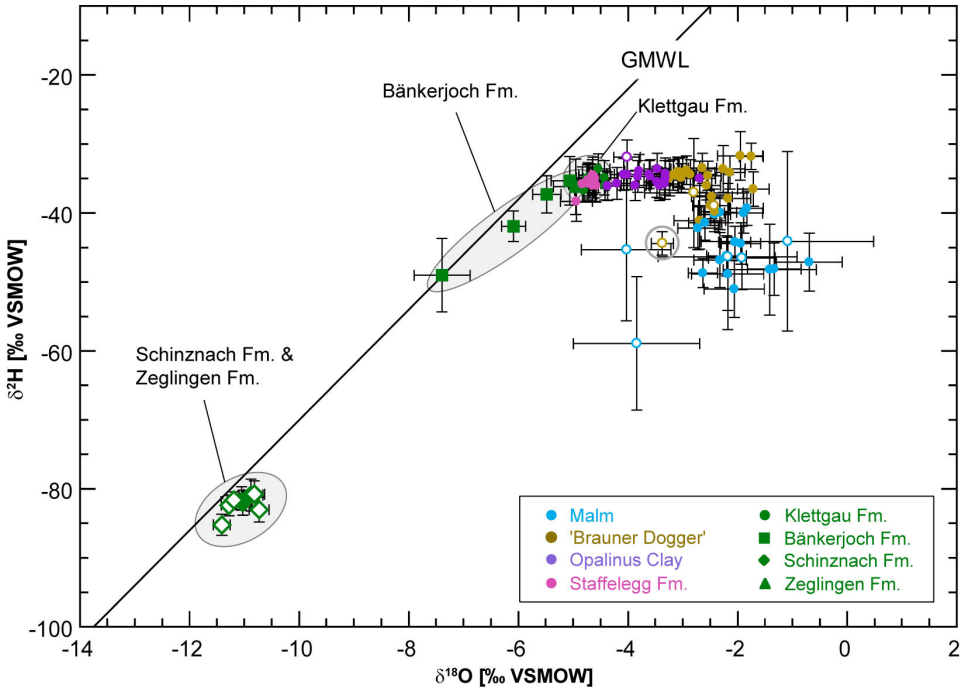


Fig. 4.8-5: $\delta^{2}H$ vs. $\delta^{18}O$ values of porewater obtained from isotope diffusive-exchange experiments

GMWL = Global Meteoric Water Line ($\delta^{2}H = 8 \times \delta^{18}O + 10$ ‰ VSMOW; Craig 1961), open symbols refer to porewater isotope values which are less reliable owing to experimental artefacts (see text). The sample with a grey circle shows signs of contamination by drilling fluid (*cf.* Section 4.4).

# 5 Discussion of porewater data

## 5.1 Chloride data and estimation of Cl and Br-accessible porosity

*Paul Wersin, Carmen Zwahlen, Martin Mazurek, Thomas Gimmi*

Chloride, a major component in the porewater, has been determined by squeezing (Section 4.6), advective displacement (Section 4.7) and aqueous extraction (Section 4.4). This anion is considered to behave as a conservative species with no or very limited interaction with the minerals. The same can be said for bromide, which occurs at much lower concentrations in the porewater. In argillaceous rocks, anions are repelled from the negative structural charge of the clay-mineral surfaces and are thus affected by ion exclusion. In other words, they only 'see' part of the total water-filled porosity, the fraction of which is often termed anion-accessible porosity (Pearson 1999, Pearson et al. 2003) or also 'free' porosity. Ion exclusion is not complete according to theory and depends on distance from charged surfaces, but here this simplifying assumption is made for adopting a simplest possible model.

Knowing the concentration of Cl per bulk (total) porewater in a sample from aqueous extraction ($C_{Cl\ in\ bulk\ porewater}$), the Cl-accessible porosity fraction, $f_{Cl}$, can be estimated from Cl measurements in squeezing ($C_{Cl\ in\ squeezed\ water}$) or advective-displacement ($C_{Cl\ in\ adv.\ displaced\ water}$) experiments, assuming that the latter two represent the composition of the 'free' porewater:

$$f_{Cl} = \frac{n_{anion-accessible}}{n_{total}} = \frac{C_{Cl\ in\ bulk\ pore\ water}}{C_{Cl\ in\ squeezed\ or\ adv.displaced\ water}}$$

$C_{Cl\ in\ bulk\ porewater}$ is calculated from:

$$C_{Cl\ in\ bulk\ pore\ water} = \frac{C_{Cl\ in\ aq.extract}}{WC_{dry}\ {}^{S}/_{L}}$$

with $C$ = concentration [mg/L], $n$ = porosity [–], $WC_{dry}$ = water content relative to dry rock mass [g/g], $S/L$ = solid/liquid ratio of aqueous extraction experiment [g/g]. The Br-accessible porosities are derived in an analogous fashion.

The anion-accessible porosity fractions have been derived according to the above equation for squeezed and advectively displaced porewaters (Tabs. 4.6-8, 4.6-9 and 4.7-17). Both methods enable to mobilise porewater that is thought to represent the mobile porewater and a proxy of the so-called 'free' porewater (not affected by the negatively charged clay surface). It should be noted, however, that the two methods operate by entirely different mechanisms. Whereas porewater is mobilised by mechanical compaction implying a deformation of the pore space in the squeezing method, this is achieved by a strong hydraulic pressure gradient and an artificial porewater in the advective-displacement method. Thus, method-specific artefacts may be expected and likely not the same volume of the pore space is sampled by the two methods. In the case of Cl, experimental artefacts appear to be minor as suggested from previous studies (e.g., Mazurek et al. 2021). In the case of the squeezed waters, it is generally assumed that the waters squeezed at the lowest pressure best reflect the in situ porewater (Mazurek et al. 2015, Wersin et al. 2016). For the advectively displaced waters, the first two measured aliquots are assumed to be the most representative of the in situ porewater (Section 4.7).

The derived values of the Cl-accessible porosity fraction ($f_{Cl}$) for the two datasets are shown as a function of the clay-mineral content in Fig. 5.1-1, with the SQ values derived according to the preferred method 1 (from POST data, see Section 4.6, Tab. 4.6-8). Porosity fractions obtained

from the two methods range between about 0.4 and 0.5 except for one AD sample (744.48 m) from the Wedelsandstein Formation which shows a value of 0.32. The corresponding mean value from both methods, excluding sample 744.48 m, is 0.453 ± 0.05. This value is in the same range as the corresponding ones from previous boreholes, such as TRU1-1 (Aschwanden et al. 2021), MAR1-1 (Mäder et al. 2021), BOZ1-1 (Wersin et al. 2022a) and BOZ2-1 (Gimmi et al. 2022), but slightly below that estimated for BUL1-1 (with mean $f_{Cl}$ = 0.52; Mazurek et al. 2021). It should be noted, however, that $f_{Cl}$ data from AD are systematically lower than those of SQ (Fig. 5.1-1). Differences between both methods were also observed in the previous boreholes, but generally not in such a systematic manner.

There is no clear trend with a clay-mineral content above 30 wt.-%. The sample with the lowest clay-mineral content (30 wt.-%) from the Wedelsandstein Formation actually exhibits a lower $f_{Cl}$ although an increase would be expected based on previous boreholes (e.g. BUL1-1, see Fig. 5.1-1). This sample contains a different clay mineralogy compared to the other samples, thus contains no kaolinite contrary to the other samples.

It would be important to know the anion-accessibility because within the sampled interval, the lithologies in the STA3-1 profile vary substantially. In order to derive a porewater profile for Cl, the anion accessibility in these lithologies must be known or assumed. In BUL1-1, which also lies in the Nördlich Lägern siting region, an increasing trend of $f_{Cl}$ with decreasing clay-mineral content was suggested below a clay-mineral content of 20 wt.-% (Fig. 5.1-1; even though the precise relationship could not be discerned). In other boreholes, such as TRU1-1, the increasing trend of $f_{Cl}$ seemed to start already at 40 wt.-% clay-mineral content, whereas in BOZ1-1 this "threshold" seemed to occur at about 25 wt.-%. Given these premises, we consider a uniform $f_{Cl}$ value of 0.45 for clay-mineral contents > 20 wt.-% as "reference" for deriving the Cl profile for the entire sequence, but also explore the effect when assuming a value of 40 wt.-% clay-mineral content (Section 5.2). Below these "threshold" clay-mineral contents, a linear increase of $f_{Cl}$ to a value of 1 at a clay-mineral content of zero is assumed.

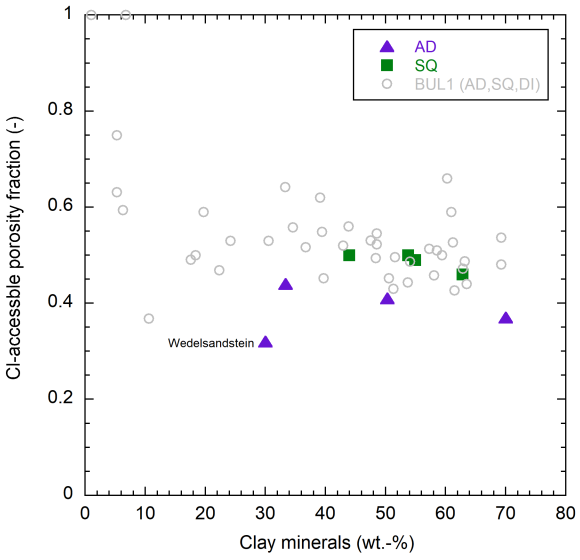


Fig. 5.1-1: Cl-accessible porosity fraction as a function of the clay-mineral content from AD and SQ data as well as data from the BUL1-1 borehole

BUL1-1 data comprises AD, SQ and through-diffusion data (Mazurek et al. 2021).

The fact that $f_{Cl}$ shows considerable scatter when plotted against the clay-mineral content suggests that the latter is not the only parameter that determines anion accessibility. Mineralogical composition of the clay fraction, mean pore size, grain-size distribution, fabric and other factors are expected to affect anion accessibility as well. Note that the negative structural charge of the clay-mineral surfaces is predominately carried by the smectite and illite components. Furthermore, according to theory, anion accessibility also varies with the salinity and composition of the porewater, i.e., it is not just a material property. All these partly interdependent effects cannot be properly quantified at this stage, which severely limits the application of theoretical models.

An uncertainty range of ± 20% is considered for $f_{Cl}$, which is probably sufficient for clay-rich lithologies but may still be an underestimation for clay-poor rocks. This uncertainty propagates into the calculated Cl concentrations in the anion-accessible porewater, i.e., an error of ± 20% must be considered in addition to the propagated analytical error.

For Br, only advective-displacement data are available. The derived $f_{Br}$ values as a function of the clay-mineral content are illustrated in Fig. 5.1-2. The mean $f_{Br}$ value for the four samples where these values could be derived is 0.52 ± 0.09. The mean $f_{Br}$ value is higher than relative to the mean $f_{Cl}$ value for the same AD samples (0.39 ± 0.05). It should be pointed out that in three of the four samples uptake of Br by the Ag filters occurred used for those experiments (Section 4.7.2). Notwithstanding this methodological issue, the difference between $f_{Cl}$ and $f_{Br}$ values inferred from AD data has already been observed in previous boreholes (without Ag filters). The reason for this difference is not clear at this stage, but Br may not behave in an entirely conservative manner, as suggested by its behaviour during drying to 105 °C (Section 4.4.3).

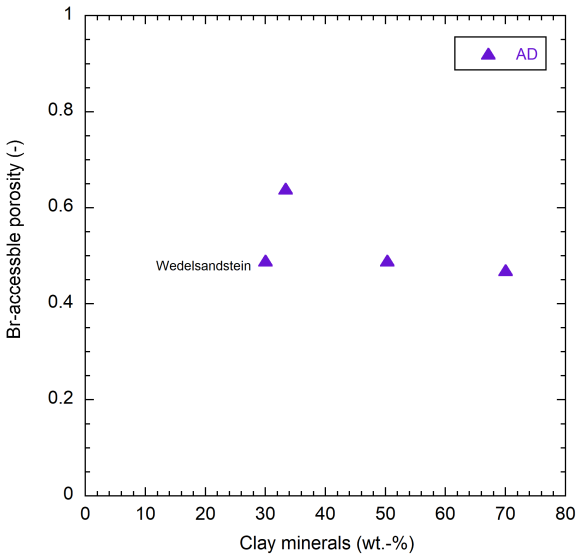


Fig. 5.1-2: Br-accessible porosity fraction as a function of the clay-mineral content derived from AD data

Fig. 5.1-3 illustrates the Cl-accessible porosity fraction as a function of depth. No clear trend for the sampled interval («Brauner Dogger» – Staffelegg Formation) can be discerned based on the limited dataset, rather suggesting constant values with depth. Again, the systematic difference between AD and SQ data is illustrated.

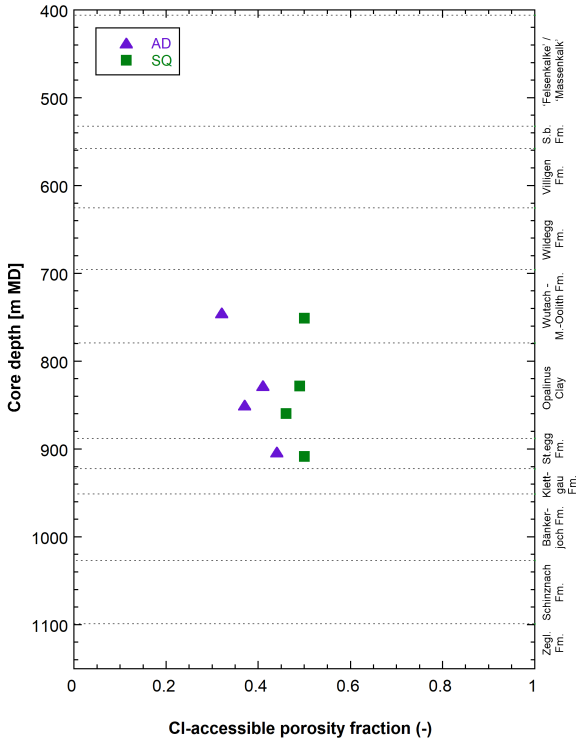


Fig. 5.1-3: Cl-accessible porosity fraction as a function of depth

## 5.2 Chloride, bromide, Br/Cl and $\delta^{37}Cl$ profiles

*Paul Wersin, Carmen Zwahlen, Martin Mazurek, Thomas Gimmi*

The chloride profile depicted in Fig. 5.2-1 includes aqueous extraction data re-calculated to in situ conditions assuming the relationship between clay-mineral content and $f_{Cl}$ (with a clay-mineral content of 20 wt.-% as "threshold" value) as discussed in Section 5.1. The Cl concentrations obtained from squeezing and advective displacement, as well as those for the groundwaters in the Malm and the Muschelkalk (Table 2.3 in Lorenz *in prep.*), are also shown in Fig. 5.2-1. The error bars include the propagated analytical uncertainty and, for aqueous extraction data, an additional 20% that reflect the uncertainty related to $f_{Cl}$ (see Section 5.1, Fig. 5.1-1).

Data from all three methods are consistent within the extended error bars[12]. The Cl profile is reasonably well constrained and supported by the dense sampling, in particular in the Opalinus Clay. In some lithologies in the upper and lower confining units, however, Cl concentrations show considerable variations (see below). In general, a flat profile with concentrations scattering around ~ 8 g/L is observed across most of the cored section, namely between the Klettgau Formation and the Malm aquifer in the lower «Felsenkalke» + «Massenkalk» as illustrated in Fig. 5.2-1 (left). In that figure, porosity determined from water-loss is considered to re-calculate Cl in aqueous extracts. Considering pycnometer porosity (Section 4.3.4) instead leads to a similar profile, but a general shift to slightly higher concentrations (Fig. 5.2-1 right) scattering around ~ 9 g/L can be discerned. This difference is because of the slightly lower porosities deduced from grain and wet density measurements. Also, the scatter in the Opalinus Clay and the «Brauner Dogger» appears

[12] One should keep in mind that three out of the four AD experiments exhibit increased $NO_3$ contents, even though this probably does not affect Cl.

somewhat higher with the latter choice. The reasons for these slight differences are not known at this stage. Samples from the «Felsenkalke» + «Massenkalk» show exceptionally high Cl concentrations when re-calculated from water-loss porosity, which is clearly due to desaturation of the samples (Section 4.3.4) amplified by low porosities. Thus, the use of pycnometer porosity leads clearly to a more realistic profile for this unit.

Looking at the Cl profile from the Malm aquifer down to the Muschelkalk aquifer in more detail, one can note:

- A slight general increase with depth is indicated in the Malm units (down to 700 m depth), but the scatter is considerable owing probably to the heterogeneity in lithologies and/or methodological issues for determining Cl levels in low porosity limestone-rich samples.
- The «Herrenwis Unit» (reef facies) in the upper part of the «Brauner Dogger» is limestone rich with strongly variable clay-mineral contents and displays large variations. These are mainly related to methodological uncertainties of these heterogeneous low porosity rocks. The uncertainty releated to $f_{Cl}$ values is probably larger than the 20% considered here. On the other hand, the low concentration at the top of the unit of some samples and the increasing trend with depth for a large part of the samples are suggested, at least when considering the profile from water-loss porosity (Fig. 5.2-1 left). This trend is, however, less obvious when pycnometer-porosity is considered (Fig. 5.2-1 right).
- The profile across the OPA-Staffelegg Formation-Klettgau Formation sequence is rather flat but shows condiderable variations in the lower part. A slightly decreasing trend with depth seems to be discernible for the AqEx data in the uppermost part, but there are no SQ and AD data available in this region which could confirm this trend. These latter two datasets show a systematic difference in Cl concentrations, with SQ data yielding lower values than those of AD. It should be noted that three of the four AD samples were affected by nitrate perturbation (Section 4.7). This, however, does not appear to explain the differences, because the OPA sample at 849.98 m depth with no nitrate perturbation also shows a clear shift relative to the two SQ samples in the vicinity. Note that Cl data from all four AD samples were considered to be reliable as discussed in Section 4.7.5.5). The scatter in the Staffelegg Formation and Klettgau Formation displayed by the AqEx data is considerable, in particular at the top of the Staffelegg Formation: The calcareous clay-poor sample at 891.98 m from the Gross Wolf Member exhibits a low Cl concentration, whereas the opposite is seen in the nearby less calcareous and clay-richer sample at 896.60 m from the Rietheim Member. Uncertainties related to the anion-acessible porosity fraction are the likely cause for this apparent mismatch, which has also been consistently observed in the other TBO profiles.
- The profile shows a strong decrease from the top of the Bänkerjoch Formation down to the Muschelkalk aquifer with minimum values at about 1'000 m depth, but with strong variations. Looking more closely, one could envision two minima, one at ~ 970 m and the other at ~ 1'030 m depth. These are, however, separated by only one sample point at 1'008.64 m with a high Cl concentration of 12 g/L. The same trend is indicated from the Br profile (Fig. 5.2-3). Note that the water isotope and $\delta^{37}Cl$ profiles show a regularly decreasing trend with depth from the Bänkerjoch Formation down to ~ 1'030 m (but not already at ~ 970 m) (see below). From this section, which consists of porous dolostones, a regular increase of Cl levels from 1.4 g towards the sampled aquifer in the Muschelkalk at 1'050 m – 1'100 m) is noted, where Cl levels reach ~ 4 g/L both in porewaters and in the groundwater.

As mentioned above, the relationship used to derive the Cl-accessible porosity fraction for samples with low and intermediate clay-mineral content is based on the arbitrary assumption of of a linear relationship with clay-mineral content < 20 wt.-% (towards a value of 1 for clay-free rock). Fig. 5.2-2 compares the profiles obtained for a "threshold" value of 20 wt.-% (left) with

those using a threshold value of 40 wt.-%. The two profiles are similar, showing slightly more scatter in the «Herrenwis Unit» but slightly less scatter in the lower Malm units for the left profile (20 wt.-%) compared to the right one (40 wt.-%). On the other hand, the Cl profile with the 40% "threshold" displays less scatter in the Staffelegg Formation and in particular the sample at 896.60 m from the Rietheim Member is more in line with the general trend.

In summary, a broadly consistent Cl profile above the Muschelkalk aquifer is obtained from squeezing, advective-displacement and aqueous extraction data. A well-defined profile is identified, with some scatter. This scatter is related predominantly to the uncertainty in anion-accessible porosity (which may not only vary as a function of the clay-mineral content), and to a lesser extent to the uncertainty in the water content. In this analysis, a simple relationship of the anion-accessible porosity with the clay-mineral content (as proxy of surface charge) based on squeezing and advective-displacement data was used. Other relationships with the clay-mineral content (e.g., linear extrapolation from clay-mineral content < 40 wt.-%) do not result in a less scattered profile. The lower part of the Cl profile is clearly influenced by the Muschelkalk aquifer. However, the negative excursion observed above the sampled aquifer in the center of the Bänkerjoch Formation cannot be explained so far and is not supported by $\delta^{2}H$, $\delta^{18}O$ or $\delta^{37}Cl$ data.

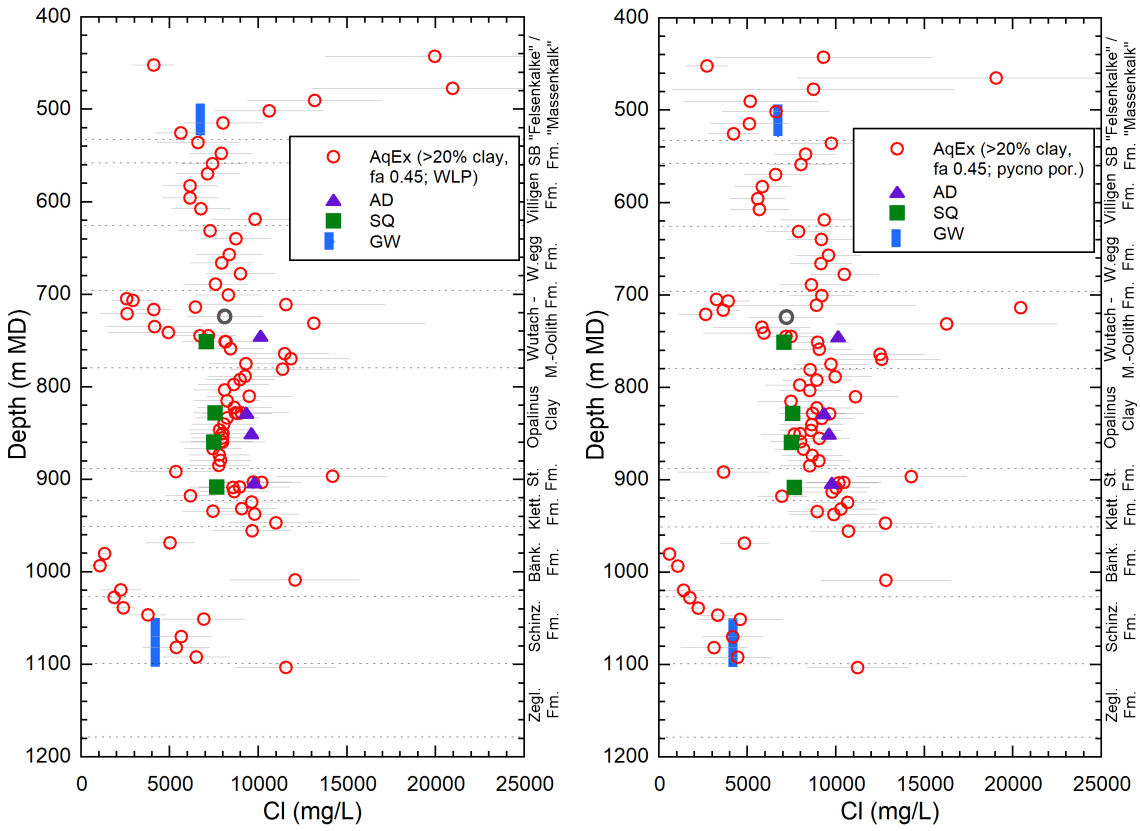


Fig. 5.2-1: Cl profile with data from squeezing, advective displacement, aqueous extraction, and groundwater samples

AqEx data recalculated from water-loss porosity (left) and pycnometer porosity (right) assuming 20 wt.-% clay-mineral content as "threshold" (see text). Aqueous extraction data re-calculated to Cl-accessible porosity assuming the relationship between accessibility and clay-mineral content as discussed in Section 5.1. Error bars on the data from aqueous extraction include propagated analytical uncertainty plus another 20% that reflect the uncertainty related to $f_{Cl}$. See comment in text regading possible disturbance of AD values.

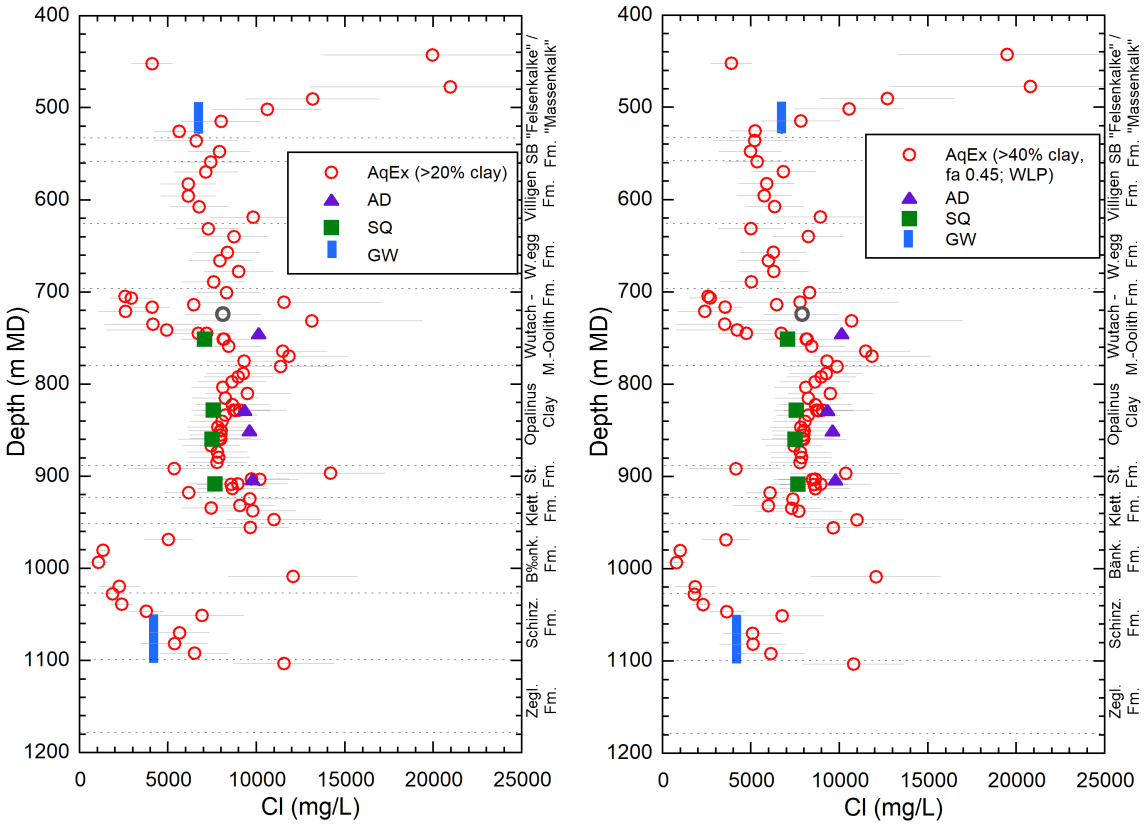


Fig. 5.2-2: Cl profile with data from squeezing, advective displacement, aqueous extraction, and groundwater samples

AqEx data recalculated from water-loss porosity using 20 wt.-% (left) and and 40 wt.-% (right) clay-mineral content as "threshold" (see text). Aqueous extraction data re-calculated to Cl-accessible porosity assuming the relationship between accessibility and clay-mineral content as discussed in Section 5.1. Error bars on the data from aqueous extraction include propagated analytical uncertainty plus another 20% that reflect the uncertainty related to $f_{Cl}$.

The Br profile (Fig. 5.2-3) reveals a similar shape as the one of Cl, albeit with somewhat more scatter, which is likely related to the larger analytical uncertainty of this minor element. Using the pycnometer porosity (Fig. 5.2-3 right) instead of the water-loss porosity (Fig. 5.2-3 left) to calculate porewater concentrations from aqueous extracts leads to somewhat more scatter, a feature that is more pronounced for Br compared to Cl (Fig. 5.2-1).

In the upper section, from the Bänkerjoch Formation up to the Malm aquifer, the Br profile shows considerable scatter with average values of about 20 – 35 mg/L. In fact, an increasing trend with depth in the Malm is suggested, a feature that is not seen in the Cl profile. Below, the concentrations decrease strongly showing a very similar trend as Cl. In the sampled groundwater test interval of the Muschelkalk, porewater values tend to be higher than that measured in the groundwater.

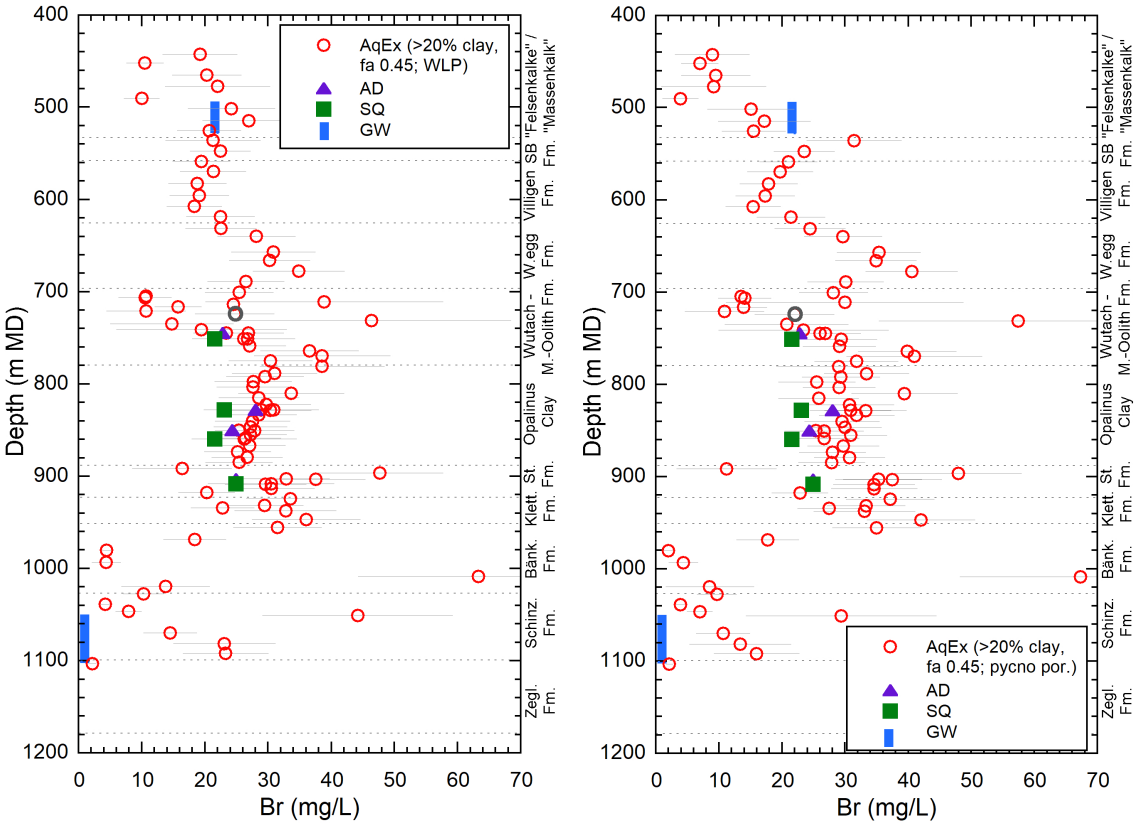


Fig. 5.2-3: Br profile with data from squeezing, advective displacement, aqueous extraction, and groundwater samples

AqEx data recalculated from water-loss porosity (left) and pycnometer porosity (right) assuming 20 wt.-% clay-mineral content as "threshold" (see text). Groundwater data of Malm aquifer are based on a preliminary extrapolation. Aqueous extraction data in the Br profile re-calculated to Br-accessible porosity assuming the relationship between accessibility and clay-mineral content for Cl as discussed in Section 5.1. Error bars on Br data from aqueous extraction include propagated analytical uncertainty plus another 20% that reflect the uncertainty related to $f_{Br}$. See comment in text regading possible disturbance of AD values.

The Br/Cl profile (Fig. 5.2-4) shows less scatter than the individual Cl and Br profiles. This is mainly because heterogeneity and uncertainty related to anion-accessibility and water content do not affect the Br/Cl ratio, contrary to the individual concentrations. AqEx, SQ and groundwater data show consistent datasets whilst three of the four AD samples indicate ratios slightly below the overall trend (see below).

Rather constant 1'000*Br/Cl ratios of about 1.5 are depicted from the Klettgau Formation up to the Malm aquifer, similar to that of modern seawater. In the upper part of the «Brauner Dogger» unit, values are more scattered, in particular in the «Herrenwis Unit». Above, ratios appear to decrease slightly in the lower Malm units towards the Malm aquifer. In the Bänkerjoch Formation, Br/Cl ratios increase with depth, but show very variable values in the underlying Schinznach Formation. The lowest sample at 1'103.22 m depth in the top of the Zeglingen Formation displays a low ratio of 0.08, consistent with the corresponding groundwater sample. The halite-rich layer at about 1'160 m depth exhibits an even lower ratio of ~ 0.01.

It is interesting to note that the Br/Cl ratios of ~ 1.5 over most of the profile are higher than what was observed in BUL-1-1 and the boreholes from ZNO (TRU-1-1 and MAR-1-1). However, the boreholes BOZ1-1 and BOZ2-1 from JO display similar ratios (although showing a slightly decreasing trend with depth). The positive excursion in the Bänkerjoch was also observed in those latter two boreholes and in the MAR1-1 borehole.

The reason for the lower Br/Cl ratios in the AD samples is not entirely understood. As discussed in Sections 4.7.5 and 4.7.6, Br was affected by interaction with the Ag filter in three of the four samples. Moreover, these samples were impacted by microbially induced nitrate production. The fourth sample (from 849.48 m depth), however, should not have been affected by these phenomena because an improved set-up was used to minimise microbial effects and interaction of Br with filters. Nevertheless, this sample also shows an offset in Br/Cl ratio relative to the general trend.

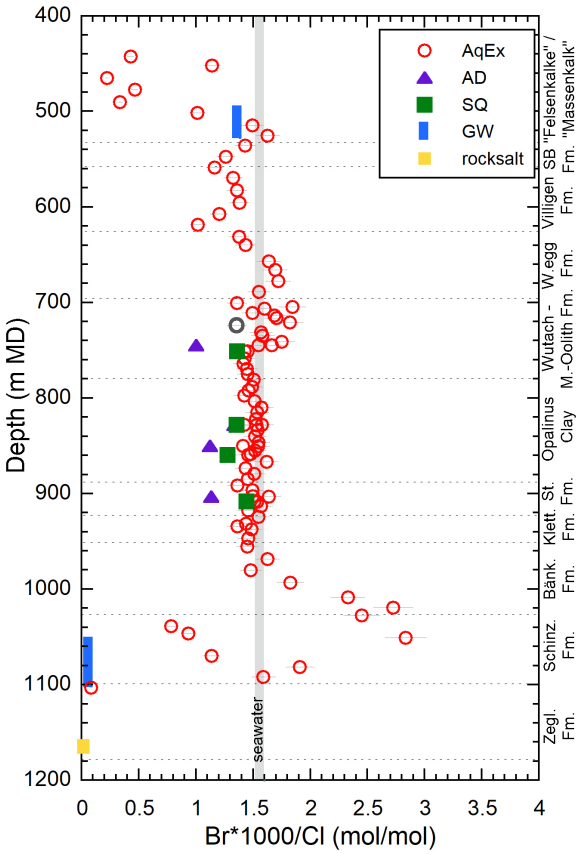


Fig. 5.2-4: 1'000*Br/Cl (molar units) profile with data from squeezing, advective displacement, aqueous extraction, groundwater and halite samples

Groundwater data of Malm aquifer are based on a preliminary extrapolation. Grey bar: range in modern seawater. The propagated uncertainty for SQ data assumes the same analytical uncertainty as for the other samples (4% for Br). See comment in text regading possible disturbance of AD values.

The profile for $\delta^{37}Cl$, which has already been discussed in Section 4.4.4, is shown in Fig. 5.2-5. In the lowest part of the profile, it reveals rather high δ values > 0, which are in a similar range as that for the halite layer below and the sampled groundwater from the Muschelkalk. Above this aquifer, a steadily decreasing trend to the base of the Opalinus Clay can be inferred. In the upper part of the profile the profile exhbits more variability, in particular in the upper part of the «Brauner Dogger». The data suggest rather constant values within the Opalinus Clay and a tendency to decrease within the Malm unit up to the top of the samples profile. Note that due to significant contamination of the sampled Malm groundwater by drilling mud, the δ value is likely not meaningful (not shown in Fig. 5.2-5).

It is worth mentioning that anion tracer profiles (Cl, Br) do not indicate any excursions in the prominent deformed interval in the Opalinus Clay at 850.20 – 851.80 m depth (Section 2.2).

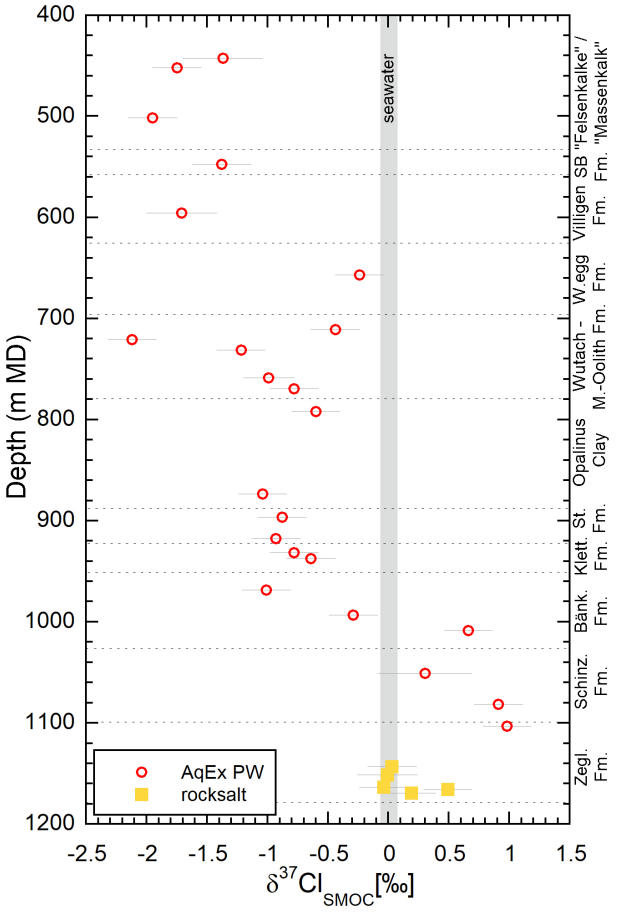


Fig. 5.2-5: $\delta^{37}Cl$ profile for aqueous extracts, rock forming halite and Muschelkalk groundwater

Due to high contamination of Malm groundwater with drilling mud, no value indicated for this sample.

## 5.3 Sulphate and $SO_4$/Cl profiles

*Paul Wersin, Martin Mazurek, Thomas Gimmi*

Sulphate data from squeezing, advective displacement, aqueous extraction and groundwaters are illustrated in Fig. 5.3-1. Data from aqueous extraction were re-calculated to concentrations in bulk porewater (Fig. 5.3-1 left) or to concentrations in anion-accessible porewater (using the same accessibility as for Cl with the relationship based on 20 wt.-% clay-mineral content "threshold", Fig. 5.3-1 right), assuming conservative behaviour of sulphate. This assumption is not true at least in anhydrite-bearing lithologies in the Bänkerjoch Formation where mineral dissolution contributed to $SO_4$ concentrations in the extracts, as is evident from the AqEx samples with re-calculated unrealistically high $SO_4$ concentrations of more than 50 g/L, way above the solubility of gypsum or anhydrite (not shown in Fig. 5.3-1).

$SO_4$ concentrations based on squeezing and advective displacement yield distinctly lower and less scattered values in comparison with the concentrations per bulk water or per accessible porewater re-calculated from aqueous extraction. A closer look at the sequence «Brauner Dogger» – Staffelegg Formation reveals broadly consistent concentrations between squeezing and advective-displacement data, although AD data display slightly higher values. Both datasets suggest a slightly decreasing trend with decreasing depth in the lower part of the sequence, followed by approximately constant concentrations (2.5 – 3 g/L) from the lower part of the Opalinus Clay to the «Brauner Dogger». The Muschelkalk groundwater exhibits a slightly lower concentration (~ 1.5 g/L) than the AD and SQ porewaters above. The sampled Malm groundwater displays a much lower concentration of ~ 5 mg/L compared to the porewater analyses of AD and SQ.

The re-calculated aqueous extraction concentrations exhibit systematically higher and more variable concentrations than the SQ, AD and groundwater data. The discrepancy between aqueous extraction and squeezing/advective-displacement data becomes even larger when anion exclusion is considered, e.g. by assuming the same relationship between anion-accessible porosity and clay-mineral content as that applied for Cl (Fig. 5.3-1 right). However, it should be noted that the anion-exclusion effect of $SO_4$ in the considered rocks is not well known. From double layer theory, the exclusion of $SO_4$ in clayrocks is predicted to be higher because of its higher charge (Gimmi & Alt-Epping 2018). On the other hand, $SO_4$ has a larger tendency to form weak complexes, such as with alkaline earths, thus partly compensating the charge effect. Also, data for selenate (which displays similar chemical properties as sulphate) in Opalinus Clay from Mont Terri suggest a similar diffusion regime as for Cl (Gimmi et al. 2014), even though no exact values for anion accessibility are available. A similar discrepancy between squeezing or advective-displacement data on the one hand and aqueous extraction data on the other hand has been observed for other boreholes, such as Schlattingen-1 (Wersin et al. 2013), the BUL1-1 borehole (Mazurek et al. 2021), the TRU1-1 borehole (Aschwanden et al. 2021), the BOZ1-1 borehole (Wersin et al. 2022a) or the BOZ2-1 borehole (Gimmi et al. 2022) as well as in the Mont Terri Rock Laboratory (Wersin et al. 2020). In the latter case, waters sampled from packed-off boreholes exhibited similar sulphate concentrations and $SO_4$/Cl ratios as waters squeezed from nearby drillcores. The reason for the higher sulphate levels derived from aqueous extraction compared to squeezing or advective-displacement data is not understood at this stage, in spite of a recent systematic aqueous extraction study on Opalinus Clay including Mont Terri and BUL1-1 samples (Debure & Gailhanou 2019, Aschwanden & Wersin 2020).

The porewaters from squeezed samples are close to saturation with respect to celestite (SI: -0.07 to +0.03), while those from advectively displaced samples are somewhat oversaturated (SI: +0.25 to +0.38). Celestite could be identified in some samples of the rock matrix of the Opalinus Clay

and overlying formation samples at Mont Terri and Schlattingen-1 by a combined SEM/microprobe study (Jenni et al. 2019). Samples from advective displacement and squeezing are generally undersaturated with regard to gypsum, and gypsum is not thought to play a role in this issue.

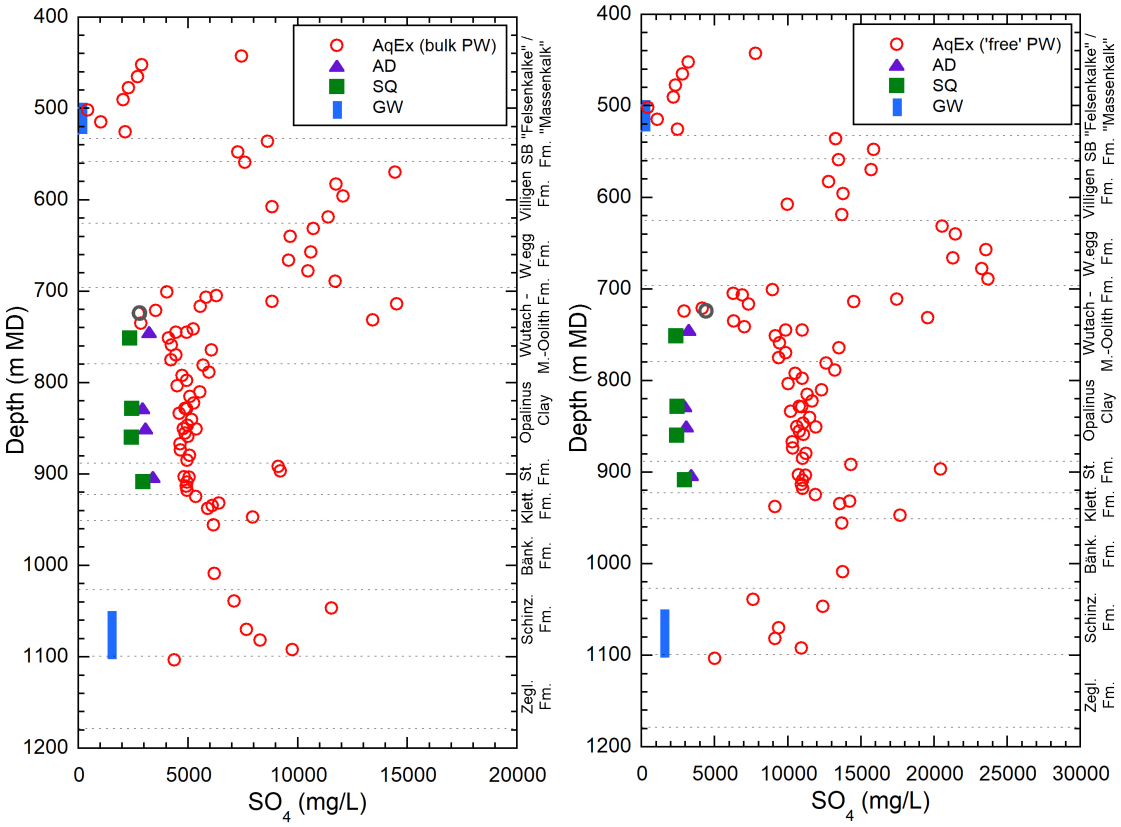


Fig. 5.3-1: $SO_4$ profiles with data from squeezing, advective displacement, aqueous extraction, and groundwater samples; left: AqEx data re-calculated to bulk porosity; right: AqEx data re-calculated to anion-acessible porosity

Groundwater data are based on a preliminary extrapolation. Aqueous extraction data re-calculated to contents in bulk porewater using water content. Aqueous data re-calculated to $SO_4$-accessible porosity assuming the same relationship between accessibility and clay-mineral content as applied above for Cl (20 wt.-% clay-mineral content "threshold").

The depth profile of $SO_4/Cl$ ratios (Fig. 5.3-2) shows a similar trend as the $SO_4$ profile. The general discrepancy between AD and SQ data on the one hand and AqEx data on the other are clearly evident and not discussed further.

In the «Brauner Dogger» – Opalinus Clay, $SO_4/Cl$ ratios in AD and SQ data are constant with values of 0.12, much higher than that of the overlying Malm groundwater ($\sim 3 \times 10^{-4}$). The lowest samples in the Staffelegg Formation display slightly increased ratios of 0.13 – 0.14. The underlying Muschelkalk groundwater displays a higher value of 0.25. Note that $SO_4/Cl$ ratios are generally higher than that of modern seawater (0.052) (red line in Fig. 5.3-2 right).

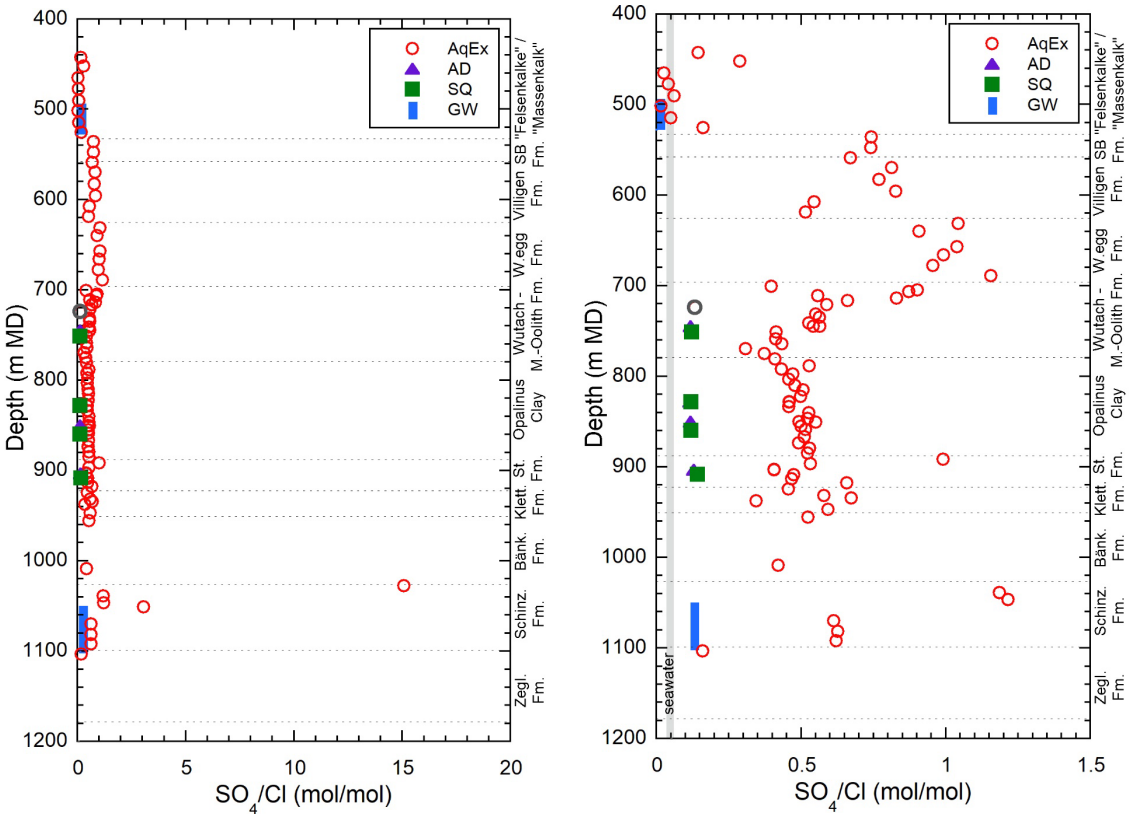


Fig. 5.3-2: Profiles showing molar $SO_4/Cl$ ratios obtained from different methods at different scales

Groundwater data are based on a preliminary extrapolation. Dashed line: modern seawater ratio.

## 5.4 Cation concentrations in porewaters

*Paul Wersin, Eric Gaucher, Thomas Gimmi*

Squeezing and advective displacement are the two methods that yield direct information on the cation concentrations in the porewater. Moreover, these can be estimated by simple modelling from the cation exchange data, notably from the cation occupancies on the exchanger. Aqueous extraction data, on the other hand, do not enable straightforward determination of porewater cations because of their modification via cation exchange and mineral reactions during the extraction process.

Both the squeezing and advective-displacement method may potentially induce some changes in porewater composition, thus also affecting cation composition and distribution. Data from previous boreholes and the Mont Terri rock laboratory, however, suggest that using not too high squeezing pressures and very early samples in the case of squeezing and advective displacement, respectively, experimental artefacts are relatively minor (e.g., Wersin et al. 2016, Wersin et al. 2020, 2022b), or at least some level of consistency between AD and SQ data is obtained (Mazurek et al. 2021, Aschwanden et al. 2021, Mäder et al. 2021, Wersin et al. 2022a, Gimmi et al. 2022). It should be pointed out that microbial processes probably occured during the advective displacement of three of the four experiments of STA3-1, as indicated for example by anomalous nitrate

levels in the water samples (Section 4.7). This obviously also affects the cationic charge. It is important to note that two of the three affected AD samples (827.93 m, 903.38 m) exhibit very elevated nitrate levels, whereas the third affected AD sample 744.88 m exhibits only a moderate nitrate concentration.

Depth profiles for Na, Ca, Mg and K in porewater are illustrated in Fig. 5.4-1. Overall, a differentiated picture regarding consistency between AD and SQ datasets can be seen. Looking at first at the main cations Na, Ca and Mg, AD data show higher and more variable concentrations relative to SQ data. The shift is more pronounced for the samples affected by microbially induced high nitrate levels (encircled points). The higher cationic charge of AD is thus largely explained by the high nitrate levels (Section 4.7.5). Whereas the cationic charge of $Na^+$ and $Ca^{2+}$ is compensated almost entirely by $Cl^-$ and $SO_4^{2-}$ for SQ samples and the two AD samples non-affected or only moderately affected by nitrate, this is not the case for the two high-nitrate AD samples, where an anion charge deficit is evident (Fig. 5.4-2 left). For K, an opposite trend between AD and SQ data is noted (Fig. 5.4-1) and nitrate-affected AD samples display slightly lower concentrations than SQ samples. The non-affected AD sample (849.98 m) on the other hand shows a slightly higher K concentration relative to SQ samples. Sr depicts analoguous differences as the other divalent cations (not shown).

The porewater composition in the Dogger and Liassic is Na-Cl dominated with little variations (omitting highly nitrate perturbed AD samples). According to the classification of Jäckli (1970)[13] the porewaters are of Na-(Ca)-Cl-($SO_4$) type, showing slightly increased $SO_4$ levels in the lowest sample from the Staffelegg Formation.

The Ca/Na molar ratio shows constant values of about 0.08 for SQ data, and somewhat higher values of around 0.1 for AD data. Note that a low Ca/Na ratio of 0.06 is indicated for the overlying Malm groundwater, but a high value of 0.3 for the underlying Muschelkalk groundwater.

The relationships of cations and their consistency with exchangeable cation populations are further discussed in Section 5.6.

[13] Ions with > 50 eq.-% are underlined; ions with 20 – 50 eq.% are not underlined, ions with 10 – 20 eq.% are put in brackets.

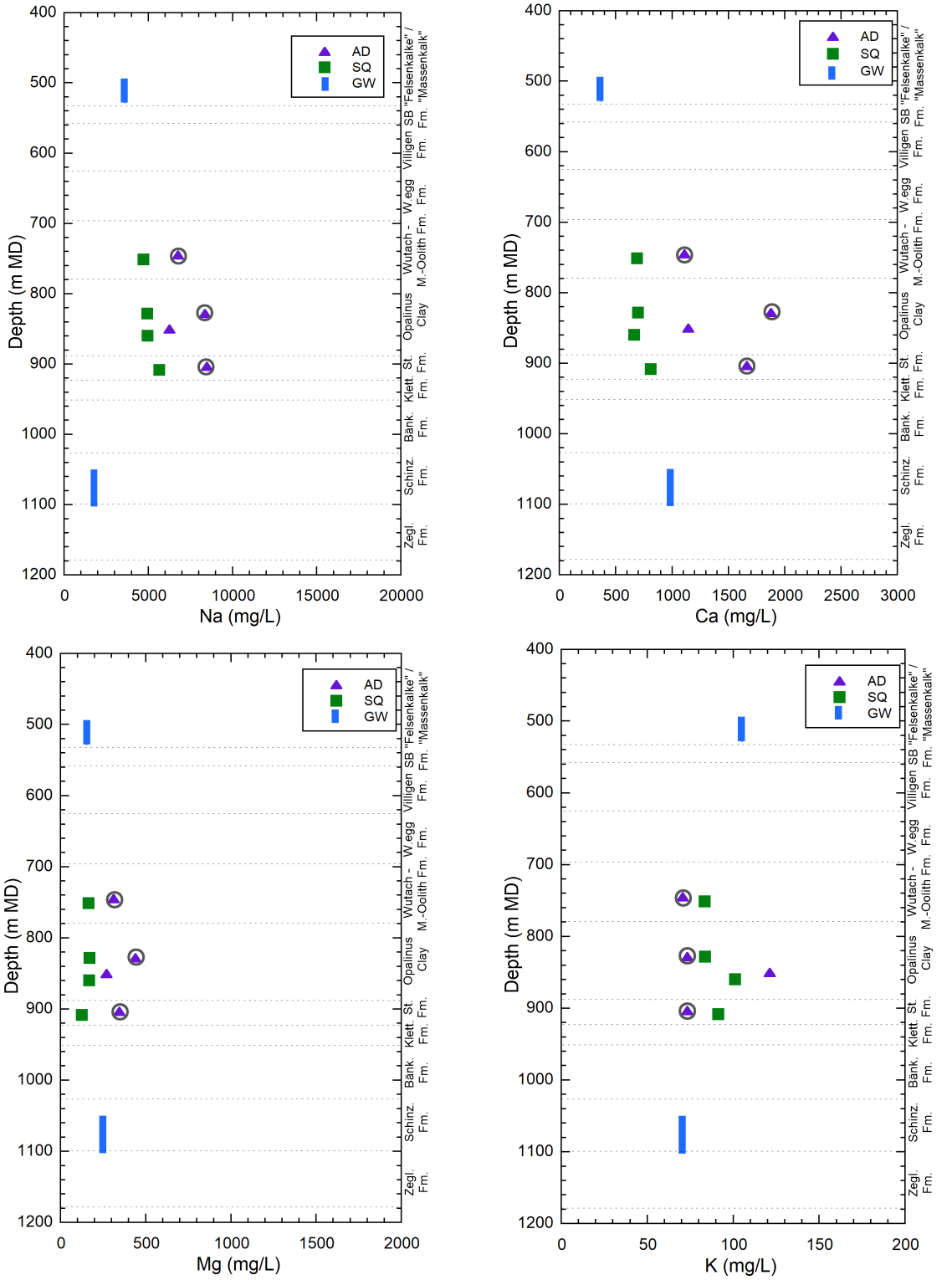


Fig. 5.4-1: Profiles for Na, Ca, Mg, K and Sr in porewater with data from squeezing, advective displacement and groundwater samples

Groundwater data are based on a preliminary correction. The values of the AD samples indicated by circles, are most likely disturbed by microbial reactions (see text and Fig. 5.4-2).

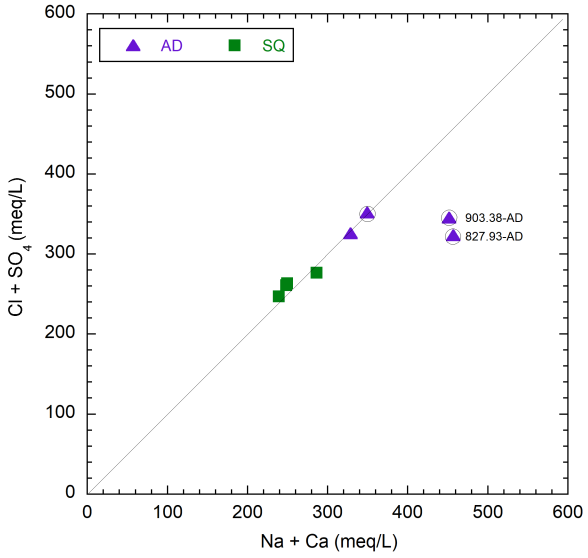


Fig. 5.4-2: $Cl + SO_4$ concentrations vs. Na + Ca concentrations (meq/L) for AD and SQ samples

Dashed line: 1:1 relationship between $Cl + SO_4$ conc. and Na + Ca conc. The values of the AD samples indicated by circles, are most likely disturbed by microbial reactions (see text).

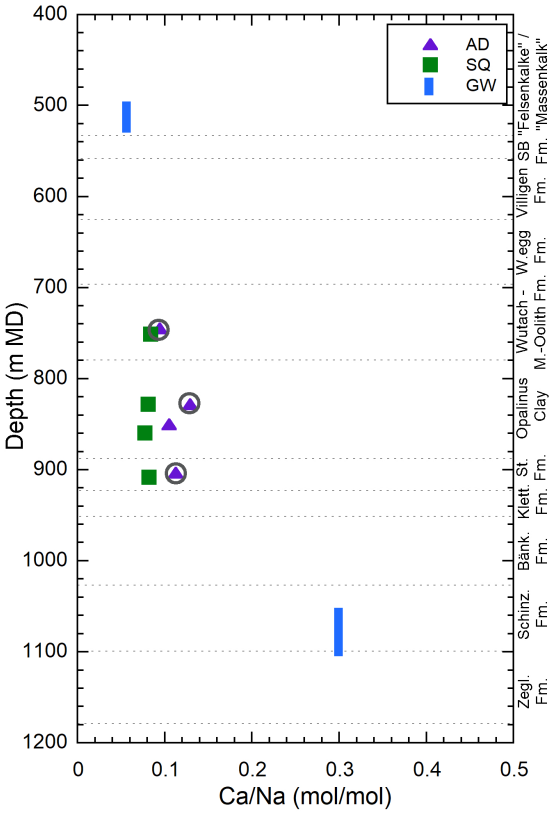


Fig. 5.4-3: Ca/Na ratio (molar units) for SQ and AD samples and groundwater

Groundwater data are based on a preliminary correction. The values of the AD samples indicated by circles, are most likely disturbed by microbial reactions (see text and Fig. 5.4-2).

## 5.5 Dissolved carbon species (inorganic, organic), alkalinity, pH and $pCO_2$

*Paul Wersin, Eric Gaucher, Thomas Gimmi*

### 5.5.1 Dissolved inorganic carbon, alkalinity, pH & $pCO_2$

The two methods yielding information on the carbonate system of the porewater are squeezing and advective displacement. These two methods enable the measurement of TIC, alkalinity (determined by titration) and pH. Alkalinity may include other compounds (e.g. low-molecular organic acids) than carbonate species ($HCO_3^-$, $CO_3^{2-}$) and thus TIC is considered to be a more reliable parameter for constraing the carbonate system of the porewaters (Wersin et al. 2020).

Knowing pH and TIC, the (dissolved) carbonate system is entirely constrained (at constant temperature and pressure) according to Gibbs phase rule and the $CO_2$ partial pressure can be calculated. It should be noted that it is not straightforward to obtain reliable measurements on these parameters which are prone to perturbations. For example, degassing of $CO_2$ during the squeezing process may alter pH and TIC parameters[14] (Tournassat et al. 2015, Wersin et al. 2020). In the case of advective displacement, an important perturbation that may arise is related to microbial activity inducing high nitrate levels (Section 4.7.5). Equilibrium with calcite, omnipresent in the sedimentary sequence, imposes a further constraint on pH/$pCO_2$. Thus, from the measured Ca, TIC and pH, the saturation state with regard to calcite can be calculated, providing a plausibility test of the dataset regarding the carbonate system. It is worth noting, however, that calculated saturation indices for calcite close to zero do not a priori confirm that measured parameters, such as pH and TIC, reflect in situ conditions. In fact, perturbations during the experimental procedure might lead to a new equilibrium with calcite at different pH/$pCO_2$ conditions.

Tab. 5.5-1 shows the measured pH, TIC data together with the derived $pCO_2$ and saturation index for calcite from speciation calculations with PHREEQC. Note that for the AD data pH was measured inline and offline after sampling, but only offline data (lab data) are considered here (differences between these two measurements are rather small). In general, pH values for AD are in the range of 7.0 – 7.7, whereas those for SQ are much higher, in the range of 8.3 – 8.8, as also illustrated in Fig. 5.5-1 (left, closed symbols). Conversely, TIC values are higher for AD (4 – 120 mM) compared to SQ (1.4 – 2 mM), even for the two AD samples where $NO_3$ concentrations are less elevated. Regarding $pCO_2$, measured AD data indicate values of -1.3 to -2.5 bar in log units, whereas much lower values (-3.4 to -4.0) are derived for SQ data, as also illustrated in Fig. 5.5-1 (right, closed symbols). All samples are oversaturated with regard to calcite, but oversaturation is higher for SQ samples.

Most of the $pCO_2$ data obtained from pH/TIC measurements represent rather extreme values relative to the expected ones (about -2 to -3 log(bar); Wersin et al. 2020). Thus, $pCO_2$ values from two AD samples appear too high, in fact those ones exhibit the highest nitrate concentrations (Tab. 5.5-1) which is likely related to the microbial perturbation. Although the details of the nitrate-producing pathway remain unknown at present, it is reasonable to assume that it involved a redox process with the production of acidity. This in turn would have led to the dissolution of carbonates and the production of $CO_2$ and alkalinity, as schematically illustrated by the following reaction:

$$2\ CaCO_3 + 3\ H^+ \rightarrow 2\ Ca^{2+} + HCO_3^- + CO_2(g) + H_2O$$

[14] But alkalinity is not affected by changes in $CO_2$ partial pressures as long as no dissolution/precipitation reaction occurs.

This would explain both the high TIC and $pCO_2$ derived from these AD data[15]. In the case of SQ data, $CO_2$ degassing, which is a known phenomenon occuring during the squeezing process, may explain high pH and increase of $CO_3^{2-}$ activity (leading to calcite oversaturation), schematically represented by the two reactions (where ↑ represents degassing):

$$HCO_3^- \rightarrow CO_2(g)\uparrow + OH^-$$

$$2\ HCO_3^- \rightarrow CO_2(g)\uparrow + CO_3^{2-} + H_2O$$

Tab. 5.5-1: Measured pH and TIC as well as calculated $pCO_2$, $SI_{calcite}$ and pH from AD and SQ experiments (see text)

| | | From measured parameters | | | | Calculated | | |
|---|---|---|---|---|---|---|---|---|
| **Method** | **Depth** | **pH** | **TIC** | **log$pCO_2$** | **SI Calcite** | **log$pCO_2$** | **pH** | **Nitrate** |
| | [m] | (lab) | [mmol/L] | [b]ar | [-] | [bar] | | [mmol/L] |
| AD | 744.88 | 7.18 | 4.06 | -1.99 | 0.49 | | | 9.6 |
| AD | 827.93 | 6.95 | 12.07 | -1.33 | 0.93 | | | 134.2 |
| AD | 849.98 | 7.67 | 3.88 | -2.49 | 0.99 | | | 0.4 |
| AD | 903.38 | 7.37 | 19.58 | -1.51 | 1.53 | | | 102.4 |
| SQ | 750.86 | 8.76 | 1.53 | -4.04 | 1.41 | -2.26 | 7.16 | 0.1 |
| SQ | 828.13 | 8.54 | 1.91 | -3.68 | 1.33 | -2.13 | 7.10 | 0.1 |
| SQ | 859.37 | 8.28 | 2.00 | -3.38 | 1.10 | -2.20 | 7.14 | 0.2 |
| SQ | 908.31 | 8.69 | 1.42 | -3.99 | 1.36 | -2.30 | 7.16 | 0.1 |

[15] This process would also explain the elevated Ca concentrations (Section 5.4).

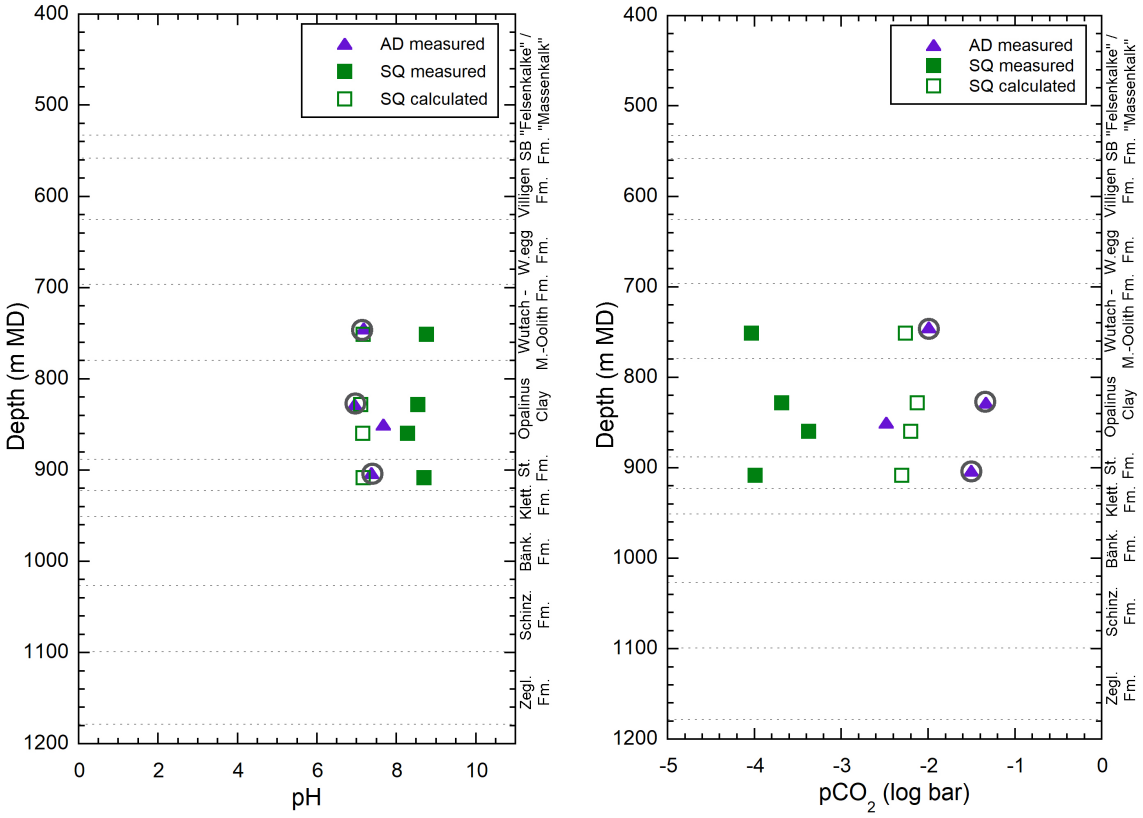


Fig. 5.5-1: pH (left) and $pCO_2$ values (right) from AD and SQ (see text)

Solid symbols: measured pH, pCO2: calc. from measured pH and TIC. Open symbols: models based on calcite equilibrium (see text). The values of the encircled AD samples are most likely disturbed by microbial reactions (see text and Fig. 5.4-2).

Assuming that SQ samples were affected by $CO_2$ degassing during the experimental procedure, $CO_2$ was added until attainment of calcite saturation with aid of PHREEQC. This leads to lower pH and higher $pCO_2$ values, depicted as open symbols in Fig. 5.5-1. These calculated pH/$pCO_2$ values seem to be in a reasonable range (pH 7.1 – 7.2, log($pCO_2$) –2.1 to –2.3) according to previous pH/$pCO_2$ data in Opalinus Clay (Wersin et al. 2020). This supports the hypothesis that the carbonate system was mainly affected by $CO_2$ degassing and much less by carbonate dissolution during the squeezing procedure.

In summary, both AD (except perhaps sample 949.98 m) and all squeezing data indicate perturbed pH/$pCO_2$ conditions. Re-calculating $pCO_2$ and pH assuming calcite equilibrium seems to lead to reasonable values in the case of SQ.

### 5.5.2 Dissolved organic carbon

Information on dissolved organic carbon is available from advective-displacement (AD) and squeezing (SQ) data as well as from aqueous extracts of AD cores (AqEx-AD):

1. SQ: TOC
2. AD: TOC, low molecular-weight organic acids (LMWOA)
3. AqEx-AD: low molecular-weight organic acids (LMWOA)

Moreover, the (solid) organic carbon content ($C_{org}$) from the corresponding SQ and AD rock samples is available besides those from PW, RP and DI samples.

Before discussing the dissolved organic carbon data it is worth mentioning some general points: The organic carbon in the sedimentary rock consists of refractory kerogen and only a small fraction is extractable by solvents (Grasset et al. 2010) The water-soluble organic carbon is even smaller, thus for example reaching a few mg C/L in the porewater of Opalinus Clay at Mont Terri or in the Callovo-Oxfordian Formation sampled from seepage boreholes (Courdouan Merz 2008; Courdouan et al. 2007a & b). Higher concentrations (several tens to hundreds of mg C/L) are generally measured in porewaters extracted from core samples, such as from squeezing or advective displacement (Wersin et al. 2013, Wersin et al. 2020). In the case of aqueous extracts, significant amounts of organic carbon are released to the solution. This indicates that a fraction of the "solid"carbon is mobilised during the extraction process. It also suggests the preferential release of loosely bound small organic molecules.

The TOC concentrations from AD and SQ data are illustrated in Fig. 5.5-2 (left). The SQ data show concentrations of about 200 mg/L, but slightly higher levels for the two OPA samples compared to the other two samples. This pattern is in qualitative agreement with the (total) organic C profile, which depicts higher $C_{org}$ amounts in OPA compared to the adjacent formations (Fig. 5.5-2 right)[16]. AD data on the other hand show higher and much more variable TOC levels. The TOC variation of AD samples is not correlated with the corresponding $C_{org}$ values of the rock. The two samples most affected by the nitrate disturbance yielded TOC of 500 and 800 mg/L, respectively. The sample with no nitrate disturbance displays a lower value of 340 mg/L, which is, however, still above the levels obtained for the squeezed samples. Moreover, this sample contains a high concentration of acetate, making up about 63% of the TOC. The uppermost AD sample which is moderately affected by microbial nitrate production also contains a notable fraction of acetate (~ 50% of the TOC). High concentrations of this compound are commonly released during AD experiments (Mäder 2018). Conversely, the two AD samples (827.93 m and 903.38 m) strongly affected by the nitrate disturbance have low acetate levels (< 20 mg/L). This difference might also be related to the microbial activity in the AD cores by which acetate would have been transformed. Sample 827.93 m contains measurable levels of other LMWOA, such as lactate, prorionate and formate, whilst sample 903.38 m does not show any indications of increased LMWOA.

[16] Note the elevated $C_{org}$ content in one core from the Rietheim Member of the Staffelegg Formation ("Posidonienschiefer").

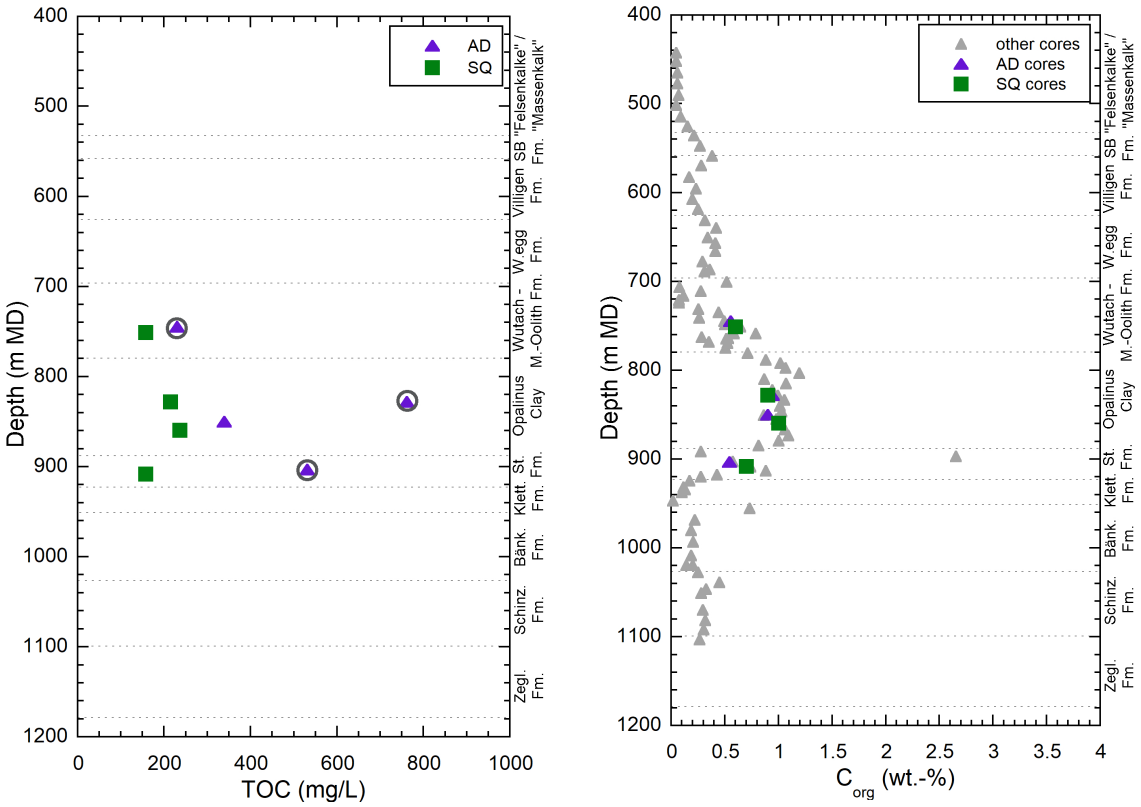


Fig. 5.5-2: TOC concentrations in porewater (left) from AD and SQ experiments and organic carbon content in rock in AD, SQ and other cores (right)

The values of the encircled AD samples are most likely disturbed by microbial reactions (see text and Fig. 5.4-2).

## 5.6 Cation exchange capacity and exchangeable cation population

*Paul Wersin*

### 5.6.1 Corrected exchangeable cation data

As mentioned in Section 4.5, in order to obtain the exchangeable cation concentrations, the extracted cation data need to be corrected for cations dissolved in the porewater and the cations released from (potential) mineral dissolution. As shown from previous work (e.g. Hadi et al. 2019) and also indicated from speciation calclations presented in Section 4.5 (Tab. 4.5-4), carbonate mineral dissolution is minimised with the appropriate *S/L* ratio, extraction time and pH conditions. Such conditions were applied to the Uni Bern dataset.

Two correction methods for cations dissolved in the porewater were applied based on the concentrations of the main anions chloride and sulphate (Bradbury & Baeyens 1998, Hadi et al. 2019). The first correction method ($NaCl/Na_2SO_4$) attributes dissolved Cl and $SO_4$ from the Ni-extracts to Na and leaves the other cations unchanged. The second method ($NaCl/CaSO_4$) attributes Cl to Na and $SO_4$ to Ca, leaving the other cations unchanged. In both methods, the CEC is calculated from the sum of cations (ΣCAT) minus the concentrations (normalised to $meq/kg_{dry\_rock}$) of Cl and $SO_4$. The corresponding data are shown in Tab. 5.6-1. The relative difference between the uncorrected and corrected sums of extracted cations (ΣCAT) is 6 – 10% for the three samples.

The values for the corrected ΣCAT are close to those of Ni consumption, albeit generally slightly lower by -6% to -10%. The good match between the two datasets supports the validity of the correction procedure for deriving the CEC based on the sum of cations.

Fig. 5.6-1 shows the CEC parameters as function of the clay-mineral content. No clear trend can be discerned, but it should be noted that the small sample number does not allow any conclusions in this regard. Further correlations are discussed in the following section where data from PSI is included.

The exchangeable cations are expressed as cation fractional occupancies (in equivalent fractions) in Tab. 5.6-1. Na and Ca are the main exchangeable cations, followed by Mg and K. The Sr occupancies are considerably lower (0.5 – 0.6% of the CEC).

Tab. 5.6-1: Sum of cations and cation occupancies obtained from Ni-en extraction after correction (Uni Bern data)

First line for each sample indicates fractional cation occupancies (in equivalent units) obtained by the $NaCl/Na_2SO_4$ correction method, the second line those obtained by the $NaCl/CaSO_4$ method.

| **Type** | **Depth** [m] | **Formation** | **Clay Mineral content** [wt.-%] | **Sum CAT raw** [meq/$kg_{rock}$] | **Sum CAT corr.** [meq/$kg_{rock}$] | **Na** fr.oc. | **K** fr.oc. | **Ca** fr.oc. | **Mg** fr.oc. | **Sr** fr.oc. |
|---|---|---|---|---|---|---|---|---|---|---|
| AD | 744.88 | Wedelsandstein Fm. | 23 | 121.1 | 113.8 | 0.47<br>0.49 | 0.05 | 0.35<br>0.32 | 0.12 | 0.005 |
| AD | 827.93 | Opalinus Clay | 50 | 108.5 | 100.1 | 0.52<br>0.55 | 0.05 | 0.31<br>0.28 | 0.11 | 0.005 |
| AD | 903.38 | Staffelegg Fm. | 33 | 72.7 | 65.3 | 0.49<br>0.53 | 0.06 | 0.33<br>0.29 | 0.11 | 0.006 |

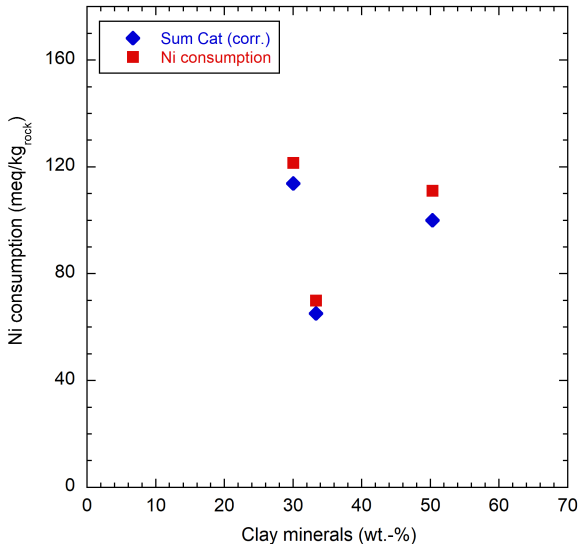


Fig. 5.6-1: Ni consumption and sum of (corr.) cations as a function of the clay-mineral content (data of Uni Bern)

### 5.6.2 Comparison with data from PSI

A dataset including 22 samples from the STA3-1 borehole was elaborated by PSI (Marques Fernandes & Baeyens *in prep.*). Samples originated from the top of the «Brauner Dogger» down to the Klettgau Formation In a first step, the CEC at PSI was estimated for all samples from Ni consumption with the Ni-en extraction method. Subsequently, the main dataset was generated via CsCl extraction, from which the CEC and the exchanger population were obtained. The CEC was derived by subtracting the anion equivalents (Cl, $SO_4$, $HCO_3/CO_3$) from those of the cations (Na, Ca, Mg, K, $NH_4$, Sr). The exchanger population was derived by two correction methods: (1) attributing Cl and $SO_4$ to Na and TIC to Ca, and (2) attributing Cl to Na and $SO_4$ and TIC to Ca. Note that these two methods are analogous to the ones used for the Uni Bern samples presented above, except for the additional consideration of TIC. The contribution of the latter is less relevant in the case of the Uni Bern data (see Tab. 4.5-4) because of the much higher solid/liquid ratios and thus a lower contribution of mineral dissolution to measured cation concentrations.

The conditions applied in the different extraction methods of PSI and Uni Bern are compared in Tab. 5.6-2. Important differences of the PSI methods relative to that of the Uni Bern are (i) the lower solid/liquid ratios, (ii) the smaller amount of solid mass and (iii) the more variable concentration of the index cation depending on the expected CEC.

Tab. 5.6-2: Extraction conditions applied by Uni Bern and PSI

| | **University of Bern** | **PSI** | **PSI** |
|---|---|---|---|
| Extraction method | Ni-ethylenediamine | Ni-ethylenediamine | CsCl |
| Initial extract solution concentration | 88 – 103 mmol/L | 3.3 mmol/L | 11 – 33 mmol/L |
| Solid/liquid ratio | ~ 0.9 kg/L | ~ 0.03 kg/L | ~ 0.03 – 0.1 kg/L |
| Amount of solid used | ~ 30 g | ~ 1 g | ~ 1 – 3 [a)] g |
| Extraction time | 24 h | 24 h | 24 h |
| Final pH | 8.3 – 8.6 | 8.3 –8.4 | 8.6 – 9.5 |
| Sample disaggregation | Disintegration by hand to a few $mm^3$ pieces | Milled and passed through 1 mm sieve | Milled and passed through 1 mm sieve |
| Sample storage time prior to preparation | 1 – 14 days | Several months [b)] | Several months [b)] |
| Extraction in glovebox | Yes | No | Yes |

[a)] *S/L* ratio adjusted to obtain the expected index cation consumption-to-CEC ratio.

[b)] in glovebox

## Cation exchange capacity and corrected sum of extracted cations

The Ni-en consumption and the corrected ΣCAT data (the latter from Ni-en extraction in the case of Uni Bern and CsCl extraction in the case of PSI) are shown in Fig. 5.6-2. From the comparison of these two datasets, the following findings can be derived:

- The CEC values obtained from Ni consumption exhibit consistent values for both datasets (to the degree the small number of samples permits a comparison; Fig. 5.6-2 left). In this context, it should be noted that the two datasets were not performed on the same samples, thus CEC variations at similar depths due to mineralogical variation can be expected.
- The CEC values obtained from the corrected sum of cations also indicate consistency between Uni Bern and PSI datasets (Fig. 5.6-2 right).
- In the case of Uni Bern data, the corrected ΣCAT data are generally slightly lower than Ni consumption (by -10 to -6%), whereas the PSI data rather show the opposite (-2 to +20%).
- In general, the expected positive trend between clay-mineral content and CEC, both for Ni consumption and corrected sum of cations is illustrated (Fig. 5.6-3). There is one clear outlier sample at 735.02 m with 35 wt.-% clay minerals from the «Herrenwis Unit» that falls off the trend and displays a high CEC.
- The trend improves when illite content or smectite content is considered instead of clay-mineral content. In fact, the CEC is primarily induced by the structural negative charge of these minerals, whereby the negative charge carried by smectite is about four times larger than that of illite. The correlation between the sum of illite and 4×smectite content and the CEC is clearly superior to that exhibited by the clay-mineral content, as illustrated in Fig. 5.6-4. Note that the outlier sample from the previous graph now roughly lies within the general trend (see previous bullet point).

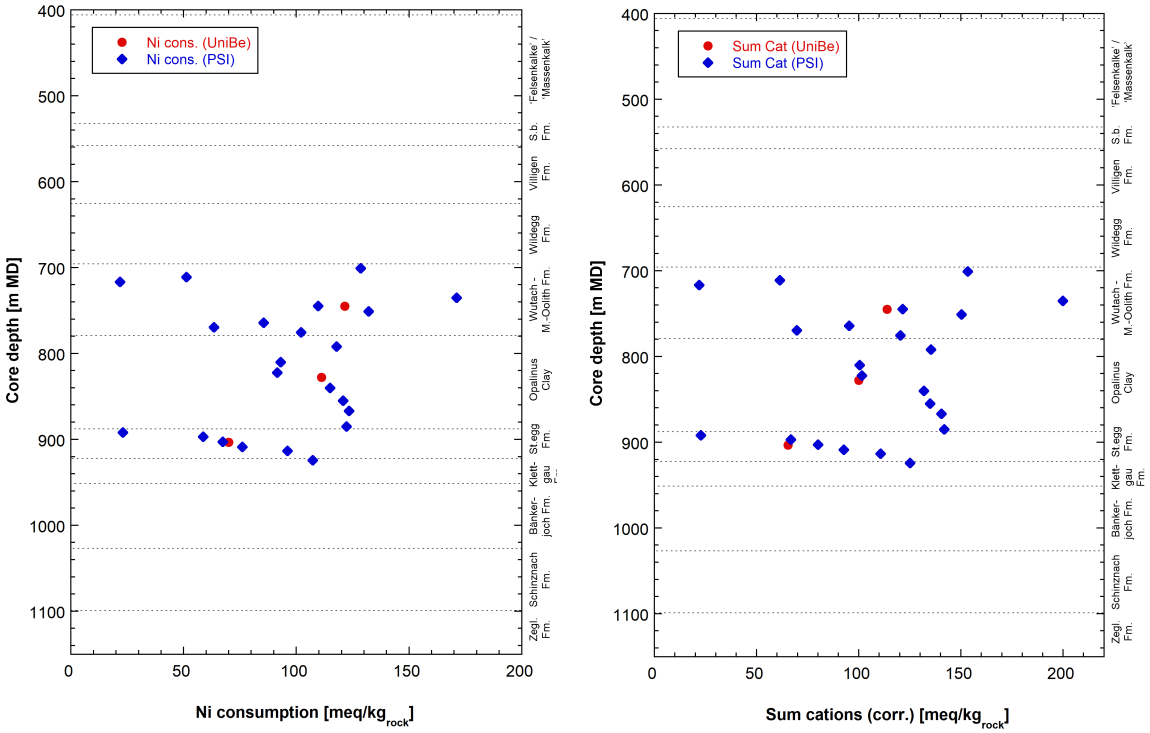


Fig. 5.6-2: Comparison of CEC data from Uni Bern and from PSI; Ni consumption data (left) and corrected sum of cations data (right)

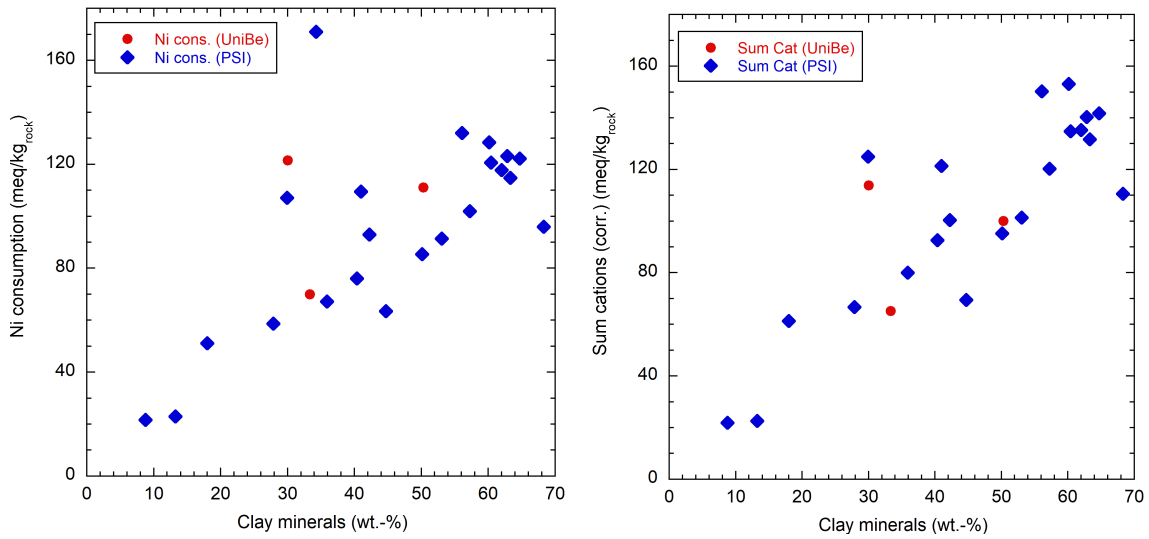


Fig. 5.6-3: CEC data as function of the clay-mineral content; left: Ni consumption data; right: Corrected sum of cations

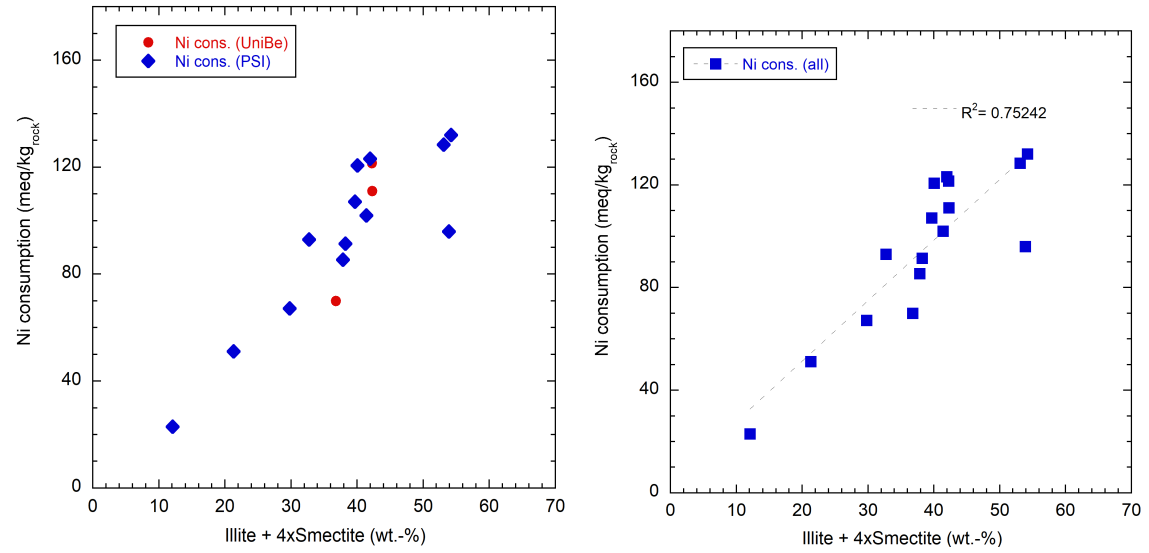


Fig. 5.6-4: Ni consumption as function of the sum of illite end-member content and 4×smectite end-member content

Note that illite and smectite contents were not measured for all samples.

## Exchangeable cation occupancies

The advantage of comparing fractional cation occupancies rather than the extracted cation concentrations is that they are normalised to the sum of cations (as proxy for the CEC) and do not directly depend on the clay-mineral content of the sample.

Fig. 5.6-5 shows the Na and Ca occupancies derived from the two correction methods. Note that in method 1 Cl and $SO_4$ are attributed to Na, whereas in method 2, $SO_4$ and, in the case of PSI data, also TIC is attributed to Ca. Thus, the Na fraction is minimised in method 1 and maximised in method 2, while the opposite is true for Ca. Besides the two datasets, the calculated occupancies

from the SQ and AD porewater data are shown. The calculations were done with the PHREEQC simulator and the well-established single-site cation exchange model for Opalinus Clay (Pearson et al. 2011, Wersin et al. 2016). Two samples with low clay-mineral content (716.58 m and 891.81 m) from the PSI datset yielded unrealistically low Ca occupancies from the correction methods and are not presented in the data below.

Comparison of "measured" Uni Bern and PSI exchangeable cation data illustrates more or less consistent trends for all measured exchangeable cations, except for K, as illustrated in Figs. 5.6-5 to 5.6-7. The "back calculated" exchangeable AD/SQ data generally support the overall trends. For K, PSI data display systematically higher occupancies, which is related to the extraction by CsCl mobilising a larger pool of K present in the illite fraction. The same mismatch was already observed in previous boreholes (Mazurek et al. 2021, Aschwanden et al. 2021, Mäder et al. 2021, Wersin et al. 2022a, Gimmi et al. 2022). The higher K occupancies of the PSI data can explain the somewhat lower corresponding Na occupancies of the Uni Bern and of the "back calculated" exchangeable AD/SQ data. This is illustrated by the consistent behaviour of the ΣNa+K for all three datasets (Fig. 5.6-5 right). The monovalent cation data suggest an increasing trend with depth in the upper «Brauner Dogger», followed constant values down to the footwall of the sampled sequence. The scatter in the uppermost part of the «Brauner Dogger» («Herrenwis Unit») is likely due to the uncertainty related to the cation occupancy correction procedure for these limestone-rich heterogeneous rocks in which a considerable fraction of carbonate mineral dissolution occurred (Marques Fernandes & Baeyens *in prep.*).

The Ca and Mg occupancies display slightly decreasing trends with depth in the upper part part of the sequence, followed by rather constant values (Fig. 5.6-6). Consistency between the "measured" and "back-calculated" datasets is improved considering Ca occupancies corrected by method 2 relative to method 1. PSI data suggest an increase in Ca and also in Ca/Na and Ca/Na+K ratios (Fig. 5.6-8) from the center to the footwall of the OPA, followed by a decrease in the Staffelegg Formation The increasing trend in the OPA is, however, not supported by Uni Bern data and the "back-calculated" SQ/AD data. Thus, at present it is not clear whether the trend for Ca suggested by the PSI data in the lower part of the OPA is real or related to some experimental artefact.

The Mg/Ca ratio decreases slightly from the «Brauner Dogger» down to the bottom of the OPA but exhibits a rise across the Staffelegg Formation (Fig. 5.6-9 left). The Sr/Ca ratio profile suggests a slight increase with depth, but the scatter in the data is substantial.

Exchangeable ammonium (only measured by PSI) displays low fractional occupancies of 0.012 – 0.017, with the exception of one sample from the «Herrenwis Unit» (0.025).

There is an outlier sample at 710.87 m depth which displays high K and comparatively low Na occupancies. The share of mobilised K via CsCl extraction appears to be particularly high for this sample from the «Herrenwis Unit» (reef facies). This may be due to drilling fluid contamination which also affected a near-by sample (Section 4.4.2.1) The sample at 896.60 m from the Rietheim Member displays a significantly higher share of extracted Sr compared to the other samples.

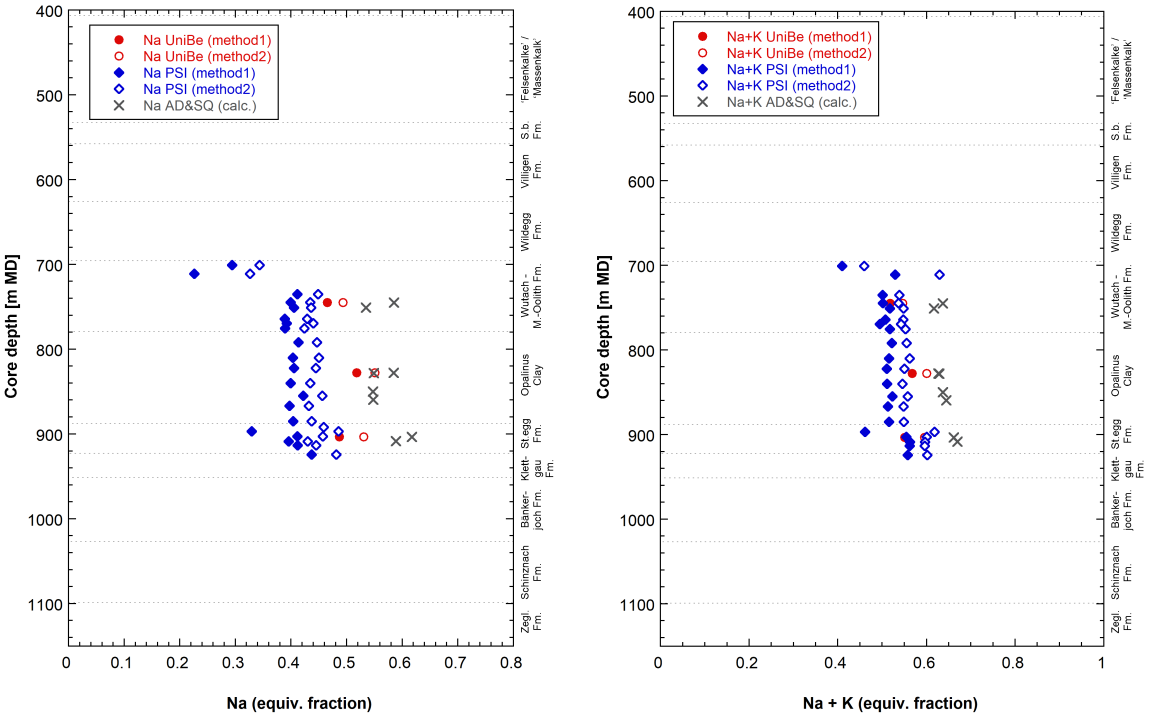


Fig. 5.6-5: Na (left) and Na+K (right) occupancies according to Uni Bern and PSI data and calculated from AD/SQ data

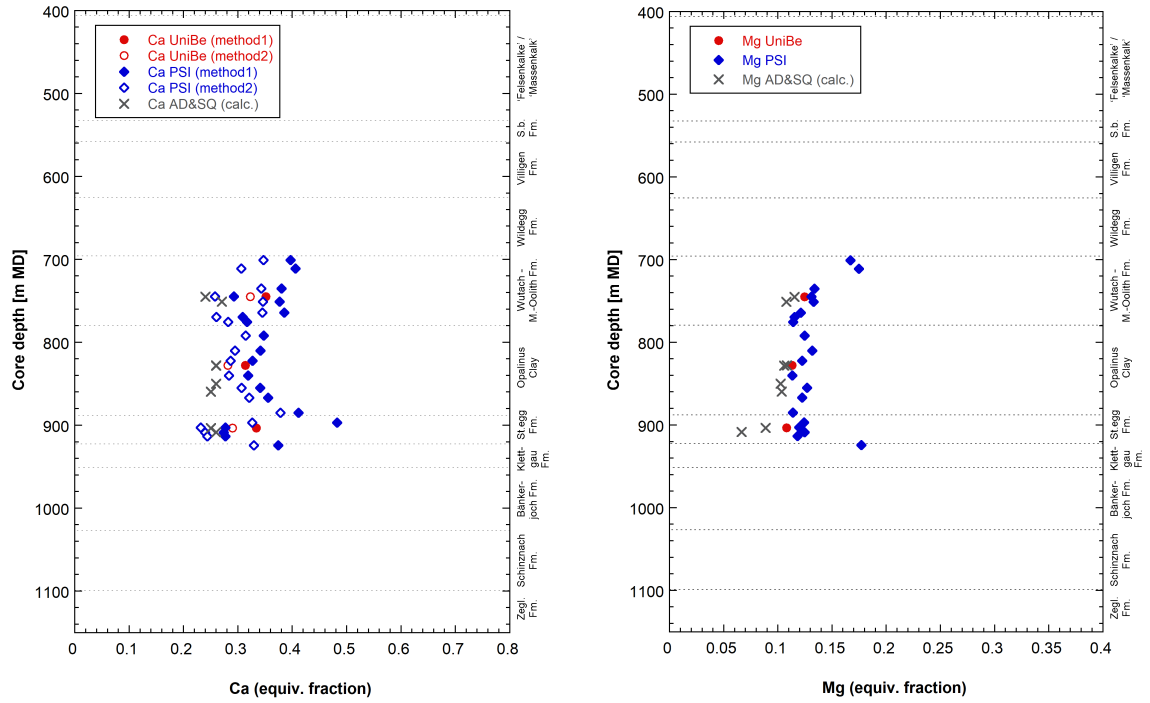


Fig. 5.6-6: Ca (left) and Mg (right) occupancies according to Uni Bern and PSI data and calculated from AD/SQ data

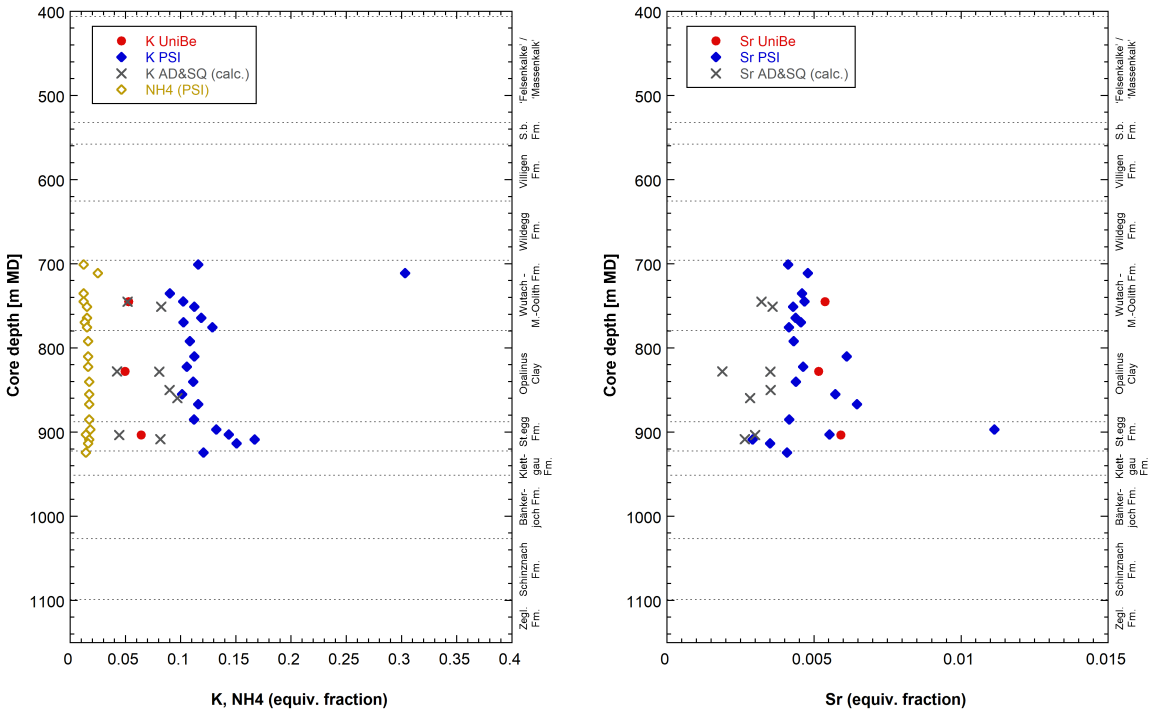


Fig. 5.6-7: K, $NH_4$ (left) Sr occupancies (right) according to Uni Bern and PSI data and calculated from AD/SQ data

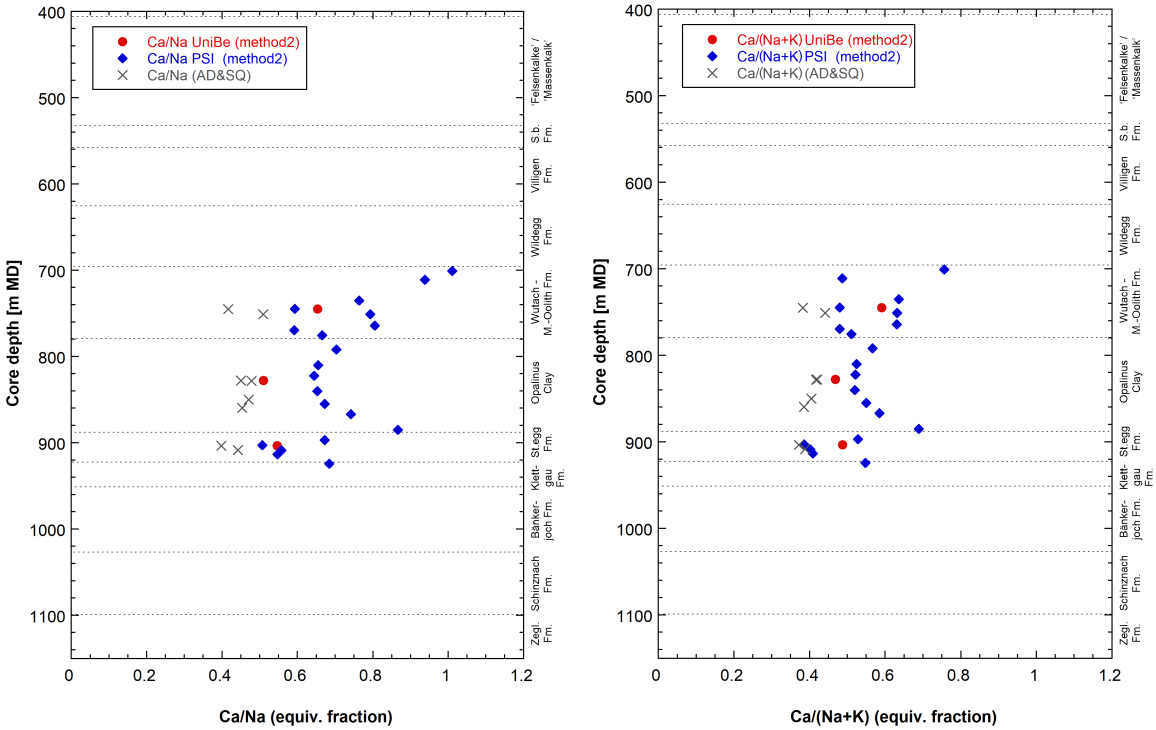


Fig. 5.6-8: Ca/Na ratios (left) and Ca/(Na+K) (right) according to Uni Bern and PSI data and calculated from AD/SQ data

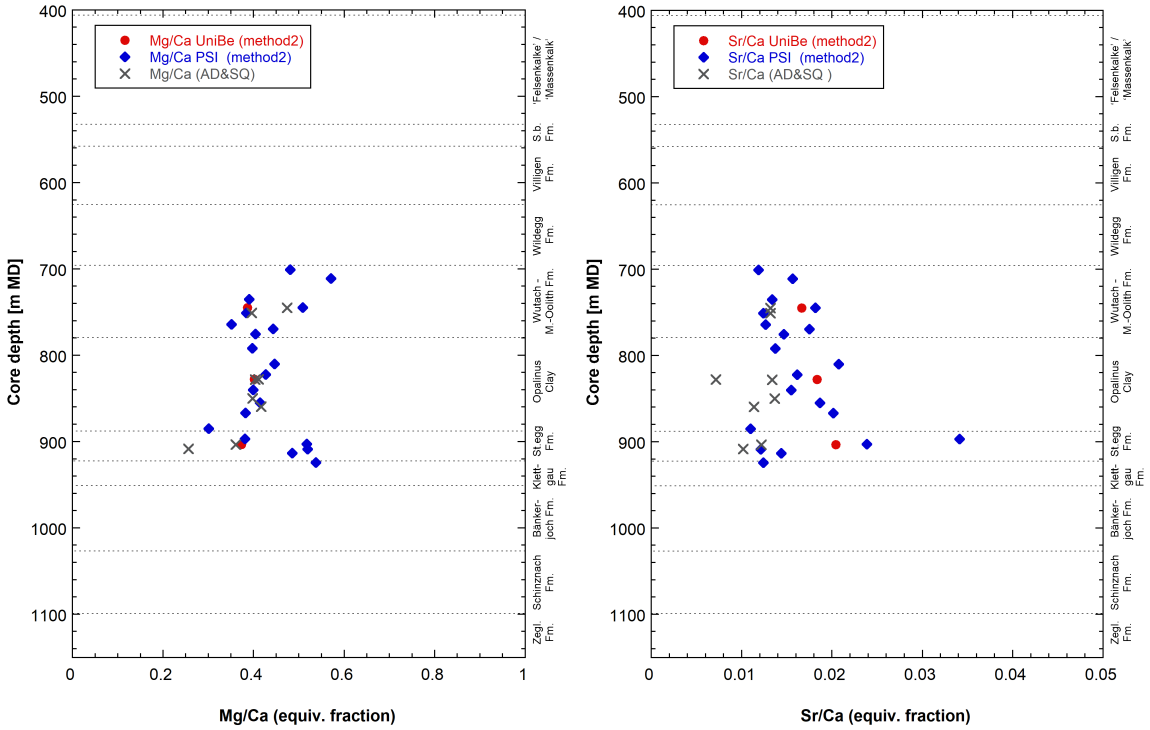


Fig. 5.6-9: Mg/Ca ratios (left) and Sr/Ca ratios (right) according to Uni Bern and PSI data and calculated from AD/SQ data

## Extracted anions

The amounts of Cl and $SO_4$ extracted are illustrated in Fig. 5.6-10. Note that for PSI data, Cl data from aqueous extraction are shown, because CsCl was used for extraction of exchangeable cations. These Cl data compare well with those analysed in the Ni-en extracts of Uni Bern. Both these datasets agree with the (larger) AqEx dataset of Uni Bern which is also illustrated in Fig. 5.6-10 (left). Regarding $SO_4$, also broad agreement between the datasets is depicted Fig. 5.6-10 (right).

The Cl concentrations (in $eq/kg_{rock}$) reveal a slightly decreasing trend with depth across the OPA. Furthermore, a conspicuous negative excursion is seen in the «Herrenwis Unit». The Cl profile is discussed in more detail in Sections 4.4.4 and 5.2.

The extracted $SO_4$ levels are generally in the same range (on an equivalent basis) as Cl levels. They are rather constant in the Opalinus Clay but display a decreasing trend with depth in the Staffelegg Formation contrary to Cl, $SO_4$ concentrations indicate a positive excursion in the upper part of the «Brauner Dogger».

Total inorganic carbon (TIC) measured in the PSI extracts is 4 – 10 $mmol/kg_{dry\ rock}$. This is higher than expected from Uni Bern extracts. TIC was not measured in the latter but calculated to be below 1 $mmol/kg_{dry\ rock}$ based on the assumption of calcite equilibrium (Tab. 4.5-4). The higher TIC in the PSI extracts is explained by the lower *S/L* ratio, which induces a higher proportion of dissolved carbonate from carbonate minerals.

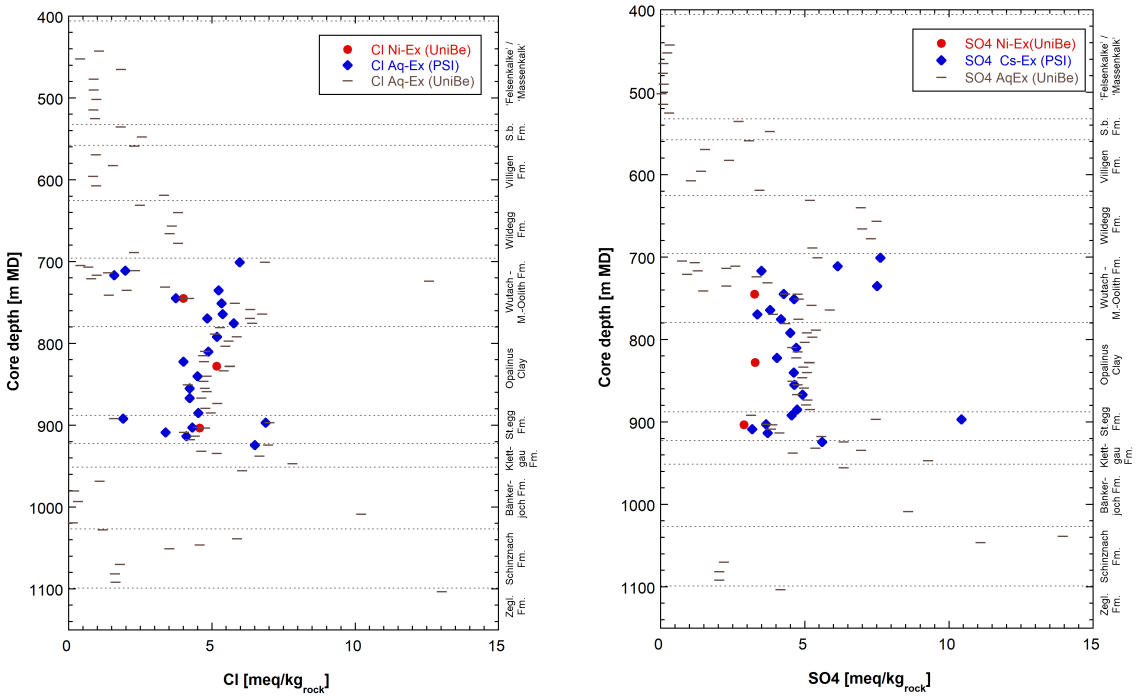


Fig. 5.6-10: Extracted Cl (left) and $SO_4$ (right) according to Uni Bern and PSI data

## 5.7 Stable water isotopes

*Lukas Aschwanden & Thomas Gimmi*

### 5.7.1 Comparison between different methods for the determination of stable porewater isotope compositions

The porewater oxygen and hydrogen isotope compositions were determined using three different methods including the isotope diffusive-exchange (Section 4.8), advective displacement (Section 4.7) and high-pressure squeezing (Section 4.6) methods. Data of the three techniques are available for the section 740 – 910 m where clay-rich rocks dominate and all methods can be applied. For the clay-poor rocks of the Malm and the Muschelkalk only data from isotope diffusive-exchange experiments are available. For the advective-displacement technique, the average of the first two displaced solution aliquots is considered as being most representative for the in situ porewater. For the squeezed water, the one obtained at the lowest squeezing pressure (200 MPa or 300 MPa) is considered as being most representative for the in situ porewater.

All the porewater isotope data, together with those for the groundwater samples from the aquifers in the Malm and the Muschelkalk (*cf.* Section 2.3), are shown in Fig. 5.7-1 as a function of depth. For isotope data from isotope diffusive-exchange experiments the error bars reflect the propagated experimental and analytical uncertainty. For isotope data from advective-displacement and high-pressure squeezing experiments only the analytical error is illustrated. In general, for $\delta^2H$, the three methods agree well (within the uncertainty). However, for $\delta^{18}O$ both isotope data from high-pressure squeezing and from advective displacement show slightly lower values compared to the data from isotope diffusive-exchange experiments. The reason for this is currently unknown. Note that three of the advective-displacement experiments were affected by microbially-induced nitrate production. However, the effect of elevated nitrate concentrations on the water isotopes is small (*cf.* Section 4.4).

### 5.7.2 Comparison with groundwater data and depth profiles

The $\delta^{18}O$ and $\delta^{2}H$ values of groundwater from the Malm aquifer agree well with those of the porewater obtained from the two samples in the packed-off interval. Owing to low hydraulic conductivity ($7.7 \times 10^{-12}$ m/s) no groundwater sample could be collected in the Keuper of STA3-1. From the Malm aquifer down to the base of the Klettgau Formation the porewater isotope composition shows a continuous evolution in $\delta^{18}O$ and $\delta^{2}H$ before sharply evolving towards most negative values in the water-conducting zone of the Schinznach Formation. Note that none of the isotope tracers show any irregularities or excursions in the deformed interval (850.20 – 851.80 m) of the Opalinus Clay (*cf.* Section 2.2) and neither do the anionic tracers Cl and Br (*cf.* Section 5.2). Thus, based on the tracer profiles there are no indictations for recent advective flow in this interval.

The $\delta^{2}H$ values of groundwater from the Muschelkalk aquifer agree well (i.e., within the propagated uncertainty) with those of the porewater obtained from samples in the packed-off interval but porewater $\delta^{18}O$ values are slightly enriched. The Muschelkalk groundwater appears to represent minima of $\delta^{18}O$ and $\delta^{2}H$ and the adjacent porewaters in the Bänkerjoch Formation indicate remarkably steep gradients towards heavier values upwards. Such steep gradients indicate either that the isotope signal in the groundwater is geologically young, and/or the diffusion coefficients in the anhydrite-rich Bänkerjoch Formation are very low.

As described in Section 4.8, although both $\delta^{18}O$ and $\delta^{2}H$ values of the porewater indicate the same general trends between the aquifers in the Malm and the Muschelkalk, some differences exist in the interval Schwarzbach Formation – Klettgau Formation: Porewater $\delta^{18}O$ values generally evolve towards more depleted values, whereas $\delta^{2}H$ signatures first increase down to the base of the «Herrenwis Unit» (701.7 – 742.0 m) and then remain remarkably constant down to the base of the Klettgau Formation. This different behaviour likely reflects inherited trends from the initial porewater isotope profiles (i.e., before the isotope signatures in the confining aquifers changed to present-day values) with rather constant $\delta^{2}H$ but decreasing $\delta^{18}O$ values across the Jurassic and eventually Late Triassic sequence. Interestingly, similar differences, partly less pronounced, were observed in data from other boreholes (Mazurek et al. 2021, Aschwanden et al. 2021, Mäder et al. 2021, Wersin et al. 2022a, Gimmi et al. 2022) or even in the older data from Benken (Gimmi & Waber 2004, Gimmi et al. 2007).

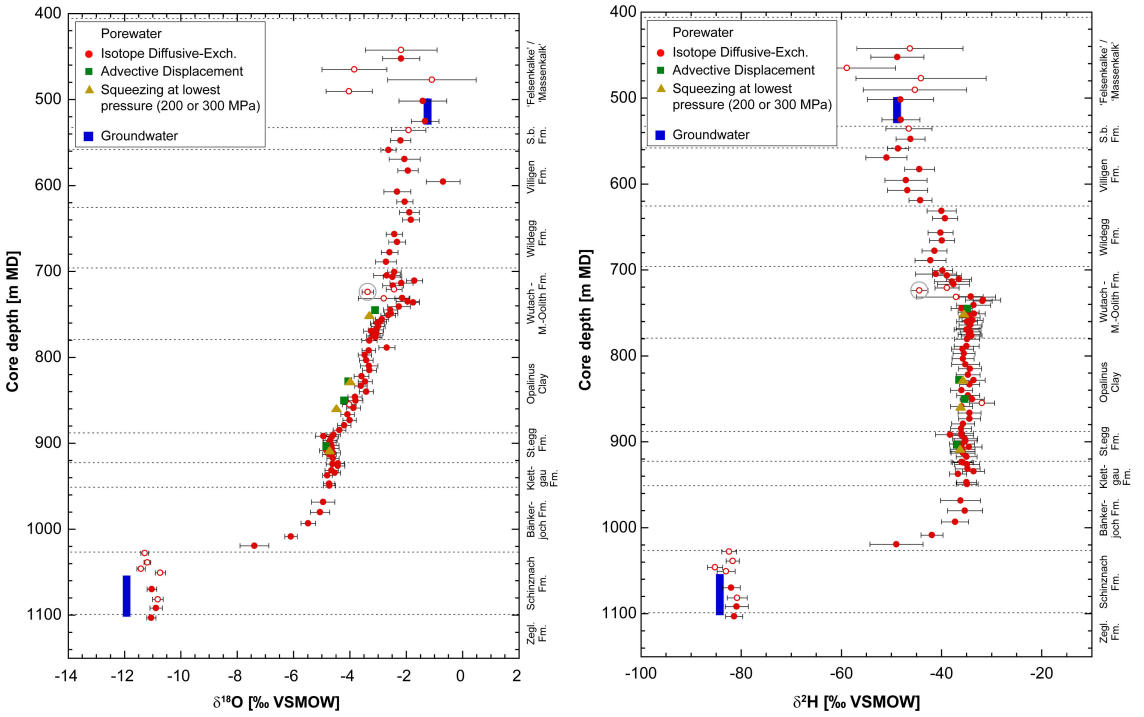


Fig. 5.7-1: Depth trends of $\delta^{18}O$ and $\delta^{2}H$ in groundwater and porewater derived by all techniques

Bars indicate propagated analytical errors (diffusive exchange) or simple analytical errors (squeezing, advective displacement). Groundwater data are from Lorenz (*in prep.*). Open symbols refer to porewater isotope values which are less reliable owing to experimental artefacts (*cf.* Section 4.8). The sample with a grey circle shows signs of contamination by drilling fluid (*cf.* Section 4.4).

### 5.7.3 $\delta^{2}H$ versus $\delta^{18}O$ and comparison with Global Meteoric Water Line

Fig. 5.7-2 illustrates all data in a $\delta^{18}O$ vs. $\delta^{2}H$ diagram. Such diagrams provide information on e.g. climatic conditions during recharge, on water-rock interactions, and/or on mixing of different water components.

Porewater isotope signatures in the Malm plot far to the right of the Global Meteoric Water Line (GMWL), as do porewaters in the underlying «Brauner Dogger» (but enriched in $^{2}H$). The porewater isotope composition continuously evolves from the «Brauner Dogger» to the base of the Klettgau Formation towards values depleted in $^{18}O$, as shown by the solid red arrow 1 in Fig. 5.7-2, thereby closely approaching the GMWL. This suggests a dominant meteoric component in the latter porewaters. The pronounced deviation of the porewater $\delta^{18}O$ – $\delta^{2}H$ signatures with respect to the Global Meteoric Water Line at the top of the section in the Malm and the «Brauner Dogger» indicates long residence times of these porewaters, with values affected by exchange with groundwater in over- and underlying water-conducting zones, and possibly by water-rock interactions. Similar to the porewater at the base of the Klettgau Formation, porewater in the Bänkerjoch Formation has a meteoric signature evolving – with increasing depth – along the GMWL towards values more depleted in $^{18}O$ and $^{2}H$ but still distinctly enriched compared to modern recharge (solid red arrow 2 in Fig. 5.7-2). Note that modern recharge does not only refer to recent or post-glacial recharge but rather recharge under climatic conditions similar to recent

conditions (e.g., during an interglacial period in the Quaternary). At the base of the Bänkerjoch Formation porewater $\delta^{18}O$ and $\delta^{2}H$ signatures sharply drop to distinctly more negative values in the water-conducting zone of the Muschelkalk (solid red arrow 3 in Fig. 5.7-2) still falling on or slightly to the right of the GMWL and somewhat depleted relative to modern recharge, indicative for infiltration under cold-climate conditions. The deviation of the porewater isotope composition from the GMWL is likely due to mixing with isotopically different water components and/or water – rock interactions.

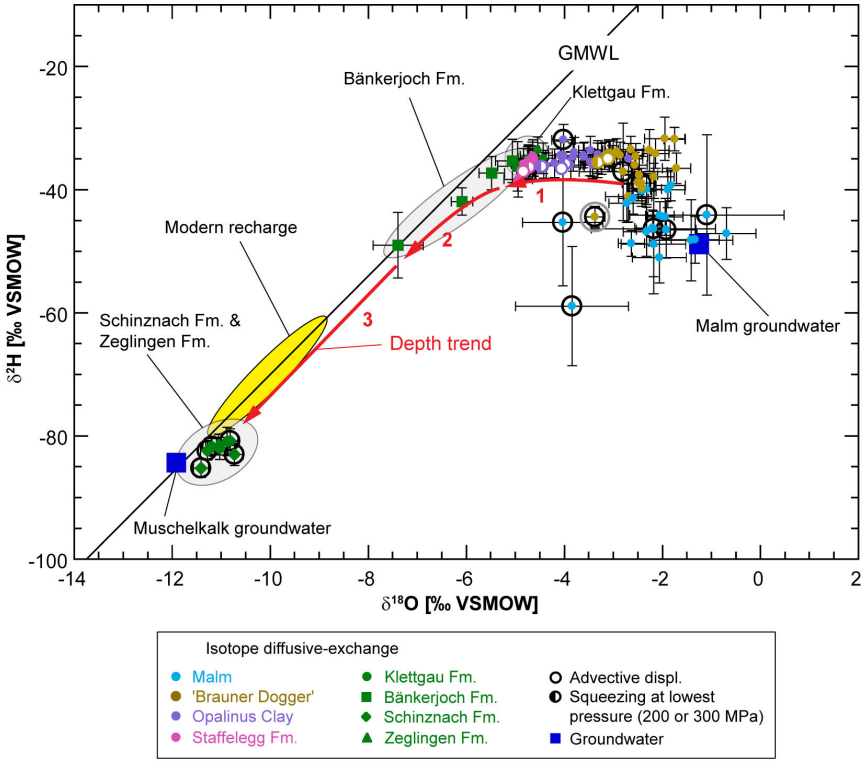


Fig. 5.7-2: $\delta^{2}H$ vs. $\delta^{18}O$ for groundwater and porewater derived by all techniques

Bars indicate propagated analytical errors (diffusive exchange) or simple analytical errors (squeezing, advective displacement). Groundwater data are from Lorenz (*in prep.*). GMWL = Global Meteoric Water Line (defined as $\delta^{2}H = 8\ \delta^{18}O + 10$; Craig 1961). Range of modern recharge from Kullin & Schmassmann (1991). Samples in circles are less reliable owing to experimental artefacts (black circles; *cf.* Section 4.8) and/or possible contamination by drilling fluid (grey circles; *cf.* Section 4.4). See text for details on the numbering of red arrows (depth trend).

# 6 Final remarks and main conclusions

*RWI team*

High-quality cores could be extracted from the STA3-1 borehole as planned between the top of the «Felsenkalke» + «Massenkalk» and the top of the Zeglingen Formation. Groundwater could be sampled from the «Felsenkalke» + «Massenkalk» (Malm aquifer) and the Schinznach Formation (Muschelkalk aquifer). The porewater samples enabled to acquire high quality mineralogical, petrophysical and porewater data using a well-established procedure. Drilling operations proceeded without major problems down to a maximum depth of 1'281.1 m (Weitenau Formation, Permian). No significant quantities of drilling mud (12 $m^3$ max.) were lost during drilling of STA3-1.

As in previous boreholes, a number of systematic depth trends were observed for the contents of clay minerals, quartz and calcite. Above a strong upward decrease of clay minerals in the Staffelegg Formation, the base of the Opalinus Clay marks a major mineralogical discontinuity towards high clay-mineral contents. As seen previously, the 'Mixed clay-silt-carbonate sub-unit' can be subdivided into 2 parts with contrasting mineralogical trends. Marked trends also exist in the «Murchisonae-Oolith Formation» and in the Wedelsandstein Formation. The ratio of the illite-to-kaolinite end-member clays also shows a systematic variation with depth. It is low in the Opalinus Clay and increases marginally towards the top of the «Murchisonae-Oolith Formation», then it becomes much higher towards the top of the Dogger.

The depth trends of mineral contents correlate well with those of petrophysical parameters and can be even clearer (e.g. water content). Water content and porosity correlate positively with the clay-mineral content, even though the correlation is far from perfect. This indicates that apart from clay-mineral content, other rock characteristics, such as depositional environment, pore-space architecture and diagenesis have an influence on porosity. The most prominent deviations include dolostones of the Schinznach and Zeglingen Formations, where diagenetic dissolution occurred.

Nitrogen adsorption data were obtained for 7 samples from the upper and lower confining units of the Opalinus Clay only. The samples are lithologically very different, but the general trends match with those observed for the larger dataset from the BUL1-1 borehole. There is a broadly positive correlation of the external specific surface area (BET, $N_2$ adsorption) with clay-mineral contents and a weaker correlation with water contents. Also, average radii of external pores (assuming negligible interlayer water) tend to decrease with water content or with clay-mineral content, but with larger scatter of the values for samples with low water or low clay-mineral content.

Drilling fluid contamination was identified in one aqueous extraction sample in the «Herrenwis Unit». It was noticed that aqueous extraction on dried rock yielded substantially lower Br and in the case of the Rietheim Member sample also lower Cl concentrations compared to extracts conducted on wet rock. This might be related to complexation with transformed organic matter during the heating to 105 °C, but further investigations would be needed to check this hypothesis.

Across the interval Schwarzbach Formation – Schinznach Formation both $\delta^{18}O$ and $\delta^{2}H$ values of the porewater show well defined, curved profiles. None of the isotope tracers show any irregularities or excursions in the deformed interval (850.20 – 851.80 m) of the Opalinus Clay. Porewaters in the Malm and the «Brauner Dogger» are enriched in $^{18}O$ and $^{2}H$ and plot far to the right of the Global Meteoric Water Line (GMWL) indicating long residence times. From the «Brauner Dogger» to the base of the Klettgau Formation the porewater isotope composition continuously evolves towards values depleted in $^{18}O$, thereby closely approaching the GMWL. This suggests a dominant meteoric component in the latter porewaters. The different behaviour

of $\delta^{18}O$ and $\delta^{2}H$ values in this section of the borehole may reflect inherited trends resulting from the earlier evolution (i.e., before the isotope signatures in the confining aquifers changed to present-day values) with rather constant $\delta^{2}H$ but $\delta^{18}O$ values decreasing with depth across the low-permeability formations of the Dogger and the Liassic. Similar to the porewater at the base of the Klettgau Formation, porewater in the Bänkerjoch Formation has a meteoric signature evolving – with increasing depth – along the GMWL towards values more depleted in $^{18}O$ and $^{2}H$ but still distinctly enriched compared to modern recharge. Porewaters in the Bänkerjoch Formation indicate remarkably steep gradients towards general minima of $\delta^{18}O$ and $\delta^{2}H$ in the water-conducting zone of the Muschelkalk. Such steep gradients indicate either that the isotope signal in the groundwater is geologically young, and/or the diffusion coefficients in the anhydrite-rich Bänkerjoch Formation are very low. The isotope composition of porewater in the Muschelkalk still falls on or slightly to the right of the GMWL and is somewhat depleted relative to modern recharge, indicative for infiltration under cold-climate conditions.

Anion-accessible porosities could be derived from squeezed (SQ) and advectively displaced (AD) porewaters. These yield Cl-accessible porosity fractions ($f_{Cl}$) with a mean value of ~ 0.45 ± 0.05[17]. This is similar to values derived for previous boreholes (e.g. BOZ1-1, BOZ2-1, TRU1-1, MAR1-1) but slightly lower than that for BUL1-1. The same linear relationship of $f_{Cl}$ with clay-mineral content as for this latter borehole was used to derive Cl and Br concentrations per accessible porewater from aqueous extraction.

Broadly consistent Cl and Br profiles are revealed from squeezing, advective-displacement and re-calculated aqueous extraction data. Using pycnometer porosities instead of water-loss porosities when scaling the aqueous extract data to concentrations per bulk porewater or accessible porewater leads to a more coherent profile in some sections, but to more scatter in others. The Cl and Br profiles show a rather flat shape between the Klettgau Formation and the Malm units, with Cl concentrations of ~ 8 g/L. Neither the Cl nor the Br profile show any irregularities or excursions in the deformed interval (850.20 – 851.80 m) of the Opalinus Clay. Variations are evident in the confining units, in particular in the «Herrenwis Unit». These are interpreted as being largely related to uncertainites regarding anion-accessible porosity fractions. The Cl and Br profiles are bounded by the aquifers in the Muschelkalk and the Malm, respectively. Below the Klettgau Formation, a marked decrease towards the Muschelkalk aquifer is noted, but strong variations in the lower part of the Bänkerjoch Formation are indicated. Analogous profiles were derived for $\delta^{18}O$ and $\delta^{2}H$ (but without the variations in the Bänkerjoch Formation). There are no indications of an active aquifer in the Keuper from the Cl and Br profiles.

The depth profile of the Br/Cl ratio reveals consistency between AqEx and SQ. The slightly lower values obtained from AD data are interpreted as being largely related to methodological artefacts. The Br/Cl profile shows less scatter than that of Cl or Br due to the fact that no assumptions on anion accessibility need to be made and the uncertainty regarding re-calculation to the rock porosity cancels out. Constant Br/Cl ratios close to modern seawater are found in the upper part of the profile down to the Klettgau Formation. Below, the ratios exhibit larger scatter, suggesting a positive excursion in the Bänkerjoch Formation, followed by a strong decrease towards the Muschelkalk aquifer. The low Br/Cl ratios in the porewater of the Zeglingen Formation and in the groundwater of the Muschelkalk could be related to dissolution phenomena in the underlying salt layers of the Zeglingen Formation.

The sulphate data obtained from SQ and AD, which covers the sequence Wedelsandstein – Staffelegg Formation, are broadly consistent. The corresponding $SO_4$ profile indicates constant concentrations from the Wedelsandstein to the Opalinus Clay and a slight increase below in the

[17] This excludes one AD sample with an exceptionally low $f_{Cl}$ value. If this value is included, the mean value is 0.44 ± 0.08.

Staffelegg Formation. Conversely, AqEx data yield systematically higher and more variable concentrations, as has been observed in the previous boreholes and the Mont Terri Rock Laboratory. $SO_4$/Cl ratios deduced from SQ and AD exhibit a similar shape as the $SO_4$ profile with values of ~ 0.12 (molar units) in the Opalinus Clay.

Cation data representative of the porewater could be obtained from SQ and AD data although most of the AD samples were affected by high nitrate levels. Disregarding the 2 samples with highest nitrate concentrations, regular and consistent patterns in major cations could be found.

The cation exchange capacity (CEC) correlates with the clay-mineral content. An even better correlation can be deduced with the sum of illite and smectite end-member mineral contents, the main carriers of the CEC. The main exchangeable cations are Na and Ca, followed by Mg and K. The exchanger composition (cation occupancies) is approximately constant across the sampled sequence («Brauner Dogger» – Staffelegg Formation). The exchanger composition determined from extraction methods exhibits the same trends as the "calculated" exchanger compositon obtained from modelling of the SQ and AD porewater data.

The porewaters in the Opalinus Clay and bounding formations display moderate salinities and ionic strengths with Cl concentrations of about 8 g/L over large parts of the profile. These chloride levels are somewhat lower than those of BUL1-1 from the same siting area (~ 12 g/L). The porewaters are of Na-(Ca)-Cl-($SO_4$) type (according to the nomenclature of Jäckli 1970) in the interval sampled for SQ and AD (Wedelsandstein – Staffelegg Formations).

The pH/$pCO_2$ conditions deduced for the SQ and AD data appear somewhat perturbed due to $CO_2$ exchange during the experiments in case of SQ and due to microbial processes resulting in elevated nitrate concentrations in the case of AD. Reasonable pH/$pCO_2$ conditions could be estimated from simple modelling considering $CO_2$ exchange during the SQ experiments.

SQ data yield TOC data of about 200 mg C/L. These concentrations are not thought to fully reflect in situ porewater conditions but rather the easily mobilisable fraction from the solid organic matter. AD data yield higher values, especially those that are most perturbed by nitrate.

An in-depth interpretation and comparison with data from boreholes from the same or other siting areas is beyond the scope of this report. Here, a short summary of a few points is presented:

- In the STA3-1 borehole, groundwater samples could be extracted from packed-off sections in the Malm and in the Muschelkalk, similar to the boreholes BUL1-1 and MAR1-1. At both localities tracer profiles as well as structural observations confirm the presence of active aquifers in the «Felsenkalke» + «Massenkalk» and in the Schinznach Formation.
- From the few currently available SQ and AD data, the $f_{Cl}$ value (~ 0.45 for clay-mineral contents > 30 wt.-%) is in a similar range as observed for most of the previous boreholes, however, compared to BUL1-1 it is slightly lower ($f_{Cl\ BUL1}$ ~ 0.52). Note that $f_{Cl}$ values obtained from AD are systematically slightly lower than those obtained by SQ.
- The porewaters in the Opalinus Clay from STA3-1 show chloride concentrations in the same range (~ 7.5 – 9.5 g/L) as observed for TRU1-1 and MAR1-1 but somewhat lower than those at BUL1-1 (~ 12 g/L). Porewaters at BOZ1-1 and BOZ2-1 represent the most diluted in all investigated boreholes so far (~ 2.0 – 3.5 g/L).
- The porewater in the Opalinus Clay from STA3-1 shows similar $\delta^2H$ but slightly more depleted $\delta^{18}O$ values compared to the porewater of BUL1-1. In all other investigated boreholes the Opalinus Clay porewater shows more negative isotopic compositions than in STA3-1.

# 7 References

Allison, J.D., Brown, D.S. & Novo-Gradac, K.J. (1991): MINTEQA2/PRODEFA2, a geochemical assessment model for environmental systems: Version 3.0 user's manual. Environmental Research Laboratory, Office of Research and Development, U.S. Environmental Protection Agency, 106 p.

Aschwanden, L. & Wersin, P. (2020): Experimental study of sulphate in the Opalinus Clay: Results from extraction tests. Nagra Arbeitsbericht NAB 20-17.

Aschwanden, L., Camesi, L., Gimmi, T., Jenni, A., Kiczka, M., Mäder, U., Mazurek, M., Rufer, D., Waber, H.N., Wersin, P., Zwahlen, C. & Traber, D. (2021): TBO Trüllikon-1-1: Data report Dossier VIII. Rock properties, porewater characterisation and natural tracer profiles. Nagra Arbeitsbericht NAB 20-09.

Bradbury, M.H. & Baeyens, B. (1998): A physicochemical characterisation and geochemical modelling approach for determining porewater chemistries in argillaceous rocks. Geochim. Cosmochim. Acta 62, 783-795.

Courdouan Merz, A. (2008): Nature and reacivity of dissolved organic matter in clay formations evaluated for the storage of radioactive waste. PhD thesis. ETH Zurich.

Courdouan, A., Christl, I., Meylan, S., Wersin, P. & Kretzschmar, R. (2007a): Characterization of dissolved organic matter in anoxic rock extracts and in situ pore water of the Opalinus Clay. Applied Geochemistry 22, 2926-2939.

Courdouan, A., Christl, I., Meylan, S., Wersin, P. & Kretzschmar, R. (2007b): Isolation and characterization of dissolved organic matter from the Callovo-Oxfordian formation. Applied Geochemistry 22, 1537-1548.

Craig, H. (1961): Isotopic variations in meteoric waters. Science 133, 1702-1703.

Debure, M. & Gailhanou, H. (2019): GD experiment: Experimental study of sulphate in Opalinus Clay. Unpubl. Mont Terri Technical Note. Mont Terri Project, Switzerland.

Gimmi, T. & Alt-Epping, P. (2018): Simulating Donnan equilibria based on the Nernst-Planck equation. Geochim. Cosmochim. Acta 232, 1-13.

Gimmi, T. & Waber, H.N. (2004): Modelling of tracer profiles in porewater of argillaceous rock in the Benken borehole: Stable water isotopes, chloride and chlorine isotopes. Nagra Technical Report NTB 04-05.

Gimmi, T., Waber, H. N., Gautschi, A., & Rübel, A. (2007): Stable water isotopes in pore water of Jurassic argillaceous rocks as tracers for solute transport over large spatial and temporal scales. Water Resources Research 43, W04410, doi:10.1029/2005WR004774.

Gimmi, T., Leupin, O.X., Eikenberg, J., Glaus, M., Van Loon, L.R., Waber, H.N., Wersin, P., Wang, H.A.O., Grolimund, D., Borca, C.N., Dewonck, S. & Wittebroodt, C. (2014): Anisotropic diffusion at the field scale in a four-year multi-tracer diffusion and retention experiment. I: Insights from the experimental data. Geochim. Cosmochim. Acta 125, 373-393.

Gimmi, T., Aschwanden, L., Camesi, L., Gaucher, E.C., Jenni, A., Kiczka, M., Mäder, U., Mazurek, M., Rufer, D., Waber, H.N., Wersin, P., Zwahlen, C. & Traber, D. (2022): TBO Bözberg-2-1: Data report Dossier VIII. Rock properties, porewater characterisation and natural tracer profiles. Nagra Arbeitsbericht NAB 21-22.

Grasset, L., Brevet, J., Schäfer, T., Claret, F., Gaucher, E.C., Albrecht, A. & Amblès, A. (2010): Sequential extraction and spectroscopic characterisation of organic matter from the Callovo-Oxfordian Formation. Organic Geochemistry 41, 221-233.

Hadi, J., Wersin, P., Mazurek, M., Waber, H.N., Marques Fernandes, M., Baeyens, B., Honty, M., De Craen, M., Frederickx, L., Dohrmann, R. & Fernandez, A.M. (2019): Intercomparison of CEC method within the GD project. Mont Terri Technical Report TR 2017-06. Mont Terri Project, Switzerland.

Isler, A., Pasquier, F. & Huber, M. (1984): Geologische Karte der zentralen Nordschweiz 1:100'000. Herausgegeben von der Nagra und der Schweiz. Geol. Komm.

Jäckli, H. (1970): Kriterien zur Klassifikation von Grundwasservorkommen. Eclogae geol. Helv. 63/2, 389–434.

Jenni, A., Aschwanden, L., Lanari, P., de Haller, A. & Wersin, P. (2019): Spectroscopic investigation of sulphur-containing minerals in Opalinus Clay. Nagra Arbeitsbericht NAB 19-23.

Kullin, M. & Schmassmann, H. (1991): Isotopic composition of modern recharge. *In:* Pearson F.J., Balderer, W., Loosli, H.H., Lehmann, B.E., Matter, A., Peters, Tj., Schmassmann, H.-J. & Gautschi, A. (1991): Applied Isotope Hydrogeology – A Case Study in Northern Switzerland. Studies in Environmental Science 43, Elsevier, Amsterdam, 65-89.

Lorenz, G.D. (*in prep.*): Borehole STA3-1 (Stadel-3-1): Fluid sampling and analytical hydrochemical data report. Unpubl. Nagra Interner Bericht.

Mäder, U. (2018): Advective displacement method for the characterisation of porewater chemistry and transport properties in claystone. Geofluids 2018, Article ID 8198762, doi.org/10.1155/2018/8198762.

Mäder, U. & Waber, H.N. (2017): Results of advective displacement / multi-component transport experiments from claystone samples of the Schlattingen borehole. Nagra Arbeitsbericht NAB 17-16.

Mäder, U., Aschwanden, L., Camesi, L., Gimmi, T., Jenni, A., Kiczka, M., Mazurek, M., Rufer, D., Waber, H.N., Wersin, P., Zwahlen, C. & Traber, D. (2021): TBO Marthalen-1-1: Data report Dossier VIII. Rock properties, porewater characterisation and natural tracer profiles. Nagra Arbeitsbericht NAB 21-20.

Marques Fernandes, M. & Baeyens. B. (*in prep.*): Sorption measurements of Cs, Ni, Eu, Th and U on rock samples of Opalinus Clay and confining geological units from deep boreholes at the potential siting regions for a deep geological repository for radioactive waste in Switzerland: Jura Ost, Nördlich Lägern and Zürich Nordost. Nagra Technical Report NTB 22-02.

Mazurek, M. (2017): Gesteinsparameter-Datenbank Nordschweiz – Version 2. Nagra Arbeitsbericht NAB 17-56.

Mazurek, M. & Aschwanden, L. (2020): Multi-scale petrographic and structural characterisation of the Opalinus Clay. Nagra Arbeitsbericht NAB 19-44.

Mazurek, M., Oyama, T., Wersin, P. & Alt-Epping, P. (2015): Pore-water squeezing from indurated shales. Chemical Geology 400, 106-121.

Mazurek, M., Aschwanden, L., Camesi, L., Gimmi, T., Jenni, A., Kiczka, M., Mäder, U., Rufer, D., Waber, H.N., Wanner, P., Wersin, P. & Traber, D. (2021): TBO Bülach-1-1: Data Report Dossier VIII. Rock properties, porewater characterisation and natural tracer profiles. Nagra Arbeitsbericht NAB 20-08.

Naef, H., Büchi, M., Bläsi, H.R., Deplazes, G. & Gysi, M. (2019): Lithology Manual – Lithological description of drill cores and cuttings in Northern Switzerland. Nagra Arbeitsbericht NAB 19-11.

Nagra (2008): Vorschlag geologischer Standortgebiete für das SMA- und das HAA-Lager. Geologische Grundlagen. Nagra Technischer Bericht NTB 08-04.

Nagra (2014): SGT Etappe 2: Vorschlag weiter zu untersuchender geologischer Standortgebiete mit zugehörigen Standortarealen für die Oberflächenanlage. Geologische Grundlagen. Dossier II: Sedimentologische und tektonische Verhältnisse. Nagra Technischer Bericht NTB 14-02.

Parkhurst, D.L. & Appelo, C.A.J. (2013): Description of input and examples for PHREEQC Version 3: A computer program for speciation, batch-reaction, one-dimensional transport, and inverse geochemical calculations. No. 6-A43. US Geological Survey.

Pearson, F.J. (1999): What is the porosity of a mudrock? *In*: Aplin, A.C., Fleet A.J. & Macquaker, J.H.S. (eds.): Muds and Mudstones: Physical and Fluid Flow Properties. Geological Society, London, Special Publications 158, 9-21.

Pearson, F.J., Arcos, D., Bath, A., Boisson, J.Y., Fernandez, A.M., Gäbler, H.E., Gaucher, E., Gautschi, A., Griffault, L., Hernan, P. & Waber, H.N. (2003): Mont Terri project – geochemistry of water in the Opalinus Clay formation at the Mont Terri rock laboratory. Federal Office for Water and Geology Rep. 5, Bern, Switzerland.

Pearson, F.J., Tournassat, C. & Gaucher, E.C. (2011): Biogeochemical processes in a clay formation in situ experiment: Part E – Equilibrium controls on chemistry of pore water from the Opalinus Clay, Mont Terri underground research laboratory, Switzerland. Applied Geochemistry 26, 990-1008.

Pietsch, J. & Jordan, P. (2014): Digitales Höhenmodell Basis Quartär der Nordschweiz – Version 2013 (SGT E2) und ausgewählte Auswertungen. Nagra Arbeitsbericht NAB 14-02.

Rufer, D. (2019): Field Manual: Drillcore sampling for analytical purposes. Nagra Arbeitsbericht NAB 19-13.

Rufer, D. & Mazurek, M. (2018): Pore-water extraction and characterization: Benchmarking of the squeezing and adapted isotope diffusive exchange methods. NWMO Technical Report NWMO-TR-2018-14. Nuclear Waste Management Organization, Toronto, Canada.

Thoenen, T., Hummel, W., Berner, U. & Curti, E. (2014): The PSI/Nagra Chemical Thermodynamic Database 12/07. PSI Bericht Nr. 14-04, Paul Scherrer Institut, Villigen, Switzerland.

Thommes, M., Kaneko, K., Neimark, A.V., Olivier, J.P., Rodriguez-Reinoso, F., Rouquerol, J., Sing, K.S. (2015): Physisorption of gases, with special reference to the evaluation of surface area and pore size distribution (IUPAC Technical Report). Pure and Applied Chemistry 87, 1051-1069.

Tournassat, C., Vinsot, A., Gaucher, E.C. & Altmann, S. (2015): Chemical conditions in clayrocks. *In:* Tournassat, C., Steefel, C.I., Bourg, I.C. & Berrgaya, F. (eds.): Natural and Engineered Clay Barriers. Developments in Clay Science 6, Chapter 3, 71-100. Elsevier.

Van Loon, L.R. & Glaus, M. A. (*in prep.*): Diffusion measurements of HTO, $^{36}Cl^-$ and $^{22}Na^+$ on rock samples of Opalinus Clay and confining geological units from deep boreholes at the potential siting regions for a deep geological repository for radioactive waste in Switzerland: Jura Ost, Nördlich Lägern and Zürich Nordost. Nagra Technical Report NTB 22-01.

Waber, H.N. (ed.) (2020): SGT-E3 deep drilling campaign (TBO): Experiment procedures and analytical methods at RWI, University of Bern (Version 1.0, April 2020). Nagra Arbeitsbericht NAB 20-13.

Wersin, P., Mazurek, M., Waber, H.N., Mäder, U.K., Gimmi, T., Rufer, D. & de Haller, A. (2013): Rock and porewater characterisation on drillcores from the Schlattingen borehole. Nagra Arbeitsbericht NAB 12-54.

Wersin, P., Mazurek, M., Mäder, U.K., Gimmi, T., Rufer, D., Lerouge, C. & Traber, D. (2016): Constraining porewater chemistry in a 250 m thick argillaceous rock sequence. Chemical Geology 434, 43-61.

Wersin, P., Pekala, M., Mazurek, M., Gimmi, T., Mäder, U.K., Jenni, A., Rufer, D. & Aschwanden, L. (2020): Porewater chemistry of Opalinus Clay: Methods, modelling & buffering capacity. Nagra Technical Report NTB 18-01.

Wersin, P., Aschwanden, L., Camesi, L., Gaucher, E.C., Gimmi, T., Jenni, A., Kiczka, M., Mäder, U., Mazurek, M., Rufer, D., Waber, H.N., Zwahlen, C. & Traber, D. (2022a): TBO Bözberg-1-1: Data report Dossier VIII. Rock properties, porewater characterisation and natural tracer profiles. Nagra Arbeitsbericht NAB 21-21.

Wersin, P., Mazurek, M. & Gimmi, T. (2022b): Porewater chemistry of Opalinus Clay revisited: Findings from 25 years of data collection at the Mont Terri Rock Laboratory. Applied Geochemistry, 138.

Zwahlen, C., Aschwanden, L., Camesi, L., Gimmi, T., Jenni, A., Kiczka, M., Mäder, U., Mazurek, M., Rufer, D., Waber, H.N., Wersin, P. & Traber, D. (*in prep.*): TBO Stadel-2-1: Data report Dossier VIII. Rock properties, porewater characterisation and natural tracer profiles. Nagra Arbeitsbericht NAB 22-02.